The influence of manufacturing variables on the static and dynamic compressive strength of pre-preg moulded materials

THE INFLUENCE OF MANUFACTURING VARIABLES ON THE STATIC AND DYNAMIC COMPRESSIVE STRENGTH OF PREPREG MOULDED MATERIALS

SWEE CHENG YAP

THE INFLUENCE OF MANUFACTURING VARIABLES ON THE STATIC AND DYNAMIC COMPRESSIVE STRENGTH OF PREPREG MOULDED MATERIALS

by

SWEE CHENG YAP

A Doctoral Thesis
submitted in partial fulfilment of the requirements
for the award of

Doctor of Philosophy

of the Loughborough University of Technology

Institute of Polymer Technology and Materials Engineering
IPT & ME

June 1991

DEDICATION

In Memory to My Grandmother.
To My Beloved Parents, Brothers, Sister,
and My Fiance´,
For Their Love and Support.

ACKNOWLEDGEMENTS

I would like to thank my supervisor, Mr J F Harper, for his interest in this research.

I would like to express my sincere thanks to Dr R W Dyson and Dr J Fox in the London School of Polymer Technology (LSPT), Mr G E Carr, Mr N A Miller and Mr S Yang, for their help, support and encouragement in this research.

I received help and encouragement from a number of persons within the IPTME. I am grateful for their direction, encouragement and provision of facilities for completing this research.

I am thankful to Lucas Aerospace, Burnley, for providing the materials for this work, without which my work here would not have been possible.

Financial support for this work was provided by the Oversea Research Students Award and the debt is gratefully acknowledged.

Finally, I am most grateful, for the encouragement I have received, to all my family, friends and relations. In particular to my beloved parents who always carried the burden of educating and supporting me; to my brothers Yoke Sin, Yoke Lim and my sister Swee Peng for their understanding and encouragement; and not to forget my fiance´ Dr Pan Zhang for his help, patience and support throughout the work of this project.

SYNOPSIS

Fibre reinforced plastic (FRP) composites consist of two or more components combined to give a synergistic effect for a better performance in service. One of the phases comprises layers of fibrous material while the other phase comprises of a polymer matrix. In this project, carbon fibre prepreg material was used.

All materials contain imperfections. Materials constituents and manufacturing anomalies are the main causes of faults in FRP composites. The presence of voids in FRP composites is the most common defect.

The aim of this project was to determine the influence of voids on the static and dynamic compressive properties of carbon fibre reinforced plastic (CFRP) composites. The influence of voids on fatigue life and failure behaviour were also investigated.

Several methods of creating voids were investigated. Variation of partial cure time proved to be the most effective way to produce a range of void contents.

As well as void content, the density, fibre volume fraction and thickness were determined for all the laminates.

Static tests were used to determine mechanical properties (strength, modulus and failure strain) in compression. In the absence of an internationally recognised test method, a variety of anti-buckling guides was used. It was demonstrated that the type of jig used influences the test results.

Dynamic fatigue tests were carried out at different stress levels and stress/log life (S/N) curves plotted. The results of both static and dynamic tests confirmed that the presence of voids had a deleterious effect on the mechanical properties of CFRP composites. A fatigue hypothesis, which details the failure mechanism of CFRP composites during fatigue cycling, is presented.

Different types of void are defined based on their shape, size, distribution, quantity and frequency. During fatigue cycling, these voids act as sites of weakness which lead to cracking and debonding before failure in a catastrophic way.

It is concluded that an optimum partial cure time is required to obtain a composite with a minimum void content and good strength properties. Using plots of fibre volume fraction and void content versus laminate thickness, non-destructive determination of the fibre volume fraction and void content is possible by measuring the average thickness of the CFRP composites.

TABLE OF CONTENTS

LIST OF TABLES

LIST OF GRAPHS AND FIGURES

LIST OF PLATES

CHAPTER 1 INTRODUCTION

1.1 Fibre Reinforced Plastic (FRP) Composites

1.2 Pre-impregnated Laminates (Prepregs)

1.3 Imperfections

1.4 Aims

CHAPTER 1 INTRODUCTION

Fibre reinforced plastic (FRP) composites are extensively used in commercial and military aircraft, automobile and space industries. The nature of FRP composites allows the enhancement of the mechanical properties by the process of combination.

1.1 FIBRE REINFORCED PLASTIC (FRP) COMPOSITES

FRP composites typically consist of two phases, one of which comprises layers of fibrous materials. These may be natural, synthetic, organic or inorganic fibres, e.g. carbon, glass and Aramid (Kevlar). The fibres may be employed as short lengths or continuous filaments, depending on their types and applications. They are impregnated and bonded with a polymer matrix to form a rigid solid composite. The other phase comprises of the polymer matrix which can be either thermoplastics, such as PEEK (Polyetherether Ketone) or PES (Polyether Sulphone) or thermosets such as epoxy, vinyl ester or phenolic [70, 76]. These two phases are then presented in forms such as compression moulding compounds, sheet moulding compounds (SMC), dough moulding compounds (DMC), or in forms such as unidirectional filament tape, papers or woven fabrics.

The FRP composites are increasingly used because of their attractive inherent high specific strength (strength/weight ratio), specific stiffness (stiffness/weight ratio), chemical corrosion resistance, dimensional stability, heat and electrical conductivity and superior long term properties such as fatigue resistance. Most of all, they can be tailored to suit the particular applied stress field during service, as well as being moulded into complex shapes [48, 175]. Their ease of fabrication allows saving of manufacturing costs.

However, FRP composites are inherently heterogeneous, orthotropic or completely anisotropic and frequently elastically non-linear [5, 19, 20, 40, 61, 73, 136, 185]. Poor control of manufacturing process or misappropriate use in service can lead to premature failure same as in isotropic materials, such as steel and aluminium, because the performance of any materials depends inherently on the production history and service environment [4]. A greater understanding of the processing-structure-property relationship of the fibres, matrix and interphase constituents will result in improved mechanical properties [99].

1.2 PRE-IMPREGNATED LAMINATES (PREPREGS)

Prepregs are resin pre-impregnated fibre laminate materials for the manufacture of FRP composites. Prepregs have been used since the late 1940's, but they have only achieved wide prominence and recognition since the development of the higher performance reinforcing fibres [119].

Prepregs consist of thin sheets of uni- or multi- directional reinforcing fibres with a resin matrix which has been partially cured. The partial cure process provides some measure of physical integrity at room temperature to facilitate handling [141].

The advantages of prepregs over other processing methods such as wet lay-up, filament winding, resin injection, etc., are the elimination of formulation problems, less variance in the mechanical properties, 'workability' for complex shapes and lower inventory levels since no resins or catalysts need to be stocked [68, 119, 161]. Prepregs also allow the placement of the reinforcement in exactly the right place during the fabrication process, so as to carry the load efficiently during service [86, 119].

There are two major physical forms of prepregs: the unidirectional tapes or non-woven fabrics and the woven fabrics.

For a given fibre volume fraction, a composite containing non-woven fabric is stronger in the fibre direction than is the case for woven fabric. This is because all the fibres in the non-woven fabric are in the load path in the structure. However, non-woven fabric would still lead to higher strength values because of inherent defects in the woven fabric. These defects relate to the cross-over point of the rovings where air may be entrapped, the fibres are more difficult to wet thoroughly and there is some fibre misalignment [39, 40, 119].

However, the advantages of woven fabric composites over the non-woven fabrics composites include the constrained lateral movement of the fibres, dimensional stability, deep-draw shapability and better toughness. The interlaced fibre structure of woven fabrics limits the extent and growth of damage. Therefore, a high notch strength can be produced. The ease of handling and the low fabrication cost of the fabrics have made them attractive for structural applications. More over, these composites create the opportunity for complex shape mouldings including structures with holes [22, 39, 40].

The woven fabrics can be of basically three weave patterns, i.e. the plain weave, the twill weave and the satin weave (see Figure 1). The woven fabric used in this project was of the satin weave type with five shaft .

The plain weave is the simplest and the most stable. It is best suited to the

manufacture of flat FRP composites. However, it provides the lowest strength contribution to composites among all the weave patterns. The twill weave has better strength properties and better drape characteristics than plain weave due to having less yarn interlacing, making it more pliable. The satin weave is the most pliable, drapes and moulds readily with excellent strength properties.

In the manufacturing of prepregs, the primary quality requirements are complete wetting and uniform alignment of fibres, with virtually no gaps between the expanded fibres rovings [103]. Basically, there are four methods of impregnating the fibres. They are the solution dip, the solution spray, the direct hot-melt coat and the film calendering [119]. In this work, the prepregs used are manufactured by the solution dip method.

For woven fabrics, the solution dip method is often preferred. This is because the other processes need to squeeze hot-melt and film into the interstices of the fabrics which can cause distortion of the weave pattern.

1.3 IMPERFECTIONS

All practical materials contain imperfections. Sometimes these imperfections do not matter very much or their significance may be simply cosmetic; whereas, in other cases, they give rise to noticeable changes in mechanical and other properties and occasionally they can lead to functional failure [138].

Materials constituents and manufacturing anomalies are the two main causes of imperfections in FRP composites. Imperfections in the materials may originate from three major sources. They are the reinforcing fibres, the resin and the fibre-resin interface [86, 137, 138, 152]. In manufacturing anomalies, imperfections can arise from surface imperfections, small scratches, misalignment during the stacking of each individual prepreg, the presence of flaws and dust or dirt [126, 131, 135, 150]. The most common of all the microstructural defects which occur during manufacturing are the inclusion of air pockets during lay-up, insufficient removal of entrapped air and the production of volatiles during the curing process [17, 49, 80, 87, 90]. These imperfections lead to the formation of porosity and voids.

In spite of the efforts of the manufacturers to reduce the porosity and voids, it is difficult to prevent their occurrence totally within the fabricated laminate [141]. Unfortunately, it is normally assumed that these defects are eliminated through careful adherence to the manufacturers recommended curing schedule; thus the void contents are seldom reported [69].

The presence of porosity and voids affect some composite strength properties. The interlaminar shear strength, compressive strength and fatigue strength are most significantly decreased. However, some properties such as impact strength might be improved.

For the applications of high performance FRP composites, these defects must be minimised. Many methods have been developed to assess and measure void contents. Those commonly used are ultrasonic scanning and radiography. They allow very rapid assessment of a large composite by non-destructive methods.

1.4 AIMS

The main aim of the project was to determine the influence of voids on the static and dynamic compressive strengths of a commercially prepared carbon fibre woven fabric prepreg.

Various subsidiary objectives had to be met before achieving this goal. These included the determination of the influence of various manufacturing variables on the quality of the laminate produced and the most likely cause of voids. A method of detecting the distribution and the content of voids was essential.

The absence of an internationally recognised method for either static or dynamic compressive testing of FRP composites made it necessary to undertake an investigation into the effect of various compressive testing methods. The influence of void content on static compressive strength and modulus had to be determined before any dynamic testing.

The influence of voids on dynamic compressive strength was investigated for the different types and distribution of voids. The major aim in this section was to determine the influence of the type and distribution of voids on the fatigue failures. It was then followed by the examination of the relationship between the fatigue life and the void content using a fractographic method.

CHAPTER 2 LITERATURE SURVEY

CHAPTER 2 LITERATURE SURVEY

2.1 INTRODUCTION

The most important sources of voids in FRP composites are the materials and fabrication processes. Excess bleedout of resin during processing and variation of moulding parameters are also believed to cause void formation. Most authors believe that voids are normally situated in resin rich areas; others say that voids can only occur in the inter-fibre regions. This is discussed in section 2.2.

Different terms for voids and their classification according to the size, shape and distribution have also been discussed.

In section 2.3, many authors have discussed the presence of voids in FRP composites and the effect of voids on the reduction in matrix dominated mechanical properties. Some authors suggested that it is sufficient to keep the void content below a certain limit. Many reported that voids act as sites for crack initiation and stress concentrators during compressive fatigue testing. The presence or absence of particular failure modes during fatigue depend on the strength of the fibres and resin in the FRP composites and the voids present.

In the manufacturing of laminates, many authors believe that the curing pressure and temperature have great influence on the quality. Others state that the time at which the pressure is applied is the controlling factor in determining the quality of a laminate. This optimum time interval is sometimes called a 'dwell time', sometimes a 'partial cure time' or a 'pressurisation time'. The influence on void content of using solvents, excess bleed cloth, postcuring and breathing (or 'bumping of the press') during curing are discussed in section 2.4.

In section 2.5, the determination of the density, fibre volume fraction and the void content of FRP composites is discussed. The accuracy of void content measurement is highly questionable as reported by many authors. Some authors reported a negative void content which arises solely from experimental errors. Others reported that variation in each of the factors used in the calculation of void contents resulted in negative values.

In static tests, many authors agree that compressive strength data are more difficult to generate than other mechanical properties data. At present, there are no generally accepted test standards. A variety of techniques are available and their advantages and disadvantages are discussed.

In section 2.7, observations of many authors who reported that FRP

composites exhibit lower fatigue strength under compression loading and flatter S/N curves are discussed. In fatigue tests, there is debate about the use of waisted and parallel-sided specimens, length of the specimen and the loading frequency.

The use of anti-buckling guides with the specimen edges completely covered or uncovered led to some discussion between authors. It has been reported that a guide which covers the specimen edges completely has the effect of delaying the spread of initial damage.

In sections 2.8 and 2.9, failure in static and dynamic compression tests is discussed. Many authors support the view that failure in compression is by fibre microbuckling and kink-band formation. The resulting fracture surfaces consist of a plane oriented at approximately 45º to the direction of compression or a combined shear mode showing V-notched type failure.

Fatigue damage in FRP composites is more complicated than in those metal materials due to multiple failure modes reported by many authors. These failure modes are affected by many factors which are described by different authors.

Most authors agree that cracks initiate in local imperfections, stress concentrators and voids. Many authors reported that microcracks develop mainly in the matrix before the fibre microbuckling. Others reported that a fibre break might initiate a crack in the adjacent matrix. Generally, most authors agreed that visible cracks on the specimen do not lead to immediate failure.

There were reports of crack propagation in FRP composites and debonding of fibres from the matrix leading to delamination of the FRP composites. Many authors stated that delamination is the dominant failure mode in FRP composites subjected to fatigue.

The possibility of a temperature increase during fatigue loading, causing the failure of the FRP composites through softening of the matrix leading to fibre microbuckling, is discussed. Some authors reported a temperature increases at the end of the specimen life time.

Much work has shown that stiffness reduction is the best indication of property change in the FRP composites after fatigue loading. There were reports of audible cracking associated with this stiffness reduction.

2.2 VOID CONTENT

Stringer [165] based his definition of voids on the assumption that voids are present in the FRP composites in lieu of matrix resin rather than in addition to the matrix. Thompson et al [176] referred to voids as spaces within the FRP composites. Other authors [17, 35, 49, 80, 87, 98, 103, 141, 165, 176] defined conventional voids as inherent features in FRP composites that may be caused by a number of effects.

2.2.1 Sources of Voids

Both the materials and fabrication processes are contributory sources of voids. The materials are the resin and fibre rovings and the processes are pre-impregnation of fibre rovings, laminate lay-up and the curing of the resultant parts [24, 105].

Variables in the manufacturing of the resin such as its volatiles content, the reagents used and their proportions as well as the shelf life can lead to voidage in the components [46, 88, 143].

In the manufacture of resin, there is a possibility of air being either stirred-in or entrapped. Stringer [165] reported that a large number of small voids may be due to air bubbles incorporated into the resin during mixing and low vapour point constituents not being completely drawn off under vacuum during consolidation. Neither degassing the resin in the pot prior to lay-up nor reducing the vacuum level to half reduced the voids significantly.

The volatiles in the resin system are used to aid the resin handling by reducing the viscosity or by keeping the curing agent in the resin [87]. These volatiles have to be removed from the resin system during the cure cycle. In addition, the polycondensation process actually evolves volatiles by chemical reaction during cure [90]. Inadequate volatiles removal will cause extensive voids in the laminate [49, 69, 87, 103, 141, 165].

Variables in the fibre reinfocement such as entrapped air in fibre rovings, misalignment of fibres, fibre cross-over points in woven fabrics and surface imperfections can lead to void formation [88, 126, 131, 150]. These also lead to poor wetting of the fibres during pre-impregnation of the resin which affects the porosity and mechanical properties [16, 80]. Judd and Wright [90] supported this idea by stating that the viscous resin may penetrate only with difficulty in tightly packed fibre rovings. Poor wetability of the fibres will aggravate the situation and all the air will not be displaced. However, Purslow and Childs [141] stated that this

source of voids is a consequence of a mismatch between the volume of the space and the final resin content. Woven fabrics with fibre cross-over points were the most difficult areas to wet with resin, and often voids were left which initiate debonding [46].

Entrapment of air between individual fibres during lay-up is the third main source of voids [17, 35, 141, 176]. Bascom and Romans [17] called this type of void a microvoid, to distinguish it from the usually less numerous but large air pockets that envelope many fibres.

Besides these three main sources of void formation, Kardos et al [93] discussed nucleation processes as another source of voids. They reported that nucleation can occur either homogeneously within or heterogeneously at a fibre-resin or resin-particle (inclusion) interface. They said that most likely heterogeneous nucleation plays the governing role in nucleation of voids.

Stringer [165] discussed the excess bleedout of resin during curing as another source of voids. He reported that large voids, present in the resin rich areas between the rovings, are caused by overbleeding of the resin due to the resin viscosity being too low at the time of consolidation. This overbleeding of resin is probably facilitated by easy flow paths between the rovings in the woven fabric. This is supported by others [49] who say that excessive bleedout produces laminates with high void contents, poor mechanical properties and poor visual appearance.

Lee and McGarry [103] discovered that trapped air due to excessive breathing or 'bumping of the press' during processing caused high numbers of interstitial voids. Breathing is the process where pressure may be momentarily released and reapplied after a period of time under moulding pressure. This permits the resin to flow sufficiently under pressure and the trapped air and volatiles to escape during the release of pressure.

2.2.2 Occurrence of Voids

In the literature, various causes of voids have been reported. Purslow [139] stated that apart from voids in hollow fibres, voids can only occur in the resin. They tend to be found in resin rich areas which occur between rovings and individual plies. Other authors [73, 135, 141, 176] supported this view.

However, Giltrow [60] reported that voids can only occur in the inter-fibre regions. He stated that it is impossible to decide how voids are formed on the basis of their composition, whether they contain only volatiles endued from the resin or volatiles together with air. He reported that the former type could be either 'Princen

holes' (holes due to excess local vapour pressure of some volatile constituent of the resin), or their formation could have proceeded via a combination of both mechanisms. He further specified that the voids containing air might have resulted from either air previously trapped within the prepreg, air trapped during the packing of the mould, a combination of these with the 'Princen holes', or holes formed by volatiles.

2.2.3 Definition of Void Types

The types of void which occur in FRP composites have been classified in many different ways over the years, e.g. the terms; thread-, fabric-, general-, interstitial-, planar-, micro-, needle-, pocket- and interconnected voids have all been used [17, 90, 103, 176].

Bascom and Romans [17] classified interstitial voids as those within fibre rich areas, planar voids as those between layers of filaments and general voids as large voids crossing many rovings. Rotem et al [145] discussed the formation of the cylindrical voids of primary shape, where the length is much larger than the width or thickness. Lee and McGarry [103] reported that the interconnected voids appear primarily between the layers, the small interstitial voids are distributed throughout the laminate and the pocket voids, characterised by clearly defined holes, mostly appear between the fibre rovings. They stated that interstitial voids are caused by inadequate resin flow between fibres as the voids are concentrated in the fibre rich areas. They also discussed the size of pocket voids which decreased as the volatile content of the prepreg increased. Their results suggested that void size influences the mechanical properties of a laminate.

To simplify the types of void, Judd and Wright [90] classified voids into low void content ($\leq$ 1.5 %) with spherical shape and of diameter 5-20 μm and high void content, where the voids were cylindrical with the larger dimension being oriented along the fibre axis. Purslow [139] had a more detailed classification of voids with void contents of $\leq$ 0.5%, ~1% and $\geq$ 1%. He stated that it is more meaningful to quote void contents as lying within a given band than to state a specific average figure. He also argued that simple relationships between void content and mechanical properties have significance only in cases of uniformly distributed voids.

The term porosity is also used in connection with voids in FRP composites as the porosity is a measure of the volume of all pores present in a material. Brassell [24] categorised porosity as either open-cell, closed-cell, or both combined giving total porosity. He reported that the open pores are generally interconnected by

channels or capillaries, making the material permeable to liquids or gases. The closed pores may be enclosed within individual particles or form isolated spaces within the matrix; therefore the material is impermeable to liquid or gas despite its high porosity.

2.3 THE INFLUENCE OF VOIDS ON MECHANICAL PROPERTIES

Different mechanical properties are affected differently by changes in void content [135]. It is useful to review previous work on the relationship between the mechanical properties of composites and void content. The wide variation in reported physical-mechanical-property data could be due to differences in void content according to many authors [9, 48, 69, 73, 137, 169]. The nature of FRP composites is such that there is a large degree of variation in the mechanical properties of a particular moulding or component. For this reason, when using the results of mechanical tests for design purposes, a safety factor must be introduced. For example, if the coefficient of variation is 5%, then the value used in design calculations would be 85% of the mean test value [152].

The presence of voids in FRP composites results in a significant reduction in matrix-dominated properties such as interlaminar shear strength, longitudinal and transverse tensile strength and modulus, longitudinal and transverse flexural strength and modulus, compressive strength and modulus, fatigue resistance and high temperature resistance. However water absorption and impact strength may increase [4, 55, 60, 69, 87, 90, 165, 176, 185].

Harris [73] reported that voids might locally reduce the strength of the material below the required component design stress. They might also provide paths by which air can reach the carbon fibres, resulting in either oxidation of the fibres or degradation of the fibre-matrix interface [101]. It is generally accepted that the presence of voids will also affect the diffusion of moisture into the FRP composites. One possible effect of voids is suppression of the effective diffusibility due to blockage of moisture diffusion paths. The entrapment of moisture within the void can also result in non-Fickian diffusion anomalies [23, 30, 63].

The mechanical strength of a FRP composite is very dependent on the size, quantity and distribution of the voids it contains [28, 87]. Even a small quantity of voids can cause a marked reduction in the mechanical properties [176].

2.3.1 Modulus

In FRP composites, the modulus of the composite is linearly related to fibre volume fraction using the rule of mixtures:

$$E_c = E_f * \Phi_f + (1 - \Phi_f) E_m$$

equation (1)

where

E_c = composite modulus (GPa)

E_f = fibre modulus (GPa)

E_m = matrix modulus (GPa)

Φ_f = fibre volume fraction.

This assumes good bonding at the interface, where the stress applied to the composite transfers fully to the fibres through the resin and the fibres become the primary load carrying components [67].

As the modulus of the epoxy resin is low,

$$E_c \approx f * E_f * \Phi_f$$

equation (2)

where

f = a factor to take into account the adhesion between fibre and matrix.

Kavanagh [94] assumed there to be two material inconsistencies, namly, the volume percentage of voids and the fibre content. He derived a model assuming individual elastic components and the fundamental laws of statics. The void content in the model is assumed to be a property of the matrix system alone. The voids and the matrix system are considered together as an 'effective matrix system' whose modulus is given by:

$$E_m^{(eff)} = E_m (1 - \sqrt{\Phi_p}) (1 - \sqrt{\Phi_p} + \Phi_p)$$

equation (3)

where

$E_m^{(eff)}$ = effective Young's modulus (GPa)

E_m = Young's modulus (GPa)

Φ_p = void volume fraction .

2.3.2 Interlaminar Shear Strength (ILSS)

Yoshida et al [185] used statistical procedures to develop the following relationship between interlaminar shear strength and voids:

$$S_e = \sqrt{\frac{1}{n-2}\sum_{i=1}^{n}[S_i - (a + b * V_i)]^2}$$

equation (4)

where

S_e = standard error of strength values

n = number of specimens

V_i = individual measured value of voids (%)

S_i = individual measured value of ILSS (MPa)

a, b = constant.

They reported that the mechanical reliability of a composite decreases rapidly with increases in void content and that the rate of reduction depends considerably on the applied shear stress, or the standard error of strength values. They further analysed that the ILSS of carbon fibre reinforced plastic (CFRP) composites decreases almost linearly with increases in void content.

Giltrow [60] and Yamamoto [183] reported that a reduction in ILSS is in fact observed in FRP composites at about 60% fibre concentration and is usually attributed to increasing fibre-fibre contacts and the formation of porosity in an unspecified way. Other authors [4, 59, 90] supported their view by saying that ILSS reduces by about 7% for a 1% void content increase and that the reduction in ILSS with increasing void content is approximately linear up to at least 4 % void content.

2.3.3 Compressive Strength

Not much work has been carried out on the effect of voids on compressive strength properties. Prakash [135] found that increases in void content cause a steady reduction in compressive strength. Foye [53] derived an expression for the shear modulus (G) in terms of the maximum shear modulus (G_{max}), when the void content is zero, i.e.$\Phi_p = 0$. He concluded that:

$$G = G_{max} \left[\frac{(R-1)^2}{(R+1)} \right]$$

equation (5)

where

$$R = \frac{\Phi_p}{(1-\Phi_f)}$$

equation (6)

and

G = composite shear modulus (GPa)
G_{max} = effective shear modulus (GPa)
Φ_p = void volume fraction
Φ_f = fibre volume fraction.

He reported that the predicted reduction in shear modulus could be related to compressive strength changes. Joiner [87] supported this view and showed that shear strength measurements are very sensitive to the distribution of voids in FRP composites and less sensitive to the total amount of voids present. That is, a large number of small voids have a greater effect than a small number of large voids.

Garrett [55] stated that little sensitivity to severe porosity was indicated under tensile loading. Under compressive loading, strength reduction ranged between 7% and 13.3% for specimens with moderate porosity and 10% and 30.8% for specimens with severe porosity. Tang et al [170] reported that both the compressive strength and modulus increase with decreases in void content until the void content becomes about 3% to 4%. Below this value, neither the strength nor the modulus changes significantly which indicates that it is not imperative to eliminate all the voids from a laminate. For small voids, there appears to be a critical void content, below which there is little effect, but above which properties begin to deteriorate. Similar conclusions have been drawn by other authors [48, 120].

2.3.4 Compressive Fatigue Strength

High void content means lower fatigue resistance as stated in ASTM D2734 [9]. Many authors [14, 19, 46, 62, 92, 124, 128, 146, 177] reported that fatigue breakdown of material tends to be initiated from manufacturing defects such as voids, porosity, dents, pitting and flaws. These inherent defects lead to the large variation in results reported by many authors [45, 56, 132, 133, 135, 154, 163].

Harris [73] stated that voids act as sites for the initiation of fatigue damage and may facilitate the growth of a fatigue crack during cyclic loading. Other authors [111, 181] referred to the voids as microscopic stress concentrators which introduce cyclic fatigue damage of various forms such as fibre end cracking, fibre-matrix interface debonding and matrix cracking.

However, Prakash [136] reported that the void defects act as heat accumulation zones and as the promoters of crack initiation. Johnson et al [85] found that fatigue failure appears to originate as a local buckling of fibres in compression. As the compressive strength of the FRP composites depends on the shear modulus of the matrix, the most likely causes of fatigue failure are the growth of cracks and/or voids until the effective shear modulus of the structure has lowered significantly or local hot spots reduce the shear modulus of the matrix.

Bader and Boniface [13] showed evidence that cracking in 90° plies is often associated with defects or abnormalities in the laminate. If the specimen was loaded beyond the elastic limit of the FRP composites during fatigue testing, damage was caused in the matrix where cracks have propagated from areas of voids.

Mohlin [118] stated that the result of cyclic loading was a blunting effect on the many microcracks and voids which are spread randomly throughout the specimen and which also serve to arrest crack propagation. This crack propagation occurs at a later stage of the cyclic loading, causing strength degradation. Kim and Ebert [96] suggested that the direction of the shear cracks results from triaxial stress field development inside the material and also depends on the void density in a particular direction.

2.4 MANUFACTURING OF VOIDS

The technique of producing components of satisfactory quality remains more of an art than a science [4, 141, 165]. Aerospace components of consistently high quality are currently produced using empirically determined processing parameters and maintaining strict control over these parameters during production. The objective of processing is to produce a good laminate, i.e. one which is fully consolidated, has uniform thickness, has the correct resin content, does not have distorted fibres due to non-uniform resin flow, has correctly cured resin, does not have degraded resin due to excess temperature and is not porous [121].

2.4.1 Solvent Addition

In order to obtain specimens containing a wide range of void content, Yoshida et al [185] used a dilute solution of foaming agent azodi-isobutyronitrile (AZDN) $[(CH_3)_2C(CN)N.N(CN)C(CH_3)_2]$ in acetone. It was sprayed between the individual plies prior to fabricating. They reported that AZDN does not affect the hardening process of the resin and is not affected by fabrication pressure, additives, etc. They reported void contents up to 10%, but they did not mention the amount of AZDN used.

2.4.2 Effect of Curing Temperature

During the curing process, temperature and pressure are applied simultaneously. Temperature is applied to facilitate and control the chemical reaction of resin polymerisation and cross-linking. The pressure is applied to squeeze out excess resin, to consolidate the plies and to minimise void content [106, 107, 141, 170]. In some manufacturers data, it is stated that optimum properties will be achieved in the finished component by curing for a specified time at a particular temperature and pressure [29, 30, 59, 144]. One interesting point stated by Akay [4] was that a longer hold time at the cure temperature and pressure, resulted in maximum consolidation with no evidence of voids.

Yokota [184] studied the effects of several cure cycle parameters on the void content in prepregs and found that the temperature at which the pressure is applied is the most significant. High void contents were obtained whenever this temperature was below that required for complete volatile degassing or above that at which gelation occurs. Harper et al [69] stated that since this temperature range may be significantly affected by heat up rate and by normal batch-to-batch variation in prepreg properties, adherence to the manufacturer's suggested cure cycle may not always result in void free laminates. This is supported by other authors [116, 117] who reported that lower pressing temperatures resulted in greater ultimate strength.

2.4.3 Effect of Curing Pressure

Tang et al [170] analysed the effect of different curing pressures by examining photomicrographs of compacted laminates after cure. They also stated that the cure pressure had a significant effect on mechanical properties. Compressive strength and ILSS were affected by the cure pressure since they are most sensitive to void content.

Purslow and Childs [141] stated that there is an 'inherent packing fraction' for a particular material. When the prepreg is heated at the commencement of the cure cycle, the spatial constraint placed upon the fibres by the resin will be reduced. Under zero applied pressure, surface tension will act to draw the fibres together. They further stated that application of pressure will cause some further compaction and the magnitude of the pressure affects not only the resin properties but also the fibre and void contents of the final laminate. They reported in another paper [140] that quite a small increase in pressure can cause increases in fibre volume fraction of as much as 10%; but the fibre volume fraction is almost constant above a critical pressure of 150 kPa for their laminates. They further stated that a greater increase in pressure serves only to distort the fibre rovings, or break those fibres whose misalignment is restricting compaction.

Lee and McGarry [103] supported these views by saying that the increase in pressure resulted in an increase in the rate of polymerisation. Morrison and Bader [121] stated that the minimum spacing between each ply is dependent on pressure, and different fibre volume fraction laminates may be produced by varying the pressure.

2.4.4 Dwell Time and Partial Cure Time

When a large thermal mass is involved, it is common to reach the final curing temperature in two stages. An intermediate temperature is held constant for a period of time so that the laminate can reach a uniform temperature before pressurisation. This period is known as a dwell [141]. It allows the resin to remain close to its minimum viscosity for a longer period; thus allowing more resin flow and consolidation than if the temperature were raised directly to the maximum [121]. Lee and McGarry [103] stated that this dwell time should coincide with the gel time of the thermosetting resin for effective removal of volatiles.

However, Thompson et al [176] stated that the dwell time is the time that is allowed to elapse between placing the mould into a heated press and applying the pressure to close the mould. Prakash and Purslow et al [135, 141] quoted this as the partial cure time while Stringer [165] referred to it as pressurisation time.

Thompson et al [176] reported that void free specimens could be obtained for their material using a 'dwelling time' of about 10.5 minutes. They referred to laminates produced using this dwell time as 'correctly dwelled'. Laminates made with dwell times shorter or longer than the ideal were referred to as 'under dwelled' or 'over dwelled' respectively. They further pointed out that the formation of a void free microstructure depends critically on the resin viscosity at the time of closing the

mould. If pressure is applied either too early or too late, as in under and over dwelled laminates, entrapped air is less likely to escape from the mould. They stated that early pressing is less damaging since the resin has still to pass through its least viscous state; hence a large amount of air can be removed. The application of pressure when the resin is beginning to gel means that very little air can escape from the mould. Furthermore, the press force is likely to cause gross cracking in over dwelled laminates.

Similar observations were reported by Stringer [165]. He stated that gelation is determined by the moment at which the pressure is applied. Therefore, the pressurisation time becomes the controlling factor in determining the quality of a laminate. This optimum time interval, before which pressure should not be applied, is quite small (e.g. 10 minutes). If it is delayed, too little resin flow causes voids. If it is too early, the heat up rate causes the viscosity to fall and too much resin is lost before gelation.

Purslow and Childs [141] strongly supported Stringer saying that increasing the degree of partial cure, prior to pressurisation in the autoclave, may considerably improve the quality of a laminate by raising the minimum viscosity of the resin. This optimum time interval (partial cure time) allows the heat to remove the solvents and to give the sheets some physical integrity. This heat treatment causes the resin constituents to partially react and thereby raises the viscosity of the matrix.

2.4.5 Use of Bleed Cloth

To help with the removal of volatiles and excess resin, several layers of permeable bleed cloth are usually placed above and below the laminate during fabrication. Purslow and Childs [141] considered that the bleed cloth could actively extract resin from the laminate; thus if used in excess could lead to high void content.

The amount of volatiles and excess resin removed can be controlled by the degree of permeability of the bleed cloth layers, suggested Lee and McGarry [103]. However, they stated that too thick a bleed cloth has an adverse effect on the structure of the FRP composite. Resin starvation was very obvious and the laminate readily delaminated when flexed by hand.

Tang et al [170] showed experimentally that when the bleed cloth is too thin, it will saturate before all the resin is removed from the laminate. They said that the resin content of the laminate cannot be controlled by adjusting the bleed cloth thickness, as supported by Stringer [165]. However, Loos and Freeman [106] stated that the required thickness of the bleed cloth depends on the ply thickness of

the composite and the amount of resin to be bled out. They suggested a prepreg to bleed cloth ratio of about 3 to 1.

2.4.6 Other Parameters

Since a low volatile content affects the ability of the resin to flow, Lee and McGarry [103] suggested that pressure may be released and reapplied momentarily after a period of time under moulding pressure. Breathing or 'bumping of the press' permits the resin to flow sufficiently under the pressure and trapped volatiles to escape during the release of pressure. However, the time of breathing is difficult to optimise because the resin viscosity increases with time due to the advance of polymerisation.

They also suggested that postcuring can reduce the void content and change the void size. Postcure is a process of heating a cured laminate from room temperature to an elevated temperature usually in an inert atmosphere. However, they reported that although the number and size of the interconnected voids is drastically reduced, translaminar cracking becomes extensive. It is claimed that the mechanical properties of a FRP composite can be improved during postcure through the reduction of structural defects due to resin flow and/or through the further cross-linking of the resin matrix at the molecular level. Clark et al [36] reported that omission of the postcuring step reduces the fatigue life by a factor of about two while it has no significant effect on static compressive strength.

It is interesting to note that the thickness of the laminate varied as a result of varying the cure cycle in order to achieve a desired void content as discussed by Harper et al [69]. Hahn and Kim [65] supported this opinion and stated that the cured thickness may vary from laminate to laminate depending on how much resin is squeezed out during cure. The strength increases with decreasing thickness and similarly, the smaller thickness results in the higher modulus. This is true of properly consolidated laminates with no air trapped between the individual plies during lay-up, which results in thinner and lower void vontent laminates. Purslow and Childs [141] stated that the cure cycle does not give a specific thickness, but that thickness is an inherent property which is affected by the presence of imperfections in the prepreg laminate.

2.5 MEASUREMENT OF VOID CONTENT

In spite of the efforts of manufacturers, it is difficult totally to prevent the occurrence of voids in FRP composites [69, 185]; thus it is important to determine a safe working limit for voids for quality assurance purposes. A reliable measurement of the fibre volume, resin content and void content is fundamental to the prediction of the mechanical properties of FRP composites [84].

2.5.1 Density Measurement

An accurate determination of void content requires accurate values of the fibre and resin volumes and densities [90]. The density of the FRP composites can be determined using the ASTM D792 method [7].

Cilley et al [35] followed the ASTM standard using specimens approximately one gram in size and weighed to five significant figures. Five specimens were obtained from each laminate type so as to sample the variation both along the fibre direction and in the transverse direction. They used either water or octane as the immersion fluid. They concluded that by weighing in air before and after immersion in the fluid, there was no absorption of either immersion fluid by the specimens.

The density of the carbon fibre can be determined by using a density bottle with bromobenzene as the liquid [51, 81]. The maximum error quoted by Ewins and Childs [51] by this method was ± 0.005 g/cm^3. The density of the resin can also be determined using a density bottle with water as the liquid, taking care that the specimen used had undergone precisely the same cure and postcure schedules as the resin in the composite. The maximum error quoted using this technique was ± 0.0025 g/cm^3.

2.5.2 Fibre Volume Fraction Measurement

To determine the fibre volume fraction, the weights of fibre and resin need to be determined and this can be done by several methods. The most common of all is the acid digestion technique using concentrated acid to dissolve the epoxy resin [35, 77, 105]. The same specimens used previously for immersion density tests can be subjected to acid digestion as suggested by Courtaulds [174].

Haynes et al [77] stated that this is a rapid, accurate method for determining the exact amount of the fibre present in the specimen. Cilley et al [35] supported this method as they revealed no evidence of damage to the fibre by the acid after observation of unused fibres and those recovered from acid digestion tests.

Other methods for determining fibre volume fraction are by resin burnout and thermogravimetric analysis (TGA) [35, 105]. The former required heating to 425°C for four hours and the latter required heating at a constant rate whilst monitoring the weight change.

2.5.3 Void Content Determination

As the fibre and resin densities are known (values supplied by the manufacturer), then if the composite density is measured, the void content can be determined from the weight of fibre and resin. The weights of fibre and resin can be determined by the matrix incineration technique based on ASTM D2734 [9] method for calculation.

Similar methods of calculation have been performed by other authors [80, 90, 131, 185] and the equation has been presented in many different forms.

2.5.4 Accuracy

Lenoe [105] stated that a variation of 0.1% in the densities of the composite, the fibre and the resin as well as the fibre and resin volume fractions can result in an error in the estimated void content of about 2.5%. This is supported by other authors [90, 131]. He pointed out that accurate values for the resin density and especially the fibre density are difficult to obtain. The uncertainties introduced by these values decrease the validity of the calculated value, especially at low void content. For FRP composites with low void contents, the value may be lowered from a true 0.2% to a calculated -0.1% [9].

Judd and Wright [90] reported that the overall accuracy of the calculated void content is probably no more than ±0.5%; thus apparent negative values for void content are often obtained. They further discussed that the technique gives only an overall void content based on small samples and no information on the size, shape and distribution of the voids, a fact agreed by Lenoe [105] and Ewins and Childs [51]. Ewins and Childs stated that the apparent negative void contents arose solely from experiment errors and should not be greater than the calculated variation in void volume fraction. They claimed that for a typical FRP composite of $\Phi f = 0.6$, error in the assumed fibre density of -0.03 g/cm^3 which is within usual batch-to-batch variations in density, could lead to errors in fibre and void volume fractions of +0.01 and -0.01 respectively. This error in fibre volume fraction of 0.01 is only rarely significant, whilst an error in void content of 0.01 is large compared with the general level of voids.

2.5.5 Other Methods of Measurements

One method used to determine the void size, shape, and distribution is optical microscopy [24, 35, 49, 84, 90, 131]. This method can be divided into optical comparison techniques and optical counting techniques [139]. The latter method is similar to the quantitative microscopy referred to by Cilley et al [35].

Judd and Wright [90] considered that micrographic analysis gave slightly more accurate measurement of void content than the density determination method. Since the small sections examined may not be representative of the whole, they reported that the overall accuracy may be little better than ±0.5%.

Water absorption is another method of determining void content [35, 90, 131]. It requires the determination of the equilibrium water uptake of pure resin, the composite derived from it and also the resin content of the FRP composite. This method is further complicated by resin swelling, hydrolysis and leaching. The technique is less accurate than the optical microscopic and density determination methods as reported by Judd and Wright [90].

Ultrasonic techniques are at present the most generally useful non-destructive inspection techniques for FRP composites. Many authors have reported the use of ultrasonic attenuation techniques to measure void contents in CFRP composites [66, 89, 112, 164, 168]. It is used for qualitative measurement of void content, for determining deviation in thickness and fibre content and for detecting fibre misorientations, delaminations and bond failures. The advantage of this technique is that it allows the assessment of the whole laminate rather than a small portion. Judd and Wright [90] again considered that the overall accuracy cannot be greater than ±0.5%.

Other methods including radiography, X-ray, holography, thermal imaging and acoustic emission have also been carried out by many researchers with no greater accuracy.

2.6 STATIC COMPRESSIVE STRENGTH

Compressive data are more difficult to generate than tensile data for CFRP composites. Hofer et al [79] suggested that the compressive strength of FRP composites depends on the fibre stiffness and strength, matrix stiffness and strength and interface shear strength. Johnson et al [85] supported by others authors [99, 127] stated that the compressive strength of a FRP composite is affected by the shear modulus of the matrix. In another report, Tang and Springer [171] stated that compressive strength increases with an increase in the degree of cure while the tensile and shear strength decrease.

In compression testing of laminates, specimen size and geometry should be selected carefully. However, not many reports have discussed this area. In one report, Awa [12] stated that the specimen must be long enough to allow the redistribution of compressive load through the cross-sectional area and sufficiently wide that the damage propagation would not be impeded by the edge supports. Lee [104] reported that a variation of 2.5% in the laminate thickness (0.05 mm for a 2 mm laminate) will cause the apparent strength to drop to 87% of the ultimate value. Thus a reduction of this effect requires well controlled bondline thickness for the end tabs.

Harris [70] reported that the compressive strength was rarely equal to and even more rarely, in excess of the tensile strength. However, he stated that it is seldom possible to be certain that the true compressive strength is being determined. Woolstencroft et al [182] discussed the problem of the FRP composites having a high ratio of compressive strength in the direction of the fibres to shear strength in the planes parallel to the fibres; thus causing problems with shear load input.

2.6.1 Difficulties in Compressive Testing

Hofer et al [79] referred to the paucity of compressive strength data being due to three reasons. They are the high performance of FRP composites under compressive load, testing difficulties involving the specimen preparation such as end splitting, buckling of specimens, load alignment problems and the fact that more expensive methods are required to fabricate compression specimens.

Lee [104] suggested that three particular points must be considered in the design of a compression testing system. They are the brooming at the end of the specimen, axial misalignment and specimen buckling.

Brooming is overcome most easily by designing a system in which the ends of the specimen are gripped. If free-standing specimens between two flat platens are

used, then the ends of the test specimen must be perfectly flat and square. Compression wedge grips and end tabs bonded over the end of the specimen are an alternative design at the present.

Axial misalignment is another problem which can lead to an underestimate of the compressive properties as reported by Curtis and Morton [42]. Any misalignment has the tendency to induce buckling in the test specimen which introduces a bending moment causing strain divergence on either face. This type of situation must be avoided if the failure is to be of a purely compressive nature. It is therefore crucial that axial alignment is obtained by suitable system design. Often packing shims are inserted into the testing machine to ensure that the platens are parallel.

Specimen buckling can be overcome by ensuring that the column length is less than the critical Euler buckling length [178].

2.6.2 Test Methods

Highsmith et al [78] were of the opinion that much of the compression data that exists must be viewed in the light of the methods of test and special fixtures designed to restrict or prevent buckling. Thus the compression data may only represent the behaviour of specimens subjected to particular test procedures and may not be representative of the compression response of the material.

At present, there are no generally accepted International standards for obtaining the ultimate compressive strength of a FRP composite laminate. Many authors [40, 57, 91, 122, 147] simply quoted the use of anti-buckling guides that provided effective restraint against gross buckling. A substantial survey of the literature revealed a variety of techniques available for axial compression measurements [79, 158, 182].

The Celanese test method [2, 11, 38, 79, 182] uses split conical collet grips that fit into matching sleeves, which in turn fit into a cylindrical shell. However, the design is such that specimen slippage, buckling and wall friction can be problems as reported by Hofer et al [79]. Mechanically, the Celanese fixture grips may not seat properly on a cone-to-cone surface contact arrangement. Instead, contact may occur along a pair of lines on opposite sides at each end of the specimen. This causes the seat grips at each end of the specimen to shift laterally relative to each other, resulting in contact with the cylindrical shell. This promotes conditions of high frictional stresses which affect the result obtained.

Lee [104] reported that because of the very short gauge length of the Celanese specimen, a certain amount of Poisson expansion was restricted and hence a lower

energy mode of failure (eg splitting) was being suppressed. Supported by Woolstencroft et al [182], they rejected the Celanese test method as the results obtained showed a combination of low mean failure stress and high coefficient of variation. However, Schulte [150] stated that compressive testing using a Celanese jig showed that the rule of mixtures gave a good prediction of compressive modulus, provided moduli were taken at the appropriate strain level.

Other compression testing fixtures such as the sandwich beam, the TEI (Texaco Experiment Inc) compression fixture, the sandwich stabilised fixture which incorporated some of the best features of both the sandwich beam and the TEI fixture, the Narmco test 303 jig, the Federal test fixture, the IITRI (Illinois Institute of Technology Research Institute) compression fixture, ASTM D695 and D3410 test fixtures and modified Celanese jig are each reported in detail by some authors with their advantages and disadvantages discussed [2, 79, 155, 182].

Among all the authors, Adsit [2] analysed the ASTM D695 test fixture and suggested that it should be a recommended method for FRP composites. For materials other than FRP composites, he reported that the test method may be acceptable. He recommended that the ASTM D3410 test fixture be modified to include both sets of Celanese and IITRI fixtures. He stated that the conical fixture can be misused by not controlling the total thickness of the specimen. This can lead to loading of the cones along one line which results in binding of the outer shell, which will give incorrect results. He also recommended that the ASTM D3410 be modified to include the sandwich beam as the strength measured by this method appeared to be the same as measured by ASTM D3410 test fixture.

2.6.3 Scatter of Results

There is considerable scatter in the compressive properties reported by many authors [83, 104, 139, 158]. This scatter in compressive data can be caused by a number of factors including non-uniformity of stress application and poor specimen design resulting in different failure modes. The various modes that are suspected of inducing compressive failure include fibre symmetric and non-symmetric microbuckling, fibre compressive failure and delamination. Sinclair et al [158] suggested that because compressive testing is sensitive to factors such as Euler buckling, specimen misalignment in the test fixture, fibre misalignment in the specimen, bending or stretching coupling in the laminate and moisture present in the laminate, scatter in the results is further compounded.

2.7 DYNAMIC COMPRESSIVE STRENGTH

When a component is subjected to a fluctuating load, it is possible for failure to occur at a stress or strain level considerably less than that determined in static tests. This phenomenon is known as fatigue [135]. The fatigue failure of engineering components and assemblies has been a central problem in the application of materials to design for over a century. The importance of fatigue behaviour in materials can be realised from the fact that about 80% to 90% of all service failures of equipment are due to fatigue [132].

BS 3518 Parts 1 and 5 [26, 27] deal with methods of fatigue testing of metals and is a source of the definitions and nomenclatures of various terms used in connection with fatigue testing. It states that fatigue testing involves the form of the specimen and the design of the machine being intimately related. Work has been done by many authors [132, 163] to confirm that fatigue testing standards devised for metals are in general, relevant to the testing of fibre composites and to draw attention to some areas where agreement is lacking.

There are various possible loading modes for fatigue testing, such as rotating and plane bending, axial loading torsion, direct stress fatigue or combined stress fatigue. However, compressive fatigue loading of FRP composites still presents practical difficulties.

Matondang et al [113] stated that CFRP composites generally exhibit lower fatigue strengths under compressive stress than when subjected to tensile loading. Many authors [57, 64, 145, 151] supported this saying that fatigue strength of FRP composites decreases when compression becomes a larger part of the load cycle. Bader and Boniface [13] established that multiaxial laminates may fail in fatigue at even lower fractions of their static strengths.

Many fatigue test programmes currently undertaken are conducted under conditions of compressive mean stress [113]. Mandell [111] emphasised that compression fatigue testing of FRP composites introduces buckling and end-brooming problems. The fatigue data may also be sensitive to the freedom to delaminate and buckle, either as a unit, or ply by ply, which varies with specimen geometry and lateral constraint method. Bader and Johnson [14] pointed out that care must be exercised in the interpretation of fatigue data because it is strongly influenced by the test configurations.

2.7.1 Specimen Design

In the design of a fatigue specimen, Curtis et al [41] pointed out that the presence of fibre ends at a surface creates stress concentrations which provide sites for crack initiation. Harris [72] reported that choice of appropriate specimen shape is strongly influenced by the characteristic nature of the FRP composites being tested.

Much early work was carried out on waisted specimens, similar to those used in metals testing but this led to unrepresentative modes of failure in FRP composites. An alternative approach to prevent the familiar shear splitting in FRP composites of low shear resistance was to reduce the sample thickness rather than the width. This has been almost universally superseded by using parallel-sided specimens with end tabs. This eliminates the risk of grip damage (and resultant premature failure) without introducing significant stress concentrations at the ends of the test length and also failures can usually be expected to occur in the test section.

Curtis et al [41] compared the use of parallel-sided specimens and waisted specimens during fatigue testing. They reported that one problem with waisted specimens is the non-uniform stress field in the region of the waist. They further reported that although many of the parallel-sided specimens fractured in a region away from the clamping area, a number, especially those tested at the higher frequency of 5 Hz, failed within or near the end tabs. They considered the parallel-sided specimens to be unsuitable for fatigue tests at higher frequencies and the use of waisted specimens becomes a necessity as the parallel-sided specimens give an increasing number of unacceptable results. However, Sturgeon [166] pointed out that early work at RAE (Royal Aircraft Establishment) had shown that waisted specimens were not completely satisfactory in fatigue testing and other designs should be investigated.

The CRAG (Composites Research Advisory Group) recommendation [38] is that waisting of specimens is not suitable for axial fatigue testing because of the possibility of premature failure due to shear cracks initiated at the shoulders of the waist. However, many authors [47, 75] have carried out fatigue tests on parallel-sided specimens.

Matondang et al [113] argued that specimens with long gauge lengths should be used in fatigue testing to obtain representative and reproducible fatigue data. The ratio of his specimen gauge length to its width was 2.5 which agrees with the CRAG recommendation [38]. However, Camponeschi et al [29] discussed that because of the greater amount of fibre and resin in the long gauge length, there is a

greater chance of there being an imperfection in such a gauge length. Any weakness in the matrix within the gauge length would reduce the overall stiffness measurement.

2.7.2 Anti-Buckling Guides

For fatigue tests involving a compressive stress component, an anti-buckling guide is usually required to prevent buckling. Many authors [40, 91, 122, 145, 151] simply mention the use of anti-buckling guides without further information on their configurations. Lagace and Nolet [102] stated that anti-buckling plates restrict the development of delamination damage caused by ply buckling in compression.

Harris et al [75] followed one of the CRAG recommendations using an anti-buckling guide with specimen edges completely covered. They reported that with careful attention to setting up and packing between sample and jig, it was possible to obtain fatigue failures in the gauge length up to high levels of imposed compressive stress.

Gerharz [57] compared the use of one anti-buckling guide which covered the specimen completely with other which left the specimen edges exposed. He discovered that with unsupported edges, fatigue life to fracture was shortened by at least a factor of 5. During the whole life to fracture, specimens with the edges supported suffered less increase in deformation than specimens with edges not supported by the anti-buckling guide. He stated that the guide that covered the specimen completely apparently had the effect of delaying the growth of fatigue damage initiated at the specimen edges. He further reported that crack opening and local buckling associated with edge delamination is restrained by those anti-buckling plates which provide support by completely covering the specimen surface. Generally the results indicate that the influence of the anti-buckling guides is different which makes meaningful comparison difficult. This idea is supported by Matondang et al [113]. However, they stated that guides which provided specimens with edge support had no influence on the fatigue strength of matrix dominated $[\pm 45^{o}]_{8S}$ laminates. They pointed out that this was one of the errors which has been made in the past in assessing the fatigue strength of a structural member based on fatigue values obtained using this type of guide. They strongly recommended that guides should only be employed if they substantially reproduce actual support conditions found in real CFRP structures. Such guides should prevent general buckling of the structure under compression while still allowing localised buckling to take place.

2.7.3 Loading Frequency

The influence of loading frequency on fatigue behaviour is seen to be very important for FRP composites, resulting in shortened fatigue life at increased frequency [25, 44]. Among the authors, Curtis et al [41] stated that the higher the loading frequency, the larger the surface temperature rise of the specimen. While Dao [44] reported that frequency seems to influence the fracture mode of the FRP composites.

Curtis et al [41] emphasised that the laboratory fatigue strength measurement is independent of many test parameters, but it is affected by loading frequency. They also speculated that low frequency fatigue testing provides a better representation of component performance than higher frequency testing.

2.7.4 Presentation of Results

The results of fatigue can be represented graphically by either the stress/log life (alternating stress range versus the logarithm of the number of cycles to failure), or constant life diagrams (alternating stress range versus mean stress for a fixed number of cycles). The former is widely used by many authors. Sometimes, the 'step-test 'or 'stair-case' technique is also employed to determine fatigue strength at a fixed number of cycles [26, 27, 136].

It must be noted that FRP composites tend to display flatter fatigue S/N behaviour than metals [36]. This has been observed by many authors [21, 75, 99, 111] who reported that high modulus CFRP composites have excellent fatigue behaviour with nearly flat S/N curves and a low strength degradation rate. Harris et al [75] explained this by stating that the working strains in the CFRP composites are rarely so high as to exceed the matrix fatigue limit; thus the S/N curve remains almost flat. Puskar et al [142] reported that weaker materials tended to have less steep S/N curves than expected, with stronger materials more steep. He reported that woven glass fabric material has an initially steep S/N curve resulting from failure rapidly following delamination at the weave cross-over points.

2.7.5 Scatter of Results

Many authors [43, 45, 71, 143, 154, 167] reported that the scatter of fatigue life in CFRP composites is very large, but that of fatigue strength is not so large. Sturgeon [167] reported a wide spread over seven decades of cycles when the maximum fatigue stress was close to the ultimate strength of the material. This scatter of fatigue life can be explained by the Weibull distribution or logarithm normal distribution as performed by other authors [26, 27, 82, 142, 163].

De-Charentanay et al [45] explained that this scatter may be due to inhomogeneity of the materials, while Harris [71] considered the scatter increased by the random accumulation of damage. To simplify these factors affecting the scatter of results as listed in BS 3518 [26, 27], McClintock [114] classified the factors into three groups:

(1). microscopic sources of scatter such as differences in stress concentration in different phases of materials;

(2). heterogeneity among pieces such as differences in surface flatness and tool marks;

(3). sources caused by differences in production conditions for specimens, such as differences in the test specimen preparation.

Clark et al [36] proofed that by using careful control of conditions and test methods, the scatter observed in fatigue life may be reduced to a value similar to that seen in metals testing.

2.8 FAILURE IN AXIAL COMPRESSION

Due to the complex nature of FRP composites, their failure modes are strongly dependent on geometry, loading direction and ply orientation, stated Chang and Lessard [31]. Han [67] and Berg and Salama [19, 20] analysed the fracture surface of unidirectional CFRP composites and stated that it consists of two typical shapes: the shear type and a combined shear mode, showing V-notched type failure. In the latter case, each ply fails in the shear mode but adjacent plies fail in different directions. These shear failures in each ply meet at regions containing long fibres where delamination has already occurred. This inclined fracture plane is oriented so that a band of buckled fibres on this plane will undergo both shear and compressive deformation. Curtis and Moore [40] observed that these fracture planes occurred at random positions along the specimen length during compression loading. Ryder and Walker [147] supported them stating that there was no

significant end effect on the failure zone location.

2.8.1 Failure Mechanisms

The failure mechanisms reported by some authors [16, 58] were mostly of a kinking mode accompanied by extensive delamination, brooming and abrasive damage. Bascom et al [16] stated that the latter is post-failure damage resulting from the fractured surfaces being pushed against each other and is often associated with ply separation and buckling of the plies. Large areas of such surfaces are covered with debris composed of fibres and resin as reported by Shikhmanter et al [153].

Curtis and Moore [40] assumed that the test method employed obviates any macro-instability of the test specimen and ascribed the compressive failure process to just two principal mechanisms: fibre instability and failure of the fibre.

Berg and Salama [19, 20] stated that if axial cracking along the fibre direction can occur with sufficient ease, microbuckling which has nucleated on two different planes can proceed across the specimen. Thus the vertical fracture surfaces are the axial cracks, which permit microbuckling on different planes to link up and extend compressive fracture across the width of the specimen.

Ryder and Walker [147] observed that the static compression stress-strain curves exhibited an initial straight portion followed by a continuously curved portion. Just prior to failure, distinct popping sounds were heard, each accompanied by small but noticeable horizontal jumps in the stress-strain curve. They reported that failure was sudden and 'brittle-like', which they called Mode I for approximately half of the specimens and 'flat topped' followed by brittle failure (Mode II) for the other half of the specimens. Their results suggested that the compressive strength for Mode II failure was less than for Mode I failure.

2.8.2 Fractography

Shikhmanter et al [153] after analysis suggested that fracture of the laminates is transverse and is accompanied by extensive longitudinal cracking in the direction of the fibre within and at the boundaries of the plies. This feature, as referred to by other authors [15, 20, 50, 67, 135, 147], is typical of failure of the FRP composites following fibre microbuckling, which is the main mode of failure in compression. They reported that the buckling axis can be used to determine the direction of crack propagation through a region of the fracture and possibly for identification of the local failure origin. They observed that when the fracture passes through a resin rich area, it produces a relatively smooth fracture surface with flow

lines in the 'river' pattern observed in the cleavage fracture of metals. Such a surface indicates brittle fracture of the resin matrix.

However, for multidirectional laminates, Bader and Boniface [13] reported that the short term compressive strength is most likely dominated by the 0^o plies. In transverse 90^o and $\pm 45^o$ plies, cracking does not usually occur and the only influence of the off-axis plies was at the stress at which buckling instability of the 0^o plies occur. Under static loading, debonding around the fibre-matrix interface in the 90^o plies occurred at a strain lower than the cracking threshold (typically less than half) and then the transverse cracks ultimately form by the coalescence of these debonds.

2.9 FAILURE IN DYNAMIC COMPRESSION

Fatigue damage in FRP composites is more difficult to assess than in homogeneous materials, such as metals. Fatigue failure in homogeneous materials is by crack initiation, crack propagation and final failure [44, 61, 64, 65, 96, 102, 110, 132, 169, 172]. The small cracks nucleate from microscopic flaws, voids or discontinuities leading to stress concentrations. This nucleation occurs at a load level lower than the bulk ultimate strength [44, 146]. Many cycles occur before a crack appears or is initiated. However, once a crack forms, it propagates rapidly with each stress cycle until it coalesces with others or individually becomes so severe as to cause catastrophic failure [173].

Compared with the fatigue characteristics of homogeneous materials, a single crack growth does not occur in FRP composites [125]. FRP composites have several modes of failure that can occur in any combination in the fatigue process [61, 124]. Fatigue in FRP composites and metals differ in the physical process of fatigue and the fatigue performance, stated Steinbrunner [163].

2.9.1 Failure Modes

Fatigue failure modes appear to differ from static tension and compression failure modes as reported by Ryder and Walker [147]. Many authors [18, 67, 82, 91, 100, 124, 125, 132, 156] have reported different failure modes such as matrix cracking, fibre fracture, delamination, void growth and cracking. Some authors have reported that the actual progress of damage depends on the types and arrangement of the fibres, fibre-matrix bond quality, fibre length and orientation, ductility and flaw structure of the polymer matrix, the weave type, laminate lay up,

stacking sequence, specimen size and geometry. Other factors like the frequency of the stressing, the testing machine, environmental temperature and other conditions also have a significant influence on the test results [1, 32, 46, 57, 92, 132, 146, 172].

Karbhari et al [92] divided the different failure modes of fatigue into four stages: cyclic deformation causing crack nucleation, the crack nucleation itself, the related initial crack growth and crack propagation. Hahn and Kim [65] classified fatigue failure into three categories: failure due to weakness, failure by chance and failure following wear-out.

2.9.2 Crack Initiation

Bader and Johnson [14] reported that the fatigue failures might be expected to originate at local imperfections or at regions of stress concentration. Prakash [135] stated that voids act as a boundary between the two regions of the FRP composite and that possibly these internal defects act as initiation points. Other authors [37, 128] reported that resin rich areas are sites for crack development and growth.

Dew-Hughes et al [46] suggested that the cracks are initiated at voids usually at the surface under low stress conditions or internally from existing flaws. Other authors [130, 135] supported this view and reported that the failures appeared on the surface as matrix crazing and grew until they reached the internal defects. However, Smith et al [160] disagreed with this view and stated that most cracks initiate near the centre of the transverse ply at a fibre-matrix interface in a region of high stress concentration. They also stated that transverse ply cracks usually start at a fibre-matrix interface in a region of closely spaced fibres, because of the stress magnification there.

2.9.3 Matrix Failures

Wang and Chim [181] suggested that in a fibre dominant region with fibres oriented parallel to the loading direction, microcracks were developed mainly in the matrix with rather small crack lengths limited by the interfibre spacing. Naeem [123] reported that the first sign of damage was a small crack in the matrix on the surface of the specimen. Other authors [25, 177] reported that fatigue breakdown in FRP composites is dependent upon the matrix system with cracks in the matrix resulting in the fibre receiving no support; thus fibre buckling during compression.

Konur et al [99] reported that matrix cracking occurred near fibre breakage zones for CFRP composites because the matrix microcracks initiated at the interface

along the fibres and were rather isolated. They stated that at intermediate and low cycles, only fibre failures were observed. However, at high cycles, only matrix cracking and a few scattered fibre failures were observed. Lorenzo and Hahn [108] also referred to matrix microcracks nucleated in regions of densely packed fibres which were subcritical failure mechanisms, occurring early during fatigue. However, they reported that these microcracks were not deleterious and they neither triggered fibre failure nor bridged the fibres.

Harris [71] emphasised that for long life fatigue failure, the cyclic stress amplitude in FRP composites must exceed some critical value determined by the fatigue behaviour of the matrix. He stated that local matrix fatigue failures are the predominant contribution to composite fatigue failure. He also reported that the matrix and interface are the weak links as far as fatigue resistance is concerned.

2.9.4 Fibre Failures

Sato et al [148] reported that fibre breakage occurred randomly at a relatively low load and it is considered to be caused by intrinsic fibre defects. Fibre breakage is considered to be the first indication of composite failure. Other authors [32, 40, 75, 144] also reported that fibre breaks occur randomly throughout most of the loading range.

Lorenzo and Hahn [108] reported that the fibre breakage accumulated very suddenly in a cross-section leading to specimen fracture. They concluded that the fibre breakages were localised only at the fracture section. However, Charewicz et al [32] stated that in many cases most of the fibre failure and damage localisation occurred in the last 10% of the life of the test specimen.

Harris [72] in another report stated that fibre breakage may initiate a crack in the adjacent matrix. If the stress transferred to the matrix at fibre breakage is sufficiently high, it may subsequently lead to failure of neighbouring fibres. He also emphasised that this form of 'knock-on' mechanism does not occur until very high composite stresses are reached.

Konur et al [99] suggested that fibre damage occurs non-progressively as supported by Harris [72]; whereas both matrix and interfacial damage evolve progressively. They stated that fibre damage results in fibre breakage and interfacial debonding, while matrix damage is in the form of matrix cracking and interfacial damage is in the form of longitudinal splitting.

2.9.5 Crack Propagation

Mandell [110] suggested that the most obvious difference between fatigue crack growth in FRP composites and homogeneous materials is the mode of growth. Under the same conditions, most FRP composites form a complex zone of cracking which expands and may change shape during fatigue loading. Dew-Hughes et al [46] stated that crack propagation is governed by the Griffith criterion . They reported that polymer matrices show interrupted crack propagation, in which Griffith type crack growth is arrested by blunting of the crack tip. They also reported that the presence of an interface may considerably slow down crack propagation, by effectively blunting and changing the direction of crack propagation. Smith and Pascoe [159] supported this view by saying that in the presence of impurities, the crack plane may not initially lie perpendicular to the applied stress. Mohlin [118] also reported that cyclic loading has a blunting effect on the many microcracks and voids which are spread randomly throughout the specimen and which serve to arrest crack progression.

However, Jeffrey et al [83] reported that the development of fatigue damage in FRP composites containing resin rich areas appeared to be by crack propagation in the resin, rather than by interface failure. Goetchius [61] emphasised that crack propagation seems to depend on the type of laminate involved.

Sato et al [148] stated that as the stress increased, a lot of fibre breakage was observed. At the same time, matrix cracks were generated at the broken fibre tip. They concluded that the initiation and propagation of a matrix crack, accompanied by fibre breakage were the second indications of composite failure.

2.9.6 Debonding and Delamination

Debonding and delamination are the failure modes which occur during crack propagation. Dew-hughes et al [46] suggested that fibres are the likely source of flaws in the structure and hence initiation sites for debonding regardless of the efficiency of the interface. Bader and Boniface [13] reported that the major difference between static and fatigue damages is the much higher level of debonding and delamination in fatigue.

Smith et al [160] reported that debonding may occur at the fibre-matrix interface ahead of the cracking, beyond the resin rich areas. Han [67] reported that debonding of fibres from the matrix occurs at an early stage of loading, i.e. within the first 10% of the fatigue life. However Lorenzo and Hahn [108] stated that debonding, which extends from broken fibre ends, did not grow much during the

early stages of fatigue.

Goetchius [61] stated that delamination occurs in fatigue loading, under conditions of high interlaminar shear, or a combined stress state. It is suggested that combined stresses can occur at the edges of a laminate, in the vicinity of voids and defects as well as at the base of cracks.

Bascom et al [16] defined that delamination as crack propagation between plies and as the most frequently observed damage in CFRP composites. Gerharz [57] reported that for CFRP composites, besides matrix cracking, delamination is the most prevalent matrix dominated failure. Other authors [14, 54, 97, 129, 145] also supported the view that delamination is the most commonly observed damage mechanism.

Sato et al [148] suggested after analysis that as the applied load was further increased near to the failure load, fibre breakage and matrix cracks occurred frequently. The fibre breakage and matrix cracks were responsible for the occurrence of delamination. They stated that the occurrence of delamination was considered to be the third indication of composite failure.

For multidirectional laminates, Highsmith et al [78] reported that under compressive loading, the stress perpendicular to the fibres in the 90° plies is compressive and matrix cracks do not initiate in these plies. They suggested that delamination is the primary damage mode of laminates subjected to compression-compression loading. They gave an example of a $[0^{o}, 90^{o}, \pm 45^{o}]_{6S}$ laminate where the rest of the plies failed due to delamination of the first ±45° interface. Three delaminated plies will deform out-of-plane due to a decrease in their bending stiffness as the delamination grows along the length and through the width of the specimen.

2.9.7 Failure Hypothesis

A failure hypothesis proposed by Prakash [136] is that heat is generated due to hysteresis in the polymer matrix during fatigue loading of CFRP composites. Defects in CFRP composites mean that the rate of heat dissipation in such areas is less than in those areas containing more carbon fibres, which are good conductors. This results in heat accumulation leading to a local rise in temperature. With subsequent cyclic loadings, a further rise in temperature takes place. This process may lead to a reduction in the matrix shear modulus which in turn permits local buckling of the fibres. As carbon fibres are very brittle, the buckled fibres break and produce a slot or crack in the composite. This newly created slot itself is a bad conductor of heat which causes further accumulation. Furthermore, broken fibres

sufficiently raise the local stress to give rise to failure of the adjacent fibres.

Other authors [65, 92, 111, 122] supported this idea, saying that damage such as delamination and cracking results in significant local internal friction which generates heat. The heat raises the temperature of the structure and reduces its resistance to fatigue. They also noted that fatigue specimens which fracture exhibited a rise in temperature just prior to failure even when they have previously reached an apparent equilibrium. They believed that early fatigue damage is more widespread throughout the volume of material, with many small damage sites contributing to both specimen heating and modulus degradation. Later fatigue damage is the result of an agglomeration of many small sites to form a dominant defect which propagates more rapidly.

Sims and Gladman [157] measured the surface temperature rises in all their fatigue tests and found them to be less than 10°C. Sturgeon [166] reported a rise in temperature at the end of the specimen life time which was particularly sharp in the last few thousand cycles. He suggested that relatively minor failures occur throughout the life time of the specimen but the major fractures leading to failure only take place in the last few cycles.

Dao [44] explained that the initial fast temperature rise was due to establishing the primary period of heat generation. As fatigue continued, the temperature stabilised with only slight increases approximating to a steady state period of heat generation and dissipation. At the onset of final fracture, the temperature starts to rise significantly. Therefore, Johnson et al [85] concluded that the compressive strength of FRP composites depends on the shear modulus of the matrix while the fatigue performance depends on internal heating.

2.9.8 Final Failure

Goetchius [61] suggested that failure in FRP composites is not always associated with fracture. Instead, changes in properties can occur at early stages of cycling on and lead to structural failure before fracture. Some authors [52, 67, 167] even pointed out that the visible cracks do not always lead to immediate fracture. They might grow in such a way as to relieve the effectiveness of the stress concentrators by redistribution of the local stresses. Even though delamination weakens the material properties such as strength and modulus, the specimen may continue to withstand the cyclic loading for some considerable time. Dao [44] stated that the final failure period usually occurred when the material was so degraded as to fail catastrophically converting all the strain energy into fracture surface energy , heat, and sound, etc. Rotem and Nelson [145] reported that the final failure of the

laminate will occur in compression by buckling depending on the specific strength characteristics of the laminate.

The failure mode during final failure was reported by Han [67] as either whole specimen failure in shear or a combined shear mode, showing V-notched type failure which occurred at random positions along the specimens gauge lengths. These compressive failure mechanisms are similar to the axial compression failures discussed by other authors [20, 40, 153, 162, 169].

2.9.9 Stiffness Reduction and Residual Strength

Konur et al and Tsai et al [99, 180] concluded that fibre stiffness and failure strain are clearly key parameters in determining fatigue performance. Mandell [111] also reported that the progressive accumulation of cracks during fatigue breakdown might continue until the residual strength is reduced to the cycle stress resulting in failure. This change can be directly related to stress redistribution which is to be expected if internal damage occurs in a FRP laminate.

Some authors [57, 99] observed that the crack density increases with fatigue loading and stiffness reduction was proportional to the crack density as the multiple cracks increased in size and number. Kim and Ebert [96] felt that the most sensitive measure of the onset of initial fatigue damage would be a change in the shape of the stress-strain loop during the fatigue cycling.

Reifsnider and Jamison [144] showed that the relationship between stiffness and cycles had a distinct and repeatable nature. In the first region, a rapid decrease in stiffness occurs beginning with the first few fatigue cycles and ending at a stiffness reduction of 4% to 5% where the rate of reduction decreases sharply. In the second region, the stiffness reduction is approximately linear with increasing cycles. In the third region, the rate of stiffness reduction increases markedly with increasing cycles. They suggested that the formation of matrix cracks is the primary mechanism causing initial stiffness reduction in the specimens.

Other authors [149, 151] supported them concluding that the observed changes in stiffness possibly result from matrix degradation as well as delamination growth. Some authors [3, 29] reported that the large reductions in stiffness and the final fracture of the laminates can be attributed to the damage that develops in and between the off-axis plies.

Agarwal et al [3] stated that the reduction in stiffness over an interval of a few cycles is accompanied by a clearly audible sound. This is caused by the failure of the bond between the outermost fibres and the matrix system near the fixed end of the specimen. Nevadunsky et al [124] also reported an audible sound accompanied

by a change in stiffness which was detected at approximately half of ultimate load at which point a secondary linear modulus was evident. They believed that the sound emission was due to 0^{o} fibre breakage and fibre-matrix debonding. This hypothesis is supported by the fact that pure $\pm 45^{o}$ laminates which would experience only matrix failure, did not emit noise until near fracture. The audible sound is an indication that irreversible damage is being caused in the specimen. Kellas et al [95] observed that a reduction in residual compressive strength occurred when the specimens were fatigue tested for a very small number of cycles, i.e. 1,000. No further reduction was observed after a large number of fatigue cycles, i.e. 100,000. However, some authors [71, 166] pointed out that the residual strength of CFRP composites subjected to cyclic load for a moderate number of cycles, is greater than that of untested material. Morton [122] concluded that the residual compressive strength depends on the number of broken fibres together with the lateral extent of delamination associated with secondary longitudinal plies. Equally, softening of the matrix either due to temperature and/or moisture reduces the residual compressive strength.

Harris [72] suggested that, at low stress levels or early in the life of a composite undergoing cyclic loading, most types of FRP composites sustain damage of a very general kind distributed throughout the stressed region. This damage does not always immediately reduce the strength and stiffness of the composite and such reductions as it might cause ('wear-out') are often offset in the early stages of life by slight increases in strength and stiffness ('wear-in'). This is also reported by many authors [64, 65, 73, 74]. Naeem [123] proposed that for FRP composites, energy absorbed per unit cycle is directly proportional to the increase in damage per unit cycle, where the former is the difference of energy inputs into a specimen at any two consecutive cycles.

CHAPTER 3 EXPERIMENTAL WORK

CHAPTER 3 EXPERIMENTAL WORK

3.1 INTRODUCTION

Three types of prepreg material manufactured by Ciba-Geigy were used to study the influence of voids on the mechanical properties of prepregs: Fibredux 913G-E and Fibredux 914C were purchased from the manufacturer; 914C-833-40 woven fabric prepreg was supplied by Lucas Aerospace. A range of tests were conducted as outlined in Table 1 and the results of these tests are presented and analysed in the following chapters.

Fibredux 913G-E was used to investigate the effect of solvents on the void content of FRP composites (Experiment 1).

Fibredux 914C was used to study the effect of curing pressure and temperature on the void content of the FRP composites (Experiments 2 and 3). Interlaminar shear strength testing was conducted on the specimens prepared from this material.

A number of experiments (briefed below) were conducted using 914C-833-40 woven fabric. Some of this work was carried out at the request of Lucas Aerospace.

Experiment 4 was designed to examine the effect of curing pressure on the void content of laminates and the void content on static compressive strength and secant modulus. Different test fixtures were used in this experiment to investigate the influence of fixture design on the results. Compressive fatigue behaviour in zero-compression cycling was also examined.

In order to obtain representative data of the effect of curing pressure on void distribution within a laminate, three laminates were moulded at different curing pressures. Specimens were selected and tested at positions expected to be representative of the laminates (Experiment 5).

Eight laminates were moulded under different lay-up conditions to observe the stacking effect on the void distribution within individual laminates (Experiment 6). Two curing pressures were chosen. The stacking lay-ups were varied from the use of a frame and two layers of bleed cloth on each side of the laminate, to no frame and the normal single layer of bleed cloth on each side of the laminate.

Six laminates were moulded with different partial cure times. Specimens were cut out from these laminates for the determination of void distribution, from positions expected to be best representative (Experiment 7). This experiment is

designed as the trial run for Experiment 8 in order to obtain information on the effect of varying the partial cure times on the void content of the laminates.

Thirty-five laminates were also moulded with different partial cure times. Static compressive strength and secant modulus were first determined for specimens obtained from the laminates moulded at each partial cure time. This was followed by dynamic fatigue cycling under different loading conditions. The residual compressive strength and residual secant modulus were measured on those specimens which survived a million cycles. Some specimens were fatigued to a selected number of cycles and to just before failure. These specimens were sectioned and observed under the microscope.

3.2 MATERIALS

The materials used in this project were commercially manufactured by Ciba-Geigy. The manufacturer's instructions were followed with respect to storage, temperature, equilibration and exposure to air before use [33, 34].

3.2.1 Glass Fibre Prepreg- Fibredux 913G-E

Fibredux 913G-E is a modified epoxy resin pre-impregnated into unidirectional E-glass fibre cloth. The Fibredux 913 composite components can be moulded with exceptionally high resistance to water and high humidity environments as cited by the manufacturer [33]. Components manufactured from this material can be used at working temperatures in the range of -55°C to +130°C. The specified density of the fibre is 2.59 g/cm^3 and of the resin is 1.23 g/cm^3.

Both Fibredux 913G-E and 914C (described below) contain a mixture of two epoxy resins: MY750 and MY720, with the 913G-E having a greater resin content.

3.2.2 Carbon Fibre Prepreg- Fibredux 914C

Fibredux 914C is a modified epoxy resin pre-impregnated into unidirectional carbon fibre cloth. The main resin system used in Fibredux 914C confers easy processing characteristics and a sensible tolerance of the variations in technique which may be expected in general production practice [34]. Components manufactured from this material can be used at working temperatures in the range of -60°C to +180°C. The specified density of the fibre is 1.75 g/cm^3 and of the resin is 1.30 g/cm^3

3.2.3 Woven Carbon Fibre Prepreg- 914C-833-40

The 914C-833-40 was supplied by Lucas Aerospace Fabrication Division in Burnley. It is a modified epoxy resin impregnated in carbon woven fabric. The fabric is constructed from two sets of yarns. One set runs along the length of the fabric and is known as the 'warp'. The other runs across the width of the fabric and is known as the 'weft'. In this particular case, the same type of yarn is used for both the warp and weft. The weaving process interlaces these two sets of threads with each other. The frictional forces between the individual threads at the points of cross-over hold them tightly in position so that a stable cloth, capable of being cut without fraying taking place, can be produced. It has a five-shaft (harness) satin weft interlaced by warp construction. In practical weaving terminology, the warp threads are also referred to as 'ends' and the weft threads as 'picks'. The specified density of the fibre is 1.75 g/cm^3 and of the resin is 1.30 g/cm^3 .

3.3 TESTING AND MOULDING EQUIPMENT

3.3.1 Mechanical Testing Equipment

Mechanical testing was mainly performed on Dartec M1000/RE servohydraulic test machines (see Plate 1). One machine, having a 100 kN capacity, was used for both static and dynamic compressive tests; whereas the other machine, having a 50 kN capacity, was used solely for the dynamic testing. In all cases the specimen was gripped directly by hydraulically assisted jaws.

A small section of the compressive test programme was carried out on a Mand servoscrew testing machine. Compressive load was applied by means of flat platens bearing directly onto the tapered sleeves of the Celanese jig. The maximum force capacity of the machine was 100 kN.

Interlaminar shear stress tests were carried out on an Instron servo-mechanical test machine using a test fixture based on that described in ASTM D2344 [8].

3.3.2 Test Fixtures

Most of the mechanical tests involved compression loading of slender specimens. In order to eliminate buckling in such tests, the specimen needs to be supported. This is achieved by using an anti-buckling guide. Several types of anti-buckling guides were used and are shown in Plates 2, 3, 4 and 5.

The first anti-buckling guide as shown in Plate 2 enabled the edges of the specimen to be completely supported. This guide, named **ABG-1**, was designed based on the RAE method [38]. The following modifications were made to suit the purpose of this experiment (see Figure 2):

1). a window was made on each side of the guide to allow access to strain gauges placed on the specimen;

2). the body plate of the guide was of smaller dimensions to allow the use of smaller specimens;

3). the guide was modified to be freestanding on the bottom grip rather than being fixed in the grip with the specimen.

The RAE jig [38] allows for two regions of 5 mm in length of unsupported specimen at each end of the gauge length. This purpose of the unsupported region is to allow longitudinal compression of the specimen without the grip fixture coming into contact with the guide. Failure is required to be within the guide and therefore only one unsupported region is likely to improve the chances of such behaviour.

The second anti-buckling guide, named **ABG-2**, was a modification of **ABG-1**. The design included an extra large window on each side of the guide as shown in Plate 3 and Figure 3. The depth of the windows (column length L) was determined using Euler critical buckling theory on the column which is fixed at both ends:

$$P_e = \frac{(4 * \pi^2 * E * I_v)}{L^2}$$

equation (7)

where

P_e = Euler's critical force (kN)

E = Young's modulus of elasticity (GPa)

L = column length (mm)

I_v = second moment of area (mm^4)

= (b * d^3) / 12

b = specimen width (mm)

d = specimen thickness (mm)

In this case the following values were used:

P_e = 18 kN;

E = 49.8 GPa;

b = 20 mm;

d = 2 mm.

Substituting these values into equation (7), the calculated column length (L) is equal to 38 mm to the nearest whole number. A safety factor of 2.5, as recommended in the theory [178], was introduced into the design such that the window depth (in this case the column length L) becomes 15 mm (see Figure 3).

The design of the third jig, named the **CRAG jig**, as shown in Plate 4 was also based on the RAE method [38]. The following modifications were made to suit the configuration of the specimens used in this work (see Figure 4):

1). the body plate of the jig was of smaller dimensions to allow the use of smaller specimens;

2). the gripped part of the jig was eliminated to allow direct gripping of the two ends of the specimen protected with aluminium end tabs.

The fourth fixture, named the **Celanese jig**, consisted of split conical collet grips that fit into matching sleeves. These in turn fit into a cylindrical shell as shown in Plate 5. This design was based on ASTM D3410-87 [11].

3.3.3 Laminate Moulding Equipment

The FRP composite laminates were manufactured using a compression moulding press fitted with two electrically heated platens. The pressure was applied by a hydraulic ram. Temperature and pressure were kept stable throughout the moulding period. The open mould used consisted of two plates of steel with a rectangular metal frame of 2 mm thickness placed between the two plates.

3.4 913G-E PREPREG LAMINATE PREPARATION *(Experiment 1)*

3.4.1 Lay-up of Prepreg Sheets

Fibredux 913G-E prepreg was cut up into sheets of the required size using a guillotine. Each laminate consisted of 16 layers in unidirectional configuration. This made a cured composite laminate of a nominal thickness of 2 mm.

3.4.2 Solvent Addition

Three sets of laminates, each of 16 layers of Fibredux 913G-E sheets, were sprayed with different solvents in order to produce voids during the cure cycle (see Table 1). The three solvents used were pentane, Freon (dichlorodifluoromethane) and water.

After removing the protective film from each sheet, the chosen solvent for that laminate was sprayed on it. Two sheets were first pressed together, with care to avoid creating wrinkles and then passed through a hand mangle. A further coating of solvent was then applied before repeating the process on each consecutive layer until 16 layers had been pressed together to make the full thickness of the uncured laminate.

The uncured laminate was then placed in a steel frame of 2 mm thickness (nominal thickness of the laminate) and then laid up between the porous and non-porous absorbent materials (see Figure 5). Resin bleed out was enabled by the use of a perforated releasable membrane placed in contact with the laminate and backed up with an absorbent material. These materials, laid symmetrically on both sides of the laminate, permitted the escape of air and volatiles as well as bleed out of excess resin.

3.4.3 Cure Cycle for 913G-E Prepreg Laminates

The compression moulding process was used for all the mouldings as it is widely practised especially for making laboratory specimens. Each laminate was cured with a breathing or 'bumping of the press' process, where the pressure was applied and released momentarily before moulding under the curing pressure.

The uncured laminate of dimensions 150 mm by 200 mm, together with the porous releasable membrane and bleed cloths were placed between two steel plates before being put between the heated platens.

The temperature of the platens was raised to 150°C before inserting the mould. A pressure of 2000 kN/m^2 was applied for 20 minutes while the temperature was kept at 150°C. The cured laminate was then removed from the hot mould. The laminate was then conditioned for at least 48 hours at room temperature in a dessicator.

3.5 914C PREPREG LAMINATE PREPARATION

3.5.1 Lay-up of Prepreg Sheets

Fibredux 914C prepreg sheets were cut and stacked as previously described in sections 3.4.1 and 3.4.2, except that in this case no solvents were used.

Twelve sets of uncured laminates were prepared, each consisting of 16 layers of Fibredux 914C.

3.5.2 Variation of Curing Temperature *(Experiment 2)*

Six unidirectional laminates of dimensions 150 mm by 200 mm were moulded at different curing temperatures (see Table 1). The temperatures used were 150°C, 160°C, 165°C, 170°C, 175°C and 180°C. The pressure of 2000 kN/m^2 and the chosen temperature were kept constant for 1 hour. This was followed by cooling to 120°C before releasing the pressure. The laminates were then postcured at 190°C for 4 hours. The postcured laminates were then cooled and left in the dessicator for conditioning .

3.5.3 Variation of Curing Pressure *(Experiment 3)*

Six unidirectional laminates of dimensions 150 mm by 200 mm were moulded under different curing pressures (see Table 1). The pressures used were 327 kN/m^2, 653 kN/m^2, 980 kN/m^2, 1307 kN/m^2, 1633 kN/m^2 and 1960 kN/m^2. The temperature was maintained at 170°C for 1 hour followed by cooling to 120°C before releasing the pressure. The laminates were then removed from the mould and postcured at a temperature of 190°C for 4 hours before conditioning at room temperature in a dessicator.

3.6 914C-833-40 WOVEN FABRIC PREPREG LAMINATE PREPARATION

3.6.1 Lay-up of Prepreg Sheets

The 914C-833-40 woven fabric prepreg was cut into sheets of required size with a sharp pair of scissors. The stacking configuration of (0/90, +45/-45, +45/-45, 0/90)$_{2S}$ was symmetrical about the centre ply. The off-axis fibre orientation in the lay-up was accomplished by the use of suitable templates to meet the required angle tolerances. A total of 8 layers were stacked to produce a cured composite laminate with a nominal thickness of 2 mm. Each layer was added and pressed with the hand mangle as for the unidirectional prepreg sheets (Experiments 1, 2 and 3).

The uncured laminate was then placed in a 2 mm thick steel frame and sandwiched between porous releasable membrane and non-porous bleed cloths in a symmetrical lay-up as shown in Figure 5.

3.6.2 Variation of Curing Pressure *(Experiments 4 and 5)*

Laminates of dimensions 150 mm by 200 mm were moulded under curing pressures of 653 kN/m^2, 1307 kN/m^2 and 1960 kN/m^2, with eight laminates moulded for each condition (see Table 1). They were moulded at a curing temperature of 170°C for 1 hour. This was followed by cooling to 120°C before releasing the curing pressure. Each of the laminates was then removed from the mould, postcured and conditioned (Experiment 4).

In Experiment 5, a further three laminates of dimensions 150 mm by 200 mm were moulded at curing pressures of 653 kN/m^2, 1633 kN/m^2, and 2940 kN/m^2 using the same cure cycle as describe above.

3.6.3 Variation of Lay-up Conditions *(Experiment 6)*

Four laminates of dimensions 100 mm by 150 mm were moulded at each of 1000 kN/m^2 and 3000 kN/m^2 curing pressures (see Table 1). Four different lay-up conditions were chosen for each curing pressure in this experiment as follows:

1). with frame and one layer of bleed cloth on each side of the laminate;

2). without frame and one layer of bleed cloth on each side of the laminate;

3). with frame and two layers of bleed cloth on each side of the laminate;

4). without frame and two layers of bleed cloth on each side of the laminate.

The laminates were cured at 170°C for 1 hour followed by cooling to 120°C before releasing the pressure. They were postcured and conditioned at room temperature as in the previous experiments.

3.6.4 Variation of Partial Cure Time *(Experiments 7 and 8)*

Six Laminates of dimensions 100 mm by 150 mm were moulded using different partial cure times of 0, 5, 10, 15, 30 and 45 minutes (see Table 1). In this context, partial cure time was defined as the time that the uncured laminate was heated at the curing temperature without the application of the curing pressure. The curing temperature used was 170°C and curing pressure of 2000 kN/m^2 was applied for 1 hour after partial cure time. Breathing or 'bumping of the press' was carried out with momentary application and release of the pressure before the final application of the curing pressure. It was then cooled to 120°C before releasing the curing pressure. The laminates were postcured and then conditioned in the dessicator (Experiment 7).

In Experiment 8, thirty-five laminates of dimensions 190 mm by 200 mm were moulded using different partial cure times of 0, 5, 8, 12, 15, 20 and 30 minutes with five laminates moulded for each individual condition (see Table 1). The cure cycle was the same as described above. These time intervals were selected based on the findings of the trial run in Experiment 7.

3.7 PREPARATION OF TEST SPECIMENS

Before taking specimens for analysis and testing from the laminates, the edges of the laminates were discarded as these areas are unlikely to be representative of the body of the laminate.

The cutting equipment used was an electro-metallic bonded diamond slitting wheel. After cutting, the edges of the specimen were first polished on a linisher followed by a finishing polish on 400 grit silicon carbide paper. This removed scratches and burrs made by the slitting wheel.

The sampling pattern in each experiment is illustrated in Figures 6 to 11.

3.7.1 Density Determination Specimens

After being sectioned from laminates prepared in respective experiments , the specimens were degreased with acetone and conditioned for at least 48 hours at room temperature before measurements were made.

3.7.2 Acid Digestion Specimens

In order to achieve accurate fibre and resin volume fractions determination, the same specimens as used for density measurement were used for acid digestion [174]. After density measurement, they were conditioned at room temperature for at least 48 hours before digestion.

3.7.3 Static Compressive and Dynamic Fatigue Specimens

Specimens of dimensions 20 mm by 200 mm were cut from laminates prepared in Experiments 4 (Figure 8) and 8 (Figure 11). These specimens were cut slightly oversize to allow for linishing and polishing with silicon carbide paper to remove any scratches and burrs on the edges of the specimens.

Aluminium end tabs of dimensions 20 mm by 45 mm were bonded on the ends of the specimens to avoid damage of the specimen by the testing machine wedge grips. The end tabs had to be roughened to ensure good bonding and sharp edges at the point of contact with the specimen were removed in order to minimise any stress concentration effect.

The surface of the specimen in contact with the aluminium end tabs was also roughened to provide good bonding. This was followed by cleaning and degreasing using acetone. The adhesive used for bonding was made using Araldite MY750 and HY951 hardener in the ratio of 10:1. After bonding the end tabs to the ends of the specimen, pressure was applied and the adhesive allowed to cure at room temperature for at least 24 hours. The specimens were then conditioned for at least 48 hours in a dessicator before testing.

3.7.4 Celanese Jig Specimens

Specimens of dimensions 10 mm by 142.5 mm were cut from positions as shown in Figure 8 on the laminates prepared in Experiment 4. They were cut slightly oversize so that scratches and burrs could be removed by linishing and polishing.

Aluminium end tabs of dimensions 10 mm by 65 mm were bonded on the ends of the specimens as described in section 3.7.3.

3.7.5 Strain Gauges

Strain gauges were bonded to both sides of those specimens used for static compressive testing [134]. The surface where the strain gauge was to be bonded was thoroughly degreased with Freon on a clean cloth. The gauge area was then dry lapped using 240 grit silicon carbide paper to lightly roughen the surface. M-prep conditioner A was then applied to wet lap the gauge area. The residue and conditioner were then removed by slowly wiping the gauge area with a clean cloth. The wet lap and wiping procedures were repeated using 400 grit silicon carbide paper. The gauge area was then rewetted with conditioner A and was cleaned. M-prep neutraliser 5 was then applied to the gauge area. It was wet lapped and scrubbed with a cotton bud tip.

Precautions must be taken during wet lap and wiping. Firstly, evaporation of the cleaning material on the surface must be avoided since this would leave a unwanted thin film between the adhesive and the specimen. Secondly, the gauge area must not be wiped back and forth as this might cause contaminants to be redeposited on the cleaned area.

Markers were drawn on the gauge area with a specially designed ruler to ensure the proper alignment of the strain gauge on the surface. The strain gauge was removed from its acetate envelope with tweezers and placed on a clean glass plate with the bonding side of the gauge down. Terminal strips were cut as required and aligned alongside the strain gauge. Cellophane tape was used to centre the gauge and the terminal strips onto the glass plate. The tape was carefully lifted at a shallow angle, bringing the gauge and terminal strips up with it.

The gauge/tape was then positioned so that the triangle of alignment marks on the gauge were over the lay-out lines on the specimen marked using the ruler. One end of the tape was stuck to the back of the gauge area, while the other end of the tape was lifted up at a shallow angle with the bonding side of the strain gauge and the terminal strips being exposed.

The back of the gauge and the specimen were coated with 200 catalyst for about a minute. The M-bond 200 adhesive was then applied on the back of the gauge and the specimen. The lifted end of the tape was carefully replaced over the alignment marks on the specimen. A firm pressure with fingers was applied after the excess adhesive had been wiped away with a clean cloth. A soft pad, a back-up plate and a clamp were used to apply the final clamping pressure if necessary. The

adhesive was allowed to cure under the pressure for 10 minutes at room temperature. The tape was removed and the lead wires were soldered to the terminal strips.

The wires from the strain gauge connector box containing the bridge circuit were soldered to the wires from the strain gauges on the specimen mounted in the compression test fixture.

3.7.6 Interlaminar Shear Strength Specimens

Three specimens of dimensions 10 mm by 25 mm were cut from each of the six laminates prepared at different curing temperatures (Experiment 2). These specimens were taken from the positions shown in Figure 6. Another three specimens of the same dimensions were cut from the laminates prepared at different curing pressures in Experiment 3. The positions of these specimens are shown in Figure 7. The scratches and burrs were removed from the edges of the specimens using 400 grit silicon carbide paper followed by conditioning before testing.

3.8 DENSITY MEASUREMENT

The density measurement was carried out according to ASTM D792-86 [7] by the displacement method based on Archimedes' principle.

After conditioning at room temperature, the specimens were degreased with acetone and weighed to an accuracy of 0.1 mg. Each specimen was then weighed in water, suspended from the balance by a fine wire. No bubbles were allowed to adhere to the wire or the specimen, and the suspended specimen was not allowed to touch the vessel containing the water. Good wetting was achieved by a quick immersion in 50% v/v hydrochloric acid solution, as recommended by Lucas Aerospace Standards [109], prior to immersion in the water. This weight was measured rapidly in order to minimise any absorption of water by the specimen. The wire was then weighed immersed in water to the same depth as used in previous immersion. The density of the composite was calculated as:

$$D_c = \frac{a}{(a + w - b)} * 0.9975$$

equation (8)

where

D_c = composite density (g/cm^3)

a = weight of specimen with wire in air (g)

b = apparent weight of specimen completely immersed and of wire partially immersed in liquid (g)

w = apparent weight of partially immersed wire (g)

0.9975 g/cm^3 is the density of water.

3.9 ACID DIGESTION

The specimens used for density measurement (described in section 3.8) were conditioned at room temperature before carrying out thickness measurement and acid digestion. Thirteen measurements were taken on each of the specimens using a micrometer and the average thickness was taken. The acid digestion was then carried out based on Lucas Aerospace Standards [109].

The acid digestion procedure as depicted in Figure 12 was used to obtain the fibre and resin volume fractions. In stage 1, each of the specimens was placed in a tall beaker with 20 ml of concentrated sulphuric acid. The beaker was placed on a hot plate inside a fume cupboard. This was then heated until acid fumes were evolved. During this digestion (oxidation) process, the fibres were freed from and totally cleansed of resin. The fibres were dispersed in the acid solution. The beaker was then removed from the heat and 30 ml of hydrogen peroxide (100 volume) solution was added dropwise down the side of the beaker to avoid spitting of the mixture. The rate of addition was increased as the reaction proceeded. In all cases, precautions were taken in handling the two solutions. Rubber gloves and a fume hood with safety glass shield were used throughout the experiment.

As the resin oxidised, the fibres rose to the top of the solution. The reaction was considered to be complete when the hot acid solution below the fibres became clear and colourless. An additional 2 ml of the peroxide was added to the solution. This was heated for a further 10 minutes to ensure complete decomposition of the resin. The beaker was then removed from the hot plate. Approximately 50-100 ml of deionised water was added slowly to the beaker and it was then left to cool.

In stage 2, the carbon fibres were then collected by filtering through a weighed sintered glass crucible (number 3 porosity). This was carried out with the flask connected to an air suction system. Care was exercised at all times to ensure complete transfer of all fibres from the flask to the crucible. The fibres were washed thoroughly with at least 500 ml of deionised water and then with a small amount of

industrial methylated spirits (IMS).

In stage 3, the crucible was dried in an oven at 120 ± 5°C for a minimum of 2 hours, and then cooled in a dessicator. It was then reweighed to determine the mass of the fibres. The fibre volume fraction was then calculated as follows:

$$\Phi_f = [\frac{(W_f * D_c)}{(W_c * D_f)}]$$

equation (9)

where

Φ_f = fibre volume fraction
W_f = weight of fibre (g)
W_c = weight of composite (g)
D_f = fibre density (g/cm^3)
D_c = composite density (g/cm^3)

3.10 VOID CONTENT MEASUREMENT

The void content of each of the specimens was determined according to ASTM D2734 [9], assuming the density of the resin to be the same in the composite as it is in a large cast mass. Although there is no realistic way to avoid this assumption, it is nevertheless not strictly correct. Any differences in the curing pressure and temperature, as well as the molecular interactions between the resin and the fibre change the composite resin density from the bulk resin density. These changes mean that the resin density in the composite is lower than that of a large cast mass of resin, i.e. the resin density value used in the calculation is overestimated which means that the void content of the composite is underestimated.

The void content is calculated as:

$$V_p = 100 - D_c(\frac{r}{D_r} + \frac{f}{D_f})$$

equation (10)

where

V_p = void content in volume percent (%)

D_c = measured composite density (g/cm^3)

D_r = resin density (g/cm^3)

D_f = fibre density (g/cm^3)

r = resin in weight percent (%)

f = fibre in weight percent (%)

3.11 MECHANICAL TESTING

3.11.1 Interlaminar Shear Strength (ILSS) Testing

Three specimens were selected from each of the 914C unidirectional laminates prepared at different curing temperatures (Experiment 2, Figure 6) and different curing pressures (Experiment 3, Figure 7). The testing speed was set at 1 mm/min. Five measurements of the width and thickness of each of the specimens were made. The average width and thickness of each specimen were used for the calculation of ILSS. The ILSS was calculated and measured according to ASTM D2344 [8] using the following equation:

$$ILSS = \frac{0.75 * F}{b * d} * 10^3$$

equation (11)

where

ILSS = interlaminar shear strength (MPa)

F = failure force (kN)

b = specimen width (mm)

d = specimen thickness (mm)

3.11.2 Static Compressive Strength Testing

Compressive strength testing was carried out in stroke (displacement) control mode at a test speed of 1 mm/min. The specimen was gripped directly in hydraulically assisted jaws. All specimens were preloaded at a force (about 3 kN) to compress them to about 20% of their strengths before actual testing. This was to

ensure that the grips were firmly bedded into the specimen end tabs.

In the absence of an internationally recognised static compression test method, different jigs were used on specimens made in Experiment 4 in order to investigate the influence of jig design on the test results.

Five specimens were randomly selected for each set of tests using the **ABG-2** and the **CRAG jig**. Eight specimens were selected for test using **ABG-1.**

The **CRAG jig** was used for the determination of static compressive strength and secant modulus prior to the fatigue tests (Experiment 8). Two specimens were randomly selected from each of the laminates moulded under different partial cure times in Experiment 8.

In the determination of the cross-sectional area of a specimen, five measurements of thickness and width were made on each of the specimens. The mean values of the five readings were used for calculation of the cross-sectional area.

The static compressive strength was calculated as follows:

$$S = \frac{F}{A} * 10^3$$

equation (12)

where

S = static compressive strength (MPa)

F = failure force (kN)

A = specimen cross-sectional area (mm^2)

3.11.3 Celanese Jig Testing

Fifteen specimens were selected from each group of eight laminates prepared in Experiment 4 for Celanese tests on the Mand servoscrew machine. The testing speed was set at 1 mm/min. The specimens were gripped and fitted into the cylindrical shell. Each of the specimens was preloaded in compression to 3 kN (to about 20% of the failure strength) before actual compression testing.

3.11.4 Dynamic Fatigue Testing

Dynamic testing was carried out in load control mode. In Experiments 4 and 8, in order to achieve a normal distribution, the number of specimens selected from each of the experiment was in the range of 15 ~ 20 (refer to BS 3518 [26, 27]), with three to five specimens being selected from each laminate. Each specimen was gripped directly by the hydraulically assisted jaws in the same manner as in static compression testing on the Dartec machine as described in section 3.11.2. In order to eliminate any heat build up in the specimen, a low frequency sine wave, operating at 5 Hz, was used. The cycle was set such that the specimen did not experience any tensile forces, i.e. zero-compression fatigue cycling.

Having determined the average compressive failure strength (S_{ca} MPa), for a particular material, zero-compression fatigue testing was carried out at a series of intermediate stress values in the range of 50% $\bar{S}_{ca}$ to 75% S_{ca}. For example, if the average failure stress was 100 MPa, then for a fatigue test at a 60% stress level , the peak compressive stress would be set to 60 MPa. The cycle mean would be set at 30 MPa which would ensure that the specimen did not undergo any tensile loading throughout the cycle, i.e. the most positive stress would be 0 MPa.

The number of cycles to failure for each specimen was recorded. If any specimen did not fail in less than one million cycles, the test was terminated. Those specimens which survived one million cycles were then statically tested, using the **CRAG jig**, to determine the residual compressive strength and secant modulus. Stress/log life (S/N) curves were drawn for the results of tests on specimens prepared using the same cure condition.

3.12 SECANT MODULUS MEASUREMENT

In order to determine the secant modulus, the strain on the sample during testing must be known. For this reason, strain gauges were attached to specimens used for static testing. The stress-strain data obtained during the test was used to determine the secant modulus and the presence of the strain gauges also enabled the measurement of strain to failure.

The secant modulus was calculated as:

$$Mod = \frac{F}{A * 0.25} * 10^2$$

equation (13)

where

Mod = secant modulus (GPa)

F = force (kN)

A = specimen cross-sectional area (mm^2)

0.25 is the percentage strain at which the force was measured for all specimens.

3.12.1 Secant Modulus Measurement on Fatigue Specimens

Initially, strain gauges were used in the measurement of secant modulus at intervals during the fatigue tests. As expected, the strain gauges always failed or become faulty after a small number of cycles. Therefore, an empirical method, which is detailed below, was derived for the measurement of the modulus change after cycling.

Experiments were carried out so that simultaneous plots of compressive force against strain (from the strain gauge) and compressive force against displacement (reading from the machine displacement) were obtained (see Graphs 1 and 2). Thus, any value of displacement could be translated directly into a value of strain as shown in Graph 3 (a cross-plot of the overall displacement of the machine against the strain during loading). A fixed displacement was selected for all modulus measurements.

Therefore, fatigue tests were interrupted at intervals and force against displacement data were obtained in a static test. From such data the modulus was determined at a fixed displacement using the force corresponding to this displacement.

3.13 MICROSCOPIC OBSERVATION

Two specimens for microscopic examination were randomly selected from laminates moulded with 5 minutes partial cure time in Experiment 8. The specimens were cycled at a 60% stress level. This stress level was chosen as experience already gained from the fatigue tests, showed that the material would withstand a large number of cycles before failing at this stress level. Therefore, it may be

possible to observe the onset and progress of specimen damage, as too high a stress level (e.g. 70%) would cause the specimen to fail after a few cycles. Too low a stress level (e.g. 55%), a specimen would not fail before one million cycles and damage may not have been observed. The cycling was terminated for one of the specimens after completing 100,000 cycles. This specimen was sectioned, for microscopic observation, at a position where visible cracks had occurred. The other specimen was fatigued to just before failure, which was indicated by a sudden decrease in secant modulus. The specimen was then sectioned and mounted for microscopic observation.

Two specimens were also randomly selected from the laminates moulded with 15 minutes partial cure time in Experiment 8. These two specimens were cycled and prepared for microscopic observation as described above.

Two specimens were also selected from the 30 mins partial cure time in Experiment 8. One specimen was cycled to 50,000 cycles as this material was of poorer quality and might not withstand 100,000 cycles at the 60% stress level. This specimen was sectioned and mounted after cycling for microscopic observation. The other specimen was also fatigued at the same stress to just before failure. The number of cycles completed was recorded followed by sectioning and mounting.

3.13.1 Preparation of Microscopic Observation Specimens

A specimen section was mounted in Araldite epoxy resin and allowed to cure at room temperature for at least 48 hours. The face of the specimen which was to be examined was made as flat as possible [115, 179] by lightly linishing. It was then subjected to wet grinding on silicon carbide papers working from 240 grit to 400 grit, 800 grit and finally to 1200 grit. Before proceeding to the next piece of grit paper, the specimen was washed with running water, followed by washing with liquid soap solution to remove the particles or grit left from the previous paper, as they would produce deep scratches on the specimen surface. The specimen was rotated through 90° so as to grind the surface across the scratches left by the previous paper.

The specimen, with fine scratches left by the final paper (1200 grit), was then rinsed with running water and polished using a 6 μm diamond paste polishing wheel. Blue lubricant was used to prevent the cloth from becoming dry. Light pressure only was used to prevent digging into the cloth. Polishing was carried out with a circular sweep of the hand against the rotation of the wheel. The specimen was not allowed to stand still on the wheel or held at the outer edge of the wheel as the polishing would be faster due to the peripheral speed of the wheel.

The specimen was washed in running water and liquid soap solution at regular intervals during polishing. It was then rinsed in alcohol and dried under a drier before observing under the optical microscope to check that it was scratch free and then polished on a 5 μm aluminium oxide paste polishing wheel. The same procedure of polishing was carried out as described above, and the specimen was washed at intervals. Deionised water was used as lubricant. The polishing process was terminated when a mirror-like and scratch free surface was achieved.

The final stage of polishing was performed on the 1 μm diamond paste polishing wheel using blue lubricant. Very light pressure was used throughout this process and movement was towards the centre of the wheel where its rotation speed was slower. The polishing was considered complete when all the details of the constituents of the composites were visible under the microscope.

3.13.2 Optical Microscopic Observation

The optical microscopic observation was carried out on the Reichert-Jung MEF3 optical microscope. Pictures were taken which showed the detailed structure of the composites. The results are illustrated and discussed in the following chapters.

3.13.3 Scanning Electron Microscope (SEM)

SEM examination was performed on a Cambridge Instrument Steroscan 360. This electron microscope enabled very detailed observation of the areas of interest at magnifications not achievable on an optical microscope.

CHAPTER 4 RESULTS

CHAPTER 4 RESULTS

The average results of the density, fibre volume fraction, void content and thickness of all the laminates are listed in Table 2. The calculated individual values of each specimen are listed in Appendix A, Tables A1 to A30.

The average static compressive strength, secant modulus and failure strain as well as the residual strength are listed in Table 2. The individual calculated values of each specimen are listed in Appendix B, Tables B1 to B13.

The number of fatigue cycles to failure under each stress level in Experiments 4 and 8 are listed in Appendix C, Tables C1 and C2. Summary results are presented in Graphs 38 and 42. The modulus of the test specimens fatigue cycling at different stress levels are recorded at various intervals of cycles during the test. These modulus values are listed in Appendix C, C3 to C12. The summary results are presented in Graphs 53 to 62.

Graphs are plotted to indicate the relationship between the different void contents of the laminates and the density, fibre volume fraction, thickness and the static strength properties. S/N curves are plotted for the fatigue tests to indicate the relationship between the void contents of the laminates and fatigue behaviour.

4.1 THE INFLUENCE OF SOLVENT ADDITION *(Experiment 1)*

The results for the three laminates prepared with sprayed solvents on each consecutive layer are summarised in Table 2 and the results determined from each specimen are listed in Appendix A, Table A1. The density, fibre volume fraction and the void content are calculated using equations 8, 9 and 10 respectively (see sections 3.8 to 3.10). The average values of the three specimens selected from each laminate are taken for comparison.

4.2 THE INFLUENCE OF CURING TEMPERATURE *(Experiment 2)*

The results for the laminates moulded at different curing temperatures are summarised in Table 2 and the values determined from each specimen are listed in Appendix A, Table A2. The density, fibre volume fraction and the void content are calculated in the same way as in section 4.1. The ILSS values are calculated using equation 11 (see section 3.11.1). The average values of three specimens selected in each laminate are taken.

Graphs are plotted as shown in Graphs 4 to 8. In each of the Graphs 4 to 6, a best fitted curve is drawn through the points showing a peak at 165°C. No best fitted curve is drawn in each of the Graphs 7 and 8 because there is no clear trend.

4.3 THE INFLUENCE OF CURING PRESSURE *(Experiment 3)*

The results for laminates moulded at different curing pressures are listed in Appendix A, Table A3 and the summarised results are listed in Table 2. Two specimens from each laminate are used in the determination of density, fibre volume fraction and the void content with the average values of each laminate taken for comparison. Three specimens from each laminate were selected to determine the ILSS values and the average value of these three specimens was taken.

The results are plotted in Graphs 9 to 13. A straight line is drawn through each of the Graphs 9 to 11 and best fitted curves are drawn through the points in Graphs 12 and 13.

4.4 THE INFLUENCE OF CURING PRESSURE *(Experiments 4 and 5)*

The results for laminates moulded at different curing pressures are summarised in Table 2. The individual results for each specimen and the standard deviations determined from Experiment 4 are listed in Appendix A, Tables A4 to A6. The individual results of the seventeen specimens selected from each laminate with the standard deviations in Experiment 5 are listed in Appendix A, Tables A7 to A9.

A total of four graphs are plotted. The standard deviation of the variable is

also shown in each graph. Density is plotted against the curing pressure in Graph 14. It shows a reduction in void content with an increase in curing pressure. The same trend is shown in Graph 15 in the plot of fibre volume fraction versus curing pressure. In the plot of the void content versus the curing pressure in Graph 16, a reduction of the void content occurred as the curing pressure increased. The relationship between the laminate thickness and curing pressure is shown in Graph 17. It indicates that an increase in curing pressure results in a lower laminate thickness.

4.5 THE INFLUENCE OF LAY-UP CONDITIONS *(Experiment 6)*

The results of different lay-up conditions on the laminates prepared in Experiment 6 are summarised in Table 2. The values of the density, fibre volume fraction, void content and the thickness determined from the nine specimens selected from each laminate, along with the standard deviations determined are listed in Appendix A, Tables A10 to A17.

Bar charts are drawn in Graphs 18 to 21 to indicate the effect of different lay-up conditions on the density, fibre volume fraction, void content and thickness of the laminate.

4.6 THE INFLUENCE OF PARTIAL CURE TIME *(Experiments 7 and 8)*

The influence of different partial cure times on the prepreg laminates was initially examined in Experiment 7 as a trial run. This experiment was performed with laminates produced at a large range of partial cure times to determine the effect on density, fibre volume fraction, void content and the thickness. Nine specimens were selected from each laminate and the results with their standard deviations are listed in Appendix A, Tables A18 to A23. The average results for each determined variable are also listed in Table 2.

In Experiment 8, a smaller range of partial cure times was chosen with more points being selected in the range of 0 to 15 minutes partial cure time. Three specimens were selected from each of the five laminates moulded under the same moulding condition. The determined values with the standard deviations of all fifteen specimens (three from each of the five laminates) are listed in Appendix A,

Tables A24 to A30.

In Graphs 22 to 29, standard deviations of the variables (i.e. density, fibre volume fraction, void content and thickness) are taken into account in the plotting of the graphs. The plots of density and fibre volume fraction against the different partial cure times are shown in Graphs 22 and 24 respectively. These graphs indicate reductions in the density and fibre volume fraction as the partial cure time increased. The plots of density and fibre volume fraction against the void content of the laminates are shown in Graphs 23 and 25 respectively. These graphs also indicate reductions in density and fibre volume fraction as the void content of the laminate increased.

The plots of void content and thickness against the different partial cure times are shown in Graphs 26 to 29. These graphs indicate increments in thickness and void content of the laminates as the partial cure time increased.

In the plot of fibre volume fraction versus thickness shown in Graph 30, a best fitted line is drawn through the points. The graph shows an increase in the fibre volume fraction, which results in a decrease in the laminate thickness. For the plot of void content versus thickness in Graph 31, a best line is drawn through the points. It shows that as the void content of the laminates increased, laminate thickness decreased.

4.7 STATIC MECHANICAL PROPERTIES
(Experiments 4 and 8)

The static compressive strength, secant modulus and the failure strain results for the specimens from laminates prepared in Experiments 4 and 8 are summarised in Table 2. The individual results obtained from the specimens, supported by different jigs, are listed in Appendix B, Tables B1 to B8. The static strength properties of the specimens prepared in Experiment 8 are listed in Appendix B, Tables B9 to B11.

The axial compressive strength is calculated using equation 12 (see section 3.11.2). The maximum compressive load was indicated on the digital readout of the testing machine when the specimen failed under the axial compressive load.

The secant modulus is calculated using equation 13 (see section 3.12). The load corresponding to a strain of 0.25% is taken for the calculation of the secant modulus.

The results of the static strength properties obtained by the use of different jigs are shown as bar charts in Graphs 32 to 34. The graphs show greater static

compressive strength is obtained with the use of the Celanese jig but a lower secant modulus is recorded compared with the ABG-1.

The plots of the effect of different void contents on the strength properties in Experiment 8 are shown in Graphs 35 to 37. All the graphs show reductions in the strength properties as the void contents increased.

4.8 DYNAMIC FATIGUE BEHAVIOUR
(Experiments 4 and 8)

The number of fatigue cycles completed by specimens selected from laminates moulded in Experiments 4 and 8 are listed in Appendix C, Tables C1 and C2. Different stress levels were chosen from 45% to 75%. The S/N curves for specimens selected from laminates moulded at different curing pressure in Experiment 4 are shown in Graphs 38 to 41. The individual S/N curves in Graphs 39 to 41 are shown together in Graph 38 to indicate the effect of different void contents on the curves as the number of the cycles increased.

The S/N curves of the specimens moulded at different partial cure times in Experiment 8 are shown in Graphs 42 to 49. Again, the individual S/N curves in Graphs 43 to 49 are grouped in Graph 42 to indicate the effect of different void contents on fatigue behaviour. All the graphs show falling trends in the S/N curves as the number of cycles to failure increased. It is also seen that for laminates with void contents below 1%, the S/N curves are steeper. As the void content of the laminates increased to above 2%, the S/N curves became very flat. Specimens selected from the laminates between 1% and 2% void content showed S/N curves between those for the high and low void contents laminates.

4.9 RESIDUAL MECHANICAL PROPERTIES
(Experiment 8)

The residual strength, secant modulus and failure strain for those specimens which survived through one million cycles in Experiment 8 are listed in Appendix B, Tables B12 and B13.

Graphs 50 to 52 are plotted using the values obtained from the specimens fatigue cycled under 55% stress level and the average static strengths measured on specimens without undergoing dynamic tests are shown for comparison. A reduction in the strength properties is indicated for those specimens which had

fatigue cycled through one million cycles.

The modulus of specimens fatigue cycled at different levels was measured at intervals during the fatigue test. The measured values are listed in Appendix C, Tables C3 to C11. These results are plotted in Graphs 53 to 61 to show the reduction in modulus after fatigue cycling.

The graphs show similar trends for all void content laminates. A rapid reduction in modulus with the number of cycles appeared after about 10,000 cycles, for high stress fatigue cycling (e.g. 70%). At low stress levels (e.g. below 60%), a rapid modulus reduction occurred at about 100,000 cycles.

For the laminates with high void content (i.e. laminates moulded at 30 minutes partial cure time), the modulus reduction occurred earlier after about 1,000 cycles at the high stress level and after 50,000 at the low stress level.

The modulus of those specimens fatigue tested at a 60% stress level to just before failure are listed in Appendix C, Tables C12. These values are used to plot Graph 62 which shows the effect of void content on the modulus of specimens fatigue tested at a 60% stress level.

4.10 MICROSCOPIC OBSERVATION *(Experiment 8)*

Small samples were selected from the laminates moulded in Experiment 8 for microscopic observation. Samples were also sectioned from the test specimens after cycling through 100,000 cycles (50,000 cycles for specimens selected from laminates moulded with 30 minutes partial cure time) and to just before failure at 60% stress level. The preparation of microscopic specimens was in accordance with section 3.13.

4.10.1 Microscopic Observation Prior to Testing

Optical microscopic observation on low void content laminates (i.e. laminates moulded at 0 and 5 minutes partial cure times) showed voids in the form of dark holes of circular shape. They were usually smaller in diameter compared with the carbon fibres and occurred in the resin rich areas, especially in the regions between the individual plies. Small voids also occurred in the fibre rich areas in the fibre rovings but in lower quantity. Besides these, a small amount of large voids occurred in the resin rich areas as large circular holes (Plates 6, 9 and 10).

The observation on 1% to 2% void content laminates (i.e. laminates moulded

with 8 and 15 minutes partial cure times) revealed a greater amount of dark holes within the composite both in the resin rich and fibre rich areas. They appeared to be greater in size, shape, distribution and frequency. These voids tended to be of oval and elongated shape. They were usually present in the regions between the individual plies (Plates 7, 11 to 17).

Observation of the samples selected from high void content laminates (laminates moulded with 12, 20 and 30 minutes partial cure times and above 2% void content) revealed a structure which contained a very large number of dark holes in the regions between the plies. They were mainly elongated and of irregular shape. Cracks which were not present in the low void content laminates also occurred in the fibre rich areas especially in the off-axis plies (Plates 8, 11 to 18).

4.10.2 Microscopic Observation After Fatigue Cycling

The test specimens were removed from the machine once they had completed 100,000 cycles (50,000 cycles for the specimen selected from the high void content laminates) at 60% stress level. Under microscopic observation, the specimen selected from low void content (i.e. 0% to 1%) laminates revealed some cracks in the resin matrix (Plate 24). It is also clear that the number of voids appeared to have increased (Plate 25). However, very little debonding occurred in the regions between the individual plies (Plate 26).

The specimens selected from 1% to 2% void content laminates revealed extensive debonding which occurred between the individual plies. At the same time, broken segments of short fibres appeared in the resin rich areas (Plate 30). This was not apparent in the specimens sectioned from laminates of void contents below 1%.

The specimens selected from high void content (i.e. above 2%) laminates revealed a completely different structure compared with the specimens of lower void contents after fatigue cycling. The specimen under observation was covered with extensive debonding in the regions between the individual plies. Short segments of broken fibres were again observed in the resin rich areas (Plates 27 and 30).

4.10.3 Microscopic Observation Before Failure

The test specimens were removed from the machine once drastic modulus reductions were indicated on the plot of load versus displacement. Samples were sectioned from the test specimens for microscopic observations.

Under microscopic observation, the specimens selected from low void content (i.e. 0% to 1%) laminates showed greater debonding compared with the specimens which had completed 100,000 cycles (Plate 31).

The specimens selected from laminates containing 1% to 2% void contents and laminates with high void content above 2% showed very extensive debonding in the regions between the individual plies (Plate 32). At the same time, kink-bands of buckled fibres also occurred in the specimens. The frequency of these observations increased in the specimens selected from high void content laminates. Segments of broken fibres in the resin rich areas were still observable in the specimens.

CHAPTER 5 DISCUSSION

CHAPTER 5 DISCUSSION

5.1 INFLUENCE OF SOLVENT ADDITION ON VOID CONTENT *(Experiment 1)*

The effect of using different solvents on the void content of Fibredux 913G-E laminates is summarised in Table 2. The density and fibre volume fraction of the pentane sprayed laminate were greater than Freon and water sprayed laminates. The pentane sprayed laminate also consisted of the lowest void content compared with the other two laminates.

It is believed that the high volatility of the pentane solvent (boiling point of 36°C) enabled it to evaporate off quickly when sprayed on the individual sheets before lay-up. This resulted in a 'non-solvent effect' in the laminate. Whereas, Freon (boiling point of 46°C) and especially water (boiling point of 100°C), did not fully escape through evaporation during fabrication due to their higher boiling points. The solvent remaining within the laminate was unable to escape, or only partially escape, during the curing process. This resulted in the formation of void containing laminates after curing.

Many authors [49, 69, 87, 103, 141, 165] claimed that extensive void formation is produced if volatiles are not adequately removed. However, in this experiment, only a moderate void content was obtained. The microscopic observations did not show any obvious voids or porosity within all the laminates. Therefore, it is believed that the use of solvents is not a effective way of obtaining voids in composites.

It can be seen in Appendix A, Table A1, that some negative void content values were obtained for the pentane sprayed and Freon sprayed laminates. These are thought to arise due to experimental errors in density measurement of the composite and variations in the fibre and resin densities as compared with values specified by the manufacturer. The measured density could vary by ±0.14% which in turn could result in an error in void content of ±4.7%. Several methods were used in attempts to verify the densities of the fibre and resin without much success. These included solvent extraction and burn off tests using ASTM C613 and D3171 methods respectively [6, 10]. Therefore, the manufacturer's specification had to be used.

The spread of void content values in the water sprayed laminate was greater than for the other two laminates (see Appendix A, Table A1). This is because water

is not removed uniformly during the cure process. The water vapour nearer to the edges of the laminate escapes more readily than the water vapour in the centre. Therefore, the void content of specimens from the centre of the laminate was higher than for those specimens nearer to the edges.

However, a trend is observed in the results listed in Table A1 (Appendix A). The greater the density of the composite, the higher the fibre volume fraction and the lower the void content. Firstly, this is due to the fact that the density and fibre volume fraction of the composite are directly proportional. As excess resin is squeezed out, the proportion of the fibre increases; therefore, the density of the composite increases (the density of the fibre is greater than the density of the resin). Secondly, as the proportion of voids increases, the fibre and resin volume fractions decrease simultaneously. This in turn leads to a reduction in the density of the composite. The inclusion of volatiles within a laminate leads to more resin displacement, during the curing process, than would otherwise be the case. Further, the compaction process is hindered so that the laminate thickness is greater than would be the case if no volatiles were present.

The experiment showed that both the density and the fibre volume fraction were inversely proportional to the void content. However, only moderate void contents were produced by the addition of solvents and it was concluded that a large quantity of voids could not be produced by spraying solvents on the individual sheets.

5.2 INFLUENCE OF CURING TEMPERATURE ON 914C LAMINATES *(Experiment 2)*

The effect of varying the curing temperature on the density, fibre volume fraction, void content and the ILSS of the 914C prepreg laminates are shown in Graphs 4 to 8.

5.2.1 Density

The plot of density versus curing temperature in Graph 4 shows a non-linear relationship. As the curing temperature increases from 150°C, the density also increases and reaches a maximum at about 165°C. As the temperature increases above 165°C, the density decreases.

The trends show that at a temperature of 165°C, the greatest density was achieved (Graph 4). This temperature is very near to the manufacturer's specified

curing temperature of 170°C. As a laminate is heated up from room temperature to the curing temperature, the resin becomes less viscous and chemical changes occur. The viscous liquid increases in viscosity and becomes semi-solid before turning finally into a solid mass.

At a low curing temperature (e.g. 150°C), resin flow is inhibited and this results in an 'under-cured' laminate as little cross-linking occurs between the molecules. In addition, the viscosity of the resin was too high to allow removal of the volatiles evolved during polycondensation and the entrapped air between the individual plies. The high viscosity also resulted in a resin rich laminate as the resin was unable to flow from the laminate into the bleed cloth on both sides of the laminates. The end result is an undercured, low density laminate with a low fibre volume fraction and a high void content.

At a high curing temperature (180°C), the resin has low viscosity and flows more easily until gelation occurs and the resin begins to increase in viscosity because of crosslink formation. This high curing temperature enables the resin to crosslink before it flows into the bleed cloths leading to a resin rich laminate. These results agreed with those of Yokota [184], who stated that the temperature at which the curing pressure is applied is of the greatest significant. These results also showed that high void content laminates are produced at a temperature below that required for complete volatile degassing and above that at which gelation occurs.

5.2.2 Fibre Volume Fraction

The same trend in Graph 4 is observed in the plot of fibre volume fraction versus temperature in Graph 5. The maximum fibre volume fraction is achieved at about 165°C. As the density and fibre volume fraction of a laminate are directly proportional to each other, it is to be expected that the maximum density and the maximum fibre volume fraction occur at the same temperature.

The plots in Graphs 4 and 5 can be regarded as viscosity plots. The minimum viscosity occurred at the peak on the two plots.

5.2.3 Void Content

In Graph 6, the plot of void content versus temperature shows a minimum at 165°C curing temperature. This is the temperature where the viscosity is the lowest and the flow is easiest.

It should be noted that the laminate moulded at 170°C and at the recommended curing pressure of 2000 kN/m^2 did not produce a void free laminate

as stated by the manufacturer. This is possibly due to batch-to-batch variation in the prepreg properties as well as poor heat up rate during the curing process. This observation coincides with other literature [69, 116, 117] in that adherence to the manufacturer's suggested curing conditions may not always result in void free laminates.

However, the results listed in Appendix A, Table A2, indicate that the void contents measured in the laminate moulded at 170°C were more consistent than the others. This is possibly because the small number of specimens used for the measurement of void contents were not fully representative. The other possibility is that the distribution of voids in laminates moulded at high or low curing temperatures is less uniform. The results also show that the specimens selected at the centre of each laminate had the greater void contents. This is because the resin flow in the centre of the laminate is more difficult compared with that at or near the edges of the laminate.

5.2.4 Interlaminar Shear Strength (ILSS)

Graphs 7 and 8 show the effect of curing temperature on ILSS results. The inversely proportional relationship between the ILSS and the void content, as reported by many authors [4, 103, 110, 185], does not appear in the plots. At the curing temperature of 180°C, the ILSS is in fact the greatest. At high void content (above 3.2%), the ILSS is also among the greatest. One explanation for these results is that the specimens were not really representative of the whole laminate and that the laminates were produced at very similar curing temperatures. More work is required to establish the relationship between ILSS and the curing temperature and void content. The possibility of temperature fluctuation due to the 'on/off controller' may also contribute to scatter in the results.

As a large range of void contents was not produced it was concluded that the attempt to use the cure temperature to control void content was not successful and was not pursued further.

5.3 INFLUENCE OF CURING PRESSURE ON 914C LAMINATES *(Experiment 3)*

The effect of varying the curing pressure on the density, fibre volume fraction, void content and the ILSS of the 914C prepreg laminates are shown in Graphs 9 to 13.

5.3.1 Density

The plot in Graph 9 shows a linear relationship between density and the curing pressure. At low curing pressure, the density is low because it is not possible to squeeze out the excess resin and the entrapped air from the laminate. This was evident in the bleed cloth which showed a negligible amount of absorbed resin. Therefore, the end product is a resin rich laminate with voids occurring between individual plies and within the constituents of the composite.

At a high curing pressure, the resin was forced out parallel to the plies as well as through the plies towards the bleed cloth on both sides of the laminate. However, this did not result in resin-starved laminates because the two layers of bleed cloth became saturated and were not able to absorb further squeezed out resin. Sufficient resin was left within the laminate to effectively fill up the spaces. This demonstrated that a void free laminate can be produced at a properly selected curing pressure and with the correct amount of bleed cloth.

5.3.2 Fibre Volume Fraction

The same trend in Graph 9 is observed in the plot of fibre volume fraction versus curing pressure in Graph 10. This is expected as the density and the fibre volume fraction in the laminate are directly related to each other.

The results listed in Appendix A, Table A3 show that a small increase in curing pressure (300 kN/m^2) causes an increase in density and fibre volume fraction of about 3% to 5%. However, this is not as high as the 10% increase observed by some authors [140]. It is suggested that the different curing schedule may affect the properties of a laminate differently.

5.3.3 Void Content

Graph 11 shows that as the curing pressure is increased, the void content decreases. The results also show a large range of void distribution in laminates moulded at low curing pressures. It is believed that the majority of voids formed in these laminates were due to the air entrapped between individual plies during the curing process.

The laminates moulded at 1630 kN/m^2 and 1960 kN/m^2 curing pressures had high densities and fibre volume fractions with negligible void contents. The negative void contents arise as explained in section 5.1.

5.3.4 Interlaminar Shear Strength (ILSS)

The relationship between ILSS and curing pressure, as well as ILSS and void content of the laminate are shown in Graphs 12 and 13 respectively. In Graph 12, the trend shows that laminates moulded with high curing pressure gave higher ILSS compared with the laminates moulded with low curing pressure. This is expected as low void content laminates were produced at high curing pressure. In Graph 13, the plot shows that as the void content in the laminate increases, the ILSS decreases. This is expected as the voids act as sites of weakness where the shear strength is the lowest. Under the applied force, the plies between the voids shear readily; thus, the low ILSS measured for a high void content laminate.

5.4 INFLUENCE OF CURING PRESSURE ON 914C-833-40 LAMINATES *(Experiments 4 and 5)*

A more detailed examination, using more specimens, of the effect of curing pressure on void content was carried out on the 914C-833-40 woven fabric prepreg laminates. The results are listed in a summarised Table 2 and Appendix A, Tables A4 to A6.

5.4.1 Density

The plot of density versus curing pressure in Graph 14 shows a non-linear relationship as the curing pressure increases above the manufacturer's recommended pressure of 2000 kN/m^2. Above this curing pressure, only a slight increase in density is observed when the curing pressure increases to 3000 kN/m^2 because the 'inherent packing fraction' of the materials restricts further compaction of the plies during the curing process [141]. The density only increased marginally with excess resin being squeezed out until the minimum resin content within the composite had been reached, after which a constant density was maintained under further compaction.

5.4.2 Fibre Volume Fraction

The same trend is shown in Graph 15. As the curing pressure increases, a maximum fibre volume fraction is achieved within the composite. After this point, a constant fibre volume fraction is observed even with further increments of curing pressure.

5.4.3 Void Content

Graph 16 shows a reverse curvature pattern compared to the density and the fibre volume fraction plots. This is due to the fact that at high curing pressures, the volatiles evolved during curing and the entrapped air are forced out of the laminate resulting in lower void content.

These results show that high curing pressures lead to the formation of very low void content laminates, not resin-starved laminates. Excess resin is absorbed by the bleed cloth which eventually becomes saturated and ceases to absorb the resin. A small amount of excess resin flowed out from the open mould at the high curing pressure. Although the laminates were virtually void free, they were badly distorted with great variations in thickness and fibre volume fraction, as listed in the Tables A4 to A6 (Appendix A). The curing pressure was so high that as the resin was forced out of the laminate, it disrupted the fibre alignment which led to this gross distortion of the laminate.

5.4.4 Thickness

The plot of thickness versus curing pressure (Graph 17) shows that as curing pressure is increased, the plies are consolidated more tightly; thus the thickness decreases. Further increments in curing pressure above 2000 kN/m^2 did not cause a linear reduction in thickness and void content (Graphs 16 and 17) due to the 'inherent packing fraction' factor.

The use of curing pressure to control void content was not pursued further as the results were not satisfactory. The main difficulty lies in the precise control of curing pressure during the curing process. Additional problems are that high curing pressures distort the fibre alignment in the laminates and the void content is not great enough for this work.

5.5 INFLUENCE OF LAY-UP CONDITIONS ON 914C-833-40 LAMINATES *(Experiment 6)*

The effects of varying the thickness of the bleed cloth and the use of a metal frame on the density, fibre volume fraction, void content and the thickness of the prepreg laminates are shown in Graphs 18 to 21.

5.5.1 Density

The laminates moulded with a frame and a single layer of bleed cloth on each side of the laminate produced the lowest density while the laminates moulded without a frame and with an extra layer of bleed cloth on each side of the laminate resulted in the highest density (Graph 18). This showed that the bleed cloth effectively extracted resin out of the laminates. With the curing pressure of 3000 kN/m^2, the single bleed cloth on each side of the laminate was saturated before all the excess resin was removed from the laminate. However, with the use of another extra layer of bleed cloth on each side of the laminate, more resin was extracted, leading to a higher proportion of fibres, which results in a greater density of composite.

The laminates moulded with and without a frame but with a single layer of bleed cloth showed that the thickness of the metal frame had some effect on the density. With the same curing pressure applied, the laminate moulded without a frame was virtually free to be compressed until the 'inherent packing fraction' of the laminate was reached. With a frame, the curing pressure could only compress the

laminate to the thickness of the frame. However, the laminate moulded without a frame was badly distorted, especially at the high curing pressure of 3000 kN/m^2.

At high curing pressures and without the use of a frame, different density laminates could be produced by varying the number of layers of bleed cloth. This effect was not observed in laminates moulded at low pressures. The process, in this case, was such that only a limited amount of resin was extracted from the surface plies even though the curing temperature was correct. The bleed cloth contained little resin and served as an extra restriction like the metal frame during the consolidation of the plies.

Generally, the use of a metal frame resulted in laminates of lower density.

5.5.2 Fibre Volume Fraction

Laminates moulded with a frame produced the lowest fibre volume fraction while those laminates moulded without a frame yielded the highest as shown in Graphs 19. However, the laminates moulded at the high curing pressure showed greater variation in the results. This was because the high curing pressure tended to distort the fibre distribution in the woven fabric, i.e. the fibre distribution became less uniform.

5.5.3 Void Content

Graph 20 shows a plot of void content versus curing pressure. The results exhibit large scatter and different trends for the two curing pressures. Generally, the laminates moulded with a frame had lower void contents than laminates moulded without a frame for each curing pressure.

At the low curing pressure, in the presence of a frame, resin was extracted until the laminate was consolidated to the thickness of the metal frame. Whereas, without the presence of the frame, the low curing pressure could only extract resin from the surface plies of the laminate. This led to the slightly higher void content.

At the high curing pressure, the effect of using a frame was more obvious. In the presence of a frame, the curing pressure forced out excess resin and allowed the flow of resin between the individual plies. This resulted in better consolidation of the laminate as the volatiles evolved during polycondensation and the entrapped air was more easily removed; thus a low void content laminate was produced. No further resin extraction occurred when the laminate was consolidated to the thickness of the frame resulting in a constant thickness.

At the high curing pressure, without the use of a frame, excess resin was

squeezed out in an uncontrolled manner. In the presence of the two extra layers of bleed cloth, a resin-starved laminate was produced as the resin was absorbed in greater amount.

It is important to note that although the use of a high curing pressure and a frame during moulding produced lower void contents, this procedure is not recommended in normal practice. This is because at the high curing pressure, there is a greater possibility of fibre distortion and misalignment from the required orientation.

5.5.4 Thickness

Graph 21 shows that thicker laminates are produced when a frame is used. This is because the applied pressure cannot compress the laminate thinner than the thickness of the frame. However, those laminates moulded without a frame are compressed to balance the applied pressure but their shape is distorted, particularly at the edges of the laminate. Therefore, when a frame is not used, there must be a compromise between the laminate thickness and the degree of distortion.

5.5.5 Summary

This work has shown that the number of layers of bleed cloth used influences the density, fibre volume fraction, void content and thickness of the laminates. With extra layers of bleed cloth, too much resin is absorbed from the laminates leading to the formation of resin-starved laminates with higher void contents. This is especially true at high curing pressures. Similar observations have been made by other authors [103, 141], who stated that too much bleed cloth has an adverse effect on laminates leading to high void contents. However, the author agrees with others [165, 170] who have said that varying the thickness of the bleed cloth is not the best way to control the resin content of a laminate or to obtain a void free laminate. This is because excess bleed cloth results in resin-starved laminates with poor mechanical properties due to poor bonding between the fibre and the resin.

The results also show that the use of a moulding frame affects the density, fibre volume fraction, void content and especially the thickness of the laminates. This is due to the fact that a frame restricted the compression of the press. The use of a frame produces a more uniform laminate thickness and restricts the distortion around the edges of the laminate. Therefore, a metal frame of the nominal thickness of the laminate should be used.

5.6 INFLUENCE OF PARTIAL CURE TIME ON 914C-833-40 LAMINATES *(Experiments 7 and 8)*

The heating time interval before pressurisation in the curing cycle is defined as the 'partial cure time'. A comparison was carried out on the two sets of results obtained from smaller laminates (prepared in Experiment 7) and larger laminates (prepared in Experiment 8). The smaller laminates were used only to examine the effect of varying partial cure times on the void content. The larger laminates were used for the measurement of static and dynamic compressive strengths as well as void content.

The effect of varying the partial cure times on the density, fibre volume fraction, void content and the thickness are discussed below under separate headings.

5.6.1 Density

Graph 22 shows an inverse relationship between density and partial cure time (Experiment 7) such that the longer the partial cure time, the lower the density. This is because when the partial cure time is short, the resin viscosity is still low and the resin flows readily. Upon application of the curing pressure, only the excess resin is extracted from between the plies, together with the volatiles evolved during polycondensation and the entrapped air. Therefore, the density of the composite is higher as the ratio of fibre to resin approaches the optimum and the void content is negligible.

When the partial cure time is long, the resin changes its state from a flowable liquid to a highly viscous semi-solid. Consequently little resin, volatiles or entrapped air is extracted from the plies during consolidation. A very thick laminate with high void content between the plies is formed.

The relationship between density and the partial cure time is non-linear. A drastic change in density occurred as the partial cure time was increased from zero to 15 minutes. After this time, further heating caused little change in density because the viscosity of the resin had increased above a critical level.

A similar trend as in Graph 22 is observed in Graph 23 which is a plot of density versus void content for the larger laminates (Experiment 8). The data in Graph 23 is taken from five different laminates at each particular partial cure time. Therefore, the range of results at each particular point reflects the fact that, as well as there being a non-uniform distribution of voids within a laminate, there is also non-uniformity from laminate to laminate.

5.6.2 Fibre Volume Fraction

The plots of fibre volume fraction versus partial cure time (Graph 24) and void content (Graph 25) show the same trends as the plots of density versus partial cure time (Graph 22) and void content (Graph 23). This is as expected because of the directly proportional relationship between density and fibre volume fraction.

5.6.3 Void Content

Graph 26 (Experiment 7) and Graph 27 (Experiment 8) show the relationship between void content and partial cure time. At a short partial cure time, the laminate had a low void content while a higher void content occurred at a longer partial cure time. This is because the formation of a void free laminate depends critically on the resin viscosity at the time of closing the mould [176].

The pressure should be applied when the partial cure time has reached a point when the gelation of the laminate is about to start [165]. At a shorter or zero partial cure time, the resin viscosity is still high as its temperature is low. Upon application of the curing pressure, the entrapped air and volatiles are less likely to escape from the mould. This results in a high void content laminate even though the breathing process is introduced before the final application of the curing pressure. An even higher void content is obtained when the curing pressure is applied at a longer partial cure time. At longer partial cure times, the resin starts to gel before the application of the curing pressure. This results in the formation of a very weak laminate with reduced consolidation of the individual plies. In such circumstances, little or no volatiles or entrapped air are removed and remain trapped within the plies leading to the formation of a high void content laminate.

One interesting phenomenon to note is that the void content of a laminate moulded with zero partial cure time is higher than that of a laminate moulded with 5 minutes partial cure time. During the early stages of the moulding process, the resin temperature increases and therefore its viscosity decreases. In addition, chemical reaction which produces volatiles also occurs. For a zero partial cure time, the resin temperature has not increased and therefore, on application of the curing pressure, some resin flow occurs whilst it is still viscous. This leads to some distortion of the fibre alignment along with entrapment of air and volatiles which contribute to the formation of voids. As the resin temperature increases, it becomes less viscous and is squeezed out into the bleed cloth more readily and without further affecting the fibre alignment. During this stage, some of the entrapped air and volatiles are readily removed with the resin.

For a 5 minutes partial cure time, the resin is already at an elevated temperature when the curing pressure is applied. Therefore, the resin flows more easily and without distorting the fibre alignment. The ability of the resin to flow and the length of time for which it flows are critical factors influencing the void content of a laminate. Clearly, the 5 minutes partial cure time curing schedule means that the resin is under pressure and at a low viscosity for a longer period of time than is the case with the zero partial cure time laminate as this is not prewarmed. In addition, as the temperature increases, volatiles are released. These are entrapped in the zero partial cure time laminate but are more able to escape from the 5 minutes partial cure time laminate prior to the application of the curing pressure.

The author agrees with others [141, 165] that the application of the curing pressure is the determining factor in controlling the quality of a laminate. However, different prepreg materials may have different optimum temperature and time intervals before pressurisation.

It is interesting to note that a drastic change in the void content occurs between zero minutes and 15 minutes partial cure times. This is because gelation starts during this time period and the viscosity of the resin increases drastically. A small delay at this stage could make a moderate void content laminate become a high void content laminate. Therefore, the optimum 'partial cure time' should be used, as during this time, the laminate is heated to its required cure temperature and the resin viscosity decreases.

Generally, both Graphs 26 and 27 show similar trends, although more scatter in the results is observed in Graph 27. The reason that several partial cure times were selected from zero minutes to 15 minutes (Graph 27) was because a drastic change in the void content occurred within this range during the trial run (see Graph 26). Graph 27 shows that the lowest void content with the smallest standard deviation was achieved for laminates moulded at 5 minutes partial cure time. This indicated that 5 minutes is the optimum time for pressurisation. The graph also shows that after this optimum partial cure time, the non-uniformity of void distribution within each laminate increased, even with only a slight increase of partial cure time.

The void content and its standard deviation for laminates moulded with 5 minutes partial cure time was in fact smaller than that of the laminates moulded with zero minute partial cure time (Graph 27). Prior to the optimum partial cure time, laminates of low void content were obtained, although a less uniform void distribution was observed. Above this optimum time, higher void contents, with a less uniform distribution, occurred. Therefore, to obtain the best laminate with more uniform void distribution, the application of the optimum partial cure time is

necessary.

5.6.4 Thickness

Graph 28 shows a relationship between the thickness and partial cure time. Note also the scatter in the results due to the dependence of thickness on the removal of resin, volatiles and entrapped air during the curing process.

One interesting observation was that when a high void content laminate was tapped, an empty sound was heard compared with the solid sound when a low void content laminate was tapped.

Graph 29 shows a similar trend as Graph 28, except that there is more scatter in the results in Graph 29. Graph 28 shows that at a partial cure time of 45 minutes, the thickness of the laminate was reduced. This is due to the fact that once the gel point was reached, prolonging the partial cure time has little effect in reducing the thickness of the laminate. Therefore, a constant thickness was maintained after 20 minutes partial cure time when the gelation was completed. After this partial cure time, any further application of curing pressure was not able to consolidate the individual plies any further as the laminate had already been cured.

5.6.5 Fibre Volume Fraction and Thickness Relationship

Graph 30 shows the plot of fibre volume fraction versus thickness with the standard deviations of both variables indicated. A straight line of negative slope can be drawn through the points of the graph. The laminates produced with low partial cure times were better consolidated resulting in high fibre volume fractions. The thick laminates moulded with long partial cure times were already set in the mould before the application of curing pressure. This led to a higher proportion of voids within the plies resulting in a low fibre volume fraction and a thick laminate with poor consolidation between the plies.

One interesting observation was that the thickness changed drastically from 2.3 mm to 2.6 mm when the partial cure time was increased from 5 minutes to 15 minutes. This showed that this range of partial cure time was crucial and it was at this stage that the curing pressure should be applied. Too early would result in excess resin loss; whereas, too late would result in a highly voided laminate.

Therefore, those partial cure times from 5 minutes to 20 minutes selected in Experiment 8, produced no laminates with thickness between 2.3 mm to 2.5 mm (fibre volume fraction between 0.55 to 0.60). This again showed that the partial cure time (between 5 to 15 minutes) had an effect on the thickness. After being

partially cured for 5 minutes, the volatiles and the entrapped air were not able to be effectively removed, especially the entrapped air between the individual plies. This contributed to the increase in thickness of the laminate. Therefore, it shows that the optimum partial cure time is crucial in order to mould a void free laminate.

Many laminates with thickness between 2.6 mm to 3.0 mm were produced at longer partial cure times (above 8 minutes). This is because little or no entrapped air and volatiles are removed after the optimum partial cure time. Therefore, the thickness of the laminate changed little on application of the curing pressure.

5.6.6 Void Content and Thickness Relationship

The plot of void content versus thickness in Graph 31 shows that the void content changed drastically from about 0% to 2% when the partial cure time was changed from 5 to 15 minutes. Therefore, the partial cure time has a very significant influence on the void content of the laminate. Note that, for the reasons explained in section 5.6.5, no laminates were produced with thicknesses in the range 2.3 mm to 2.6 mm.

Graphs 30 and 31, which are plots of fibre volume fraction and void content versus thickness respectively, facilitate the rapid and non-destructive assessment of laminates simply by measuring their thickness. This simple approach can be very convenient especially when sophisticated equipment is not available. However, the graphs are only suitable for the same type of prepreg laminates stacked in the same configuration as in this work.

5.7 INFLUENCE OF JIG DESIGN ON AXIAL COMPRESSION

The effect of the different jigs on the measured static compressive strength is shown in Graph 32. The Celanese jig gave rise to the highest static compressive strengths for all the specimens moulded under different moulding conditions. However, the Celanese jig gave lower secant modulus values, but higher failure strain as compared to the complete edge supported ABG-1 as shown in Graphs 33 and 34 respectively.

5.7.1 Static Compressive Strength

The fact that the **Celanese jig** gives significantly higher compressive strength suggests that either the jig, the specimen dimensions or a combination of the two have some influence on the compressive behaviour of the material.

When a specimen is gripped in the **Celanese jig**, a triaxial stress field is established in the specimen between the grip faces due to the compressive clamping force of the grip. The influence of this stress field extends not only into the material in the grip region but also into the material within the gauge length. When the uniaxial compressive force is applied to the **Celanese jig** (and the specimen) during testing, another triaxial stress field is superimposed on the field already existing in the specimen. Detailed analysis of the stress fields would be required to establish the nature and extent of the interaction between those fields. However, it is clear that the region of the specimen that is under the influence of only the applied compressive force is somewhat less than the gauge length of the specimen.

A further point to consider is the constraining effect of the grips. When a compressive force is applied to a specimen, the length decreases in the direction of the applied force. This is accompanied by an increase in the cross-sectional area of the specimen. Such increases are constrained in the regions near the grips. Detailed analysis of the behaviour of the specimen would be required to quantify this effect. However, it is clear that forces other than those uniaxially applied have some influence on the behaviour of the material within the gauge length.

The design of the **Celanese jig** specimen with a gauge length of 12.5 mm is a compromise between the need to eliminate buckling of the specimen and to minimise grip effects. It is possible that a large proportion of the short gauge length is not solely under the influence of the uniaxially applied compressive force. In contrast, in tests using the **ABG-1**, **ABG-2** and the **CRAG jig**, the specimen is less constrained with a gauge length of 110 mm.

Another potential problem is related to the construction of the **Celanese jig**. Split collet assemblies are used to grip the specimen. Each grip assembly is located inside a tapered conical sleeve and there should be a matching fit between the grip and its sleeve. This is only achieved if the collet, when holding the specimen, is perfectly circular. Therefore, the thickness of the gripped part of the specimen (i.e. the end tabs, adhesive and the specimen) must be closely controlled. Any deviation from the required thickness results in a mismatch between the collet and its enclosing sleeve. This leads to point contacts between the collet and sleeve which in turn leads to high frictional forces between them. This frictional force is reflected in the indicated failure force for the specimen; thus, the failure force is overestimated.

This results in the compressive strength and secant modulus being overestimated.

Hofer et al [79] were critical of the **Celanese jig** and highlighted the problems of specimen slippage, the tendency for buckling to occur and friction within the jig. They pointed out that although there is no physical constraint on the gauge length of the specimen, the grip effect on the short gauge length is significant and leads to high compressive strength values.

The other three anti-buckling guides, namely **ABG-1, ABG-2** and the **CRAG jig**, gave similar compressive strength values but all of them were lower than the values obtained from the **Celanese jig**. Although a grip effect exists in the region of the specimen near the grips, its influence is not as significant because of the long gauge length. In the centre part of the gauge length, the grip effect is relatively small compared to the stress field arising from the applied force. When the uniaxial force is applied to the specimen, the stress field established in the gauge length causes the specimen to fracture under axial compression along a shear plane. It was found that specimens supported by these three types of jig had lower strength values compared with the specimens supported in the **Celanese jig**.

Both the **ABG-2** and **CRAG jig** gave similar compressive strength values independent of the origin of the specimens used. The **ABG-2** design included two windows in the middle of the guides with a depth equivalent to the critical Euler buckling length with a safety factor of 2.5. The gauge length of the specimen within the windows is free from any constraint from the guide. At the same time, buckling of the specimen is also prevented. The same principle applied for the **CRAG jig** which also prevents buckling without restricting the specimen from axial compression under the applied force. This indicates that the area of unsupported gauge length within a guide is not critical as long as buckling of the specimen during compression is prevented.

5.7.2 Secant Modulus

The calculated secant modulus of specimens supported by the **ABG-1** were higher than those obtained using the **Celanese jig**. This is because the small windows on the **ABG-1** caused constraint on the area of the specimen around the windows. To determine the secant modulus, the strain on the specimen was measured using strain gauges on both sides of the specimen. The gauged areas were constrained by the windows in the **ABG-1**. Therefore, the strain is lower in this region than it would be in an unconstrained situation as in the **Celanese jig**. This lower measured strain leads to a high value for the secant modulus.

In the case of the **Celanese jig**, the gauge length of the specimen is free

from any contact with the jig. Therefore, the calculated secant modulus is more representative of the material in the region of the strain gauge.

5.7.3 Failure Strain

The results show that the measured failure strain of a specimen supported by the **ABG-1** is lower than for those specimens supported by the **Celanese jig,** although there is considerable scatter in both sets of results. The gauge length of the **Celanese jig** specimen is so short that the site of failure is very likely to be located near to the strain gauges (length of sensitive element of strain gauge is 5 mm). In contrast, the gauge length of the specimen used for the three others types of jig is so long that the strain gauges may be far away from the failure site. This will result in a registered strain somewhat lower than that at the failure site. This effect was shown in the tests on specimens prepared under 1960 kN/m^2 curing pressure. Four of the six specimens used for failure strain measurement in the **ABG-1** failed within or near the gauged area. Therefore, this set of specimens gave high failure strain values compared with a similar set of specimens tested using the **Celanese jig.**

5.7.4 Remarks

As observed by other authors, the **Celanese jig** gives relatively high strength values [79, 104]. The coefficient of variation of the strength results from the **Celanese jig** are also higher as shown in Appendix B, Table B1. The **ABG-1** gives high stiffness results as there is greater constraint on the specimen at the area around the windows.

The use of an **ABG-2** or **CRAG jig** seems to be more appropriate in this work as both jigs give fairly uniform compressive strength values. More work needs to be done in this area to investigate the effect of these two jigs on the secant modulus and failure strain.

5.8 TYPES OF VOID

Different types of void present in a laminate can be classified by their quantity, distribution, frequency and shape. The different types of void observed are listed in Figure 13.

Laminates with void contents of less than 1% (see Plate 6), such as those moulded under 0 and 5 minutes partial cure time, contained the following types of void:

- microporosity within the rovings;
- microporosity between the rovings;
- interstitial voids.

Other forms of void were also present but in a much smaller quantity:

- macropores within the rovings;
- macropores between the rovings.

Laminates having void contents of 1% to 2% (see Plate 7), such as those prepared with 8 and 15 minutes partial cure times, contained the following types of void:

- macropores within the rovings;
- macropores between the rovings;
- interface voids;
- interlaminar voids;
- interroving voids.

They also contained a minority of:

- microporosity within the rovings;
- microporosity between the rovings;
- interstitial voids.

Laminates having void contents of more than 2% (see Plate 8), such as those prepared with 12, 20 and 30 minutes partial cure times, consisted mainly of the following types of void:

- macropores within the rovings;
- macropores between the rovings;
- interface voids;
- interlaminar voids;
- interroving voids;
- thread voids.

These laminates contained little or none of the following types of void:

- microporosity within the rovings;
- microporosity between the rovings;

- interstitial voids.

One other interesting feature is the presence of the translaminar cracks together with the above mentioned voids. They are also discussed here as they existed prior to any mechanical testing although they were not caused by the same factors which caused the formation of voids.

5.8.1 Micropores Within and Between the Rovings

These two types of micropore occur mainly in low void content between 1% and 2% laminates (see Plate 9). As the total void content within the laminate increases, the number and distribution of these micropores decreases. Eventually, these types of void are totally replaced by other types as the void content increases further.

These micropores are believed to be caused by volatiles and entrapped air during the fabrication of individual plies. These two sources of void formation could be reduced but not completely removed from the laminates. The other main cause of such voids is believed to be the presence of imperfections within the laminates as discussed in section 1.3. In the manufacturing of FRP composites, primary defects, such as the presence of imperfections cannot be removed as their presence is inherent within the materials. However, secondary defects, such as the entrapped air and volatiles can be minimised under very carefully controlled processing. Therefore, these micropores were only present as a result of imperfections inherently present in the prepreg materials.

These two categories of porosity tend to be found in inter-fibre regions, e.g. at the resin rich areas (see Plate 10), which occur between and within rovings of the woven fabric, especially at the cross-over points. This is because the resin contains a mixture of different solvents added to ease the fabrication and wetting processes. The bubbles entrapped during processing cause the formation of the porosity within the resin rich areas.

The micropores tended to be spherical with a diameter of about 5 μm or less, which is smaller than the 8 μm diameter carbon fibre filaments. The spherical shape was believed to be caused by the surface tension in the individual bubbles entrapped within the resin rich areas.

5.8.2 Interstitial Voids

The interstitial voids are believed to be caused by inadequate resin flow between fibres in the fibre rovings, as they mainly occurred in the fibre rich areas. This is another form of void caused by imperfections in the prepreg materials as the wetting of the fibre rovings by the resin, especially high viscosity resin, is very difficult. The incomplete wetting of the fibres within the fibre rovings leads to the presence of entrapped air. Surface tension effects give rise to the formation of the spherically shaped voids. The interstitial voids are small and like those observed in the micropores between and within the rovings, measure 5 μm or less.

The amount and frequency of the interstitial voids decreased as the void content increases within a laminate. They are believed to be replaced by other types of voids which are discussed in the following sections.

5.8.3 Macropores Within and Between the Rovings

These two kinds of macropore are believed to result from the growth of the micropores within and between the rovings. They are caused by the agglomeration of neighbouring voids as well as the diffusion of air. As their original forms were the micropores within and between the rovings, they mainly occur in the resin rich areas between the fibre rovings (see Plates 11 and 12).

The shapes of the macropores are cylindrical or oval. Their length ranges from a fibre diameter (8 μm) to about 100 μm in the laminates having 1% to 2% void content. This cylindrical shape is believed to be due to the agglomeration of the voids while trying to escape to the edges of the laminate during the curing process.

The shape and size of the macropores increased as the void content increased. Their size ranged up to 500 μm and could occupy large regions of the resin rich areas.

However, in low void content laminates, few macropores existed. This is because the curing procedure enabled more thorough removal of entrapped air and volatiles.

5.8.4 Interface Voids

The interface voids are believed to be caused by the coalescence of interstitial voids within the fibre rovings in the fibre rich areas (see Plate 13). They may be formed by the growth of interstitial voids as the void content of the laminate increases.; thus, laminates moulded with 0 and 5 minutes partial cure times did not

show this kind of void. However, their amount and frequency increased in high void content laminates and their size ranged from a fibre diameter to about 50 μm. In general, interface voids were smaller in quantity and size as compared with the macropores within and between the rovings.

5.8.5 Interlaminar Voids

The interlaminar voids usually occurred at the fibre-matrix interface, especially at the off-axis plies between 0° and 90° plies (see Plate 14), +45° and -45° plies (see Plate 15). The presence of the fibres within the individual plies causes the voids to orientate in the direction of the fibre axis and they are therefore elongated and narrow in shape, rather than spherical like the micropores within and between the rovings. These voids are believed to be caused by the air entrapped between each ply during the lay-up not being able to escape effectively during the curing cycle. Their size varied depending on the void content of the laminates. Usually, their size ranged from about 50 μm and above.

5.8.6 Interroving Voids

Interroving voids formed mainly in the vicinity of misaligned fibres where laminate compaction was restricted. They are found in the resin rich areas between rovings, particularly at the fibre cross-over point in the woven fabric (see Plate 16). They are believed to be caused by the entrapped air and volatiles which did not escape during the curing process. Their size was in the range of 50 μm and above and they were usually elongated and cylindrical in shape.

This type of void does not occur in the low void content laminates but does occur in the high void content laminates especially those with void contents above 2%. It was observed that the macropores within and between the rovings were replaced by the interroving voids as the void content increased.

5.8.7 Thread Voids

The thread voids only occurred in laminates having void contents above 2%. These voids occur within the rovings especially at the fibre rich areas (see Plate 17). Under microscopic observation, they showed a tendency to link macropores between the rovings. This phenomenon could be explained by the agglomeration of neighbouring voids at the boundary of the fibres within the rovings. This causes the formation of a thread-like structure in a similar way to the formation of interroving

voids. These thread voids are usually perpendicular to the fibre direction in the rovings.

It is believed that entrapped air and volatiles within rovings could only escape by the formation of these thread-like structures. They tend to travel towards the surface and the edges of the laminate using the shortest path during the application of the pressure. Under long partial cure time, the resin is very viscous and flow is restricted. Thus, the thread voids had no chance to extend to the edges of the laminate and their contents remained within the rovings.

5.8.8 Translaminar Cracks

Translaminar cracks only occurred in laminates with void contents above 2%. These translaminar cracks are not a type of void and are believed to be caused by the application of the pressure when the resin is beginning to gel. The force on the compression mould is believed to cause internal gross cracking within the laminate as reported by other authors [135, 141, 176]. The cracks are formed in the laminate direction and often in fibre rich areas. The irregular cross-over points between fibre rovings locally disrupt the effect of symmetry and contribute to the setting up of sufficient shear stress to cause cracking in the laminate direction.

The cracks usually occur in closely packed fibre areas which are themselves surrounded by resin rich areas (see Plate 18). These are believed to be the weakest sites within the laminates. Poor wetting of the fibres during the long partial cure times contributes to the ease of crack formation when the pressure is applied during moulding. Thus translaminar cracks are only present in high void content laminates of 2% and above.

Lee and McGarry [103] stated that residual stresses, induced during cooling of the laminate to room temperature, give rise to the development of translaminar cracks during postcuring. However, the current work shows that no translaminar cracks develop in low void content laminates. It is therefore suggested that in high void content laminates, cracks are initiated at the voids during the curing process. The subsequent postcuring process allows the cracks to propagate under the influence of the residual stresses induced during the cooling of the laminate.

5.9 AXIAL COMPRESSION OF 914C-833-40 LAMINATES *(Experiments 4 and 8)*

Axial static compressive strength tests were carried out on specimens moulded under different curing pressures (Experiment 4) and different partial cure times (Experiment 8). All the specimens failed in a compressive failure mode randomly along the gauge length of the specimen. There was scatter in the results as expected as the variation of void content within each laminate was great. The static compressive strength, the secant modulus measured at 0.25% strain and the failure strain showed that the presence of voids within the composite affects the mechanical strength properties even when they are present in small quantities.

5.9.1 Effect of Voids on Static Compressive Strength

The bar chart of the effect of varying curing pressures on the static compressive strength (Experiment 4) is shown in Graph 32. For all the types of anti-buckling guide used during compression testing, the specimens moulded under a low curing pressure of 653 kN/m^2 gave the lowest static compressive strength and the specimens moulded under the manufacturer's recommended curing pressure of 2000 kN/m^2 gave the highest strength values. This was because the specimens moulded with low curing pressure had the greatest void content. Whereas, specimens moulded at high curing pressure had lower void contents. This proved that the presence of voids, no matter how small the quantity, can significantly affects the strength properties.

The effect of different void contents on the static compressive strength (Experiment 8) is shown in Graph 35. The same trend is again observed, i.e. as the void content increases, the static compressive strength decreases.

The linear relationship between the static compressive strength and the void content within this composite can be represented as follows:

$$S = 360 - V_v * 3.2 * 10^3 \qquad \text{equation (14)}$$

where

S = static compressive strength (MPa)

V_v = void content in volume fraction

It is believed that the presence of voids within the composite act as sites of stress concentration. During axial compression of the specimen, the voids are compressed and will tend to elongate in the plane perpendicular to the loading axis. This is especially true for micropores and macropores within and between the rovings (laminates of void content less than 2%). These voids are mainly spherical or oval in shape. Thus, these micropores and macropores will take an elliptical shape and there will be stress concentration in the perpendicular plane. These sites, especially in the interlaminar regions of the plies are sites where crack initiation is likely. As a greater number of voids are present in high void content laminates (void content greater than 2%), there will be more interaction between these sites of high stress concentration. If the elongated and cylindrical interroving and interlaminar voids are present in the direction of the axial compressive force, less force will be needed to initiate cracks in the perpendicular plane of the voids as the stress concentration at these voids will be higher than in the spherical micropores and oval macropores. Once the cracks are initiated in these voids, a plane is developed which acts as a site of weakness and becomes the shear failure plane. Therefore, high void content laminates (void content greater than 2%) exhibit premature failure with the failure strength very much lower than in those good laminates having lower void contents of less than 1%.

The results also show that the low void content laminates moulded at 5 minutes partial cure time (void content of 0.22%) gave the greatest compressive strength. It is suggested that a low quantity of voids can act to relieve the stress built up during compression. This stress redistribution within the test specimen resulted in higher compressive strength. They also showed a lower coefficient of variation in the results compared with laminates moulded at 8 to 15 minutes partial cure time (void content of 1% to 2%), even though the difference in the partial cure time is very small. This was because at 8 to 15 minutes partial cure time, the resin viscosity is low enough to cause sufficient bonding between the individual plies. However, it was insufficient to allow the complete removal of volatiles and entrapped air from between the plies. This high resin viscosity does not allow the volatiles and the entrapped air to further progress towards the edges of the laminate; thus resulting in a greater variation of void distribution within the laminate. Since the specimens selected for static compressive strength testing were randomly chosen from each laminate, a greater variation in strength values was expected from the specimens selected from the laminates within this range of partial cure times.

5.9.2 Effect of Voids on Secant Modulus

In the plot of secant modulus versus void content shown in Graph 36, the results show that as the void content increased, the secant modulus is decreased. This is because the voids act as sites of weakness within the test specimen. Under the applied compressive force, gross cracking develops from these areas. These cracks propagate rapidly throughout the whole structure of the test specimen, linking together whilst propagating. As the number of voids increases, crack initiation and propagation from these areas occurs rapidly and with ease since more sites are present for crack initiation. Therefore, a lower secant modulus is detected for high void content laminates (void contents above 2%).

It is suggested that voids also act as heat accumulation points. It can be a subsidiary effect since voids are also poor heat conductors. During compression, friction occurs in the interlaminar regions. Heat builds up at the voids and reduces the shear modulus of the matrix surrounding the voids. This in turn leads to microbuckling of the individual fibres, especially for fibres nearer to the sites of the voids. Under the compressive force, the weakest fibres fail initially. Together with the gross cracking develops from the voids, the specimen fails non-progressively. As the number of voids increased, more heat build up occurs in these areas. The matrix shear modulus is further reduced along with more fibre microbuckling occurring. Therefore, a lower secant modulus is detected for high void content laminates.

5.9.3 Effect of Voids on Failure Strain

The plot of failure strain versus void content is shown in Graph 37. There is a large scatter of results with a very high standard deviation for each value.

It is suggested that the failure strain decreases as the void content of the laminate increases. For a high void content laminate (void content above 2%), the presence of a large quantity of voids results in areas of high stress concentration, especially in the matrix surrounding the voids as explained in section 5.9.1. Such a specimen subjected to an axial force does not need a large deformation before catastrophic failure occurs.

As for the specimen with void content of 1% to 2% within the structure, more deformation is believed to occur in the voids before cracks are initiated and propagated from these sites. Therefore, a higher failure strain was observed in these laminates.

The low failure strain recorded in good laminates (void contents less than 1%)

suggested that the specimens selected from these laminates behaved more like homogeneous materials. Once cracks are initiated from the small micropores, no large deformation occurs as the cracks propagate in a shear failure plane. Therefore, a low failure strain was also observed in good laminates with void contents less than 1%.

The considerable scatter in the results is believed to arise because of the random failure along the long gauge length of the specimen. If the failure occurs away from the gauged area, the failure strain detected is lower than it would be if the gauge was at the actual site of failure. Therefore, the local strain as measured by the strain gauge is dependent on the local properties of the laminate.

5.9.4 Failure Mode in Axial Compression

All the specimens tested under axial compression failed within the gauge length although the majority failed nearer to the ends of the gauge length than the centre. The compressive strength values obtained show no correlation with failure position indicating that end effects (i.e. grips, end tabs, etc.) do not influence the test results.

The specimens failed in two modes under axial compression. They either fractured at approximately 45° to the direction of axial force or they showed a V-notched type failure (see Plates 19 and 20), with the former being the more common type of failure mode. The 45° shear plane arises due to a band of fibres buckling under shear compression deformation. The V-notched shape type failure is believed to be caused by each ply failing in the shear mode with adjacent plies failing in opposite directions. These shear failures in each ply meet at regions containing long fibres, which are the 0° plies in the centre plane of the laminate, to form the V-notch [20, 67]. This type of failure mode is less frequent and was believed to require greater compressive force to cause the V-notched shape.

It is interesting to note that the low void content specimens (void contents less than 1%), moulded under low partial cure times, failed in a different way to the high void content specimens (void content above 2%), moulded with longer partial cure times. For the low void content specimens, the specimen broke into two separate pieces at the fracture surface (see Plate 21). However, for the high void content specimens, cracking was heard at an early stage and they failed with the two separate pieces of the specimen still adhering loosely together at the fractured surfaces (see Plate 22). For the high void content specimen, the individual plies were relatively lightly bonded to each other due to the presence of a high quantity of interlaminar voids between the individual plies. During compressive loading,

brooming of the fibres occurred at these sites and the specimen fractures like a bunch of dried fibres. A post failure damage effect is believed to cause the plies to interlink at the fracture surfaces and attach the fractured plies together.

5.10 THE EFFECT OF VOIDS ON FATIGUE BEHAVIOUR

In order to examine the nature of the fracture in the carbon fibre woven fabric prepreg laminates, microscopic observations were carried out on the specimens moulded at different partial cure times (Experiment 8). Specimens were taken from the untested laminates, test specimens fatigued to 100,000 cycles and test specimens fatigued to just before failure. The fatigue specimens were compared with the untested specimens to observe any changes.

Microscopic observations were carried out using both the optical microscope and the SEM. These observations revealed a complex system of voids and cracks. A fatigue failure mechanism is proposed in order to explain the failure behaviour observed for the prepreg laminates. It should be noted that fatigue failure mechanisms are influenced by the type of the constituents in the composite, the stacking sequence, the weave pattern, specimen geometry and many other factors. The proposed hypothesis is based on this work on carbon fibre woven fabric prepreg laminate with a $(0/90,+45/-45,+45/-45,0/90)_{2S}$ stacking sequence. Failure modes such as matrix damage, void growth, interlaminar debonding, and fibre failure are observed and discussed in the following sections.

5.10.1 Matrix Damage

Damage to the matrix was in the form of matrix cracking. The development of this type of damage can be subdivided into crack initiation and crack propagation. Local imperfections, voids and the resin rich areas act as sites of crack initiation (see Plate 23) as stated by several other authors [14, 36, 46, 128, 135].

In laminates moulded at low partial cure times and having low void contents in the range 0% to 1%, there were micropores within and between the rovings, interstitial voids and resin rich areas. All these are poor thermal conductors compared with the carbon fibre and therefore the rate of heat dissipation from these areas is less than in those areas containing a more uniform distribution of carbon fibres. Under continuous fatigue cycling, heat is generated by elastic deformation processes and hot spots develop at the areas mentioned above. This heat build up (1-2°C recorded) may be a contributory cause to the development of fatigue cracks

in the matrix in those areas nearer to the voids.

Microscopic observation revealed that the cracks usually initiated near the surface of those voids present in the off-axis 90° and ±45° plies, especially in the resin rich areas (see Plate 24). This observation has been reported by several authors [65, 75, 122, 129, 169] in their work. It is believed that cracks initiate from these sites because the transverse 90° plies are subjected to the greatest shear stresses during the compression fatigue cycle. Under continuous fatigue cycling, the cracks begin to grow and propagate. The microscopic observations showed that the cracks propagated in both lateral and longitudinal directions. Basically they travelled by the easiest path and were only slowed down at the interlaminar region of the matrix and the fibres. Sometimes, crack tip blunting changed the crack growth direction before propagation continued.

Some authors [46, 135] have suggested that cracks are initiated at the surface of the laminate and propagate towards the plies. The microscopic observations in this work showed that cracks initiate near the surface in the 90° plies and spread to the specimen surfaces.

No observable matrix cracks occurred in high void content laminates of above 2% voids in the specimens fatigue cycled 50,000 times at a 60% stress level.

5.10.2 Void Growth

Void growth is believed to start at a very early stage of fatigue loading. It is believed that it starts at about the same time as the matrix cracking.

It is interesting to note that in specimens with void contents between 1% and 2% after cycling through 100,000 cycles, the numbers of macropores between and within the rovings, as well as the interface voids has increased compared with the untested specimen (see Plate 25). This is believed to be caused by a small quantity of micropores between and within the rovings expanding to form macropores between and within the rovings and the interstitial voids which expand to form the interface voids. However, void growth did not occur in high void content laminates. This may be due to the laminate having a large quantity of interroving, interface and interlaminar voids which occupy nearly all the interlaminar regions of the laminate; thus, there is no motivating force for the voids to expand in these areas.

The void growth mechanism and its influence on failure behaviour has been discussed by very few authors. Novadansky et al [124] described void growth in general terms. It is believed that void growth is one of the modes of fatigue failure damage but it is usually overshadowed by the presence of other failure modes. Void

growth is more obvious in low void content laminates (i.e. void contents between 0% and 1%), as the laminates do not consist of a large variety of voids which would otherwise mask the occurrence of void growth.

5.10.3 Interlaminar Debonding

Interlaminar debonding in the regions between individual plies occurred at a relatively early stage under fatigue loading. This appears to be the most prevalent matrix dominated failure mode in multidirectional laminates, as reported by Gerharz [57]. The debonding process extends throughout the interlaminar regions between the individual plies. Interlaminar debonding in less than 1% void content laminates (see Plate 26) was not as extensive as in the high void content laminates (void contents between 1% to 2% and above 2%) after cycling through 100,000 cycles and 50,000 cycles (see Plate 27) at a 60% stress level respectively. Matrix damage was the dominant failure mode in the low void content laminates with isolated debonding occurring at the boundaries of 0^{o} and 90^{o} plies, as well as the boundaries of $\pm 45^{o}$ plies. This was because the low void content laminates had stronger bonds between individual plies. Very few obvious voids exist between the plies and therefore cracks cannot easily join and cause interlaminar debonding. Isolated and localised debonding occur frequently at interlaminar regions in high void content laminates as shown in specimens obtained from laminates having void contents of 1% and above.

In high void content laminates, i.e. those having void contents above 1%, no obvious matrix cracks occurred which is in contrast to the low void content laminates. This is because in high void content laminates, under continuous fatigue loading, cracks initiate in macropores between rovings, interface voids, interroving voids and interlaminar voids. In particular the macropores between the rovings and the interlaminar voids grow and join rapidly, which gives rise to interlaminar debonding along the regions between the individual plies. Microscopic observation revealed that debonding occurs between the individual plies along the weave pattern of the fibre rovings. Therefore, the presence of micropores in the resin rich areas of low void content laminates resulted in matrix cracking, while the presence of macropores between the rovings in high void content laminates resulted in interlaminar debonding.

It is believed that in multidirectional laminates having low void contents, matrix cracks occur in the off-axis plies during the early loading cycles and increase in density with the number of cycles until a stable crack density for a particular configuration is reached. Once a stable crack density is achieved, no further matrix cracks occur during continuous fatigue loading. Instead, interlaminar debonding is initiated and continues at an increasing rate. For the high void content laminates, the initiation of cracks quickly develops into interlaminar debonding and spreads throughout the specimen.

In high void content laminates, the presence of the micropores between and within the rovings are only cosmetic. The macropores between and within the rovings, interlaminar voids and other macrovoids discussed in section 5.8 are the main sites of damage in the composite structure. This damage takes the form of cracking and debonding along the interlaminar region.

5.10.4 Fibre Failure

The repeated application of a fatigue load continuously in sinusoidal form leads to an increasing displacement in the specimen. The specimen strength properties change as a result of damage propagation. Thus, the specimen becomes more compliant as shown in the stress-strain curves.

Under continuous fatigue cycling for specimens having 1% to 2% void contents, matrix cracking and interlaminar debonding cause local internal friction between the individual plies which in turn results in heat build up within the body of the specimen. This process continues until a stage is reached where the matrix shear modulus is reduced to a sufficiently low level to permit local buckling of the fibres in random fashion (see Plate 28). This has been observed by many authors [32, 40, 75, 144, 148] in their specimens after fatigue cycling. In addition to local heat build up, there are local imperfections of the fibres (non-uniform diameter, etc.). If the imperfections and heat build up occur in the same area, then fibre failure will be further enhanced; thus, fibre buckling occurs at much lower apparent stress levels in these areas.

As the carbon fibre itself is very brittle, the buckled fibres break and produce a gap (slot) in the isolated fibre rovings within the composite. This newly created gap itself is a bad conductor of heat. The heat further accumulates around this gap during fatigue cycling and any fibres in this region are increasingly likely to buckle.

The failure of the fibres occurs in a step-wise mode to produce a kink-band formation as observed under the microscope (see Plate 29). This kink-band appears with its plane oriented at approximately 45º to the compressive load. The frequency

of kink-band formation was greater in the high void content laminates (void contents above 2%).

One interesting phenomenon observed in the damage zone of the high void content laminates is short segments of fractured fibres which appeared as though they had 'flowed' into the resin rich areas (see Plate 30). This was also observed by Evan [50] in his work. However, this phenomenon is not observed in the low void content laminates (void content below 1%). This is believed to be caused by fibre buckling that produces areas of broken segments of fibres at the kink-band interface. Heat build up in this area creates a reduction in the matrix shear modulus which results in thermal creep of the matrix. During compression, the broken segments of fibres are forced out from the damage zone into the resin rich areas where restriction by surrounding fibres is low. This phenomenon is not observed in the low void content laminates because of the low number of isolated and random fashion fibre failures which occur.

Fibre failure continues to spread throughout the structure of the composite with many damage sites contributing to both the strength and modulus degradation. As the number of damage sites increases, a state is developed where the next applied compressive load will cause the agglomeration of many damage sites to form a dominant defect which leads to catastrophic failure.

5.10.5 Final Failure

The final failure occurs quite rapidly as the composite is so badly damaged that catastrophic failure occurs by crack propagation linking several damage sites. It is believed that the specimen fails during the compressive half of the cycle rather than the 'decompressive' half of the cycle. This is because as the specimen is loaded from the zero load of the cycle to the maximum compression load, the structure is so degraded that catastrophic failure results and any strain energy not used in the creation of fracture surface is released in other forms (e.g. heat, sound, etc.). This final failure occurs very suddenly and randomly along the gauge length of the specimen, accompanied by audible cracking. Plates 31 and 32 show the specimens selected from laminates moulded with 5 and 30 minutes partial cure time after cycling to just before failure.

It is interesting to note that microscopic observation of the specimens cycled to one million cycles show a damage structure containing many isolated and localised damage sites (see Plates 33 and 34). Interlaminar debonding is observed over almost the entire interlaminar region between the individual plies. These damage sites give rise to visible cracks in the specimen. However, the specimens

were still able to hold together as a structure and completed one million cycles without failure. Obviously damage did not lead to immediate failure. Damage sites may grow and extend along the boundary so as to relieve the stress concentration on the fibres in compression loading. Even though the separation of the rovings by interlaminar debonding weakens the composite, the residual strength of the specimen enables it to withstand the fatigue loading until a damage state occurs such that the applied load is greater than its residual strength. This highlights one of the advantages of FRP over homogeneous materials. Whilst structural integrity is retained within the body of the composite, the fibres provide a stress relief route when an applied load is experienced by the composite. This remains the case until the integrity of the structure deteriorates such that applied forces are not transferred to the fibres.

5.11 DYNAMIC COMPRESSIVE BEHAVIOUR

The fatigue behaviour of specimens moulded at different curing pressures (Experiment 4) and specimens moulded with different partial cure times (Experiment 8) is presented in stress/log cycle curves. At least fifteen specimens were randomly selected from each moulding condition to conduct fatigue tests. All the specimens failed in a typical compressive failure mode, randomly along the gauge length of the specimen with some scatter in the fatigue life.

5.11.1 Frequency

The frequency used in this experiment was chosen as 5 Hz as this allowed fatigue of the specimens without causing undue secondary heating. Some authors [25, 44] have indicated that increased frequency results in shortened fatigue life. Heat builds up within the specimen due to hysteresis. The higher the frequency, the less able is the specimen to conduct the heat away. In order to monitor the situation in the current work, thermocouples were connected on both sides of the specimens to measure any temperature change over a two-day period. It was shown that after an early increase of 1°C to 2°C, the temperature remained constant throughout the test; thus, the heating effect of testing at 5 Hz is assumed to be minimal.

5.11.2 Specimen Geometry

All the static and fatigue tests were carried out on parallel-sided specimens. The specimens failed randomly along the gauge length with some failure near the end tabs but none within the end tabs. This differs from the findings of Curtis et al [63], who stated that parallel-sided specimens, when tested at a frequency of 5 Hz, may fail within the end tabs. The fatigue results showed that the number of cycles to failure was independent of where the specimen failed.

5.11.3 Effect of Voids on the S/N Curves

The results of fatigue tests at different stress levels are presented in graphs of stress (S) versus the logarithm of the number of cycles to failure (log N) and are referred to as S/N curves. The S/N curves of laminates moulded in Experiments 4 and 8 are shown in Graphs 38 to 41 and Graphs 42 to 49 respectively.

All the S/N curves showed an increase in slope as the number of cycles to failure increased. The specimens selected from laminates of low void content showed much steeper slopes compared with the specimens selected from laminates of high void content (see Graph 42). However, this trend does not show very clearly in Graph 38, which gives similar slopes for the three laminates prepared in Experiment 4. This is because the void content variation between these three laminates is very small.

The low void content laminates showed steeper S/N curves in Graph 42. This suggests that matrix cracking and void growth are the two main failure modes during the early stages of fatigue cycling of low void content laminates. These two main modes of failure lead to the development of an initial crack density within the specimen. Once this is achieved, then interlaminar debonding can occur (see section 5.10.3).

At high stress levels, the low void content specimens can survive a much greater number of fatigue cycles compared with high void content specimens. At lower stress levels, more time is required for crack initiation and formation of the critical crack density within the structure before the interlaminar debonding can begin. Therefore, more cycles to failure will result. However, compared with high void content laminates (above 1%), the increase in the number of cycles at low stress levels is not marked. It is suggested that, in the early stages, matrix cracking is the dominant failure mode for low void content laminates. More time is required for the development of matrix cracking at low stress levels. Once the critical crack density is achieved, the interlaminar debonding process links these cracks before

fibre failure, which leads to catastrophic failure. Therefore, this resulted in very steep S/N curves for low void content laminates compared with the flat S/N curves of high void content laminates.

For laminates with void contents between 1% to 2%, very little time is required for matrix cracking and void growth as discussed in section 5.10, since the quantity of the macrovoids is greater. Interlaminar debonding is the dominant failure mode and is more widespread throughout the structure in the early stages with many damage sites contributing to both specimen heating and modulus degradation. This is a lengthy process lasting from early in the test until the specimen is just about to fail. Specimen heating contributes to the reduction of matrix shear modulus which, in turn, allows fibre microbuckling to occur leading to fibre failure. Therefore, with the interlaminar debonding failure mode dominating the life of the specimen, a flatter S/N curve results compared with the low void content laminates.

For laminates of void content above 2%, no observable matrix cracking and void growth occurs in the early fatigue life of the specimen. The interlaminar debonding failure mode dominates throughout the fatigue life of the specimen as the voids are large in size in terms of length as well as being distributed widely; thus no cracking is required. This failure mode is a lengthy process with more cycles to failure required, especially at low stress levels, before catastrophic failure occurs. This results in very flat S/N curves compared with the low void content laminates.

Therefore, specimens selected from laminates of high void content (above 1%) can be considered as having a premature failure structure with many damage sites (i.e. voids) already present within the structure. At high stress levels, the applied force need only to agglomerate the isolated damage sites without the need for gross matrix cracking as occurs in laminates of low void contents; thus, very few cycles were required to cause catastrophic failure. For low void content laminates, crack initiation and propagation from the voids started early at high stress levels. This was followed by interlaminar debonding and agglomeration of the damage sites which initiated in the early damage stage. Thus, more cycles were required for the final failure of the specimen.

However, at low fatigue stress levels, specimens selected from high and low void content laminates withstood a large number of cycles before failure and survived through one million cycles. This is because interlaminar debonding is the controlling failure mode at low stress levels, especially for high void content laminates. After fatigue cycling through nearly 75% of the specimen fatigue life, the structure contained a large number of damage sites with debonding at the interlaminar regions of the laminate.

In the low stress fatigue tests, debonding at the interlaminar regions predominates and some isolated fibre failure occurs progressively. At this low stress level, the local hot spots at the damage sites from the continuous fatigue cycling did not reduce the shear modulus of the matrix sufficiently to allow rapid fibre failure. Therefore, the specimen retains its overall integrity and lasts for one million cycles. This was confirmed by those specimens, which after cycling for one million cycles, showed visible cracks along their thickness. At the same time, the thickness of the specimen was increased slightly due to the expansion of the cracks within structure.

Therefore, the different void contents in the FRP composites were evident in the different slopes of the S/N curves. The results for the weaker laminates with high void contents showed less steep S/N curves [142]. The stronger laminates with low void contents showed steeper curves, similar to those observed for homogeneous materials.

It is worth noting that specimens fatigued at a low stress level showed a large number of cycles before failure. however, the quality of a laminate may depend on its failure performance at high stress levels. A good and strong laminate with low void content will be preferred in either high or low stress service environments as the laminate can withstand a large number of cycles at a high stress level with a decreased chance of premature failure.

The plot of the individual S/N curves for the laminates moulded at each selected curing pressure and partial cure time are shown in Graphs 39 to 41 and Graphs 43 to 49 respectively. The large scatter in the results is as expected for this type of test and material (heterogeneous and anisotropic). It may be possible to reduce the degree of scatter in the results by improving the control of parameters during fabrication, moulding and preparation of the specimens for testing.

5.11.4 Failure Mode in Dynamic Compression

Specimens which failed in fatigue fractured in a typical 45° shear mode or a V-notched shape mode randomly throughout the gauge length of the specimen. This showed that the jig was able to support the specimen against any buckling without preventing a true compressive failure. Basically the failure mode in dynamic compression was similar to the failure mode in axial compression.

Audible sounds are emitted by the test specimens. Sometimes this may occur just prior to failure or it may occur well in advance of failure. The audible sound was believed to be due to the breaking of brittle fibres at the weakest points. If the breaking of the fibres occurred in the major load carrying longitudinal axis,

therefore the 0° plies, the specimen failed suddenly. If the breaking occurred in off-axis fibres, although the residual strength of the composite was reduced, it still was able to withstand the load during fatigue cycling; therefore, this specimen was able to survive longer. The specimens which survived one million cycles were badly damaged with cracks between the plies but they were able to hold together as individual structures.

5.12 FATIGUE DAMAGE MEASUREMENT

Those specimens which survived one million cycles of zero-compression fatigue were statically tested to determine their residual compressive strength, secant modulus and failure strain. The effect of the different moulding parameters was assessed on the basis of residual property values for those specimens fatigued at a 55% stress level as all the specimens completed one million cycles at this level.

5.12.1 Residual Compressive Strength

In general, a specimen subject to fatigue will decrease in strength. The strength remaining after a period of fatigue is called the residual compressive strength (Graph 50). The observed increases in average residual compressive strengths for the 12 and 20 minutes partial cure time specimens were within the scatter of the static compressive strength results.

A reduction in compressive strength is expected as, after fatigue cycling, the specimen consists of many damage sites within its structure. The presence of interlaminar debonding and fibre failure degrade the strength properties. When a compressive load is applied to the specimen, the low matrix strength of the degraded specimen was exceeded and the specimen failed catastrophically. Any stored strain energy not used in fracture surface creation was released in the form of heat and sound, etc.

During the final compressive failure, audible sounds were heard which are believed to be due to fibre cracks agglomerating at the damage sites in a 'knock-on' fashion. It is believed that the residual compressive strength of an individual specimen depends on the extent of the debonding and the number of isolated and localised broken fibres present in the specimen. The greater the number of damage sites within the structure, the lower is the residual strength. Therefore, specimens which were fatigue cycled at a 60% stress level had a lower residual compressive strength than those fatigued at lower stress levels (see Appendix B, Table B13).

5.12.2 Residual Secant Modulus

The reduction of secant modulus after fatigue cycling is shown in Graph 51. This reduction is as expected because the matrix shear modulus is seriously reduced in degraded specimens. Those specimens subjected to high stress fatigue loading showed a lower residual modulus than the specimens subjected to low stress fatigue loading (see Table B13). This indicates that a specimen at a higher fatigue stress level is more susceptible to premature failure as a result of the number of damage sites within the structure being greater.

5.12.3 Residual Failure Strain

The residual failure strain of specimens after cycling is shown in Graph 52. Generally, the residual failure strain was lower than the failure strain before fatigue cycling. However, the residual failure strain of some specimens was higher and this can only be explained by the general scatter in results. It was confirmed by microscopic observation that, after fatigue cycling, the specimen contained a large number of damage sites between the individual plies. Such specimens required little deformation before catastrophic failure occurs and so the recorded failure strain is low.

5.12.4 Modulus Reduction During Fatigue Cycling

The fatigue results indicate that growth of damage sites occurs within the structure until the whole specimen fails catastrophically. Therefore, the reduction in modulus of the specimen can be used to give an indication of changes in the specimen structure throughout its fatigue life.

The modulus reduction during fatigue cycling for specimens moulded at different pressures (Experiment 4) and partial cure times (Experiment 8) are shown in Graphs 52 to 54 and Graphs 55 to 61 respectively. All the graphs show the same type of relationship between modulus and the number of fatigue cycles and had a distinct and repeatable shape.

Those specimens subject to a 70% stress level showed no change in modulus up to about 10,000 cycles, but subsequently, drastic modulus reductions are observed before failure occurs. The specimens tested at a 65% stress level showed no modulus change until about 50,000 cycles. Again, drastic modulus reductions followed before failure. For the specimens tested at stress levels up to 60%, modulus reductions were recorded after about 100,000 cycles and continued up to

one million cycles. This behaviour was observed for all the specimens from the laminates prepared at a range of curing pressures in Experiment 4 and the laminates prepared with partial cure times less than 20 minutes in Experiment 8. The specimens selected from laminates moulded with 30 minutes partial cure time gave a lower number of cycles to failure due to their higher void content. For the specimens tested at a 67% stress level, drastic modulus reduction occurred at about 1,000 cycles. The specimens tested at a 60% stress level showed a drastic reduction between 10,000 and 100,000 cycles. Generally, all the specimens showed drastic modulus reductions at a lower number of cycles than did specimens from laminates of lower void content for a given fatigue stress level.

It is suggested that a drastic modulus reduction is observed when interlaminar debonding within the structure has developed to a stage where fibre failure commences in an isolated fashion. In the first 50% of the fatigue life of the specimens, little or no change of the modulus occurs. Although matrix cracking and void growth occur in low void content laminates, these failure modes do not lead to drastic modulus reduction. A stable crack density must exist to create many damage sites before interlaminar debonding can occur. However, such crack formation does not immediately reduce the modulus of the composite as the stress was redistributed throughout the undamaged regions. During this stage, only small changes in modulus occur. This has been reported by other authors as a 'wear-in' or 'wear-out' process [64, 65, 73, 74].

In high void content laminates, these modes are less obvious as the microvoids present readily act as sites for interlaminar debonding. Therefore, the fibre failure mode occurs earlier in these laminates.

In the second region between 50% to 90% of the fatigue life, the modulus reduction is approximately linear with increasing number of fatigue cycles. It is suggested that at this stage, debonding is well developed, the matrix shear modulus is reduced further and there is some fibre failure. Generally, at this stage, there is an increase in non-recoverable damage as the stress is not able to redistribute throughout the undamaged regions effectively. Therefore, the modulus decreases approximately linearly with the number of cycles.

In the last 10% of the fatigue life, a rapid decrease in the modulus corresponds to a rapid increase in the number of damage sites. At this stage, the structure of the specimen is subject to widespread cracking and interlaminar debonding in the regions between the plies. The amount of fibre failure is increased which leads to the formation of isolated kink-bands especially at the weakest sites of the structure. This drastic reduction of the modulus was accompanied by audible cracking sounds as the load bearing fibres failed. This was followed shortly by

complete failure of the specimen..

The plot of modulus reduction for the different void content laminates subject to a 60% stress level to just before failure is shown in Graph 62. Generally, drastic modulus reduction occurred at about 500,000 cycles for good laminates of void content less than 1%. As the void content of the laminates increased to about 1% to 2%, the drastic modulus reduction occurred earlier, i.e. at about 100,000 cycles. For the laminates of high void content above 2%, the drastic modulus reduction occurred at about 50,000 cycles. Microscopic examinations revealed extensive damage in the form of cracks and debonding between the plies in all the specimens. Many kink-band fibres were observed in the sectioned specimens. These kink-bands had formed where there had been a drastic reduction of modulus which allowed local fibre failure immediately prior to catastrophic failure.

CHAPTER 6 CONCLUSIONS

6.1 Manufacturing Of Voids

6.2 Determination Of Void Content

6.3 Types Of Void

6.4 Effect Of Void Content On Prepreg Properties

6.5 Design Of Compressive Test Jig

6.6 Effect Of Voids On Static Strength Properties

6.7 Effect Of Voids On Fatigue Properties

CHAPTER 6 CONCLUSIONS

The following conclusions can be drawn from the results of the tests, under the conditions and with the prepreg materials used in this project.

6.1 MANUFACTURING OF VOIDS

The spraying of solvents onto consecutive layers of the prepreg before lay-up is not an effective way of producing a wide range of void contents within the laminates.

Variation of the curing temperature and pressure produced higher void contents within the laminates compared with spraying solvents. However, the production of a wide range of void contents was still not achieved; thus, varying the curing temperature or pressure is not the best way to create a wide range of void contents.

Varying the lay-up conditions by increasing the number of layers of bleed cloth resulted in resin-starved laminates. However, this is again not an effective way of manufacturing voids as the amount of resin extracted does not increase once a minimum resin content is reached in the composite; thus, varying the lay-up conditions is not a way to create a wide range of void contents.

Variation of partial cure time was found not only easy to control, but it also allowed a large range of void contents to be produced. Therefore, varying the partial cure time was found to be the best way of manufacturing voids.

These experiments also demonstrated the importance of the cure cycle on the production of good CFRP laminates with low void content.

6.2 DETERMINATION OF VOID CONTENT

With careful preparation of the specimens, the determination of composite density by displacement, followed by acid digestion to separate the fibres from the resin, was found to be the most suitable way of measuring void contents. Optical microscopy and SEM were also easy and accurate methods for the observation of the void distribution within the composite.

6.3 TYPES OF VOID

In laminates with void contents between 0% and 1%, the voids mainly consisted of micropores within and between the rovings as well as interstitial voids, with a minority of micropores within and between the rovings. It is suggested that these voids are due to imperfections of the prepregs rather than entrapped air or volatiles produced during curing.

In laminates with void contents between 1% and 2%, the majority of the voids were macropores within and between the rovings, interface voids, interlaminar voids and interroving voids with a minority of micropores within and between the rovings. It is suggested that these voids are caused by the entrapped air and volatiles not able to escape completely during curing.

In laminates with void contents above 2%, the voids mainly consist of macrovoids as present in the 1% to 2% void content laminates. However, their quantity is greater and with negligible micropores and interstitial voids. It is suggested that these voids are mainly caused by entrapped air between the individual plies during fabrication which was not able to escape during the curing process. The high void content laminates also contained translaminar cracks which were caused by pressure on the laminate during moulding and by induced residual stress resulting from postcuring.

6.4 EFFECT OF VOID CONTENT ON PREPREG PROPERTIES

The density and the fibre volume fraction of the composite decreased as the void content increased. This was because the voids, which are less dense than the fibre or resin, increase the volume of the laminate; thus, reducing the composite density and the fibre volume fraction.

The thickness of the composite increased as the void content increased. This was the result of the presence of entrapped air between the individual plies of the laminate that is not removed completely during the curing cycle. This entrapped air resulted in the formation of interlaminar voids which restricted the compaction of the plies.

6.5 DESIGN OF COMPRESSIVE TEST JIG

The **Celanese jig** gave high static compressive strength measurements due to the high degree of support offered by the grips.

The complete-edge supported guide, **ABG-1**, was not as good a fixture for static compressive strength testing. The guide provides constraint on the specimen during testing. This constraint on the specimen, particularly in the area around the window, gave rise to high secant modulus values.

The partial-edge supported guide, **ABG-2** and the **CRAG jig** gave similar strength values with low coefficients of variation because there was less constraint on the specimen during testing. The **CRAG jig** was selected for all the fatigue testing as it was convenient to set up in the hydraulic grips of the machine.

6.6 EFFECT OF VOIDS ON STATIC STRENGTH PROPERTIES

The presence of voids reduces the static compressive strength, the secant modulus and the failure strain. This was because the voids act as stress concentrators where the cracks initiate. These cracks propagate and link the defects in the structure under the applied force. For high void content laminates, the crack propagation process is easy as the number of voids within the structure is large; thus a lower force is required to fracture the specimens selected from these laminates.

All the specimens failed in a non-progressive way. Once the applied force exceeds the residual strength of the structure, fracture occurs randomly along the gauge length of the specimen.

The compressive strength decreased linearly as the void content in the laminate increased. Similarly the secant modulus and the failure strain decrease with an increase in void content.

6.7 EFFECT OF VOIDS ON FATIGUE PROPERTIES

The voids in a CFRP composite have a direct effect on dynamic performance during fatigue cycling. The S/N curves for low void content laminates show steeper curves compared with the S/N curves for the high void content laminates. In the early stages, matrix cracking is the dominant failure mode for low void content laminates (void content less than 1%). More time is required for the development of matrix cracking at low stress levels. Once the critical crack density is achieved an interlaminar debonding process links these cracks before fibre failure which leads to catastrophic failure. This results in very steep S/N curves for low void content laminates compared with the flatter S/N curves for high void content laminates (void content above 2%).

For high void content laminates, the interlaminar debonding failure mode dominates throughout the fatigue life of the specimens as the voids are large in size and distributed widely. At low stress levels, the applied force is not great enough to initiate final failure. This results in very flat S/N curves compared with the low void content laminates.

A reduction in compressive strength was observed for all the specimens which survived one million cycles of zero-compression fatigue cycling. These specimens consist of many damage sites within the structure with the presence of interlaminar debonding and fibre failure which degrade the strength properties. The greater the number of damage sites within the structure, the lower is the residual strength. The same trends applied for the secant modulus and failure strain, where both are reduced after fatigue cycling.

Modulus reduction of the specimens during testing was negligible in the first 50% of fatigue life, a linear reduction followed in the next 40% of the life and it reduced drastically in the last 10%.

It is suggested that this drastic modulus reduction occurred when interlaminar debonding within the structure had developed to a stage such that fibre failure began in an isolated fashion. Although matrix cracking and void growth occurred in low void content laminates in early fatigue life, these two failure modes did not lead to a drastic reduction in modulus, as it was found that a critical crack density must exist before interlaminar debonding can occur.

In the last stage of fatigue, a rapid modulus reduction corresponded to a rapid increase in the number and size of damage sites and fibre failure proceeded rapidly within the structure. As the number of load carrying fibres reduced, the specimen became more vulnerable to failure. Once the applied load exceeded the ultimate residual strength of the degraded specimen, it failed catastrophically.

CHAPTER 7 FURTHER WORK

7.1 Processing Of CFRP Laminates

7.2 Jig Design For Compressive Strength Measurement

7.3 Test Procedure

CHAPTER 7 FURTHER WORK

There are several areas in which further investigation might be helpful.

7.1 PROCESSING OF CFRP LAMINATES

Ways of achieving greater control of the moulding parameters should be investigated, e.g. the curing temperature and pressure. The partial cure process variables could be examined in detail, perhaps at a lower temperature (e.g. 120°C).

To continue the study of processing parameters on the CFRP laminates, it is suggested that a dwell time at 120°C for half an hour be used, as at Lucas Aerospace in their autoclave.

It is suggested that the mould with the laminate should be placed in a fluidised bed for more effective heat transfer before being placed into the hot press for compression moulding.

7.2 JIG DESIGN FOR COMPRESSIVE STRENGTH MEASUREMENT

In the absence of an internationally recognised compression test method for slender FRP composites specimens, there is a need for further work on the current jigs in use. Such work should include the determination of their relative merits and the nature of any problems associated with these jigs. This would allow a better evaluation of the effect of different designs on the static strength properties.

It is suggested that the Celanese jig be modified to use wedge grips rather than the split conical collet grips as the Celanese jig requires careful control of the gripped part of the specimen to achieve perfect contact in the conical seat. This would minimise the effect of any deviation of the specimen thickness and the resulting mismatch between the collet and its seat.

7.3 TEST PROCEDURE

More detailed analysis of the development of compressive failure is required for a greater understanding of the failure mechanism. It is suggested that close examination of the various stages of the compressive failure mechanism during the static test be carried out. This would involve stopping some of the tests before final fracture in order to assess the internal damage under microscopic observation.

It is also suggested that compression-compression fatigue cycling tests should be carried out in order to obtain more information on the failure mechanism. Extended fatigue tests (i.e. beyond 10^6 cycles) may shed more light on the failure mechanism. In any event, more frequent observations of the internal structure may be useful.

At the same time, other techniques such as X-ray radiograph and ultrasonic scanning should be use as supporting tools to the fractography studies.

REFERENCES

REFERENCES

1. Aboudi, J.
'Micromechanics Prediction of Fatigue Failure of Composite Materials'.
J. of Reinforced Plastics and Composites, Vol. 8, No. 2, March 1989.

2. Adsit, N. R.
'Compressive Testing of Graphite/Epoxy'.
Compression Testing of Homogeneous Materials and Composites.
ASTM STP 808. (ed) Chait, R. , Papirno, R. , 1983.

3. Agarwal, B. D. , Joneja, S. K.
'Flexible Fatigue Properties of Unidirectional GRP in Transverse Direction'.
Composites, Vol. 10, No. 1, Jan 1979.

4. Akay, M.
'Influence of Curing Conditions and Post-cure Hygrothermal Treatment on the Mechanical Behaviour of CF/Epoxy Laminates'.
Interface Phenomena in Composites Materials, 1989.

5. Ashby, M. F. , Jones, D. R. H.
'Engineering Materials - 2. An Introduction to Microstructures, Processing and Design', Oxford Pergamon Publisher, 1986.

6. ASTM C613 - 67.
Standard Test Method for 'Resin Content and Graphite Prepregs by Solvent Extraction', 1985.

7. ASTM D792 - 86.
Standard Test Method for 'Specific Gravity (Relative Density) and Density of Plastics by Displacement', 1986.

8. ASTM D2344 - 84.
Standard Test Method for ' Apparent ILSS of Parallel Fibre Composites by Short Beam Method', 1984.

9. ASTM D2734 - 70.
Standard Test Method for 'Void Content of Reinforced Plastics', 1970.

10. ASTM D3171 - 76.
Standard Test Method for 'Fibre Content of Resin-Matrix Composites by Matrix Digestion', 1982.

11. ASTM D3410 - 87.
Standard Test Method for 'Compressive Properties of Unidirectional or Crossply Fibre Resin Composites', 1987.

12. Awa, V. S.
'Effect of Specimen Size on the Buckling Behaviour of Laminated Composites Subjected to Low-Velocity Impact'.
Compressive Testing of Homogeneous Materials and Composites.
ASTM STP 808, (ed) Chait, R. , Papirno, R. , 1983.

13. Bader, M. E. , Boniface, L.
'The Performance of CFRP Laminates Subjected to Complex Fatigue Loading Programmes'.
PRI Fibre Reinforced Composites'84 International Conference, 1984.

14. Bader, M. G. , Johnson, M.
'Fatigue Strength and Failure Mechanisms in Uniaxial Carbon Fibre Reinforced Epoxy Resin Composite Systems'.
Composites, Vol. 5, No. 2, March 1974.

15. Balasundaram, B.
'Compression Testing of CFRP Exposed to Humid Environments'.
Composites, Vol. 18, No. 3, July 1987.

16. Bascom, W. D. , Gweon, S. Y.
'Fractography and Failure Mechanisms of Carbon Fibre Reinforced Composite Materials'.
Fractography and Failure Mechanisms of Polymer and Composites, (ed) Roulin-Moloney, A. C., Elsevier Applied Science Publisher, 1989.

17. Bascom, W. D. , Romans, J. B.
'Microvoids in Glass-Resin Composites - Their Origin and Effect on Composite Strength'.
I & EC Product Research and Development 7172, 1968.

18. Beaumont, P. W. R.
'The Fatigue Damage Mechanics of Composite Laminates'.
CUED/C/MATS/TR 139, Cambridge University, 1987.

19. Berg, C. A. , Salama, M.
'Compressive Fatigue in Fibre Reinforced Materials'.
J. of Materials, Vol. 7, No. 7, 1972.

20. Berg, C. A. , Salama, M.
'Fatigue of Graphite Fibre Reinforced Epoxy in Compression'.
Fibre Science and Technology, Vol. 6, No. 2, April 1973.

21. Bevan, L. G.
'Axial and Short Beam Shear Fatigue Properties of CFRP Laminates'.
Composites, Vol. 8, No. 4, Oct 1977.

22. Bishop, S. M.
'Strength and Failure of Woven CFRP for High Performance Applications'.
Textile Structural Composites, (ed) Chou, T. W. , Ko, F. K.
Elsevier Science Publisher, 1989.

23. Bonnian, P. , Bunsell, A. R.
'A Comparative Study of Water Absorption Theories Applied to Glass Epoxy Composites'.
In Environmental Effects on Composite Materials, Vol. 2, 1984.

24. Brassell, G. W.
'Effect of Porosity on Strength of Carbon - Carbon Composites'.
J. of Composite Materials, Vol. 9, July 1975, pp. 288-296.

25. Broutman, L. J. , Gagger, S. K.
'Fatigue Behaviour of Epoxy and Polyester Resins'
27th Annual Technical Conference (SPI), 1972.

26. BS 3518 Part 1: General Principles.
BSI : Methods of Fatigue Testing, 1962.

27. BS 3518 Part 5 : Terms Used in the Statistical Analysis of Fatigue Experiments, BSI : Methods of Fatigue Testing, 1966.

28. Bunsell, A. R. (ed)
Fibre Reinforced for Composite Materials.
Elsevier Science Publisher, 1988.

29. Camponeschi, E. T. , Stinchcomb, W. W.
'Stiffness Reduction as an Indicator of Damage in Graphite/Epoxy Laminates'.
Composite Materials : Testing and Design (6th Conference).
ASTM STP 787, 1982.

30. Carter, H. G. , Kibler , K. G.
'Langmiur-type Model for Anomolous Moisture Diffusion in Composite Resins'.
J. of Composite Materials, Vol. 12, April 1978, pp. 118-131.

31. Chang, F. K. , Lessard, L. B.
'Damage Tolerance of Laminated Composites Containing an Open Hole and Subjected to Compressive Loading - Part I. Analysis'.
J. of Composites Materials, Vol. 25, No. 1, Jan 1991.

32. Charewicz, A. , Daniel, I. M.
'Damage Mechanisms and Accumulation in Graphite/Epoxy Laminates'.
Composite Materials : Fatigue and Fracture, (ed) Hahn, H. T.
ASTM STP 787, 1982.

33. Ciba-Geigy Fibredux 913.
Information Sheet No. FTA 46 d, May 1983.

34. Ciba Geigy Fibredux 914.
Information Sheet No. FTA 49 b, Jane 1975.

35. Cilley, E. , Roylance, D. , Schneider, N.
'Methods of Fibre and Void Measurement in Graphite/Epoxy Composites'.
3rd Conference on Composite Materials : Testing and Design.
ASTM STP 546, 1974.

36. Clark, G. , Van Blaricum, T. J.
'Load Spectrum Modification Effects on Fatigue of Impact-damaged Carbon Fibre Composites', Composites, Vol. 18, No. 3, July 1987.

37. Curtis, P. T.
'Investigation of Tensile Fatigue Behaviour of Improved Carbon Fibre Composite Materials'.
6th International Conference on Composite Materials. ICCM & ECCM.
(Second European Conference on Composite Materials).
(ed) Mattews, F. L. , Buskell, N. C. R. , Hodgkinson, J. M. , Morton, J.
Vol. 4, 1987.

38. Curtis, P. T.
'CRAG Test Methods for the Measurement of the Engineering Properties of Fibre Reinforced Plastics', RAE Tech Report 88012, Feb 1988.

39. Curtis, P. T. , Bishop, S. M.
'An Assessment of the Potential of Woven CFRP for High Performance Applications'.
Composites, Vol. 15, No. 4, Oct 1984.

40. Curtis, P. T. , Moore, B. B.
'A Comparison of the Fatigue Performance of Woven and Non-woven CFRP Laminates in Reversal Axial Loading'.
International J. of Fatigue, Vol. 9, No. 2, 1987.

41. Curtis, P. T. , Moore, D. R. , Slater, B. , Zahlan, N.
'Fatigue Testing of Multi-angle Laminates of CF/PEEK'.
Composites, Vol. 19, No. 2, 1987.

42. Curtis, P. T. , Morton, J.
'The Effect of Fibre Surface Treatment on the Compressive Strength of the CFRP Laminates', RAE Technical Report 82047, April 1982.

43. Dally, J. W. , Broutman, L. J.
'Frequency Effects on the Fatigue of Glass Reinforced Plastics'.
J. of Composite Materials, Vol. 1, 1967, pp. 424-442.

44. Dao, K. C.
'Fatigue Failure Mechanisms in Polymer Composites'.
Polymer Composites, Vol. 3, No. 1, 1982.

45. DeCharentenay, F. X. , Kamimura, K. , Lemanscon, A.
'Fatigue Delamination in Unidirectional Carbon/Epoxy Composites'.
Materials, Experimentation and Design in Fatigue.
(ed) Sherratt, F. , Strugeon, J. B.
Westbury House, 1981.

46. Dew-Hughes, D. , Way, J. L.
'Fatigue of Fibre Reinforced Plastics : A Review'.
Composites, Vol. 4, No. 4, July 1973.

47. Dickson, R. F. , Fernando, G. , Adam, T. , Reiter, H. , Harris, B.
'Fatigue Behaviour of Hybrid Composites Part 2. Carbon-Glass Hybrids'.
J. of Materials Science, Vol. 24, No. 1, Jan 1989, pp. 227-233.

48. Dorey, G.
'Effects of Defects on Advanced Composite Performance'.
Metals and Materials, Vol. 4, No. 5, May 1988.

49. Engineering Materials Handbook - Composites.
American Society of Metals (ASM) International, 1987.

50. Evans, A. G.
'A Compressional Mode of Damage in Carbon Composites'.
Fibre Science and Technology, Vol. 13, No. 1, 1980.

51. Ewins, P. D. , Childs, R.
'The Determination of the Content by Volume of Fibre, Resin and Void in CFRP'.
RAE Technical Report 72082, April 1972.

52. Found, M. S. , Howard, I. C.
'The Modelling of Damage in FRP Composites'.
Interfacial Phenomena in Composite Materials '89.
(ed) Jones, F. R. , Butterworths, 1989.

53. Foyes, R. L.
'Compressive Strength of Unidirectional Composites'.
AIAA Papers, 1966, pp. 66-143.

54. Frandsen, R. R. , Naerheim, Y.
'Fracture Morphology of Graphite/Epoxy Composites'.
J. of Composite Materials, Vol. 17, March 1983, pp. 105-113.

55. Garrett, R. A.
'Effect of Manufacturing Defects and Service-induced Damage on the Strength of Aircraft Composite Structures'.
Overcoming Materials Boundaries. National 17th SAMPE Tech Conference.
SAMPE, Oct 1985, pp. 22-24.

56. Gerharz, J. J.
'Prediction of Fatigue Failure'.
Practical Considerations of Design, Fabrication and Tests for Composite Materials, AGARD - LS - 124, Sept 1982.

57. Gerharz, J. J.
'Mechanisms of Fatigue Damage and Fatigue Testing'.
As above.

58. Ghasemi, N. M. N. , Chou, T. W.
'Compression Behaviour of Woven Carbon Fibre Reinforced Epoxy Composites with Moulded-in and Drilled Holes'.
Composites, Vol. 21, No. 1, Jan 1990.

59. Gill, R. M.
Carbon Fibres in Composite Materials.
Iliffe Publisher, 1972.

60. Giltrow, J. P.
'A Possible Source of Porosity in Composites'.
Composites, Vol. 2, No. 4, Dec 1971.

61. Goetchius, G. M.
'Fatigue of Composite Materials'.
Advance Composites III: Expanding the Technology, (ed) Steinbrunner, D. L., American Society for Metals International, 1987.

62. Green, A. K. , Pratt, L.
'The Axial Fatigue Behaviour of Unidirectional Type IIIS Carbon Fibre Epoxy Resin Composites'.
Composites, Vol. 5, No. 2, March 1974.

63. Gurtin, M. E. , Yatomi, C.
'On a Model for Two-phase Diffusion in Composite Materials'.
J. of Composite Materials, Vol. 13, April 1979, pp. 126-130.

64. Hahn, H. T.
'Fatigue Behaviour and Life Prediction of Composite Laminates'.
5th Conference in Composite Materials: Testing and Design, (ed) Tsai, S. W., ASTM STP 674, 1979.

65. Hahn, H. T. , Kim, R. Y.
'Fatigue Bahaviour of Composite Laminates'.
J. of Composite Materials, Vol. 10, April 1976, pp. 156-180.

66. Hale, J. M. , Ashton, J. N.
'Ultrasonic Attenuation in Voided FRP'.
NDT International, Vol. 21, No. 5, Oct 1988.

67. Han, K. S.
'Compressive Fatigue Bahaviour of a Glass Fibre Reinforced Polyester Composite at 300K and 77K', Composites, Vol. 14, No. 2, April 1983.

68. Handbook of Industrial Materials. First Edition.
Trade and Techanical Publisher, 1977.

69. Harper, B. D. , Staab, G. H. , Chen, R. S.
'A Note on the Effects of Voids Upon the Hygral and Mechanical Properties of AS4/3502 Graphite/Epoxy'.
J. of Composite Materials, Vol. 21, March 1987, pp. 280-289.

70. Harris, B.
'The Strength of Fibre Composites'.
Composites, Vol. 3, No. 4, July 1972.

71. Harris, B.
'Fatigue and Accumulation of Damage in Reinforced Plastics'.
Composites, Vol. 8, No. 4, Oct 1977.

72. Harris, B.
'Fatigue Testing of Fibre Composites'.
Fatigue Test Methology. AGARD - LS - 118, 1981.

73. Harris, B.
'Monitoring of Damage in Fibre Composites'.
As above.

74. Harris, B.
Engineering Composite Materials.
Institute of Metals, 1986.

75. Harris, B. , Reiter, H. , Adam, T. , Dickson, R. F. , Ferando, G.
'Fatigue Behaviour of CFRP'.
Composites, Vol. 21, No. 3, May 1990.

76. Hayes, B.
'Polymer Selection and Matrix Aspects of Processing and Manufacture of Fibre Composites'.
Composites, Vol. 14, No. 2, April 1983.

77. Haynes, W. M. , Tolbert, T. L.
'Determination of the Graphite Fibre Content of Plastics Composites'.
J. of Composite Materials, Vol. 3, Oct 1969, pp. 709-712.

78. Highsmith, A. L. , Stinchcomb, W. W. , Reifsnider, K. L.
'Effect of Fatigue-induced Defects on the Residual Response of Composite Laminates'.
Effects of Defects in Composite Materials. ASTM STP 836, 1984.

79. Hofer, K. E. , Rao, P. N.
'A New Static Compression Fixture for Advanced Composite Materials'.
J. of Testing and Evaluations, JTEVA, Vol. 5, No. 4, July 1977.

80. Hull, D.
An Introduction to Composite Materials.
Cambridge University Press, 1981.

81. Hussey, M. E.
'Measurement of Fibre Density'.
RAE Test Note (Structure) 1742, 1969.

82. Hwang, W. , Han, K. S.
'Cumulative Damage Models and Fatigue Life Prediction'.
J. of Composite Materials, Vol. 20, 1986, pp.125-153.

83. Jeffery, M. R. , Sourour, J. A. , Schultz, J. M.
'Fatigue Behaviour of Thermosetting Polyester Matrix Sheet Moulding Compounds', Polymer Composites, Vol. 3, No. 1, Jan 1982.

84. Jock, C. P.
'Quantitative Optical Microscopy Fibre Volume Methods for Composites'.
J. of Reinforced Plastics and Composites, Vol. 5, 1986, pp. 110-119.

85. Johnson, J. B. , Owston, C. N.
'The Effect of Cure Cycle on the Mechanical Properties of CF/Epoxy Resin'.
Composites, Vol. 4, No. 3, May 1973.

86. Johnson, J. W.
'Processing and Property Relationships for Fibre Composites'.
Composites, Vol. 14, No. 2, April 1983.

87. Joiner, J. C.
'The Determination of Voids in Carbon Fibre Composites'.
AQD Laboratories Report No. NM 000296, July 1973.

88. Jones, B. F. , Wilkins, B. J. S.
'Techanical Note : A Technique for the Analysis of Fracture Strength Data for Carbon Fibres'.
Fibre Science and Technology, Vol 5-6, No. 4, 1972/73, pp. 315-320.

89. Jones, B. R. , Stone, D. E. W.
'Towards an Ultrasonic Attenuation Technique to Measure Void Content in Carbon Fibre Composites'.
Non-Destructive Testing, Vol. 9, No. 1-3, April 1976.

90. Judd, N. C. W. , Wright, W. W.
'Voids and Their Effects on the Mechanical Properties of Composites: An Appraisal'.
SAMPE J., Vol. 14, No. 1, Jan/Feb 1978, pp.10-14.

91. Kan, H. P. , Patwani, M. M.
'Compression Fatigue Behaviour of Fibre Composites'.
SAMPE Quarterly, Vol. 11, No. 4, July, 1980.

92. Karbhari, V. M. , Parks, B. , Dolgopolsky, A.
"Effect of Mean Load Levels on Fatigue in Random Short Fibre Injection Moulded Composites'.
J. of Materials Science Letters, Vol. 8, No. 2, Feb 1989.

93. Kardos, J. L. , Dudukovic, M. P. , Dave, R.
'Void Growth and Resin Transport During Processing of Thermosetting Matrix Composites', Epoxy Resin and Composites IV.
Advances in Polymer Science, 1980, pp. 101-124.

94. Kavanagh, K. T.
'The Effect of Void and Fibre Variations on the Accuracy of Composites Material Characterization'.
J. of Composites Materials, Vol. 7, Oct 1973, pp. 500-515.

95. Kellas, S. , Morton, J. , Curtis, P. T.
"The Effect of Hygrothermal Environment Upon the Tensile and Compression Strengths of Notched CFRP Laminates. Part II: Fatigue Loading'.
Composites, Vol. 21, No. 1, Jan 1990.

96. Kim, H. C., Ebert, L. J.
'Axial Fatigue Failure Sequence and Mechanisms in Unidirectional Fibre Glass Composites'.
Composites, Vol. 20, No. 4, July 1989.

97. Kim, R. Y. , Soni, S. R.
'Experimental and Analytical Studies on the Onset of Delamination in Laminated Composites'.
J. of Composite Materials, Vol. 18, Jan 1984, pp. 70-80.

98. Kirk-Othmer (ed)
Encyclophedia of Chemical Technology. Third Edition.
John Wiley and Sons, 1981.

99. Konur, O. , Mattews, F. L.
'Effect of the Properties of the Constituents on the Fatigue Performance of Composites : A Review'.
Composites, Vol. 20, No. 4, July 1989.

100. Kumar, P. , Garg, A.
'Failure Modes and Fractographic Study of Glass/Epoxy Composite Under Dynamic Compression'.
J. of Materials Science, Vol. 23, No. 7, 1988.

101. Kunz, S. C.
'Themomechanical Characterisation of Graphite/Polyimide Composites'.
Composites for Extreme Environments, (ed) Adsit, N. R.
ASTM STP 768, 1982.

102. Lagace, P. A. , Nolet, S. C.
'Effect of Ply Thickness on Longitudinal Splitting and Detamination in Graphite/Epoxy Under Compressive Cyclic Load'.
Composite Materials: Fatigue and Fracture, (ed) Hahn, H. T.
ASTM STP 907, 1986.

103. Lee, B. L. , McGarry, F. J.
'Study of Processing and Properties of Graphite Fibre/High Temperature Resin Composites'.
AMMRC CTR 76 - 10, April 1976.

104. Lee, R. J.
'Compressive Strength of Aligned Fibre Reinforced Thermoplastics Laminates', Composites, Vol. 18, No. 1, Jan 1987.

105. Lenoe, M. E.
'Effect of Voids on Mechanical Properties of Graphite Fibre Composites'.
AD Report 727236, Dec 1970.

106. Loos, A. C. , Freeman, J. R.
'Resin Flow During Autoclave Cure of Graphite/Epoxy Composites'.
High Modulus Fibre Composites in Ground Transportation and High Volume Applications.
ASTM STP 873, 1985.

107. Loos, A. C. , Springer, G. S.
'Curing of Epoxy Matrix Composites'.
J. of Composite Materials, Vol. 17, March 1983, pp. 135-170.

108. Lorenzo, L. , Hahn, H. T.
'Fatigue Failure Mechanisms in Unidirectional Composites'.
Composite Materials : Fatigue anf Fracture, (ed) Hahn, H. T.
ASTM STP 907, 1986.

109. Lucas Aerospace Fabrications, Burnley.
'Determination of Density, Fibre Volume Fraction and Void Content of CFRP', No. 099/37809, Sept 1986.

110. Mandell, J. F.
'Fatigue Crack Growth in Fibre Reinforced Plastics'.
Polymer Composites, Vol. 2, No. 1, Jan 1981.

111. Mandell, J. F.
'Fatigue Behaviour of Fibre Resin Composites'.
Development in Reinforced Plastics - 2. Properties of Laminates.
(ed) Pritchard, G. , 1982.

112. Martin, B. G.
'Ultrasonic Attenuation due to Voids in Fibre Reinforced Plastics'.
NDT International, Vol. 9, No. 4-6, Oct 1976.

113. Matondang, T. H. , Schutz, D.
'The Influence of Anti-buckling Guides on the Compression Fatigue Behaviour of CFRP Laminates'.
Composites, Vol. 15, No. 3, July 1984.

114. McClintock, F. A.
'Criterion for Minimum Scatter in Fatigue Testing'.
American Society for Mechanical Engineers, Paper No. 55, 1955.

115. Metals Handbook. Ninth Edition.
Metallography and Microstructures, Vol. 9.
American Society for Metals, 1985.

116. Mijovic, J. , Wang, H. T.
'Processing Property Relationships in Autoclave Cured Graphite/Epoxy Composites. Part II', ANTEC (Boston) 86, Society of Plastics Engineers.
44th Technical Conference and Exhibition, 1986.

117. Mijovic, J. , Wijaya, J.
'Effects of Graphite Fibre and Epoxy Matrix Physical Properties on the Temperature Profile Inside their Composite During Cure'.
SAMPE J., Vol. 25, No. 2, April 1989.

118. Mohlin, T.
'Determination in Compressive Performance of a Graphite/Epoxy Laminates as a Consequence of Environmental Exposure and Fatigue Loading'.
J. of Reinforced Plastics and Composites, Vol. 3, 1984, pp. 256-263.

119. Molyneux, M.
'Prepreg, Tape and Fabric Technology for Advanced Composites'.
Composites, Vol. 14, No. 2, April 1983.

120. Morley, J. G.
'Advanced Fibre Composite Materials'.
Fibre Science and Technology, Vol. 1-2, 1968-70, pp. 209-225.

121. Morrison, C. E. , Bader, M. G.
'Computer Modelling of Resin Flow During Laminate Cure'.
Composites, Vol. 20, No. 1, Jan 1989.

122. Morton, J.
'Damage Characteristics in Notched Carbon Fibre Composites Subjected to Fatigue Loading - Environmental Effects'.
J. of Composite Materials, Vol. 22, July 1988, pp. 657-673.

123. Naeem, M.
'Fatigue Damage-Compliance Relationship for GRP'.
Composites, Vol. 19, No. 6, Nov 1988.

124. Nevadunsky, J. J. , Lucas, J. J.
'Early Fatigue Damage Detection in Composite Materials'.
J. of Composite Materials, Vol. 9, Oct 1975, pp. 394-408.

125. Newaz, G. M.
'Fatigue Damage Growth Rate in Unidirectional Composite in Flexural Loading'.
J. of Material Science Letters, Vol. 4, No. 2, 1985, pp. 197-199.

126. Nielsen, L. E.
'Fatigue Behaviour of Some Filled Polymer'.
J. of Composite Materials, Vol. 9, April 1975, pp. 149-157.

127. 'Non-Destructive Testing for the Detection of Fatigue Damage in CFRP'.
Cranfoeld Memo. No. 73, Second Annual Report 72.
Ministry of Technology AT / 2028 / 053.

128. Novak, R. C.
'Shear Fatigue Bahaviour of Unidirectional Resin Matrix Composites'.
Composite Materials : Testing and Design.
ASTM STP 540, March 1973.

129. O'Brien, T. K. , Reifsnider, K. L.
'Fatigue Damage Evaluation through Stiffness Measurements in Boron-Epoxy Laminates', J. of Composite Materials, Vol. 15, Jan 1981, pp. 55-70.

130. O'Brien, T. K. , Rigamonti, M. , Zanotti, C.
'Tension Fatigue Analysis and Life Prediction for Composite Materials'.
NASA Tech. Memo. 100549, Oct 1988.

131. Olster, E. F.
'Effect of Voids on Graphite Fibre Reinforced Composites'.
AD Report 746560, 1972.

132. Owen, M. J.
'Fatigue Testing of FRP'.
Composites, Vol. 1, No. 6, Dec 1970.

133. Pipes, R. B.
'Interlaminar Shear Fatigue Characteristics of Fibre Reinforced Composite Materials'.
Composite Materials: Testing and Design, ASTM STP 540, 1973.

134. Pole, J.
BSSM Strain Measurement Reference Book.
The British Society for Strain Measurement, 1979.

135. Prakash, R.
'Non-Destructive Testing and Fatigue Bahaviour of CFRP'.
PhD Thesis, Cranfield Institute of Technology, Dept of Materials, 1975.

136. Prakash, R.
'Significance of Defects in the Fatigue Failure of CFRP'.
Fibre Science and Technology, Vol. 14, No. 3, 1981, pp. 171-182.

137. Pritchard, G. (ed)
'Introduction: Causes of Property Variability'.
Development in Reinforced Plastics II. Properties of Laminates.
Applied Science Publishers, 1982.

138. Pritchard, G.
'Imperfections in FRP Materials'.
As above.

139. Purslow, D.
'On the Optical Assessment of the Void Content in Composite Materials'.
Composites, Vol. 17, No. 2, April 1986.

140. Purslow, D. , Childs, R.
'Autoclave Moulding of CFRP'.
RAE Technical Report 85039, April 1985.

141. Purslow, D. , Childs, R.
'Autoclave Moulding of Carbon Fibre Reinforced Epoxies'.
Composites, Vol. 17, No. 3, April 1986.

142. Puskar, A. , Golovin, S. A.
Fatigue In Materials: Cumulative Damage Processed.
Elsevier Science Publisher, 1985.

143. Rapimo, R.
'Fatigue Fracture Initiation in Notched Graphite/Epoxy Specimen'.
J. of Composite Materials, Vol. 11, Jan 1977, pp. 41-50.

144. Reifsnider, K. L. , Jamison, R.
'Fracture of Fatigue Loaded Composite Laminates'.
International J. of Fatigue, Vol. 4, No. 4, Oct 1982.

145. Rotem, A. , Nelson, H. G.
'Fatigue of a Laminated Composite Under Tension-Compression Fatigue Loading'.
Composites Science and Technology, Vol. 36, No. 1, 1989.

146. Russell, A, J.
'Micromechanisms of Interlaminar Fracture and Fatigue'.
Polymer Composites, Vol. 8, No. 5, Oct 1975.

147. Ryder, J. T. , Walker, E. K.
'Effect of Compression on Fatigue Properties of a Quasi-isotropic Graphite/Epoxy Composites', Fatigue of Filamentary Composite Materials.
(ed) Reifsnider, K. L. , Lauraitis, K. N., ASTM STP 636, 1977.

148. Sato, N. , Kurauchi, T. , Kamigaito, O.
'In situ SEM Observation of Fracture Process of Carbon Fibre Reinforced Epoxy Resin Composite'.
J. of Materials Science Letters, Vol. 4, No. 9, 1985, pp.1095-98.

149. Saunders, D. S. , Van-Blaricum, T. J.
'Effect of Load Duration on the Fatigue Behaviour of Graphite/Epoxy Laminates Containing Delaminations'.
Composites, Vol. 19, No. 3, May 1988.

150. Schulte, K.
'Mechanical Properties of Polymer Composites'.
3rd European Conference on Composite Materials (France), March 1989.

151. Schutz, D. , Gerharz, J. J.
'Fatigue Strength of a Fibre Reinforced Materials'.
Composites, Vol. 8, No. 4, Oct 1977.

152. Sharples, T.
'Reproducible Processing and Reliable Repeatability in Carbon Fibre Composites'.
Composites, Vol. 14, No. 2, April 1983.

153. Shikhmanter, L. , Eldror, I. , Cina, B.
'Fractography of Unidirectional CFRP Composites'.
J. of Materials Science, Vol. 24, No. 1, 1989, pp. 167-172.

154. Shimokawa, T. , Hamaguchi, Y.
'Distrubition Specimens of a Carbon Eight-Harness Satin Laminate'.
J. of Composites Materials, Vol. 17, Jan 1983, pp.64-76.

155. Shockey, P. P. , Waddoups, M. E.
'Strength and Modulus Determination of Composite Materials Within Sandwich Beams'.
Report FZM 4691, Sept 1966.

156. Sims, D. F. , Brogdon, V. H.
'Fatigue Behaviour of Composite Materials Under Different Loading Modes'.
Fatigue of Filamentary Composite Materials.
(ed) Reifsnider, K. L. , Laurcutis, K. N., ASTM STP 636, 1977.

157. Sims, G. D. , Gladman, D. G.
'Effect of Test Conditions on the Fatigue Strength of a Glass Fabric Laminates: Part B - Specimen Condition'.
Plastics and Rubbers: Materials and Applications, Aug 1980.

158. Sinclair, J. H. , Chamis, C. C.
'Compressive Behaviour of Unidirectional Fibrous Composites'.
Compressive Testing of Homogeneous Materials and Composites.
(ed) Chait, R, Papirno, R. , ASTM STP 808, 1983.

159. Smith, G. W. , Pascoe, K. L.
'The Role of Shear Deformation in the Fatigue Failure of a GFRP'.
Composites, Vol. 8, No. 4, Oct 1977.

160. Smith, P. A. , Gilbert, D. G. , Poursartip, A.
'Matrix Cracking of Composites Inside a Scanning Electron Microscope'.
J. of Materials Science Letters, Vol. 4, No. 7, 1985, pp. 845-847.

161. Sprenger, K. H. , Vaihingen, E.
'Prepreg Complexes - An Alternative to the Reinforcement of High Performance Composite Materials'.
Kunststoffe German Plastics, Vol. 78, No. 12, 1988.

162. Starnes, J. H. , Williams, J. G.
'Failure Characteristics of Graphite/Epoxy Structural Components Loaded in Compression', NASA Tech. Memo. 84552, Sept 1982.

163. Steinbrunner, D. L.
'Fatigue Crack Propagation of Composites'.
Advanced Composites III: Expanding the Technology.
American Society for Metals (ASM) International, 1987.

164. Stone, D. E. W. , Clake, B.
'Ultrasonic Attenuation as a Measure of Void Content in CFRP'.
Non-Destructive Testing, Vol. 8, No. 5, Sept 1989.

165. Stringer, L. G.
'Optimisation of the Wet Lay-up/Vacuum Bag Process for the Fabrication of Carbon Fibre/Epoxy Composites with High Fibre Fraction and Low Void Content', Composites, Vol. 20, No. 5, Sept 1989.

166. Sturgeon, J. B.
'Fatigue and Creep Testing of Unidirectional CFRP'.
28th Annual Technical Conference SPI, 1973.

167. Sturgeon, J. B.
'Fatigue of Multidirectional CFRP'.
Composites, Vol. 8, No. 4, Oct 1977.

168. Sturgeon, J. B. , Moore, B. B.
'Fatigue of CFRP and Detection of Damage Growth by Ultrasonic C-scans'.
RAE Technical Report 80150, Nov 1980.

169. Sturgeon, J. B. , Rhodes, F. S. , Moore, B. B.
'The Fatigue Behaviour of a Carbon Fibre Composites with Laminates Constrctions of 0°, 0 ± 45°, 90 ± 45°'.
RAE Technical Report 78031, March 1978.

170. Tang, J. M. , Lee, I., Springer, G. S.
'Effect of Cure Pressure on Resin Flow, Voids and Mechanical Properties'.
J. of Composite Materials, Vol. 21, May 1987, pp. 421-440.

171. Tang, J. M., Springer, G. S.
'Effect of Cure and Moisture on the Properties of Fiberite 976 Resin'.
J. of Composite Materials, Vol. 22, Jan 1988, pp.2-14.

172. Tanimoto, S. P. , Amijima, S.
'Fatigue Properties of Laminated Glass Fibre Composite Materials'.
29th Annual Technical Conference (SPI), 1974.

173. Tanimoto, T. , Amijima, S.
'Progressive Nature of Fatigue Damage of GFRP'.
J. of Composite Materials, Vol. 9, Oct 1975, pp. 380-391.

174. Test Methods.
Courtaulds Ltd, Carbon Fibre Unit.
Conventry, England, Aug 1970.

175. Thomas, K. T. (ed)
Engineer's Guide to Composite Materials.
American Society for Metals, 1987.

176. Thompson, S. C. , Kim, H. C. , Mattews, F. L.
'The Effect of Processing on the Microstructure of CFRP'.
Composites, Vol. 4, No. 2, March 1973.

177. Thuresson, S. , Abelin, R.
'Fatigue Testing of an all Composite using for the MFI-18 High Lift Aircraft'.
Composites, Vol. 18, No. 4, Sept 1987.

178. Timoshenko, S. P. , Gere, J. M.
Mechanics of Materials.
Van Nostrand Reinhold, 1972.

179. Tottle, C. R.
An Encyclopedia of Metallurgy and Materials.
The Metals Society, MacDonald and Evans, 1984.

180. Tsai, G. C. , Doyle, J. F. , Sun, C. T.
'Frequency Effects on the Fatigue Life and Damage of Graphite/Epoxy Composites'.
J. of Composite Materials, Vol. 21, Jan 1987, pp.2-13.

181. Wang, S. S. , Chim, E. S. M.
'The Fatigue Damage and Degradation in Random Short Fibre Composites'.
J. of Composite Materials, Vol. 17, March 1983, pp.114-134.

182. Woolstencroft. D. H. , Curtis, A. R. , Harescheugh, R. I.
'A Comparison of Test Techniques used for the Evaluation of the Unidirectional Compressive Strength of CFRP'.
Composites, Vol. 12, No. 4, Oct 1981.

183. Yamamoto, M.
'Determination of Meltability of High Modulus Carbon Fibre by its Matrix Resin'.
International Conference on Carbon Fibre, Plastic Institute, London, 1971.

184. Yokota, M. J.
'In Process Controlled Curing of Resin Matrix Composites'.
SAMPE J., Vol. 14, No. 4, 1978.

185. Yoshida, H. , Ogasa, T. , Hayashi, R.
'Statistical Approach to the Relationship Between ILSS and Void Content of CFRP', Composites Science and Technology, Vol. 25, No. 1, 1986.

TABLES

Experiment No.	Material	Curing Conditions and Other Parameters		No. of Slabs	Measured Parameters	Purposes & Comments
		Constants	Variables			
1	913G-E	Temperature = 150°C Pressure = 2000 kN/m^2 Time = 20 mins.	Solvent Addition		- Density - Fibre Volume Fraction - Void content	- Effect of solvent addition on void content. - Unidirectional stacking configuration. - Refer to Fig.6 for Sample Pattern.
			Pentane - $CH_3(CH_2)_3CH_3$	1		
			Freon - CCl_2F_2	1		
			Water - H_2O	1		
2	914C	Pressure = 2000 kN/m^2 Time = 1 hour - Cooling to 120°C before releasing pressure. - Postcure at 190°C in vacuum oven for 4 hours.	Curing Temperature (°C)		- Density - Fibre Volume Fraction - Void content - Inter-Laminar Shear Strength (ILSS)	- Effect of curing temperature on void content. - Unidirectional stacking configuration. - Refer to Fig.6 for Sample Pattern.
			150	1		
			160	1		
			165	1		
			170	1		
			175	1		
			180	1		
3		Temperature = 170°C Time = 1 hour - Cooling to 120°C before releasing pressure. - Postcure at 190°C in vacuum oven for 4 hours.	Curing Pressure (kN/m^2)			- Effect of curing pressure on void content. - Unidirectional stacking configuration. - Refer to Fig.7 for Sample Pattern.
			327	1		
			653	1		
			980	1		
			1307	1		
			1633	1		
			1960	1		

Table 1 Overview of Experiments

Experiment No.	Material	Curing Conditions and Other Parameters			No. of Slabs	Measured Parameters	Purposes & Comments
		Constants	Variables				
4	914C-833-40 Woven Fabric Prepreg	Temperature = 170°C Time = 1 hour - Cooling to 120°C before releasing pressure. - Postcure at 190°C in vacuum oven for 4 hours.	Jig Design	Curing Pressure		- Density - Fibre Volume Fraction - Void content - Thickness - Static Compressive Strength - Fatigue Compressive Strength	- Influence of jig design on the results of static compressive test. - Stacking configuration: (0/90, +45/-45, +45/-45, 0/90)$_{2s}$. - Refer to Figures 2, 3, and 4 for jig design. - Refer to Fig.8 for Sample Pattern.
			Celanese Jig	653 kN/m^2	8		
			ABG-1				
			ABG-2				
			CRAG Jig				
			Celanese Jig	1307 kN/m^2	8		
			ABG-1				
			ABG-2				
			CRAG Jig				
			Celanese Jig	1960 kN/m^2	8		
			ABG-1				
			ABG-2				
			CRAG Jig				
5		Temperature = 170°C Time = 1 hour - Cooling to 120°C before releasing pressure. - Postcure at 190°C in vacuum oven for 4 hours.	Curing Pressure (kN/m^2)			- Density - Fibre Volume Fraction - Void content - Thickness	- Influence of curing pressure on void content. - Stacking configuration: (0/90, +45/-45, +45/-45, 0/90)$_{2s}$. - Refer to Fig.9 for Sample Pattern.
			653		1		
			1633		1		
			2940		1		

Table 1 Overview of Experiments (continued)

Experiment No.	Material	Curing Conditions and Other Parameters			No. of Slabs	Measured Parameters	Purposes & Comments
		Constants	Variables				
			Curing Pressure	Lay-up Conditions			
6	914C-833-40 Woven Fabric Prepreg	Temperature = 170°C Time = 1 hour - Cooling to 120°C before releasing pressure. - Postcure at 190°C in vacuum oven for 4 hours.	1000 kN/m²	with frame; Two layers of bleed cloth	1	- Density - Fibre Volume Fraction - Void content - Thickness	- Effect of lay-up conditions on void content. - Stacking configuration: (0/90, +45/-45, +45/-45, $0/90)_{2s}$. - Refer to Fig.10 for Sample Pattern.
				no frame; Two layers of bleed cloth	1		
				with frame; Four layers of bleed cloth	1		
				no frame; Four layers of bleed cloth	1		
			3000 kN/m²	with frame; Two layers of bleed cloth	1		
				no frame; Two layers of bleed cloth	1		
				with frame; Four layers of bleed cloth	1		
				no frame; Four layers of bleed cloth	1		

Table 1 Overview of Experiments (continued)

Experiment No.	Material	Curing Conditions and Other Parameters		No. of Slabs	Measured Parameters	Purposes & Comments
		Constants	Variables			
7	914C-833-40 Woven Fabric Prepreg	Temperature = 170°C Pressure = 2000 kN/m^2 Time = 1 hour - Cooling to 120°C before releasing pressure. - Postcure at 190°C in vacuum oven for 4 hours.	Partial Cure Time (mins)		- Density - Fibre Volume Fraction - Void content - Thickness	- Effect of partial cure time on void content. - Stacking configuration: (0/90, +45/-45, +45/-45, 0/90)$_{2s}$. - Refer to Fig.10 for Sample Pattern. - Trial run for Experiment 8.
			0	1		
			5	1		
			10	1		
			15	1		
			30	1		
			45	1		
8		Temperature = 170°C Pressure = 2000 kN/m^2 Time = 1 hour - Cooling to 120°C before releasing pressure. - Postcure at 190°C in vacuum oven for 4 hours.	Partial Cure Time (mins)		- Density - Fibre Volume Fraction - Void content - Thickness - Static Compressive Strength - Fatigue Compressive Strength. - Static residual compressive strength	- Effect of partial cure time on static and fatigue compressive strengths. - Stacking configuration: (0/90, +45/-45, +45/-45, 0/90)$_{2s}$. - Refer to Fig.11 for Sample Pattern. - More points were selected between 0 ~ 15 mins based on findings of Experiment 7 (trial run). - Residual strength on samples fatigue cycling at 55% stress level.
			0	5		
			5	5		
			8	5		
			12	5		
			15	5		
			20	5		
			30	5		

Table 1 Overview of Experiments (continued)

Experiment No.	Material	Variables	Density (g/cm^3)	Fibre Volume Fraction	Void Content (%)	Interlaminar Shear Strength(MPa)	Comments
1	913G-E	Solvent Addition					- Void content range is too small.
		Pentane - $CH_3(CH_2)_3CH_3$	2.1325	0.6613	-0.06		
		Freon - CCl_2F_2	2.0825	0.6439	0.41		
		Water - H_2O	2.0469	0.6429	1.08		
2	914C	Curing Temperature (°C)					- Void content range is too small.
		150	1.5505	0.6459	3.07	46.91	
		160	1.5648	0.6548	2.19	68.33	
		165	1.5602	0.6459	2.42	74.91	
		170	1.5641	0.6531	2.56	66.94	
		175	1.5451	0.6376	3.22	66.05	
		180	1.5466	0.6389	3.15	75.61	
3		Curing Pressure (kN/m^2)					- Void content range is too small.
		327	1.5454	0.6163	2.46	79.60	
		653	1.5448	0.6518	3.74	65.47	
		980	1.5813	0.6737	0.20	68.01	
		1307	1.6115	0.6899	0.62	80.22	
		1633	1.6395	0.7070	-0.65	96.74	
		1960	1.6348	0.7002	-0.51	91.75	

Table 2 Overview of Experimental Results

Experiment No.	Material	Variables		Density (g/cm^3)	Fibre Volume Fraction	Void Content (%)	Thickness (mm)	Static Compressive Strength (MPa)	Secant Modulus (GPa)	Failure Strain (%)	Comments
4	914C-833-40 Woven Fabric Prepreg	Jig Design	Curing Pressure								
		Celanese Jig	653 kN/m^2	1.5707	0.6178	0.57	2.247	442	45.2	0.91	- Celanese jig & ABG-1 produced high compressive strength. - ABG-1, ABG-2 difficult to set up. - CRAG jig is used for fatigue testing due to its good performance.
		ABG-1						403	47.7	0.89	
		ABG-2						369			
		CRAG jig						376			
		Celanese Jig	1307 kN/m^2	1.5801	0.6306	0.27	2.202	447	47.6	0.93	
		ABG-1						416	49.1	0.87	
		ABG-2						396			
		CRAG jig						384			
		Celanese Jig	1960 kN/m^2	1.5736	0.6138	0.20	2.202	490	46.4	0.90	
		ABG-1						434	49.8	0.93	
		ABG-2						396			
		CRAG jig						387			
5		Curing Pressure (kN/m^2)									- Void content range is too small.
		653		1.5437	0.6076	2.29	2.278				
		1633		1.5735	0.6212	0.37	2.190				
		2940		1.5787	0.6240	0.17	2.167				

Table 2 Overview of Experimental Results (continued)

Experiment No.	Material	Variables		Density (g/cm^3)	Fibre Volume Fraction	Void Content (%)	Thickness (mm)	Comments
6	914C-833-40 Woven Fabric Prepreg	Curing Pressure	Lay-up Conditions					- Moulding without frame produces higher void content. - Moulding with four layers (two on each side) of bleed cloth increases void content. - Void content range is too small. - Not a good way to produce voids.
		1000 kN/m^2	with frame; Two layers of bleed cloth	1.5576	0.6179	1.57	2.230	
			no frame; Two layers of bleed cloth	1.5721	0.6317	1.59	2.188	
			with frame; Four layers of bleed cloth	1.5642	0.6290	1.44	2.200	
			no frame; Four layers of bleed cloth	1.5721	0.6481	1.50	2.146	
		3000 kN/m^2	with frame; Two layers of bleed cloth	1.5777	0.6371	0.69	2.098	
			no frame; Two layers of bleed cloth	1.5863	0.6827	0.94	1.993	
			with frame; Four layers of bleed cloths	1.5842	0.6575	0.90	2.081	
			no frame; Four layers of bleed cloth	1.5908	0.6747	0.98	2.033	

Table 2 Overview of Experimental Results (continued)

Experiment No.	Material	Partial Cure Time (mins)	Density (g/cm^3)	Fibre Volume Fraction	Void Content (%)	Thickness (mm)	Static Compressive Strength (MPa)	Secant Modulus (GPa)	Failure Strain (%)	Residual Compressive Strength (MPa)	Residual Secant Modulus (GPa)	Residual Failure Strain (%))	Comments
7	914C-833-40 Woven Fabric Prepreg	0	1.5742	0.6288	0.66	2.144							- Void content changes drastically between0 ~ 15 mins. - Large range of void content achieved. - Trial run for Experiment 8.
		5	1.5686	0.6018	0.17	2.310							
		10	1.5225	0.5294	1.21	2.652							
		15	1.4775	0.5080	3.93	2.764							
		30	1.4622	0.5024	4.91	3.091							
		45	1.4523	0.4969	5.48	2.946							
8		0	1.5835	0.6346	0.13	2.149	355	49.3	0.73	344	38.4	0.80	- Compressive strength and residual compressive strength (after fatigue) decrease as void content increases. - Large range of void content achieved.
		5	1.5779	0.6238	0.22	2.204	375	46.3	0.79	280	45.0	0.74	
		8	1.5278	0.5293	0.80	2.707	318	38.8	0.85	303	36.3	0.84	
		12	1.4952	0.4993	2.27	2.828	274	36.6	0.76	293	33.8	0.92	
		15	1.5158	0.5333	1.86	2.650	304	38.1	0.82	277	35.5	0.81	
		20	1.4762	0.5101	4.11	2.963	229	35.5	0.69	270	34.6	0.65	
		30	1.4475	0.4796	5.25	2.938	197	31.7	0.67	174	31.9	0.56	

Table 2 Overview of Experimental Results (continued)

GRAPHS

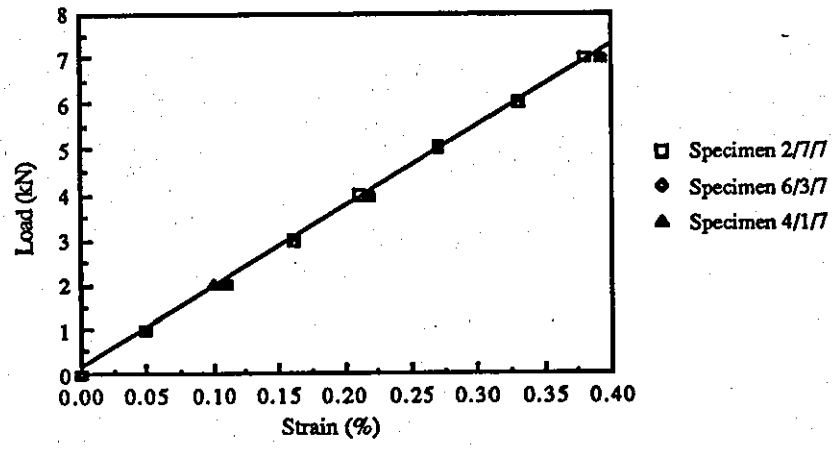

Graph 1 Load versus Strain

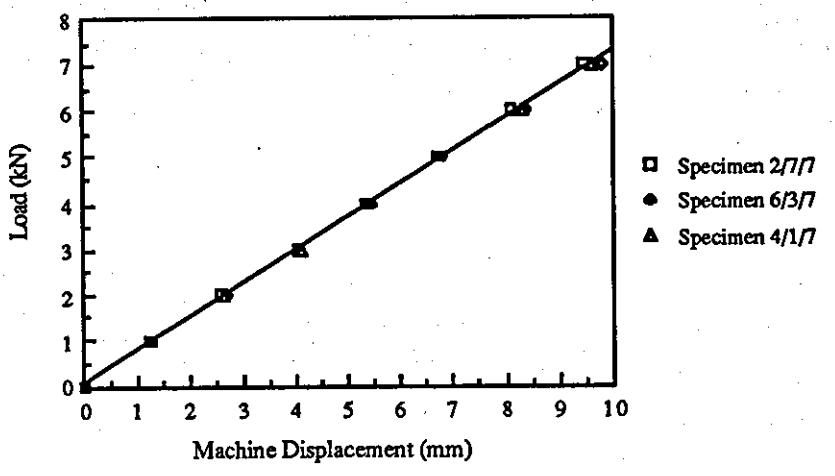

Graph 2 Load versus Machine Displacement

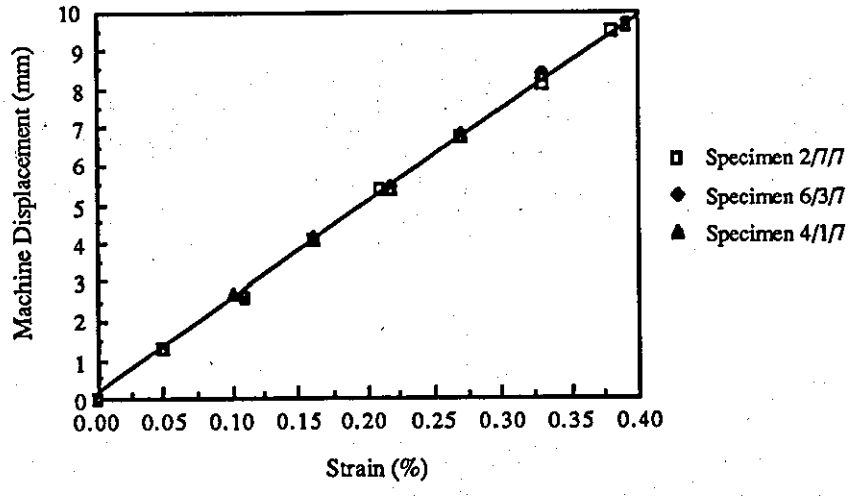

Graph 3 Machine Displacement versus Strain

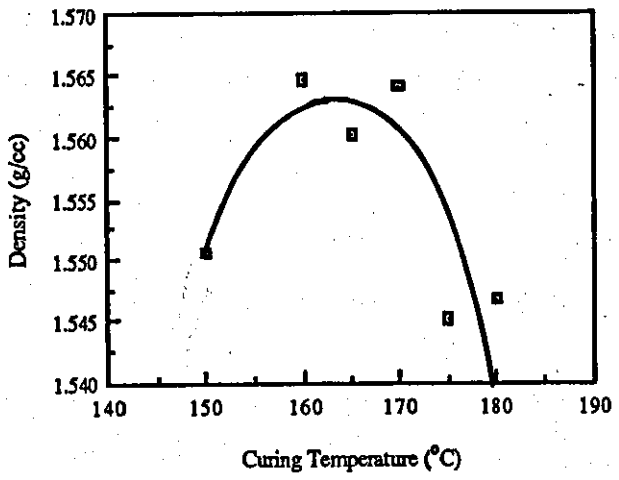

Graph 4 Density vs Curing Temperature (Expt 2)

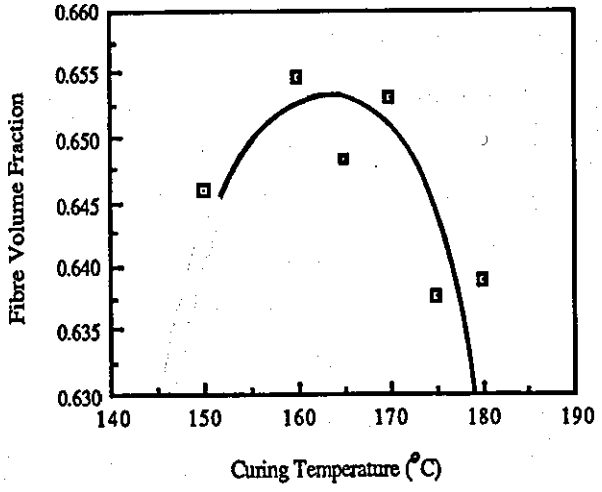

Graph 5 Fibre Volume Fration vs Curing Temperature (Expt 2)

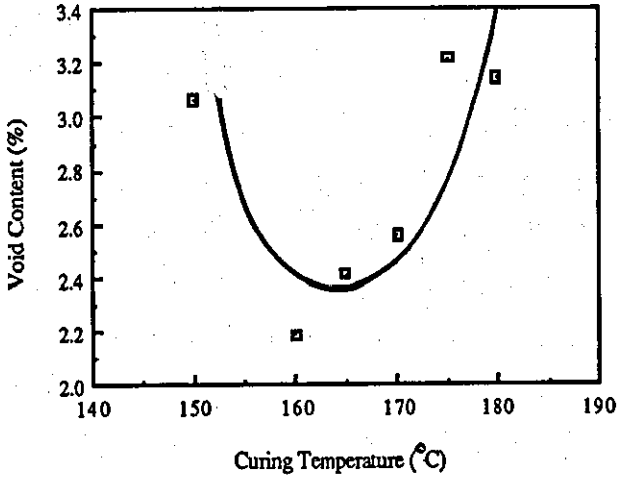

Graph 6 Void Content vs Curing Temperature (Expt 2)

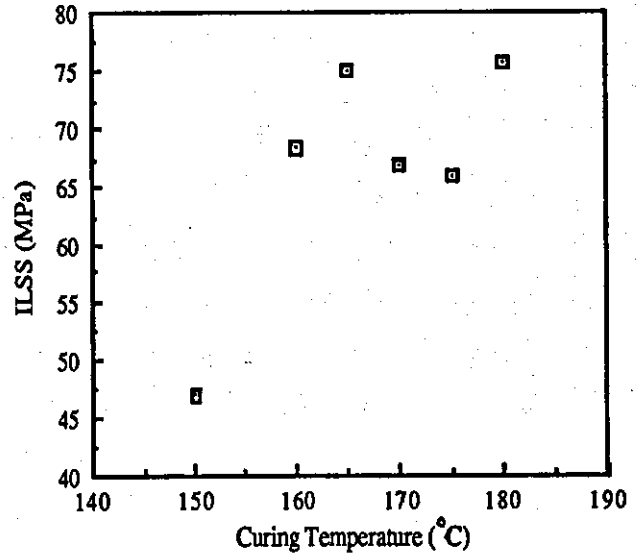

Graph 7 ILSS vs Curing Temperature (Expt 2)

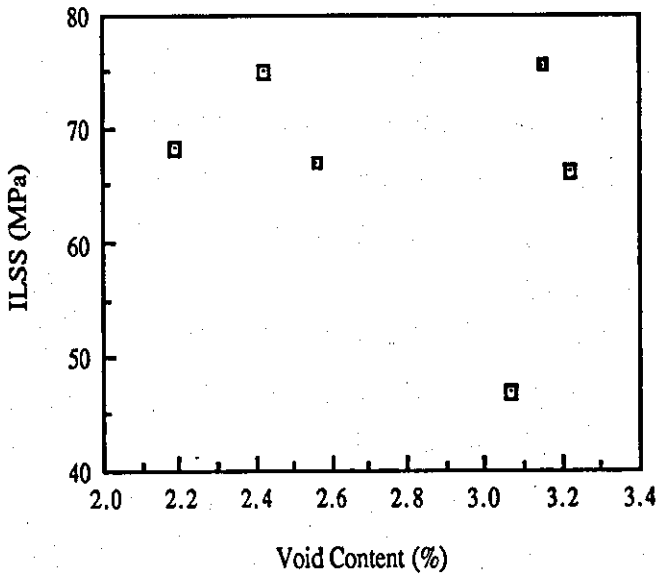

Graph 8 ILSS vs Void Content (Expt 2)

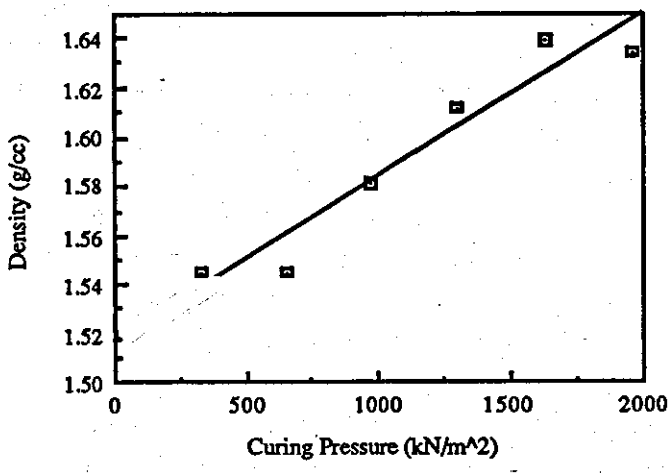

Graph 9 Density vs Curing Pressure (Expt 3)

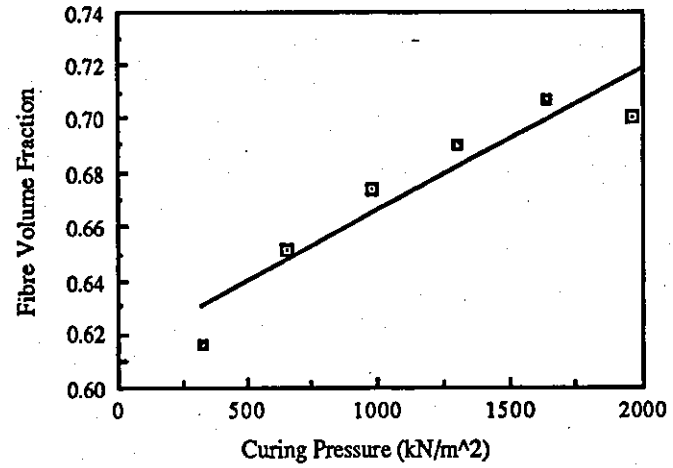

Graph 10 Fibre Volume Fraction vs Curing Pressure (Expt 3)

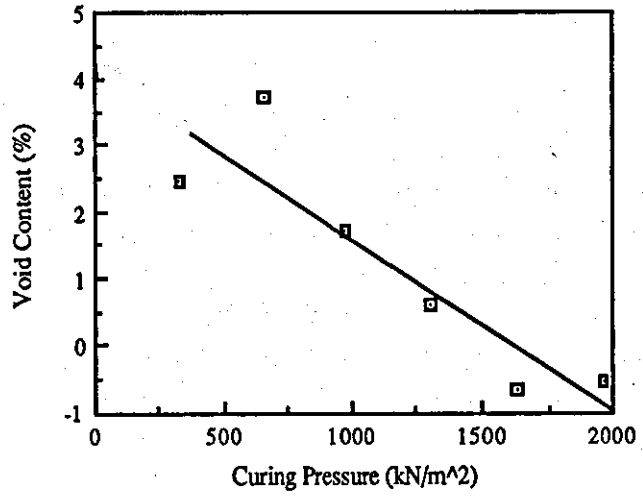

Graph 11 Void Content vs Curing Pressure (Expt 3)

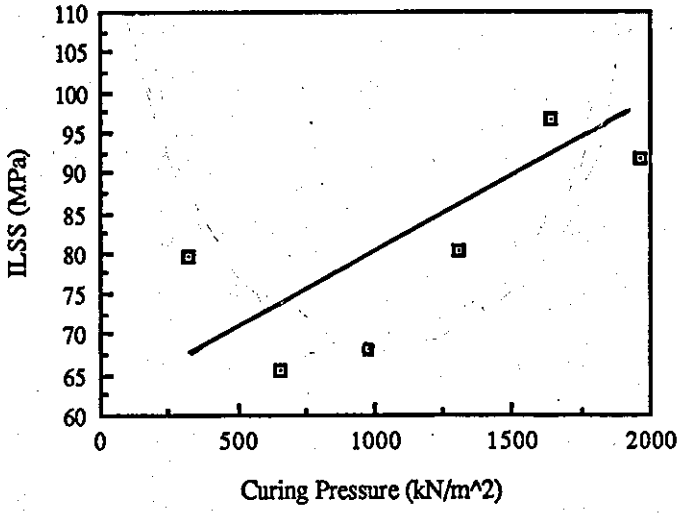

Graph 12 ILSS vs Curing Pressure (Expt 3)

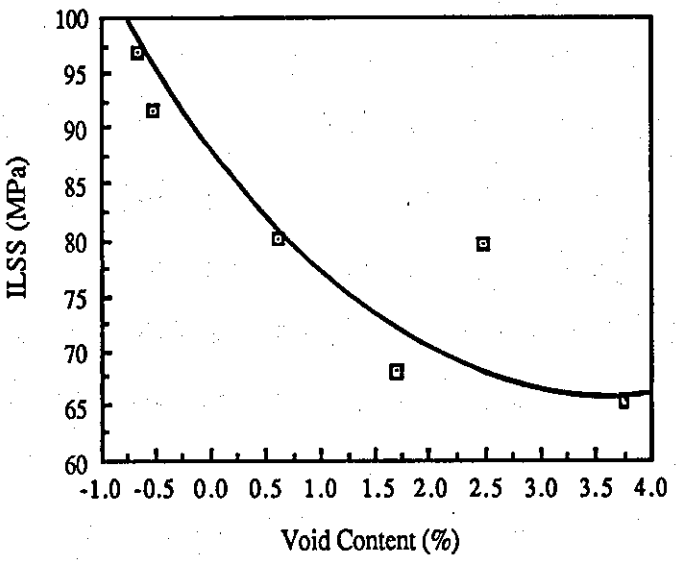

Graph 13 ILSS vs Void Content (Expt 3)

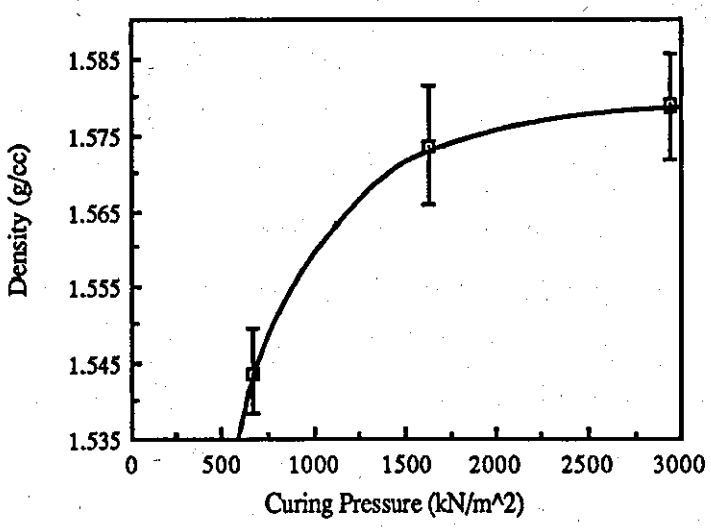

Graph 14 Density vs Curing Pressure (Expt 5)

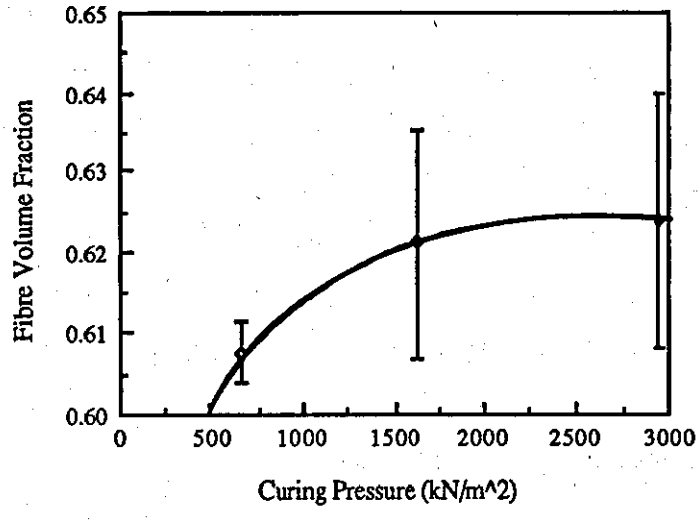

Graph 15 Fibre Volume Fraction vs Curing Pressure (Expt 5)

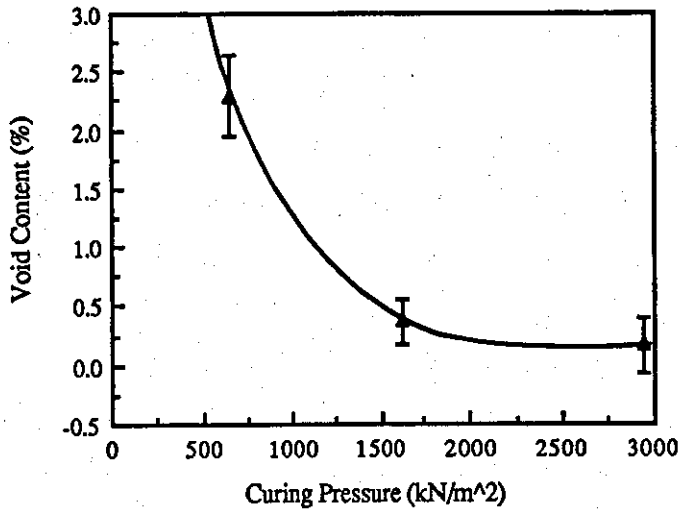

Graph 16 Void Content vs Curing Pressure (Expt 5)

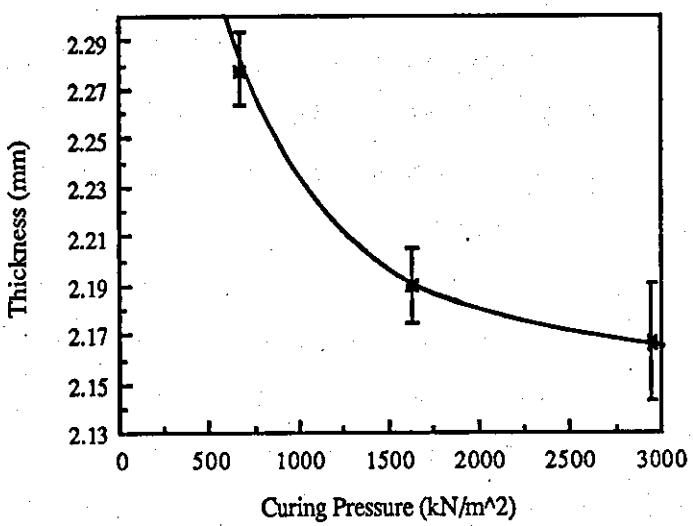

Graph 17 Thickness vs Curing Pressure (Expt 5)

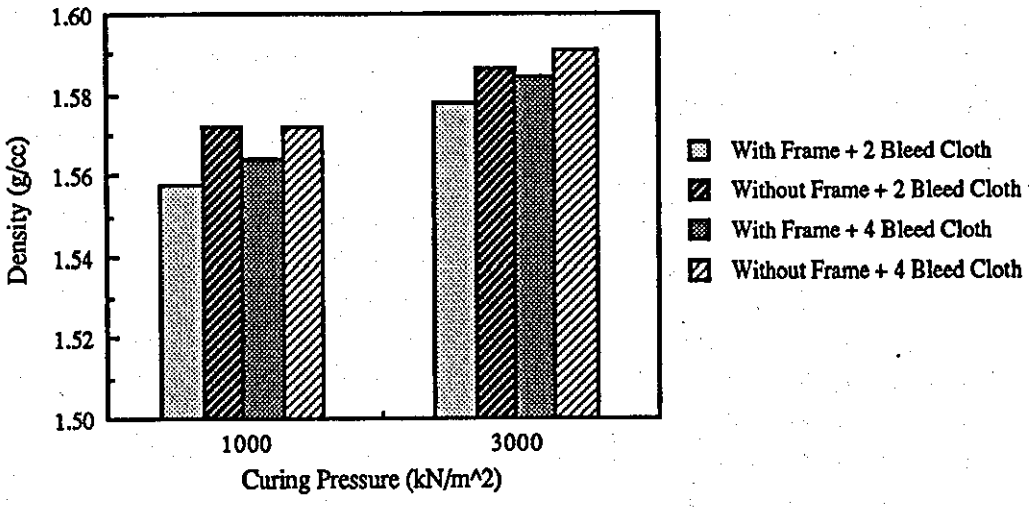

Graph 18 Density vs Curing Pressure for Different Lay-up Conditions (Expt 6)

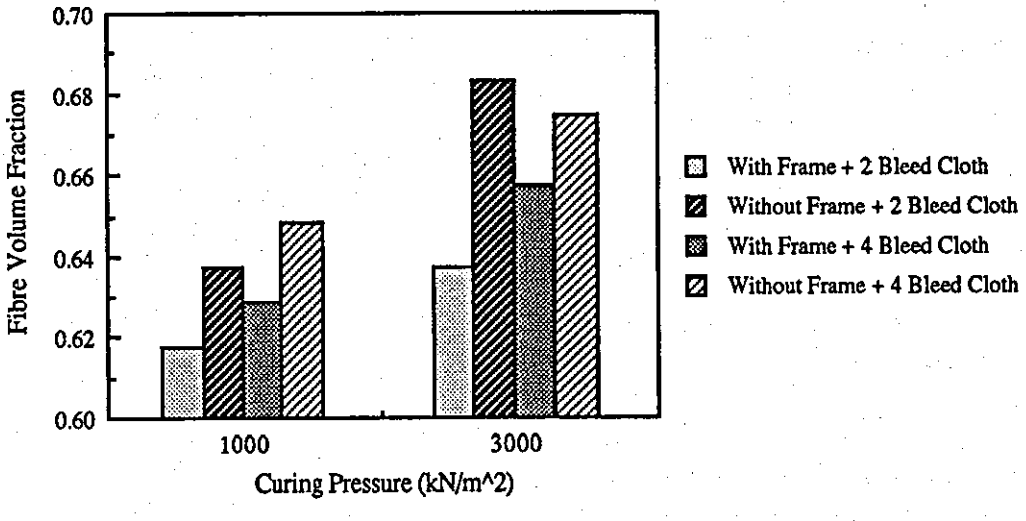

Graph 19 Fibre Volume Fraction vs Curing Pressure for Different Lay-up Conditions (Expt 6)

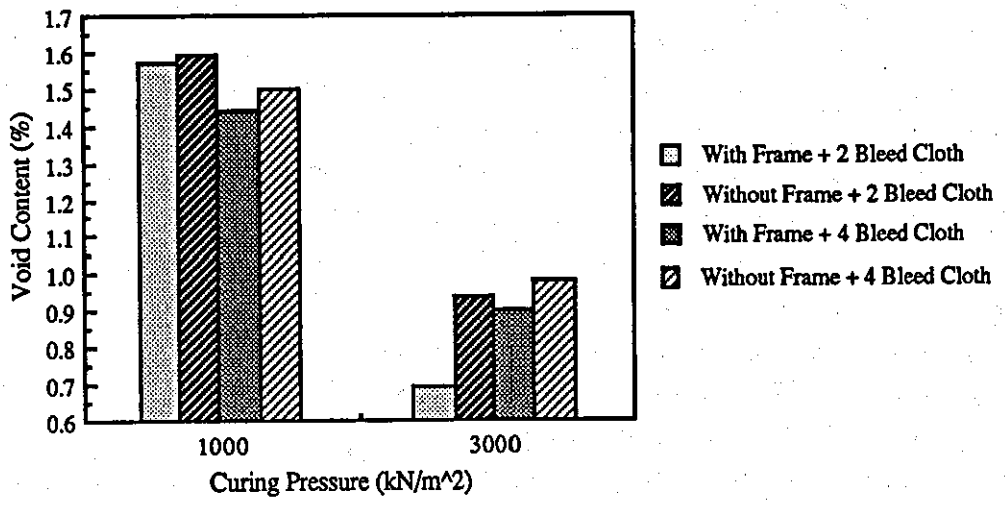

Graph 20 Void Content vs Curing Pressure for Different Lay-up Conditions (Expt 6)

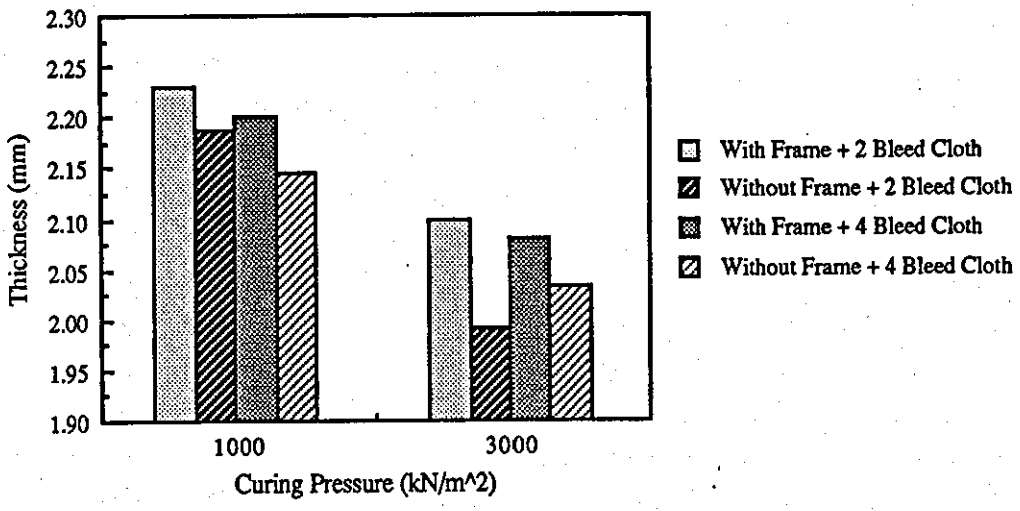

Graph 21 Thickness vs Curing Pressure for Different Lay-up Conditions (Expt 6)

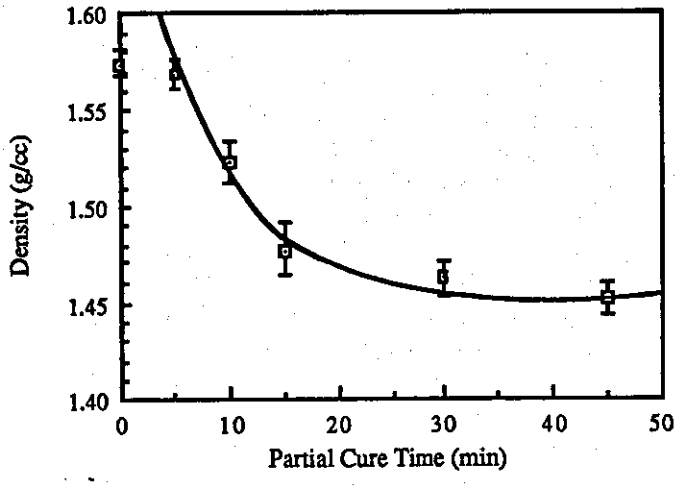

Graph 22 Density vs Partial Cure Time (Expt 7)

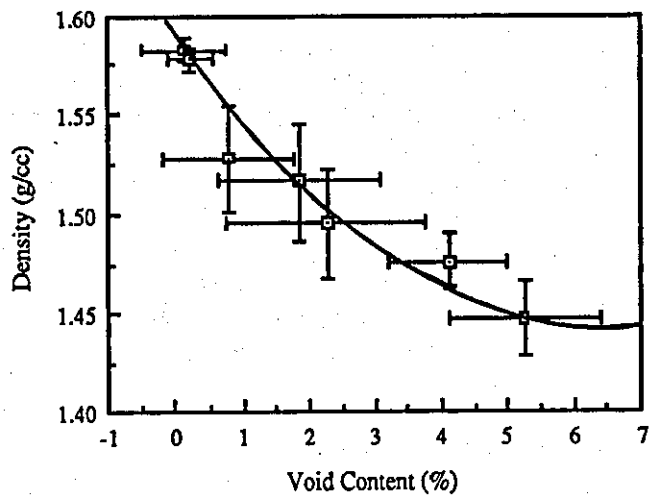

Graph 23 Density vs Void Content (Expt 8)

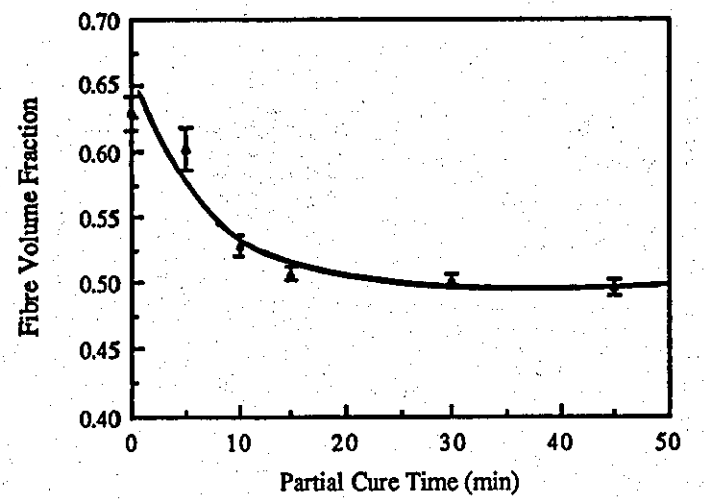

Graph 24 Fibre Volume Fraction vs Partial Cure Time (Expt 7)

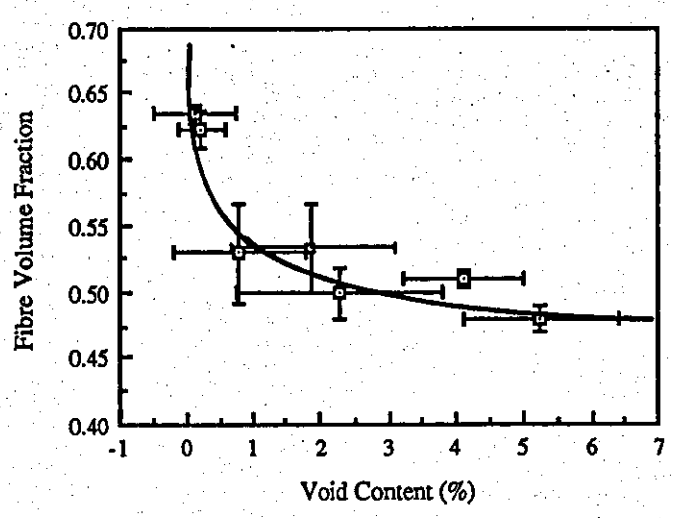

Graph 25 Fibre Volume Fraction vs Void Content (Expt 8)

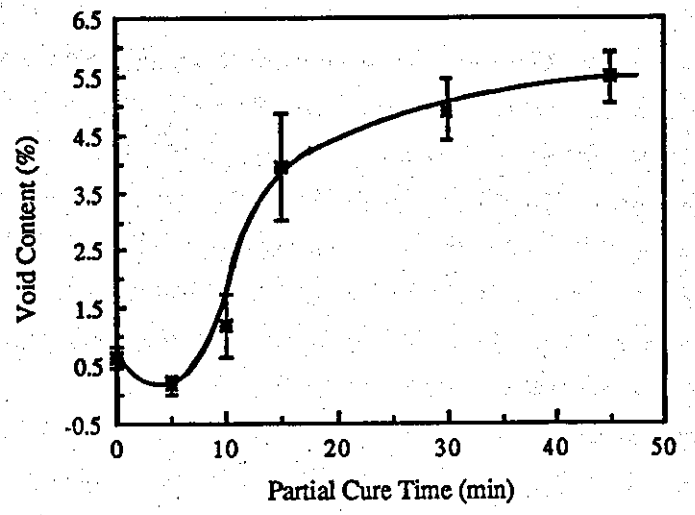

Graph 26 Void Content vs Partial Cure Time (Expt 7)

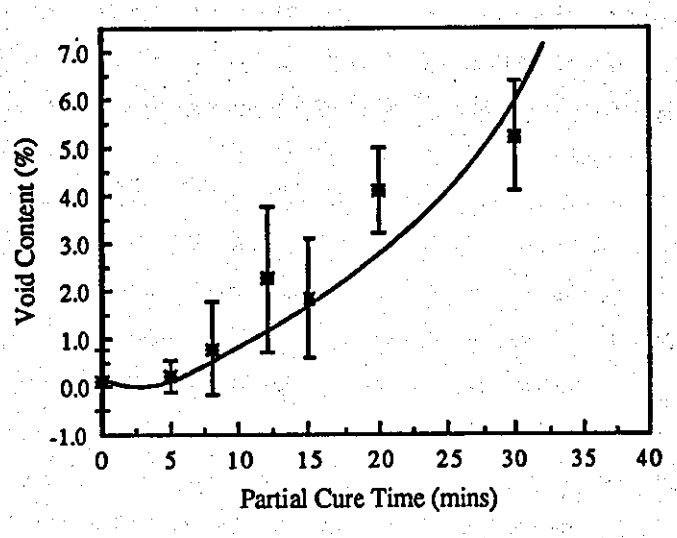

Graph 27 Void Content vs Partial Cure Time (Expt 8)

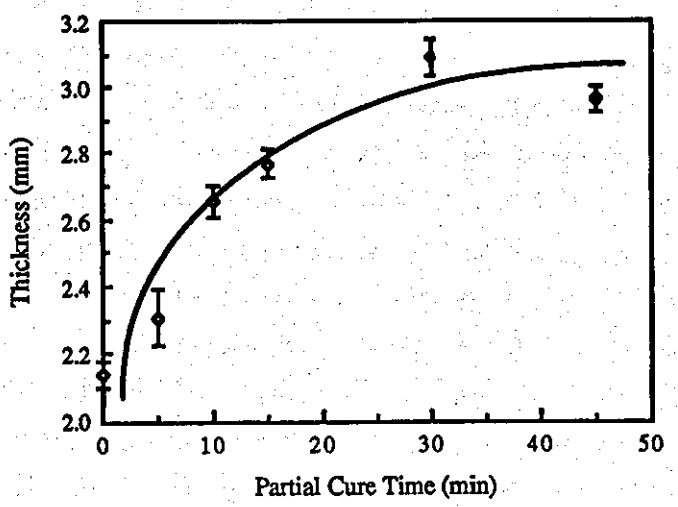

Graph 28 Thickness vs Partial Cure Time (Expt 7)

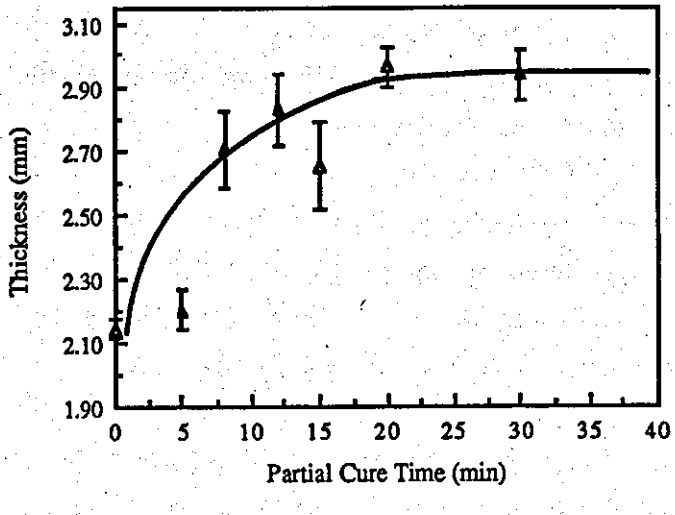

Graph 29 Thickness vs Partial Cure Time (Expt 8)

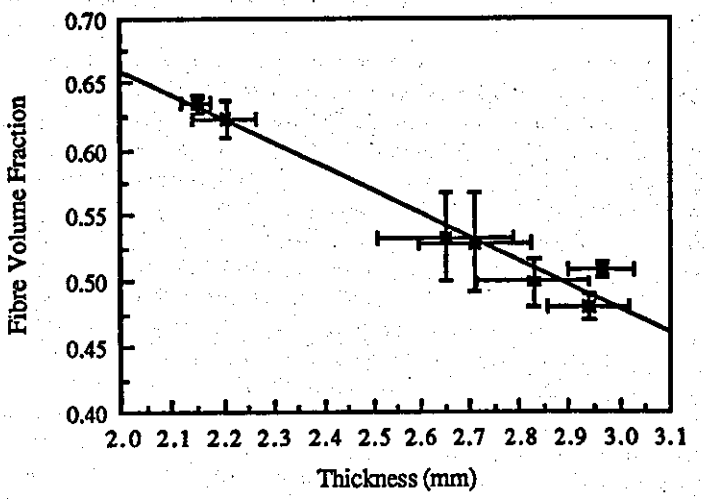

Graph 30 Fibre Volume Fraction vs Thickness (Expt 8)

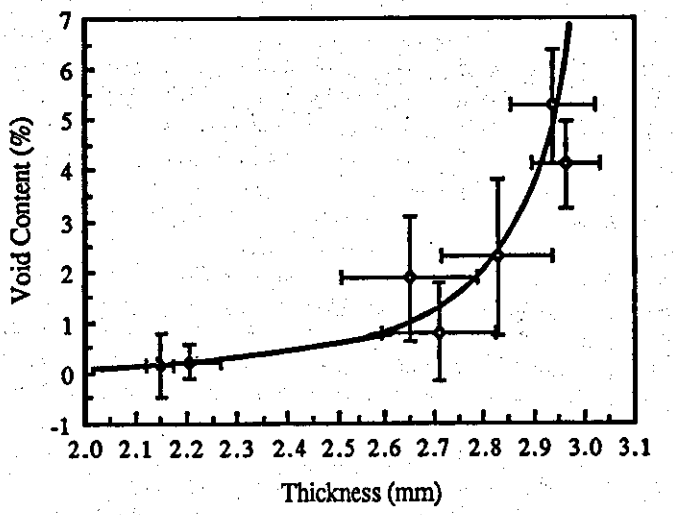

Graph 31 Void Content vs Thickness (Expt 8)

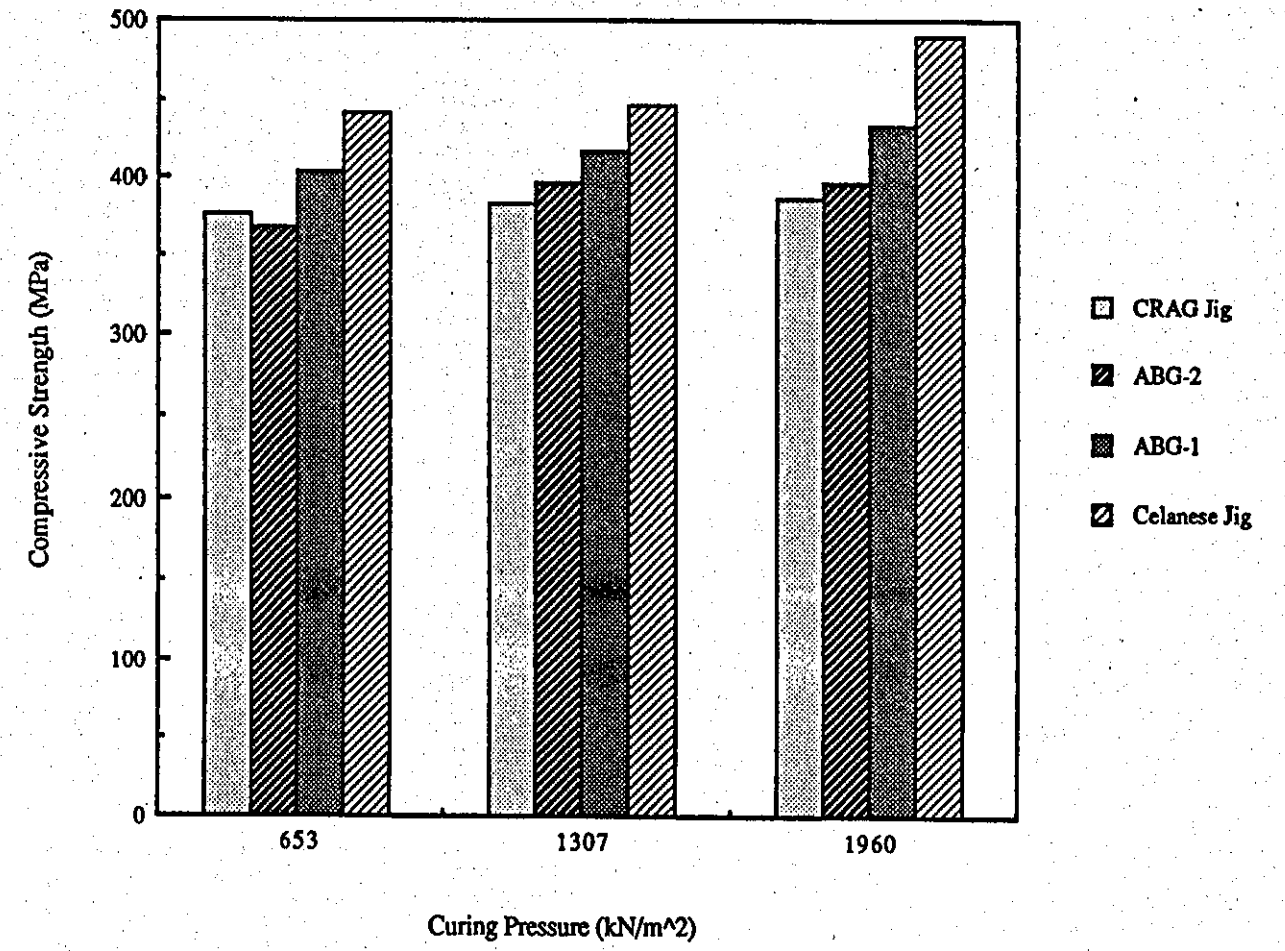

Graph 32 Different Jig Design on Static Compressive Strength (Expt 4)

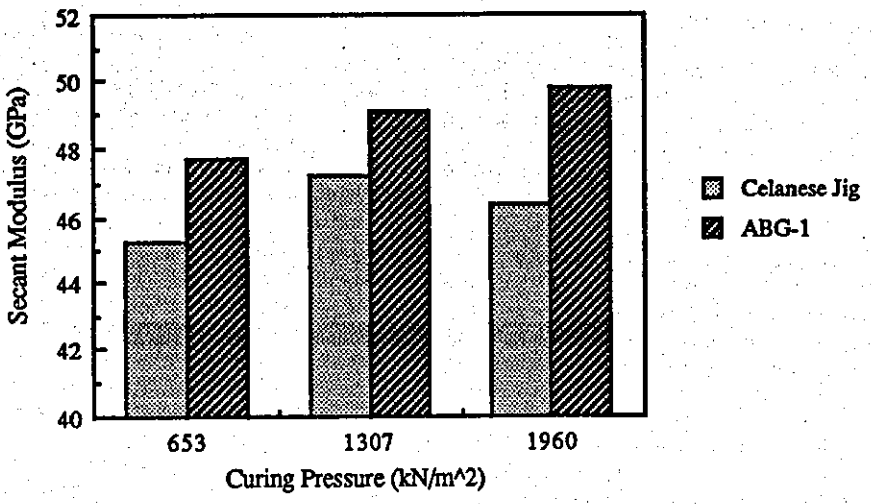

Graph 33 Secant Modulus vs Curing Pressure (Expt 4)

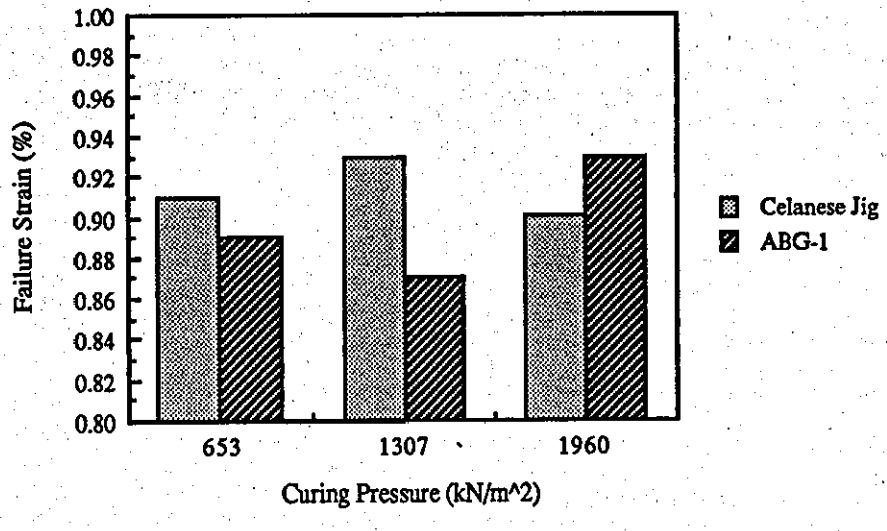

Graph 34 Failure Strain vs Curing Pressure (Expt 4)

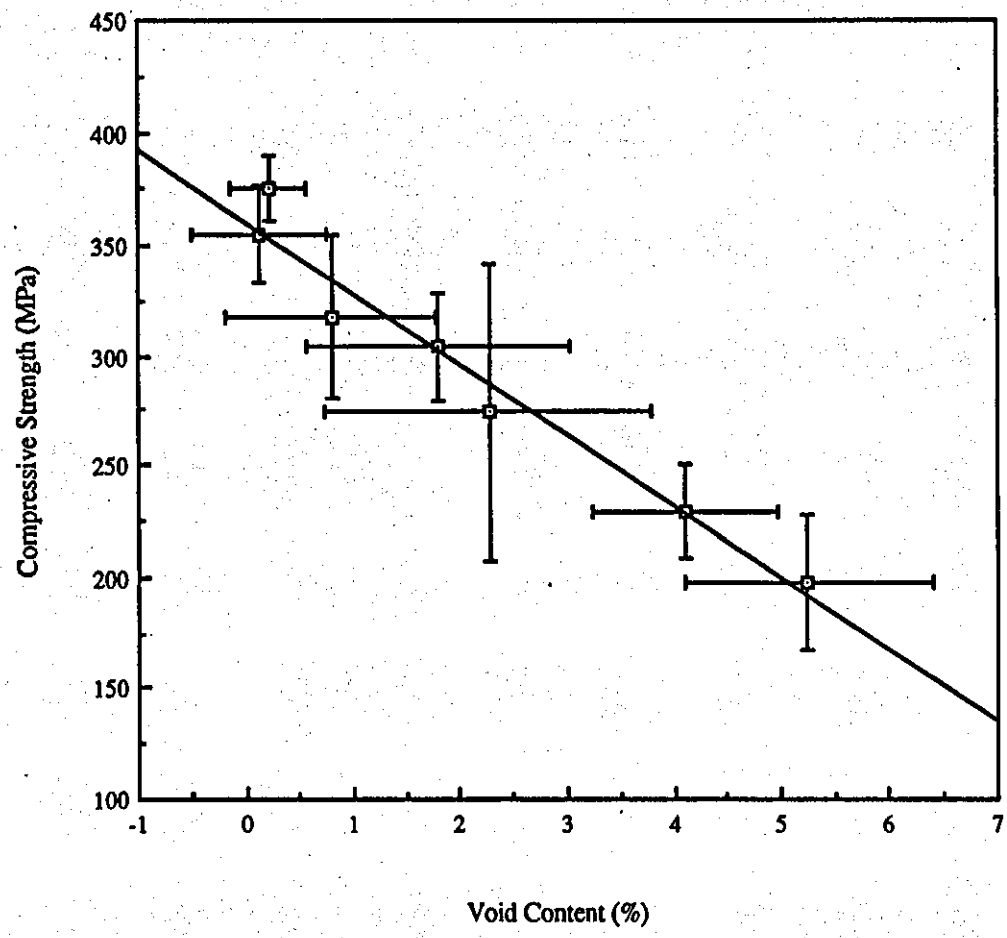

Graph 35 Compressive Strength vs Void Content (Expt 8)

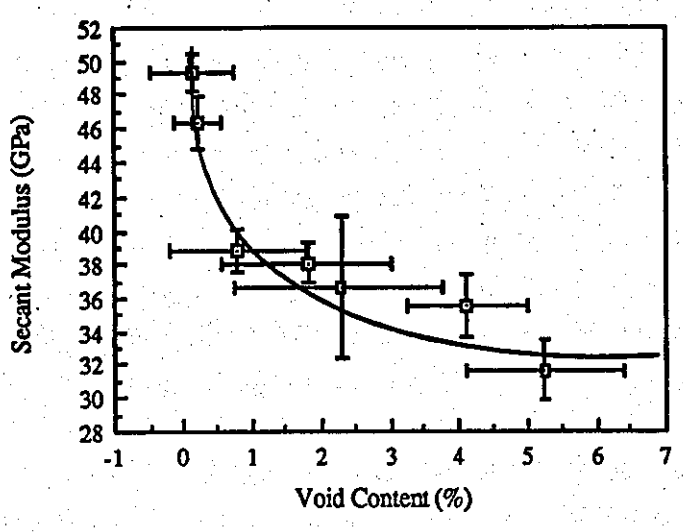

Graph 36 Secant Modulus vs Void Content (Expt 8)

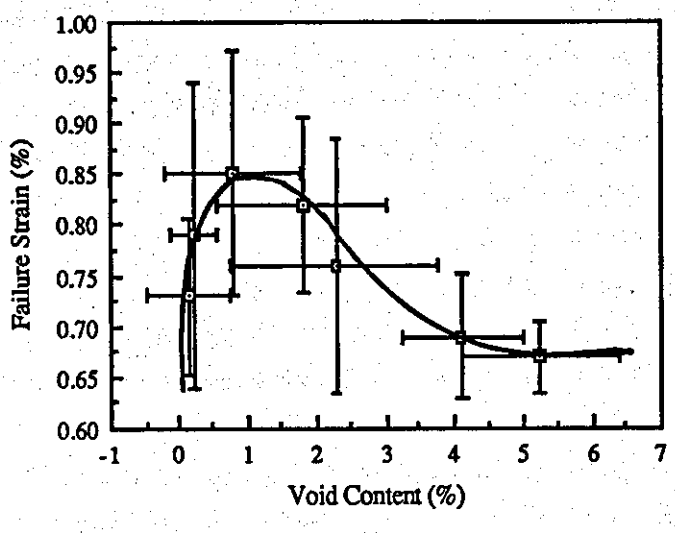

Graph 37 Failure Strain vs Void Content (Expt 8)

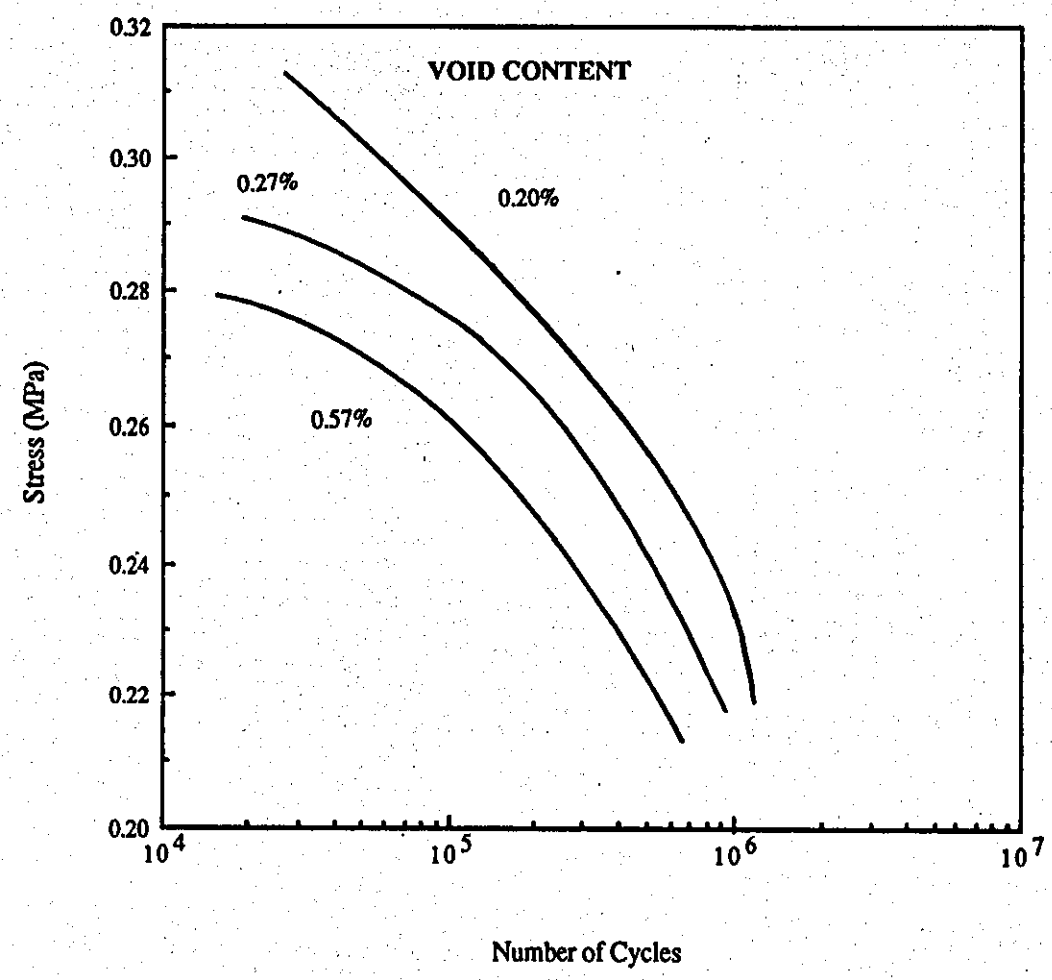

Graph 38 S/N Curves for Mouldings With Different void contents (Expt 4)

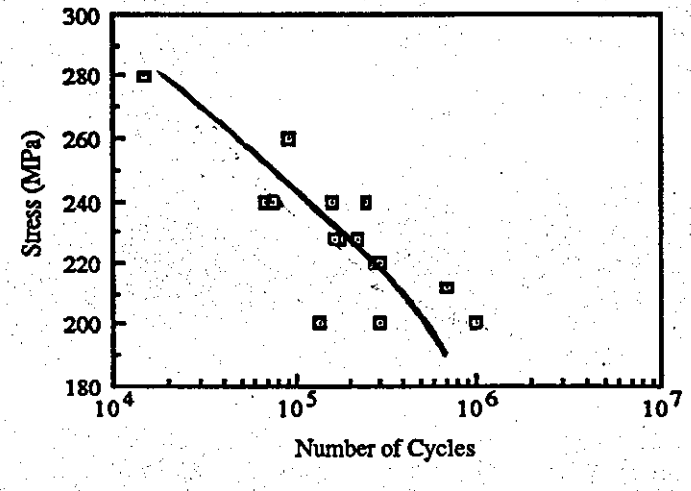

Graph 39 S/N Curve for 653 kN/m^2 Curing Pressure (Expt 4)

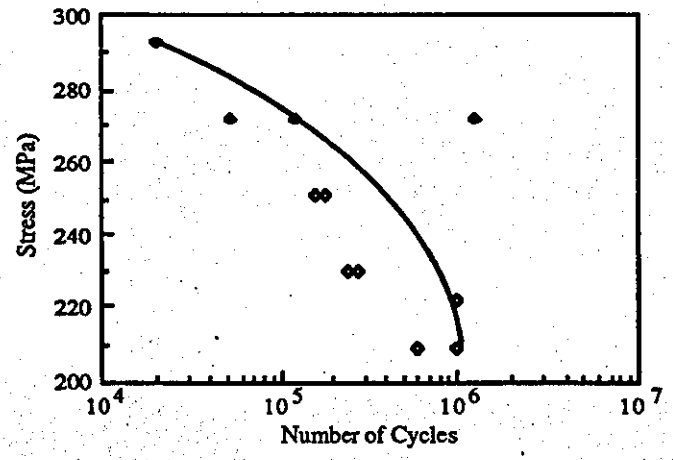

Graph 40 S/N Curve for 1307 kN/m^2 Curing Pressure (Expt 8)

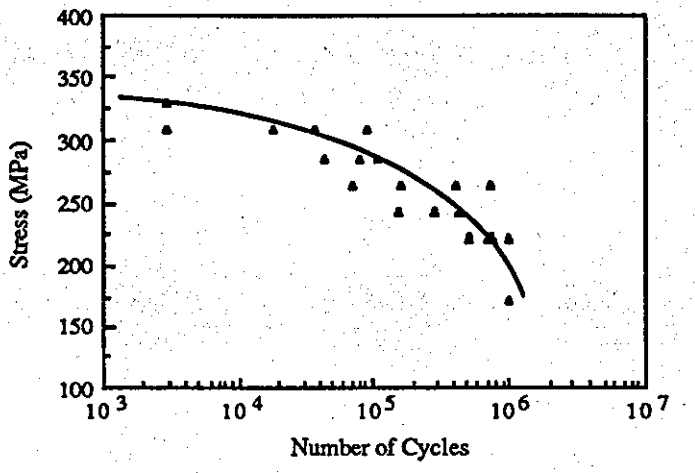

Graph 41 S/N Curve for 1960 kN/m^2 Curing Pressure (Expt 8)

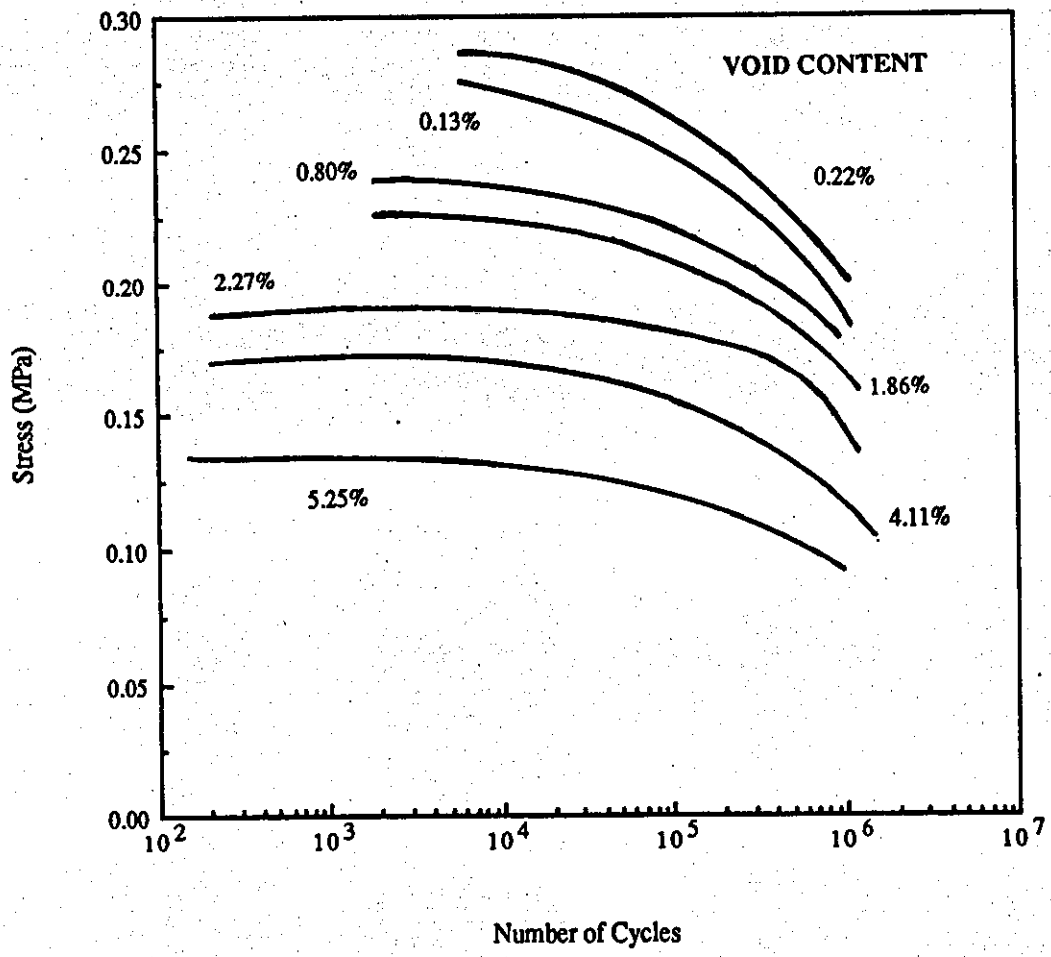

Graph 42 S/N Curves for Mouldings With Different void contents (Expt 8)

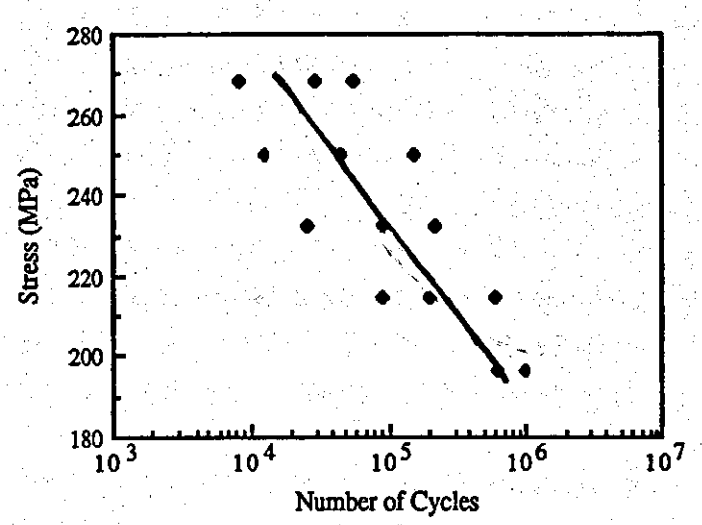

Graph 43 S/N Curve for Zero Minutes Partial Cure Time (Expt 8)

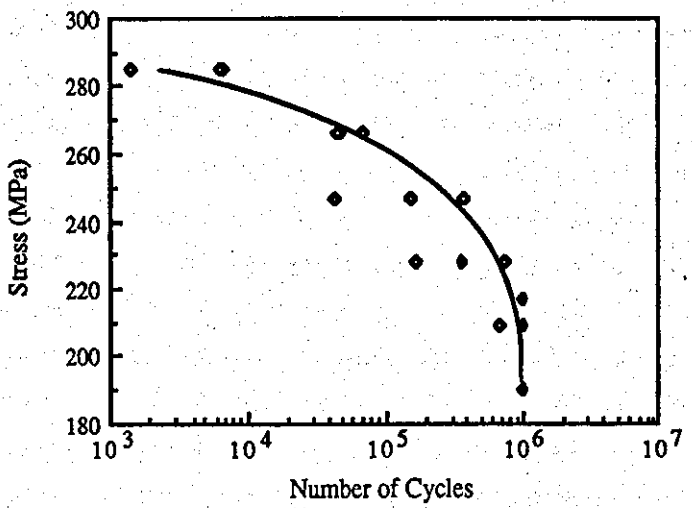

Graph 44 S/N Curve for 5 Minutes Partial Cure Time (Expt 8)

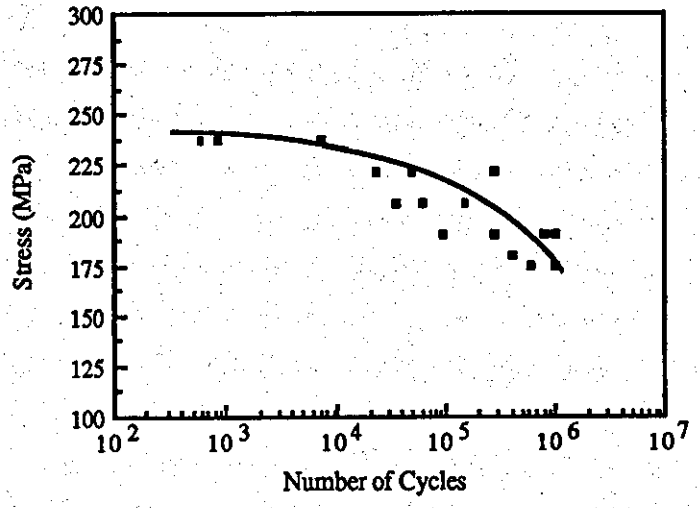

Graph 45 S/N Curve for 8 Minutes Partial Cure Time (Expt 8)

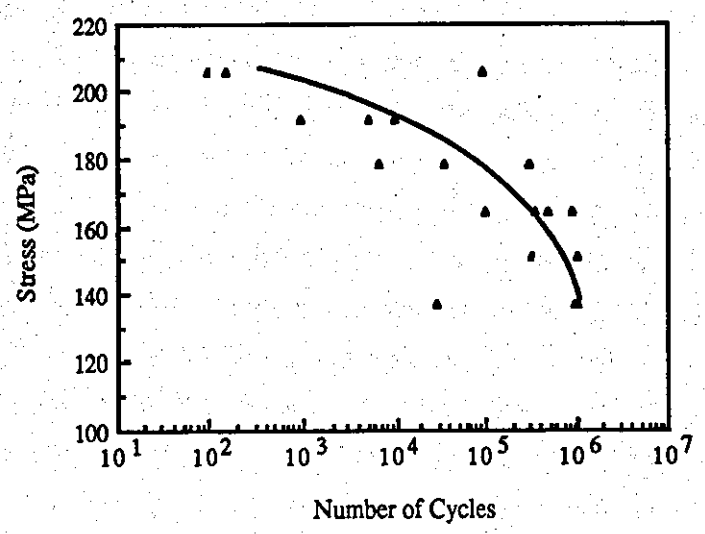

Graph 46 S/N Curve for 12 Minutes Partial Cure Time (Expt 8)

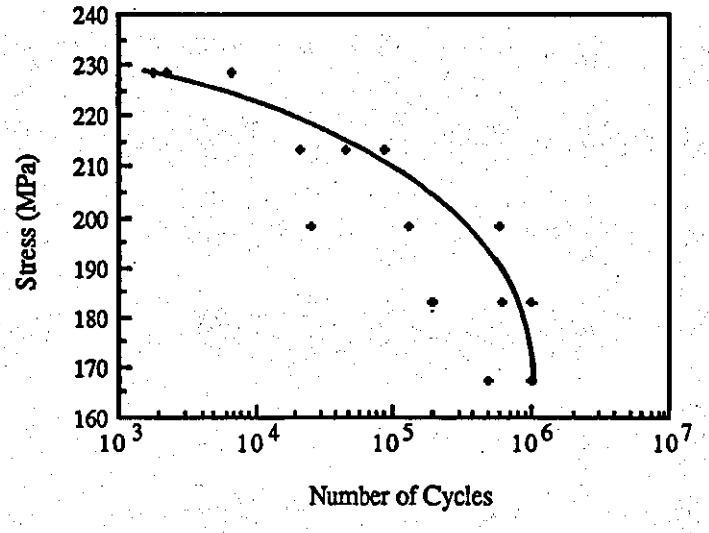

Graph 47 S/N Curve for 15 Minutes Partial Cure Time (Expt 8)

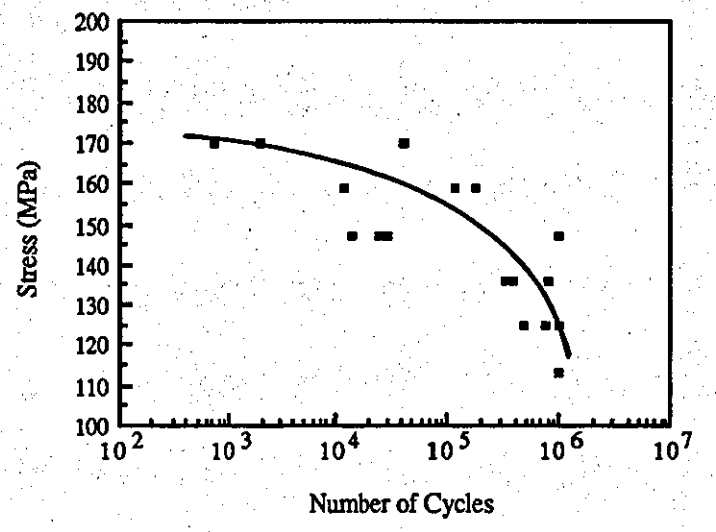

Graph 48 S/N Curve for 20 Minutes Partial Cure Time (Expt 8)

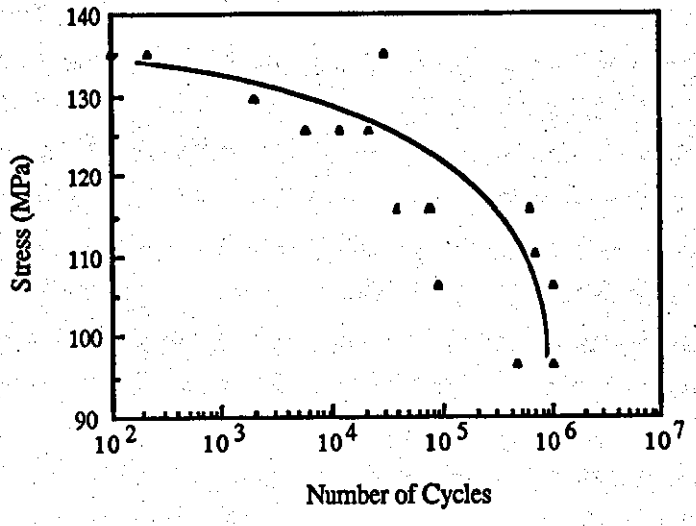

Graph 49 S/N Curve for 30 Minutes Partial Cure Time (Expt 8)

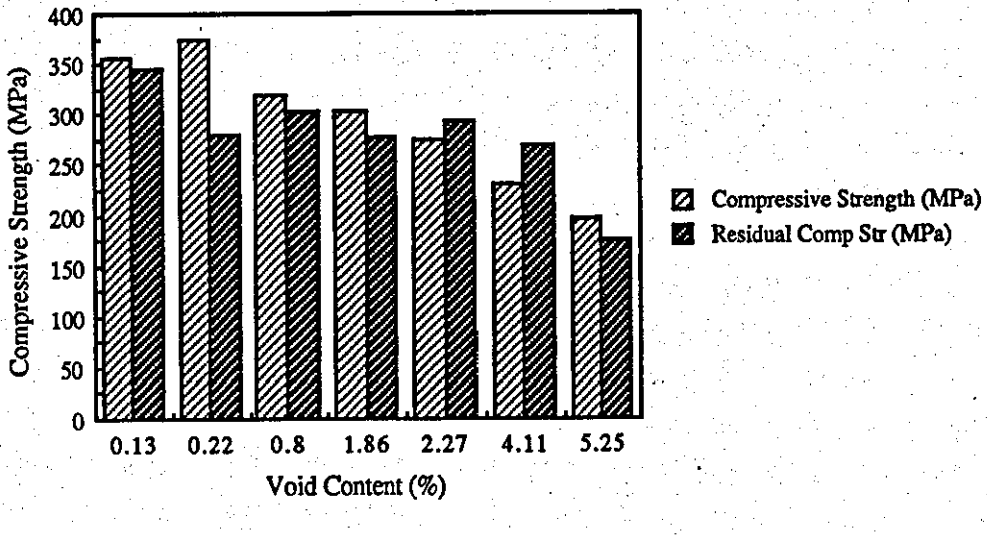

Graph 50 Effect of Fatigue on Static Compressive Strength (Expt 8)

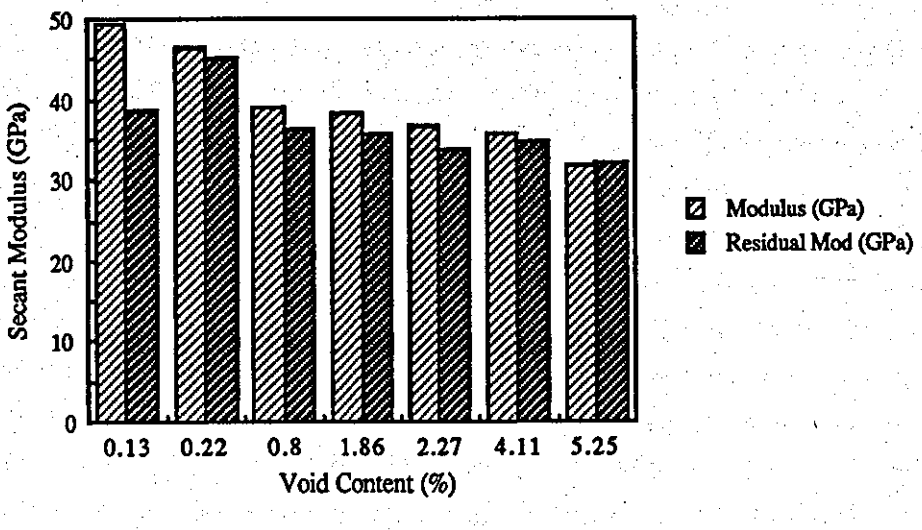

Graph 51 Effect of Fatigue on Secant Modulus (Expt 8)

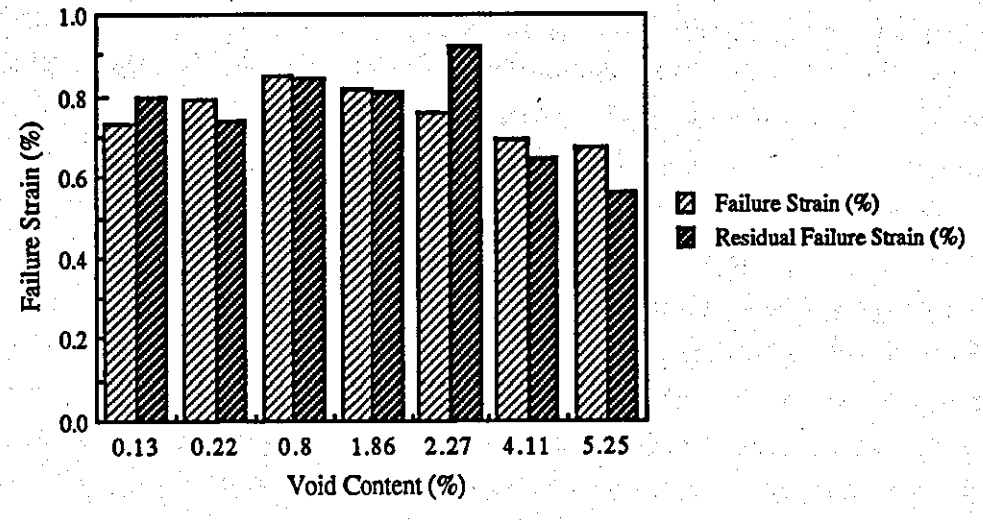

Graph 52 Effect of Fatigue on Failure Strain (Expt 8)

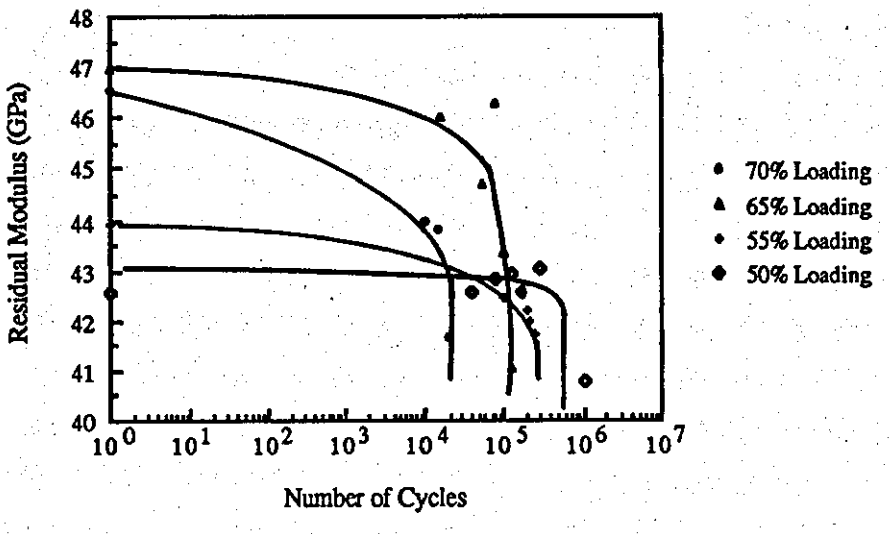

Graph 53 Residual Modulus for 1307 kN/m^2 During Cycling (Expt 4)

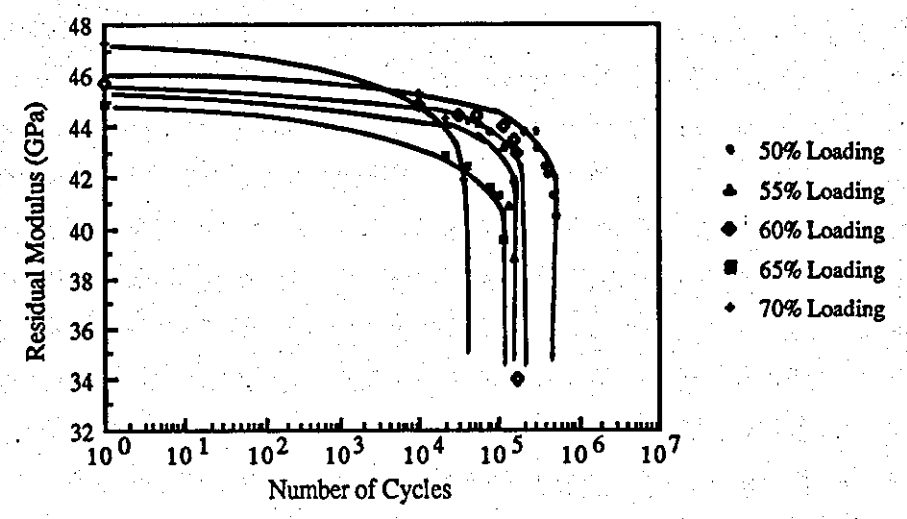

Graph 54 Residual Modulus for 1960 kN/m^2 During Cycling (Expt 8)

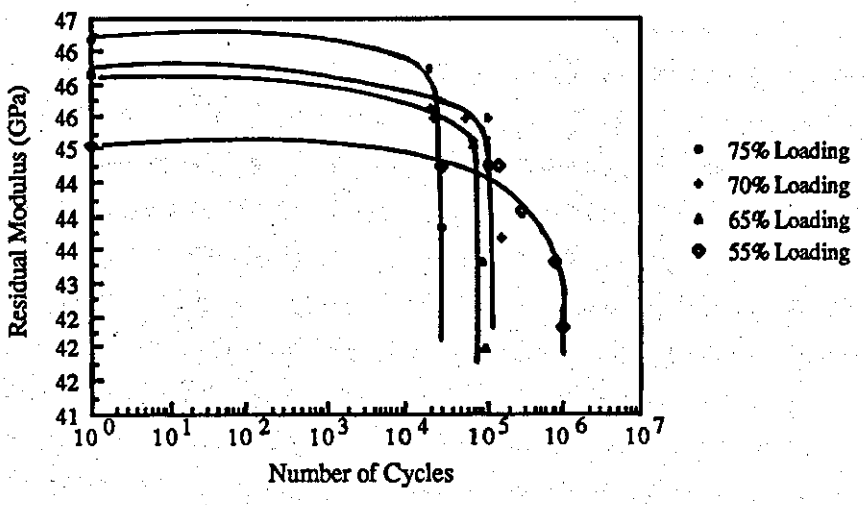

Graph 55 Residual Modulus for Zero Minutes Partial Cure Time During Cycling (Expt 8)

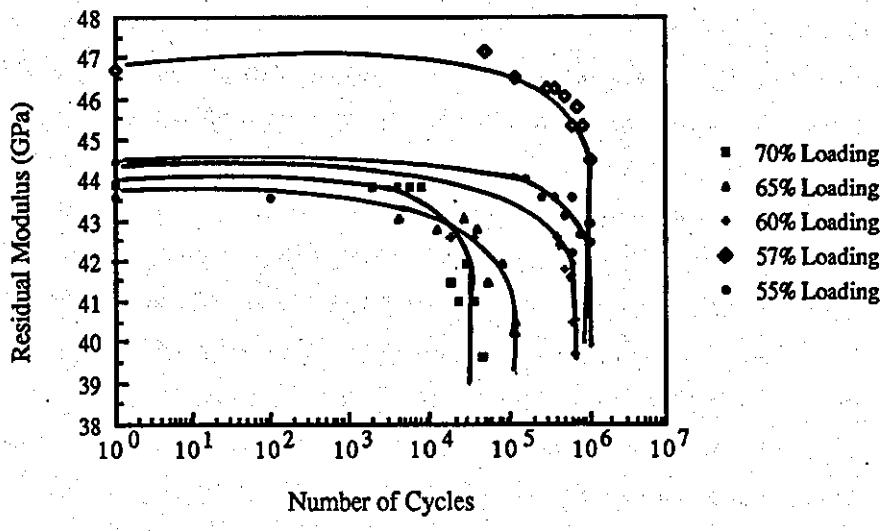

Graph 56 Residual Modulus for 5 Minutes Partial Cure Time During Cycling (Expt 8)

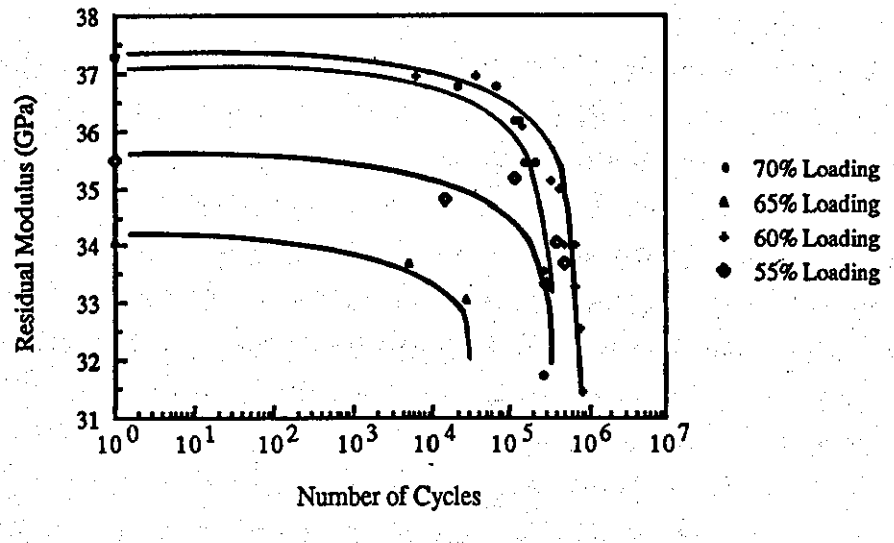

Graph 57 Residual Modulus for 8 Minutes Partial Cure Time During Cycling (Expt 8)

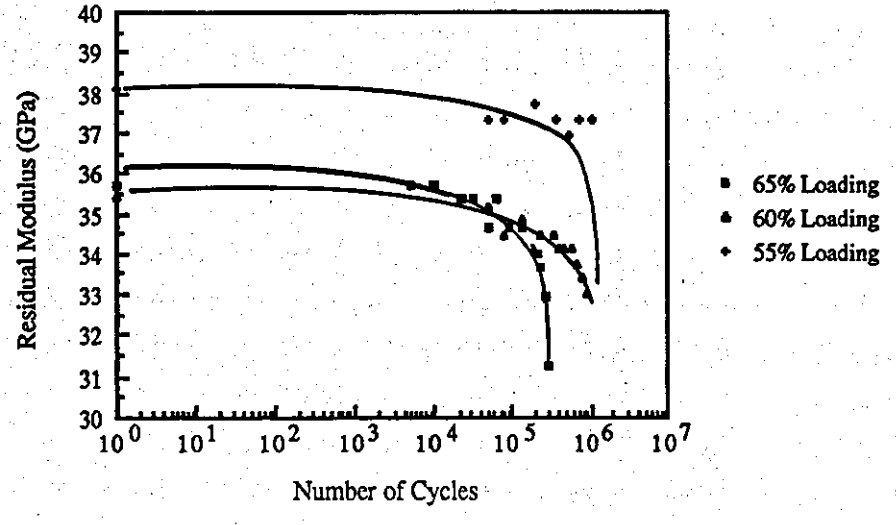

Graph 58 Residual Modulus for 12 Minutes Partial Cure Time During Cycling (Expt 8)

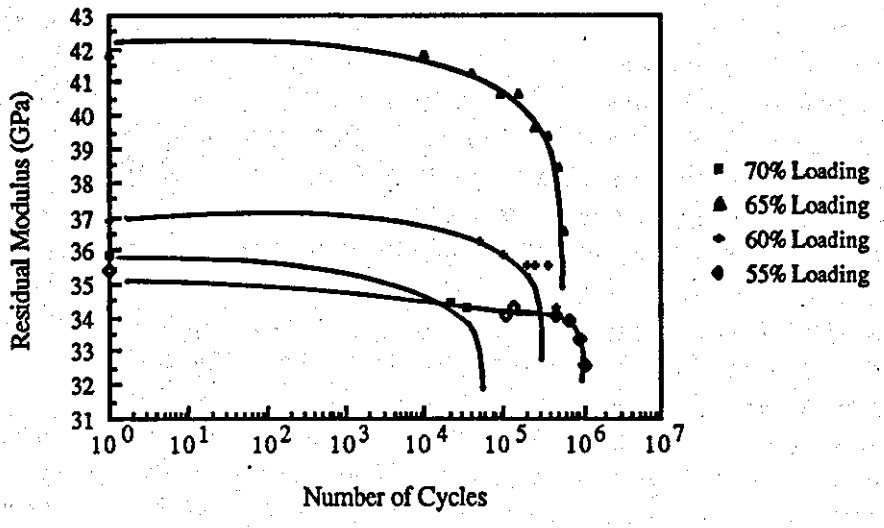

Graph 59 Residual Modulus for 15 Minutes Partial Cure Time During Cycling (Expt 8)

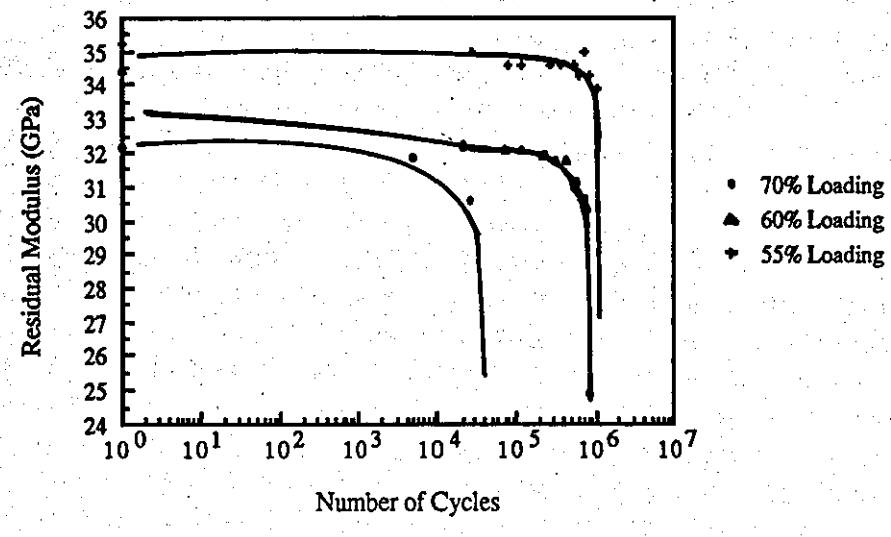

Graph 60 Residual Modulus for 20 Minutes Partial Cure Time During Cycling (Expt 8)

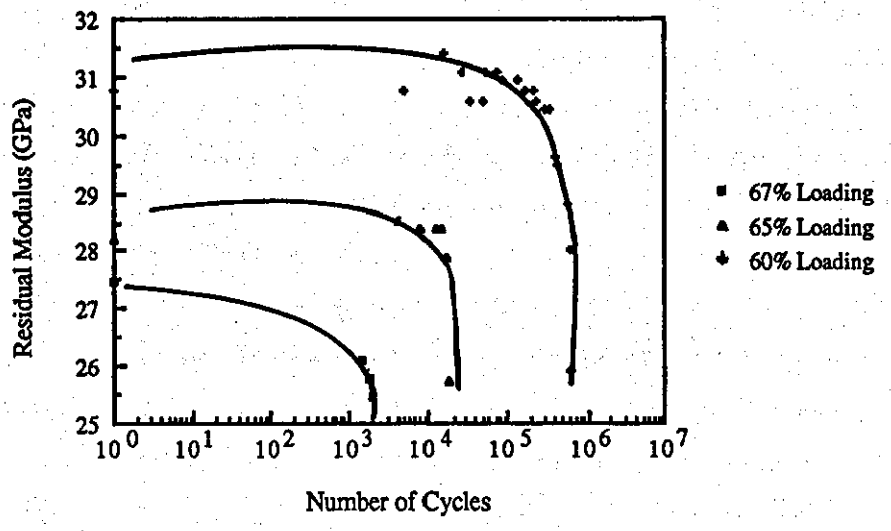

Graph 61 Residual Modulus for 30 Minutes Partial Cure Time During Cycling (Expt 8)

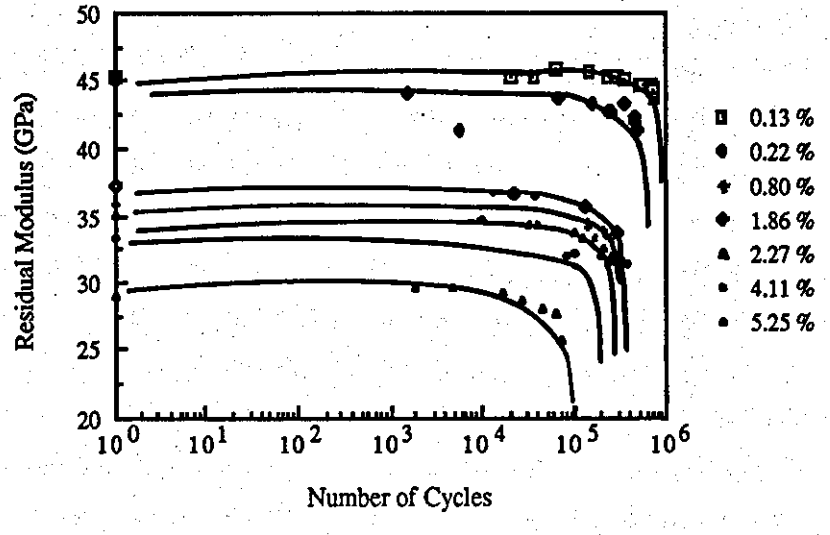

Graph 62 Residual Modulus for Specimens Fatiguing at 60% Stress Level (Expt 8)

FIGURES

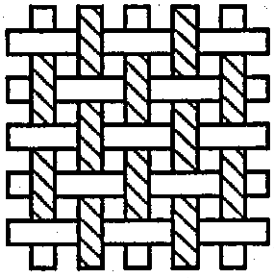

Fig. 1.1 Plain Weave

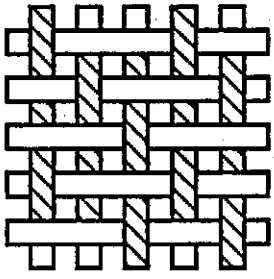

Fig. 1.2 Twill Weave
(Crowfoot Satin)

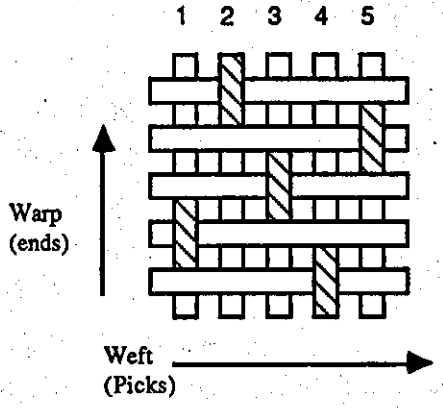

Fig. 1.3 Five-shaft Satin Weave

Figure 1 Types Of Weave Pattern

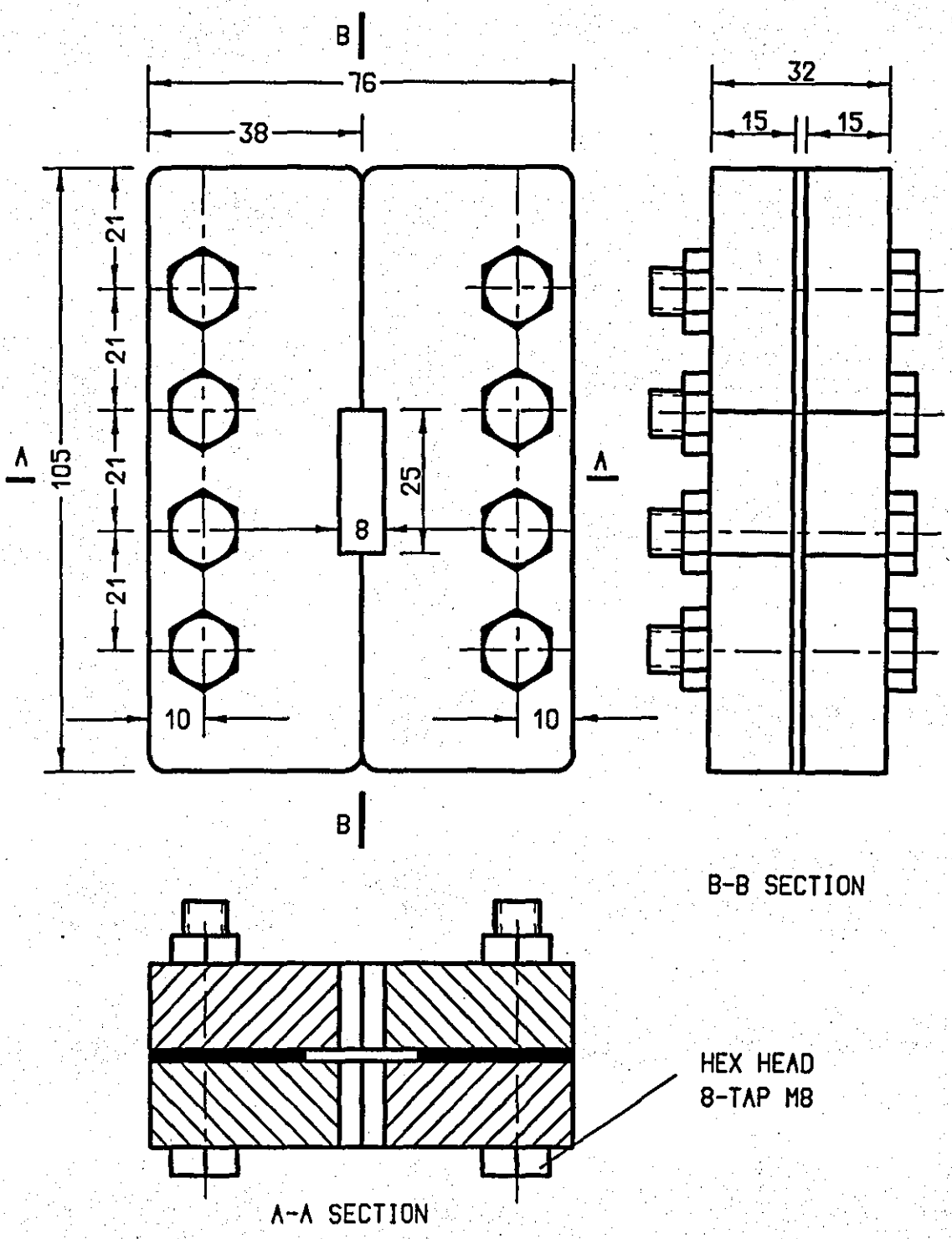

FIGURE 2 COMPLETE-EDGE SUPPORTED ANTI-BUCKLING GUIDES(ABG-1)

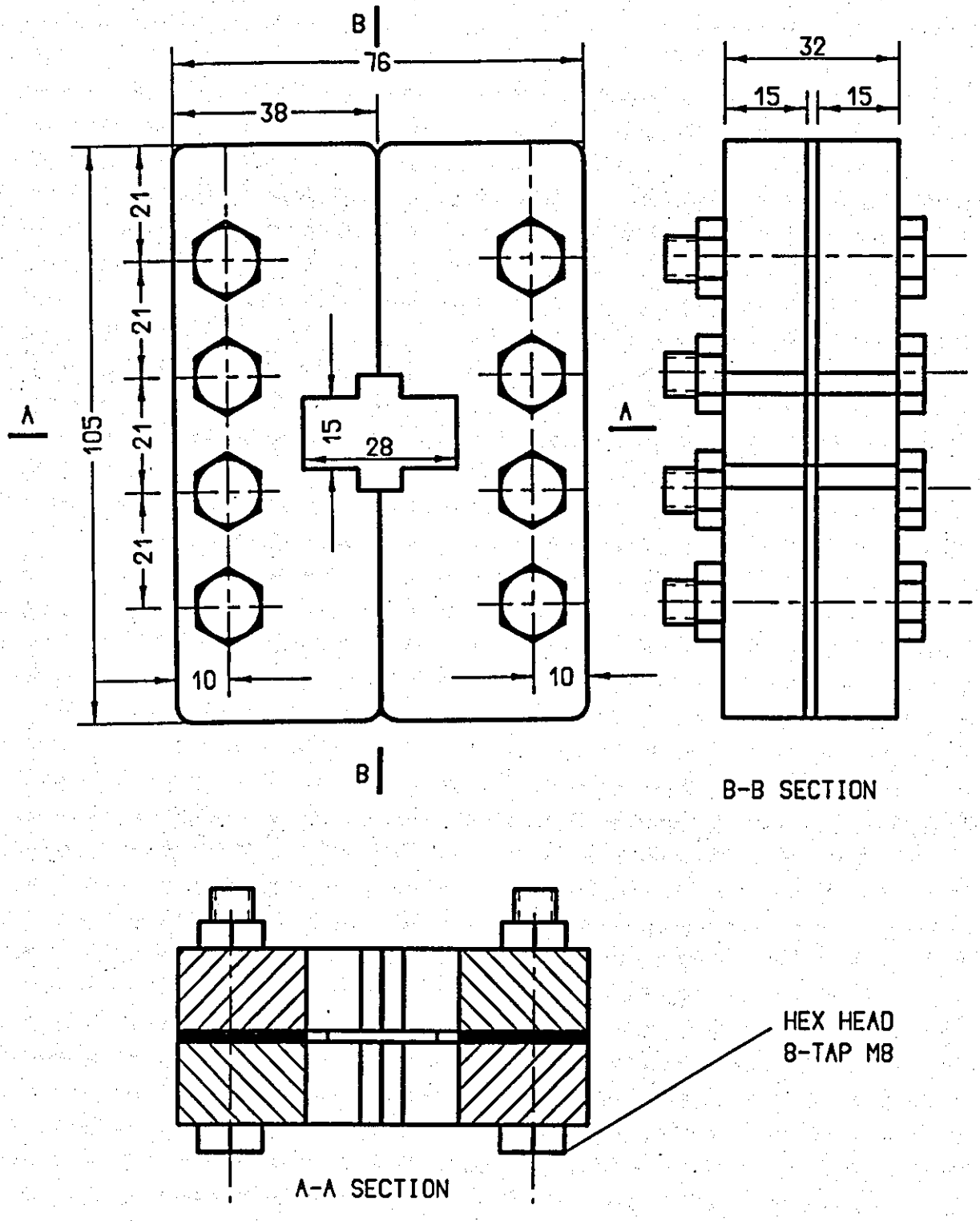

FIGURE 3 PARTIAL-EDGE SUPPORTED ANTI-BUCKLING GUIDES (ABG-2)

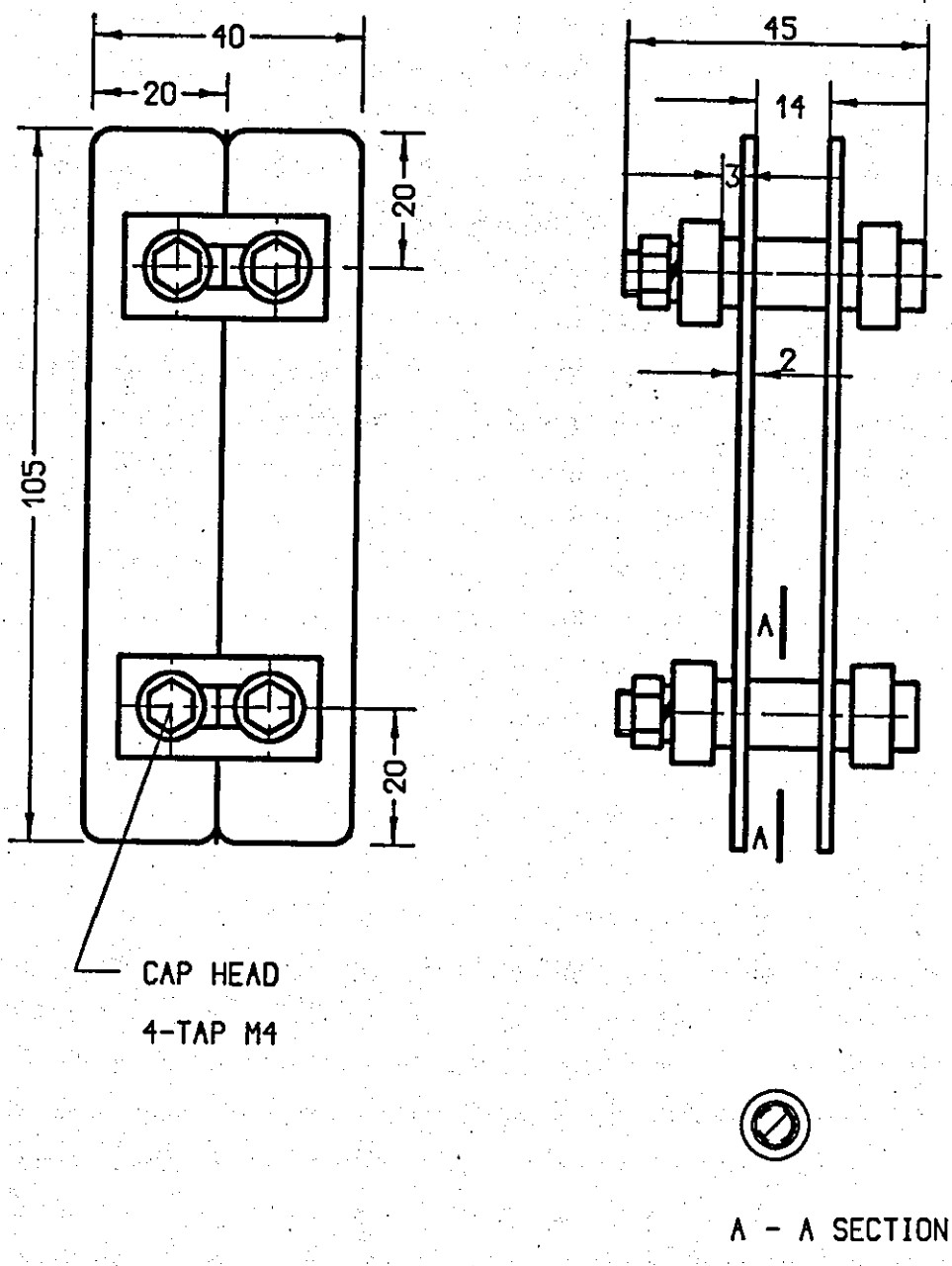

FIGURE 4 CRAG JIG

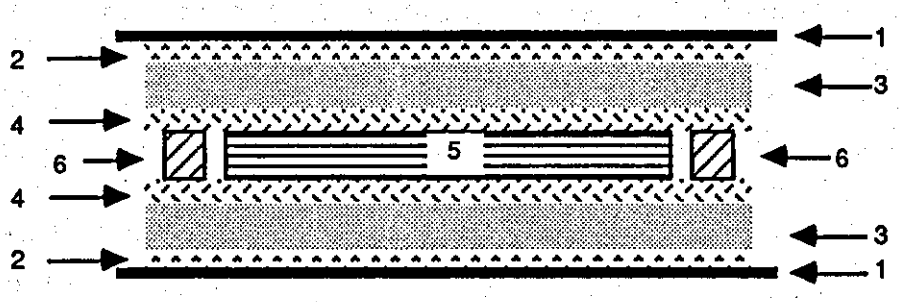

1 = steel plate
2 = Tygavac TFGO 75 non-porous PTFE
3 = Tygavac NW 153 medium weight bleed cloth
4 = Tygavac TFGO 75P porous PTFE coated glass fabric
5 = prepreg laminate
6 = metal frame

Figure 5 Lay-up of Prepreg Laminate in Mould

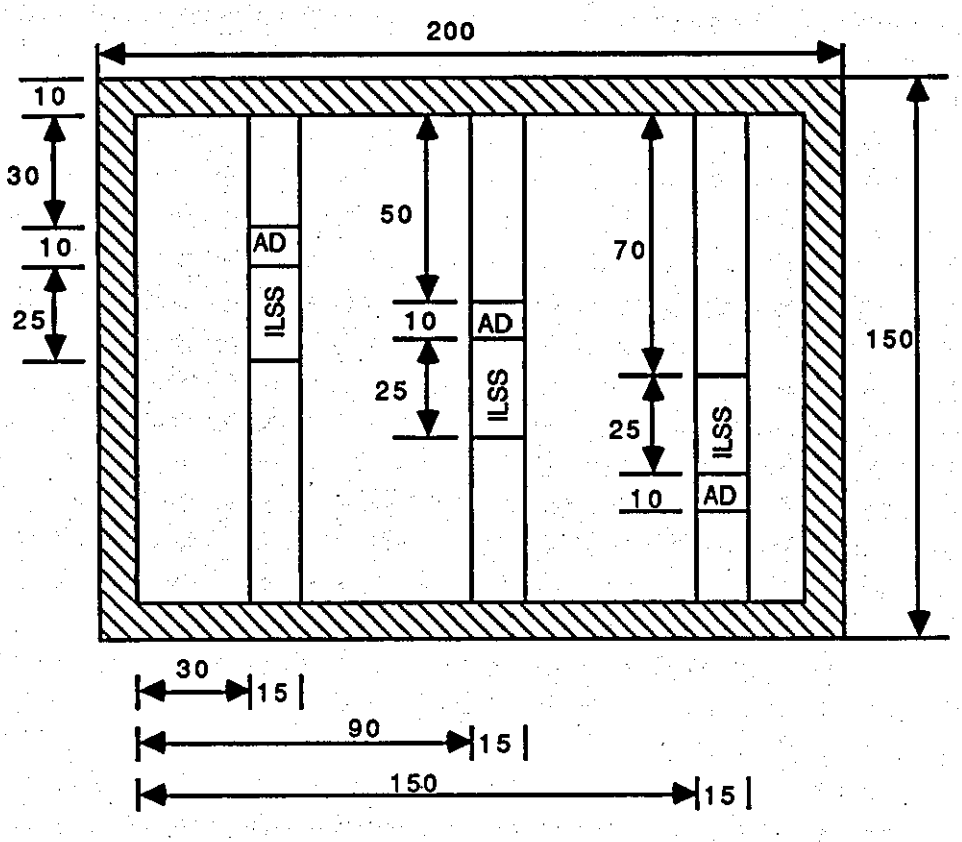

Figure 6 Sample Pattern For Experiments 1 and 2 (Scale 1: 2)

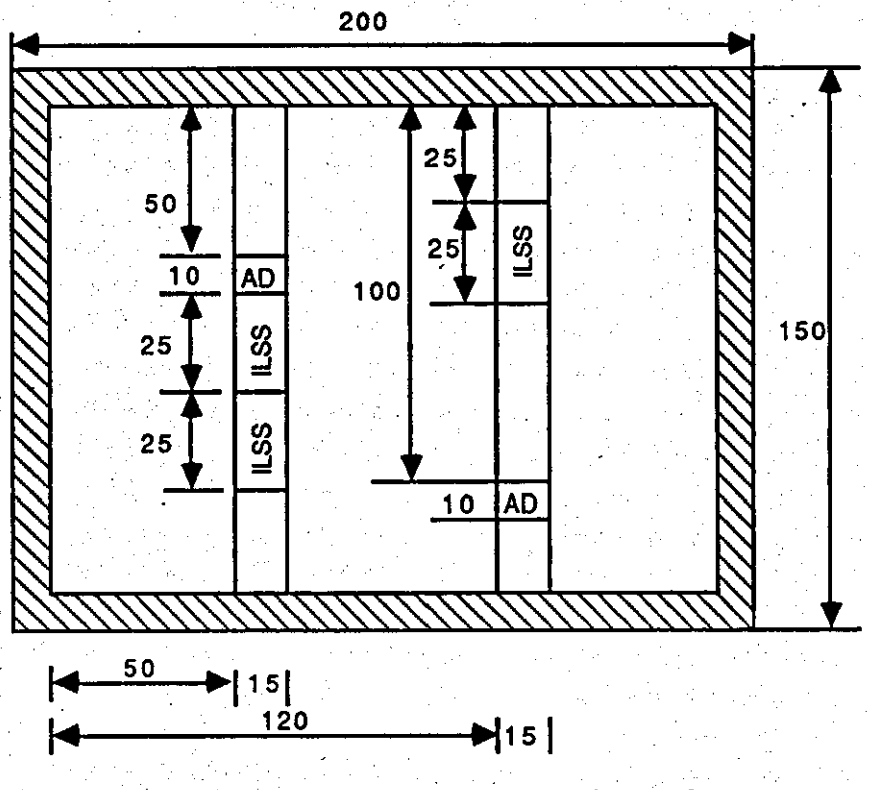

Figure 7 Sample Pattern For Experiment 3 (Scale 1: 2)

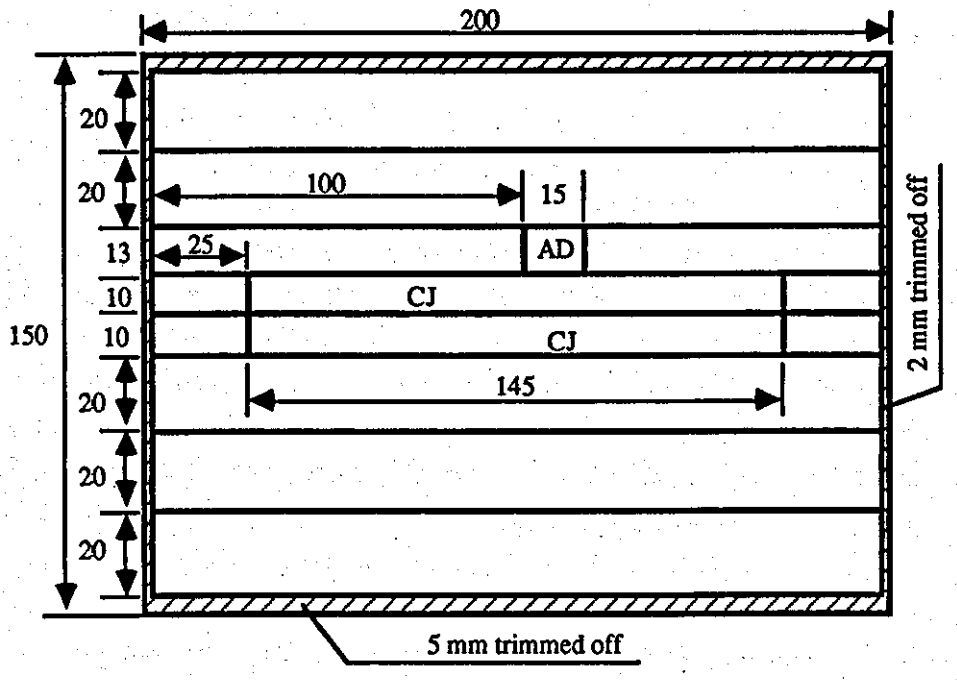

Figure 8 Sample Pattern For Experiment 4 (Scale 1: 2)

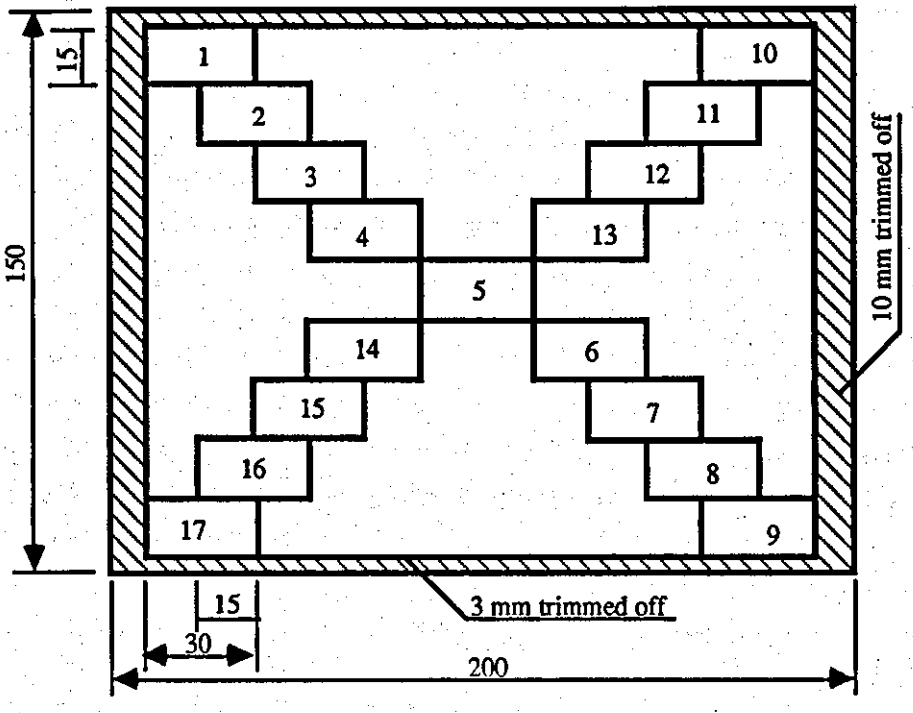

Figure 9 Sample Pattern For Experiment 5 (Scale 1: 2)

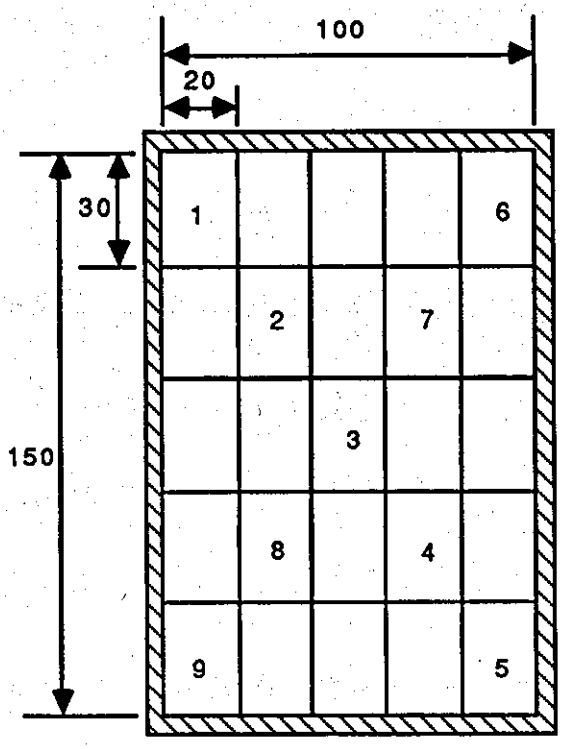

Figure 10 Sample Pattern For Experiments 6 and 7 (Scale 1: 2)

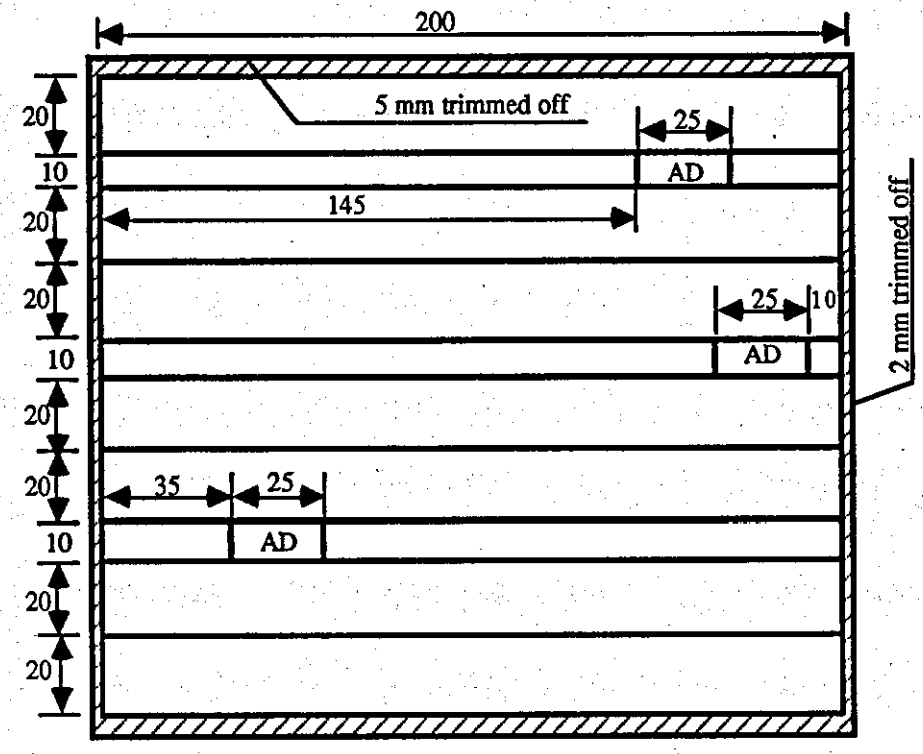

Figure 11 Sample Pattern For Experiment 8 (Scale 1: 2)

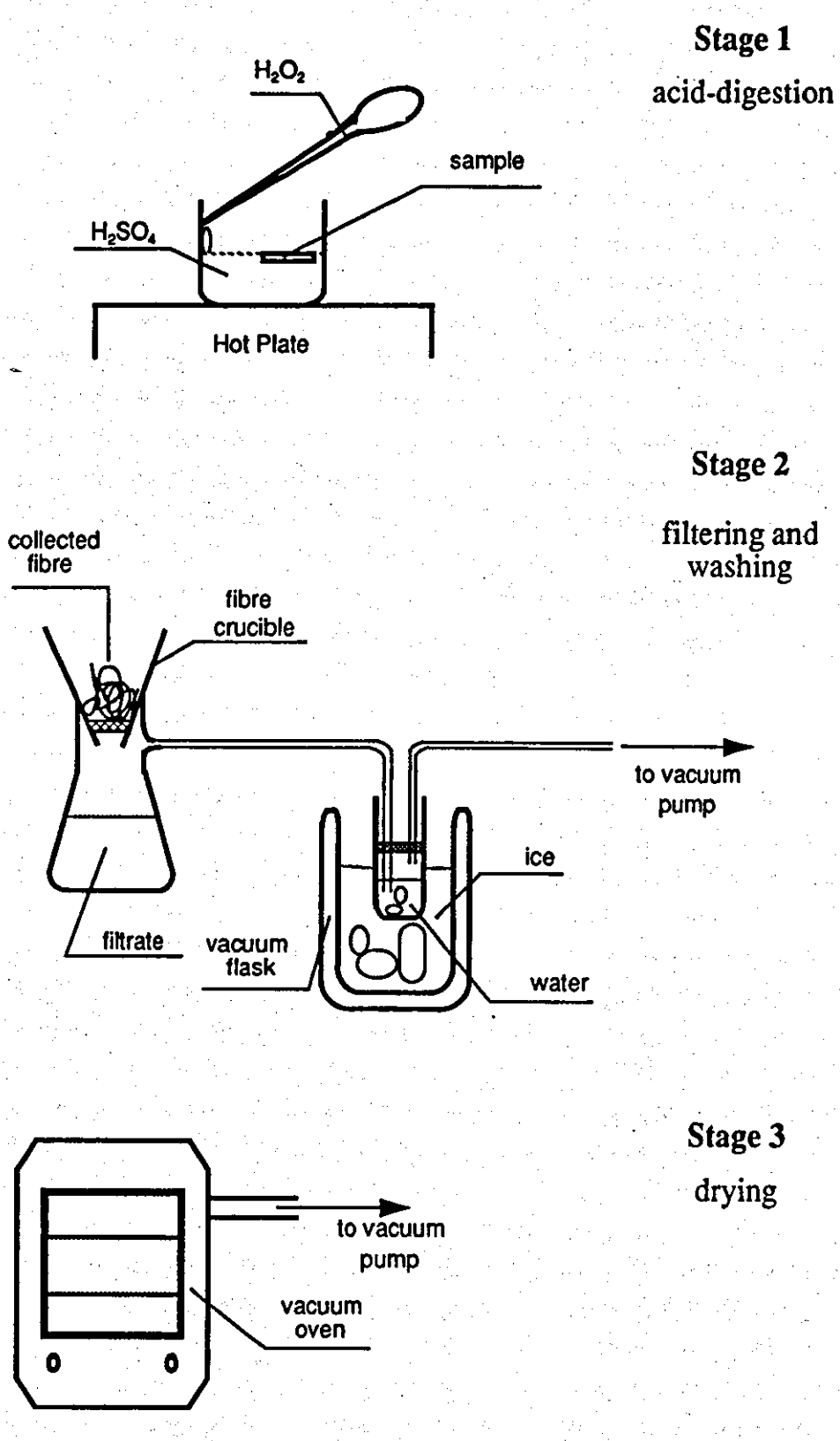

Figure 12 The Acid Digestion Process of Volume Fraction Measurement

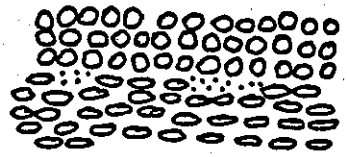

(a) Micropores Between the Rovings

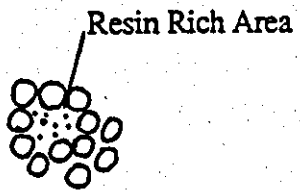

(b) Micropores Within the Rovings

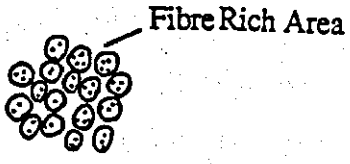

(c) Interstitial Voids

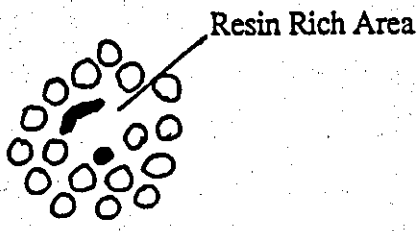

(d) Macrpopres Within the Rovings

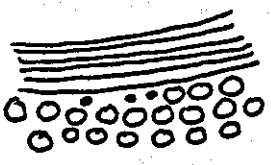

(e) Macropores Between the Rovings

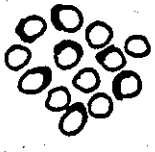

(f) Interface Voids

(i) between 0°/90° plies

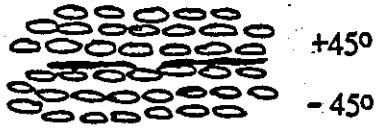

(ii) between ±45° plies

(g) Interlaminar Voids

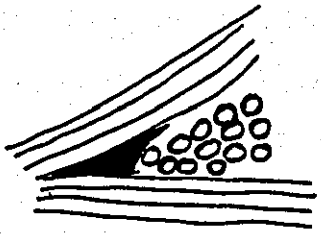

(h) Interroving Voids

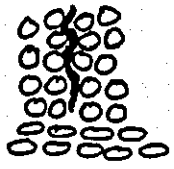

(i) Thread Voids

Figure 13 Types of Void

PLATES

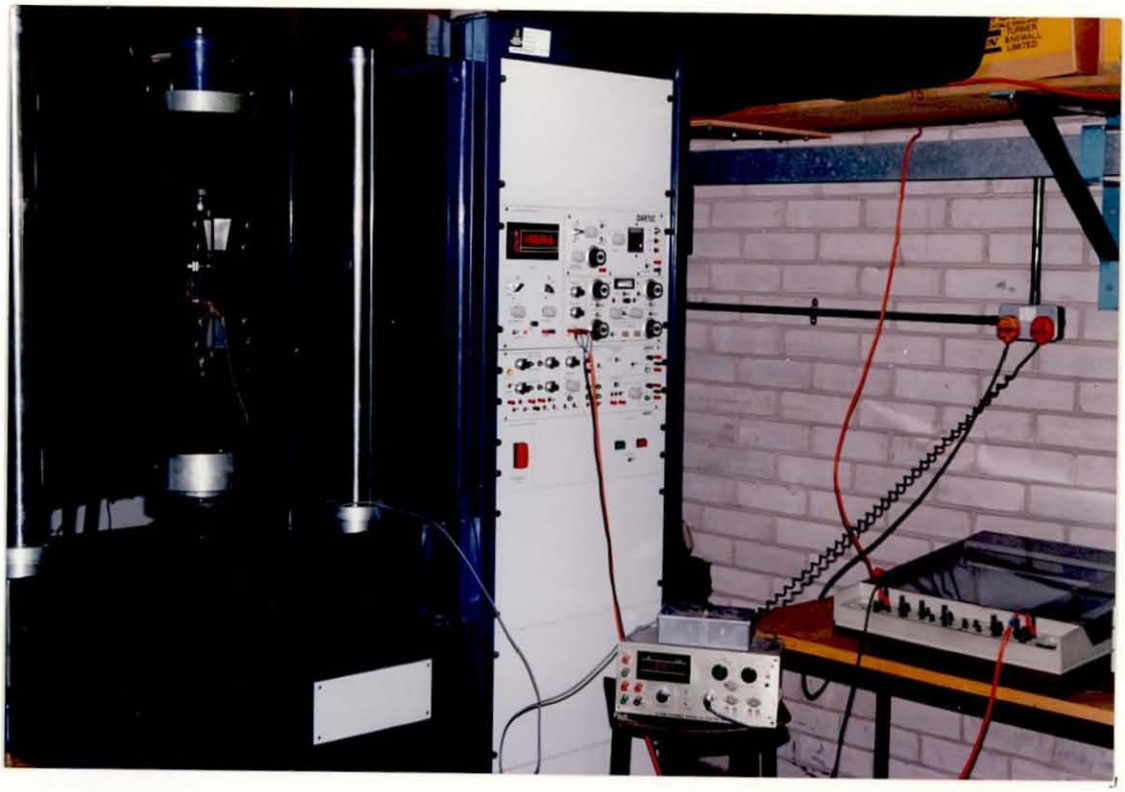

Plate 1 Dartec M1000/RE Servohydraulic Test Machine

(a) Front View

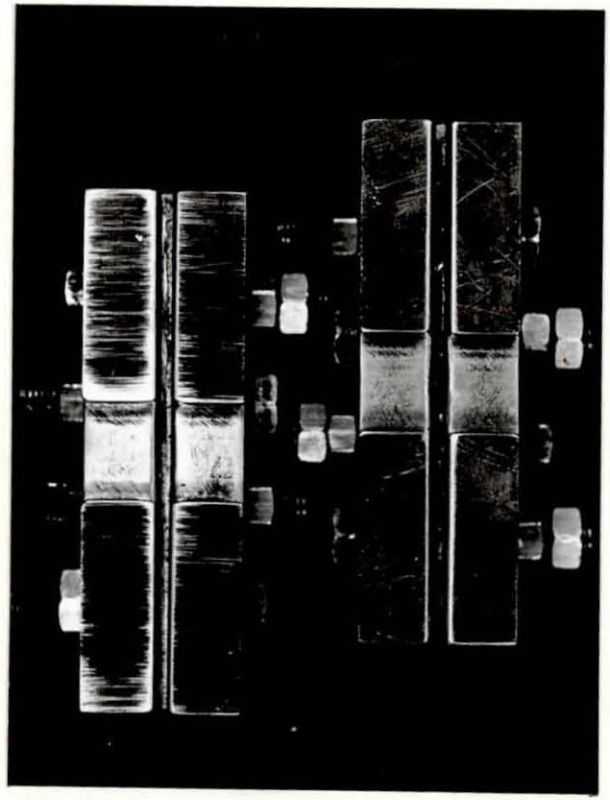

(b) Side View

Plate 2 Complete Edge Supported Anti-Buckling Guide (ABG-1)

(a) Front View

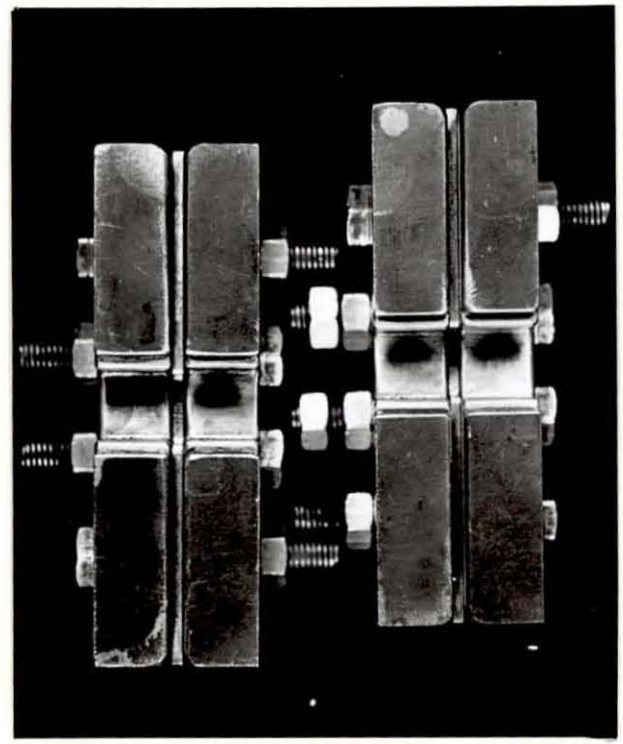

(b) Side View

Plate 3 Partial Edge Supported Anti-Buckling Guide (ABG-2)

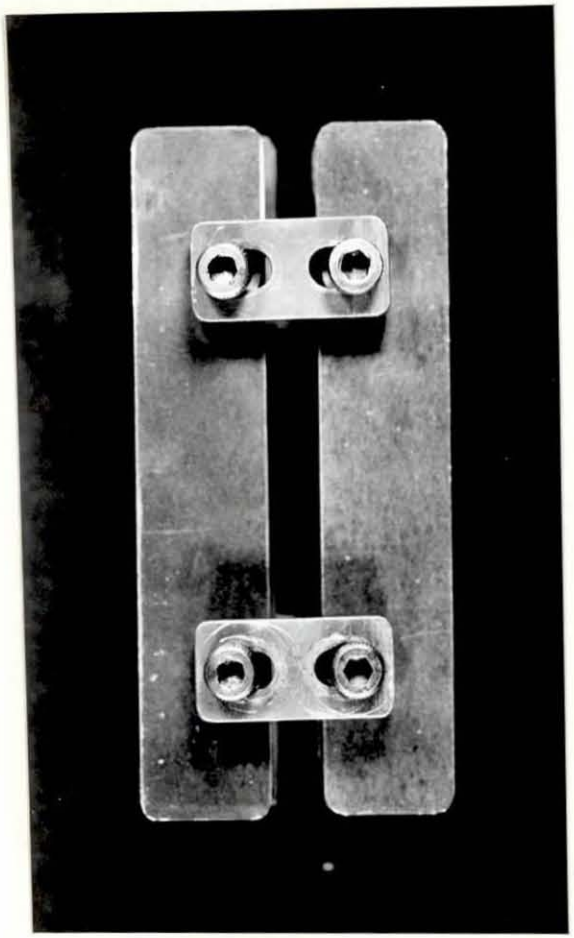

(a) Front View

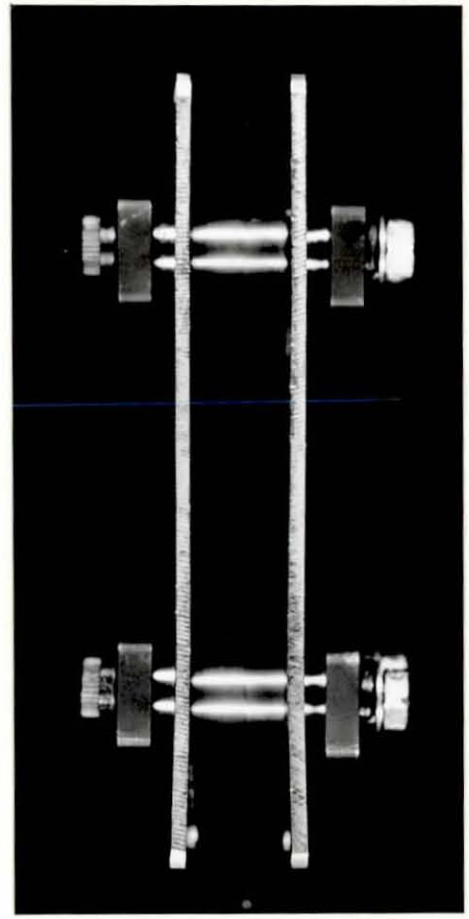

(b) Side View

Plate 4 CRAG Jig

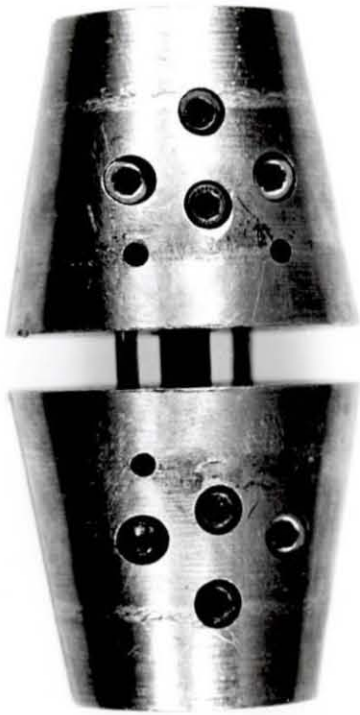

(a) Split Collet Assemblies

(b) Collet Grips Inside Conical Seats Located in Cylindrical Sleeve

Plate 5 Celanese Jig

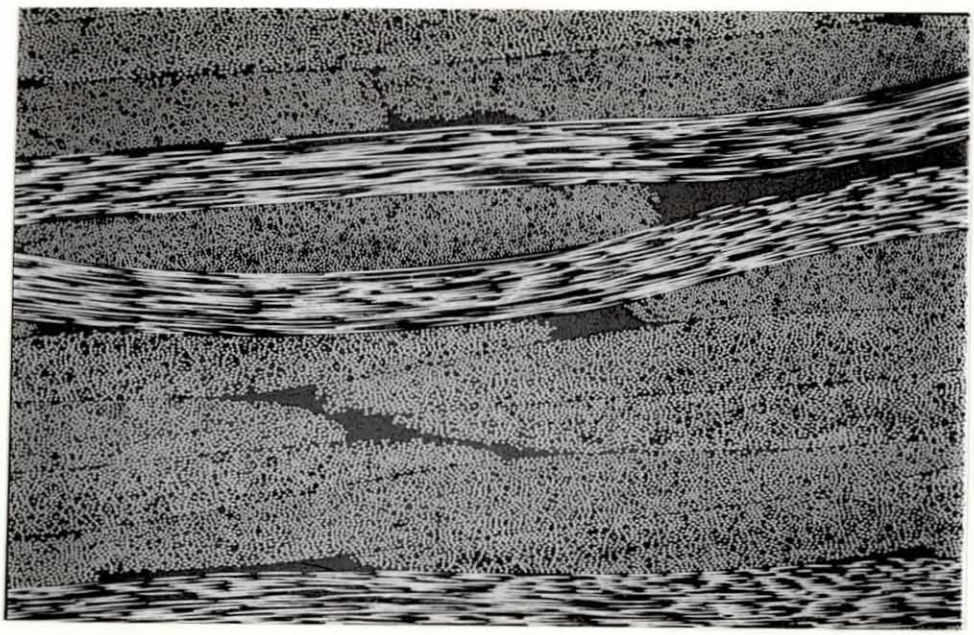

Plate 6 Laminate With 0-1% Void Content (Magnification x63)

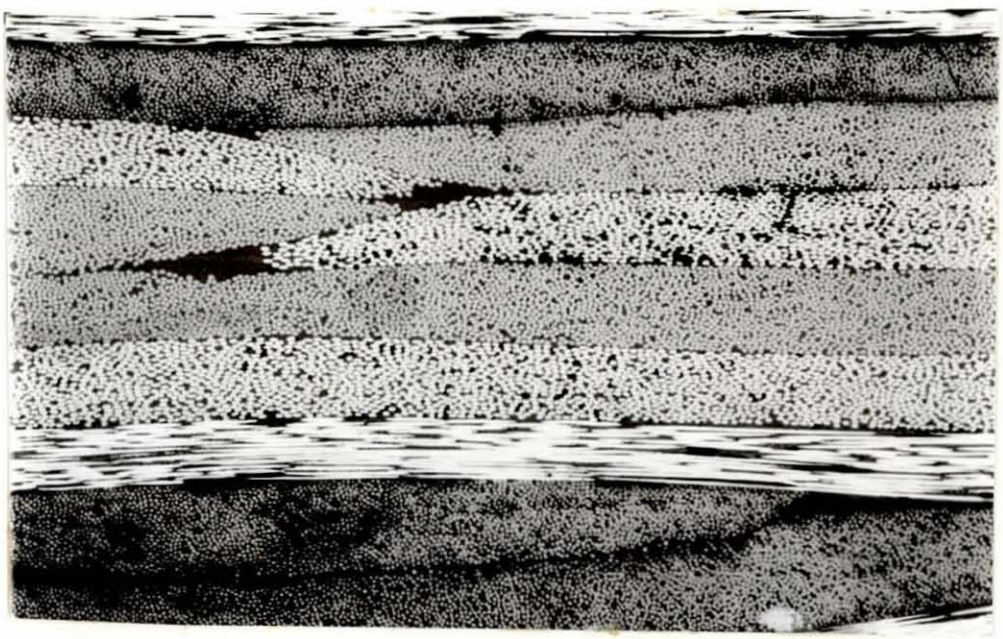

Plate 7 Laminate With 1-2% Void Content (Magnification x80)

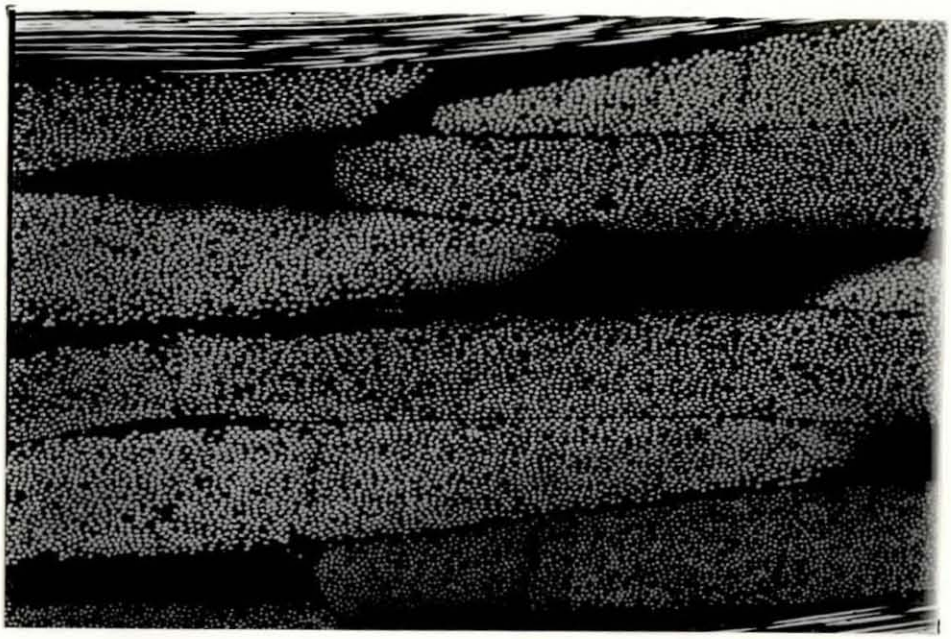

Plate 8 Laminate With Above 2% Void Content (Magnification x80)

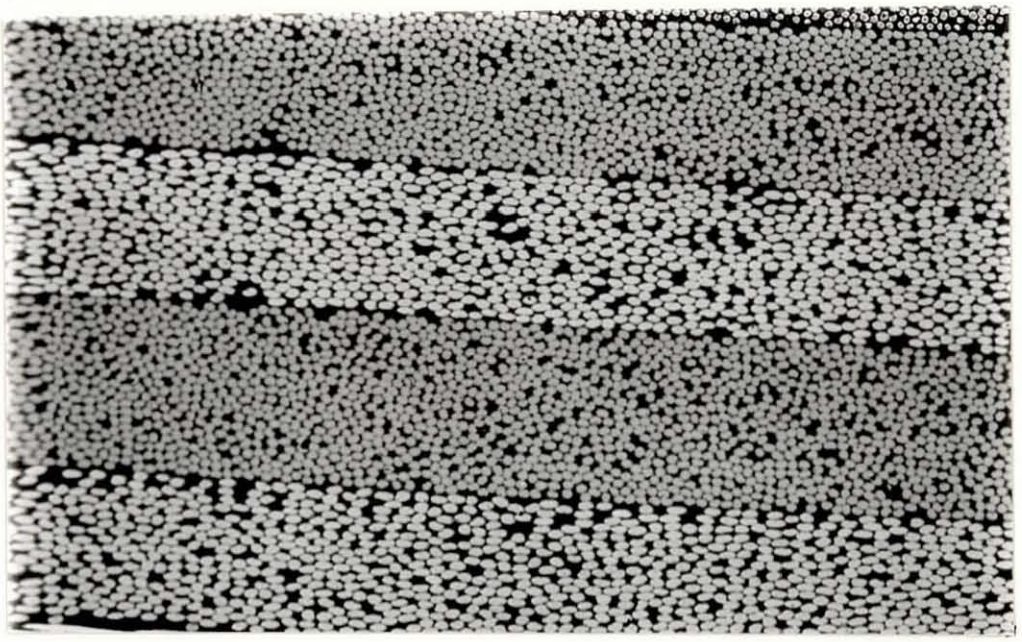

Plate 9 Micropores Within and Between the Rovings (Magnification x158)

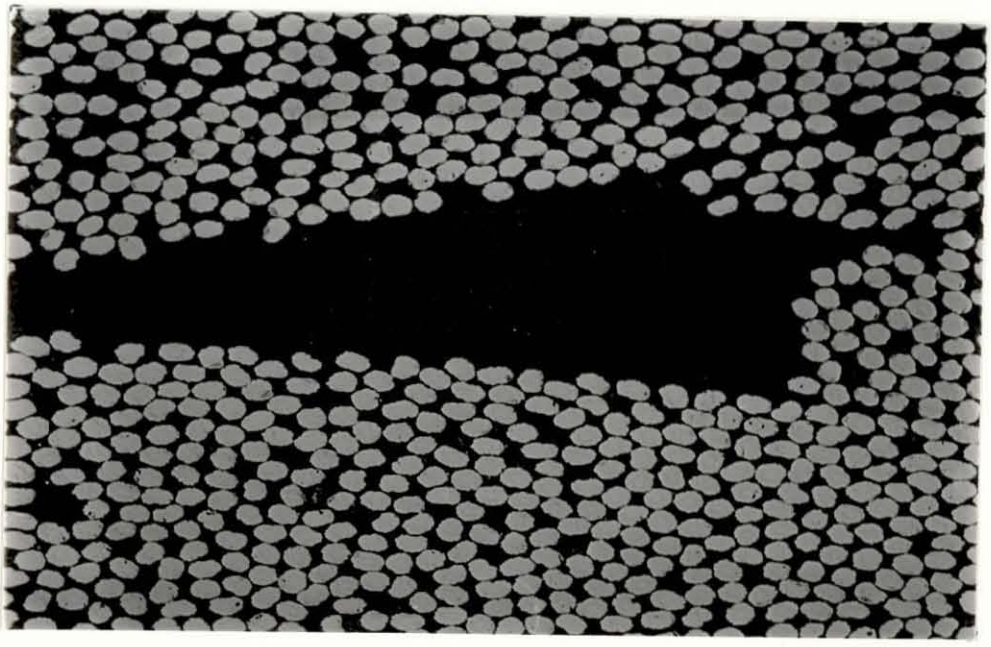

Plate 10 Resin Rich Area (Magnification x394)

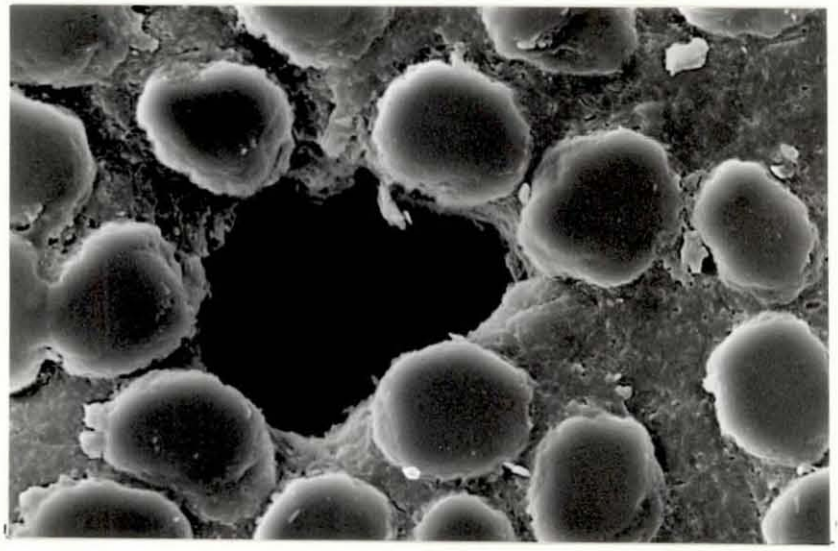

Plate 11 Macropore Within the Rovings (Magnification x31K)

Plate 12 Macropore Between the Rovings (Magnification x155)

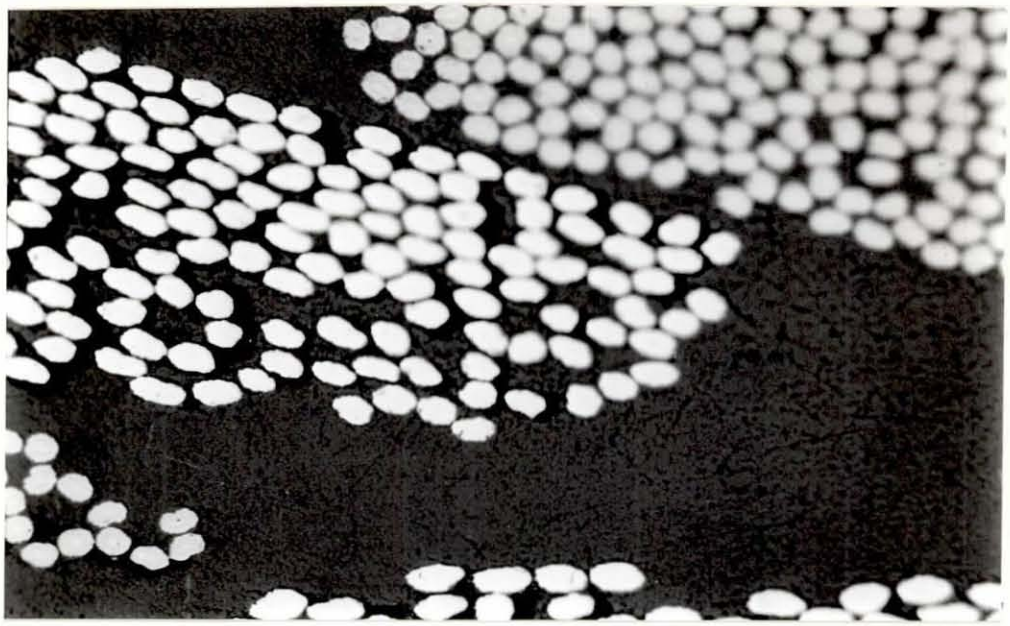

Plate 13 Interface Voids (Magnification x492)

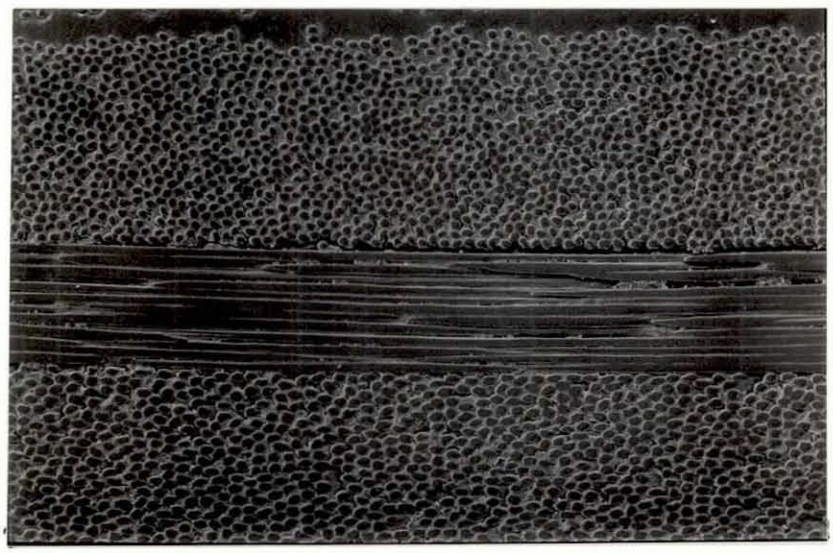

Plate 14 Interlaminar Void Between $0^{o}/90^{o}$ Plies (Magnification x230)

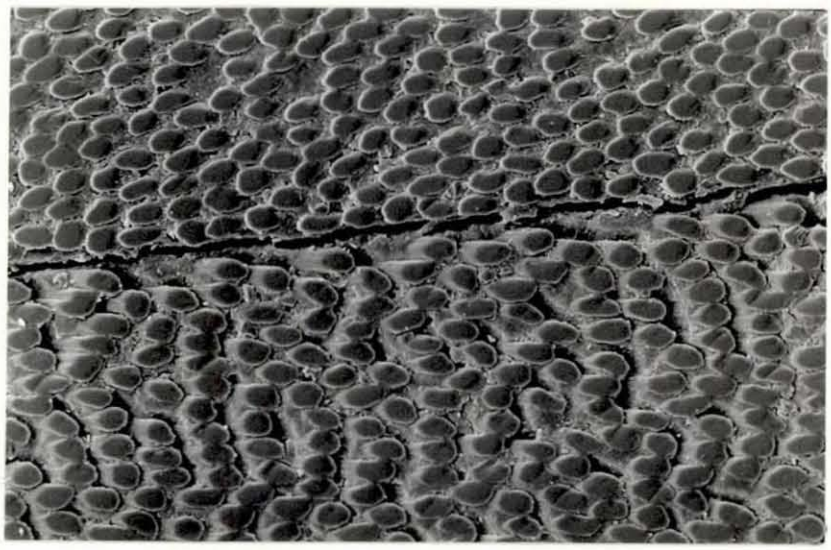

Plate 15 Interlaminar Void Between ±45° Plies (Magnification x520)

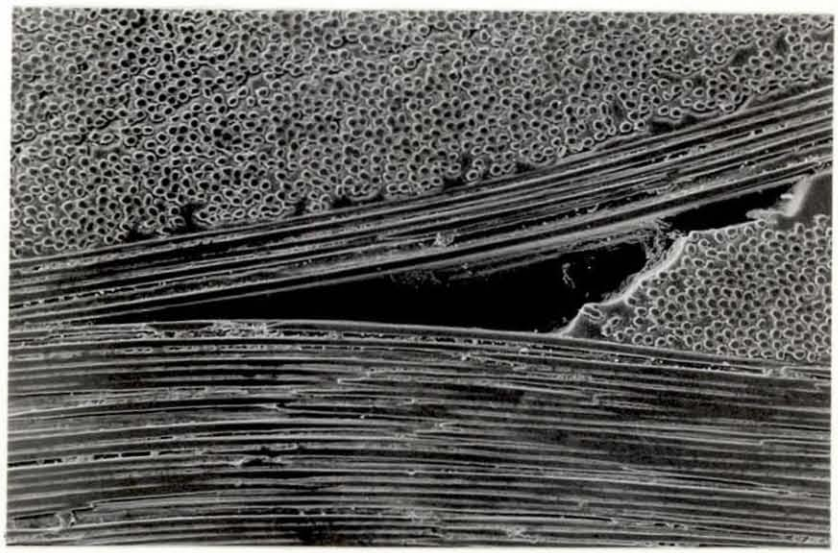

Plate 16 Interroving Void (Magnification x230)

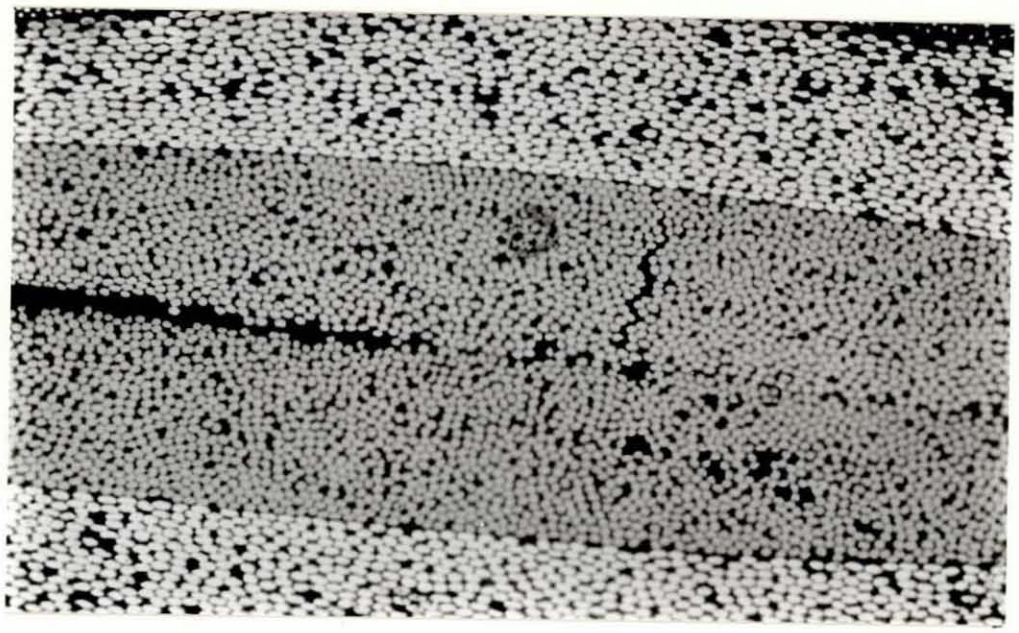

Plate 17 Thread Void (Magnification x158)

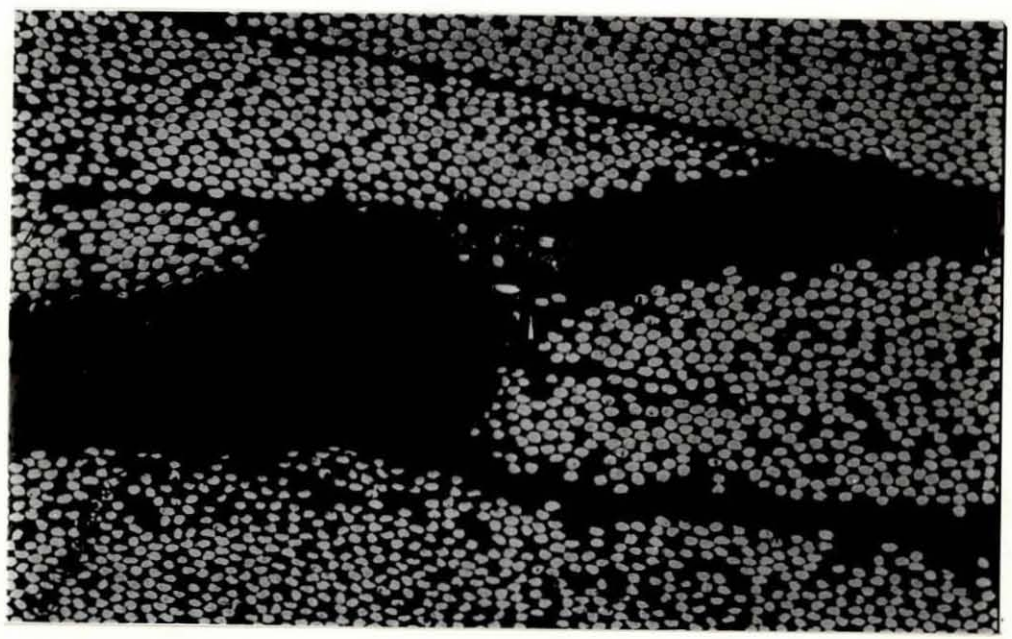

Plate 18 Translaminar Crack (Magnification x197)

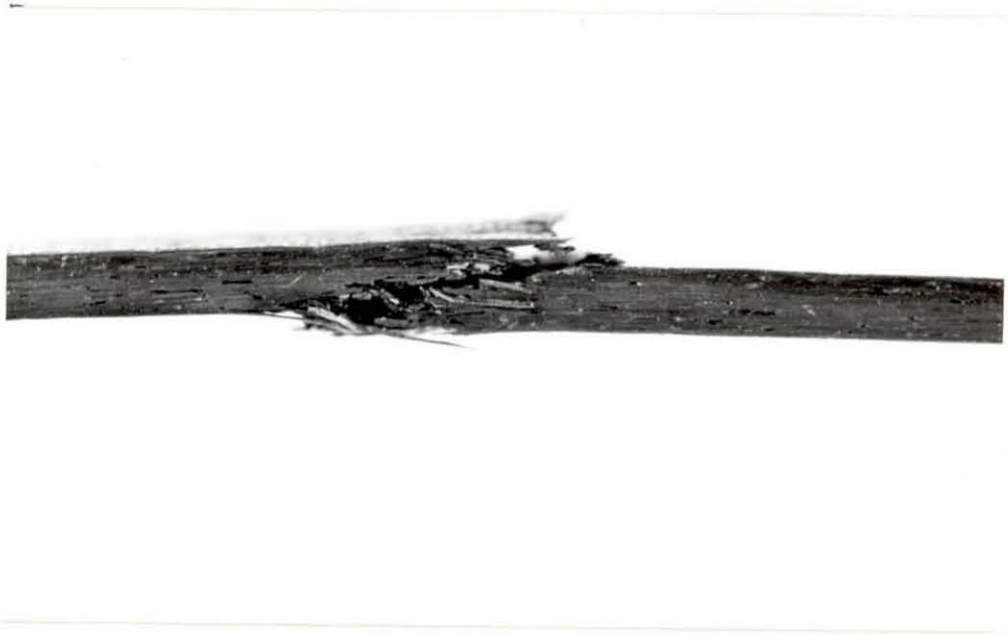

Plate 19 45° Shear Plane

Plate 20 V-Notched Failure

Plate 21 Low Void Content Failure Mode

Plate 22 High Void Content Failure Mode

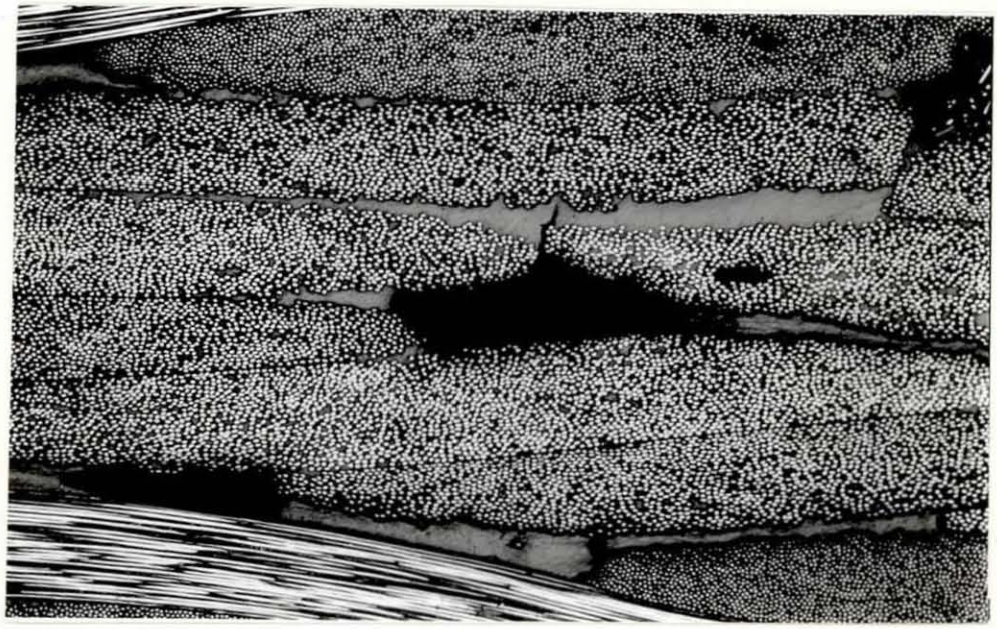

Plate 23 Crack Initiation From Void (Magnification x80)

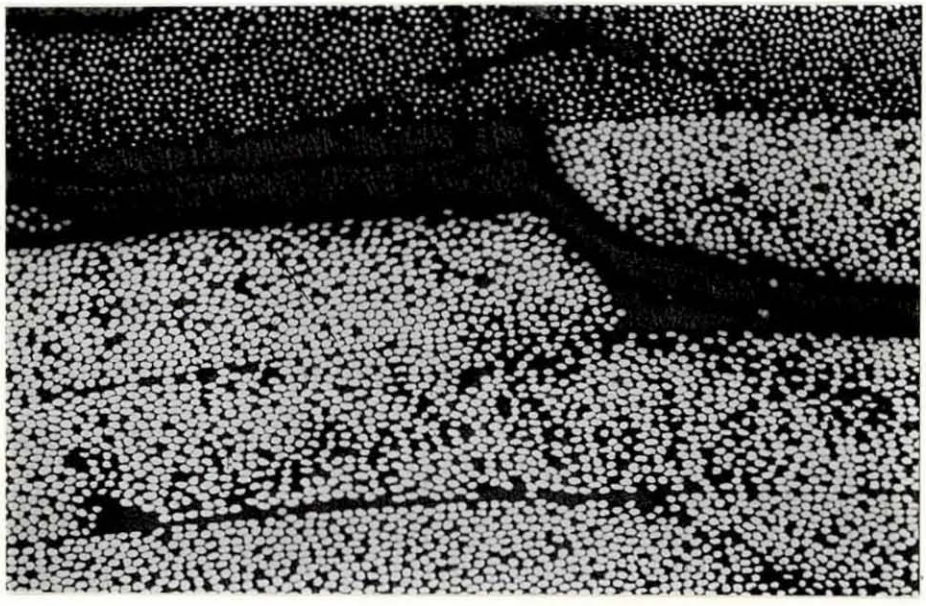

Plate 24 Matrix Cracking (Magnification x158)

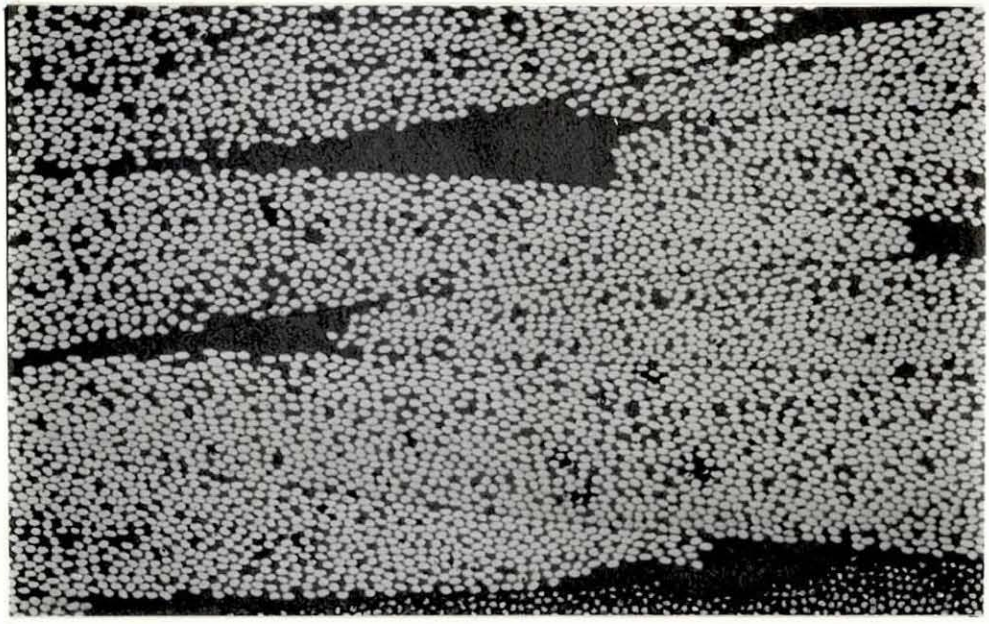

(a) Before Cycling (Magnification x158)

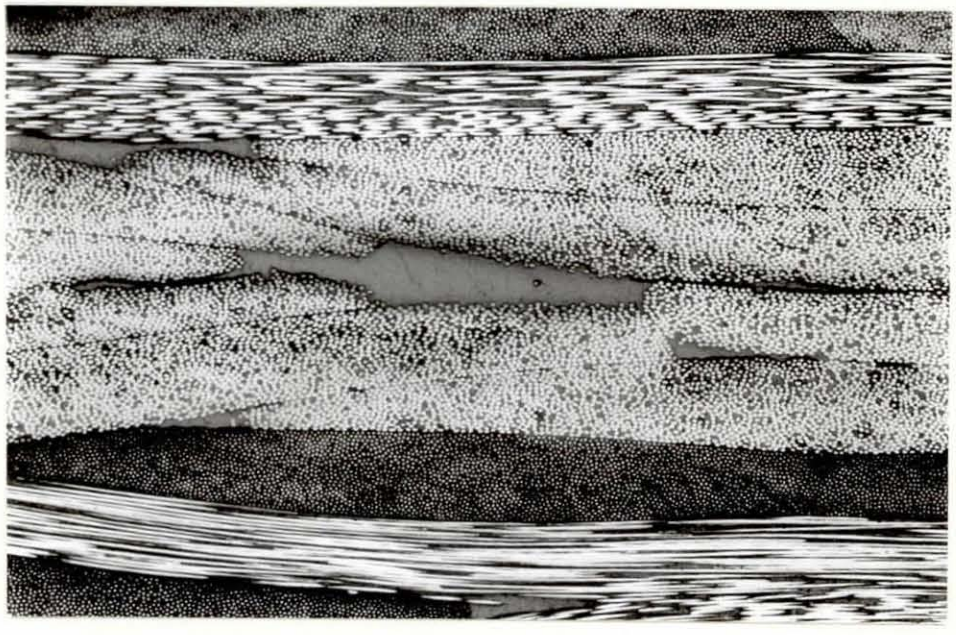

(b) After Cycling (Magnification x80)

Plate 25 Void Growth

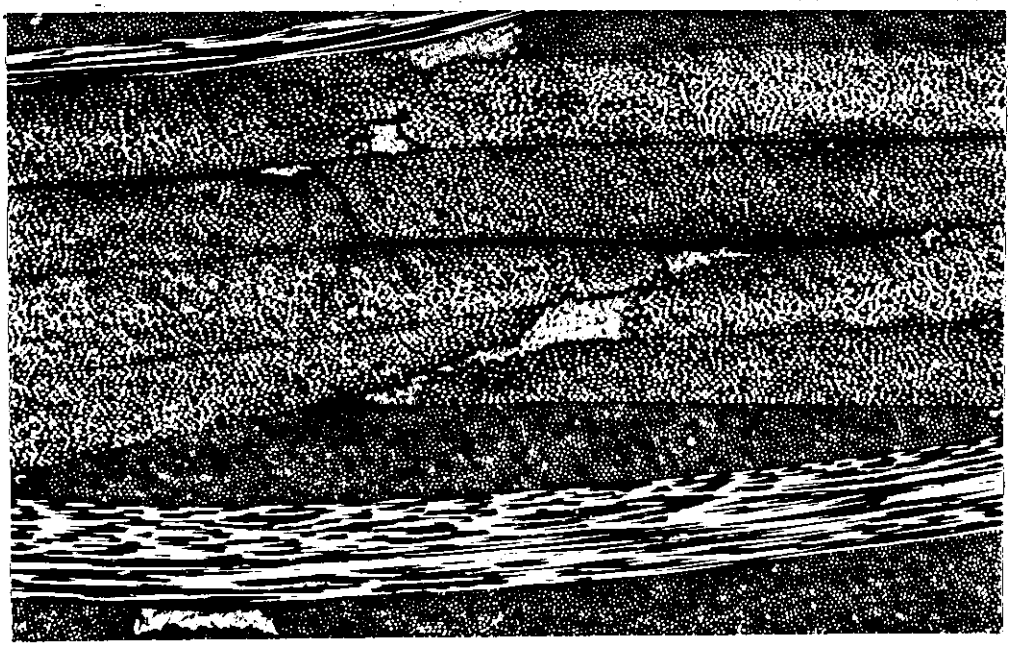

Plate 26 Interlaminar Debonding in Laminate With 0-1% Void Content

(Magnification x80)

Plate 27 Interlaminar Debonding in Laminate With Above 2% Void Content

(Magnification x31.5)

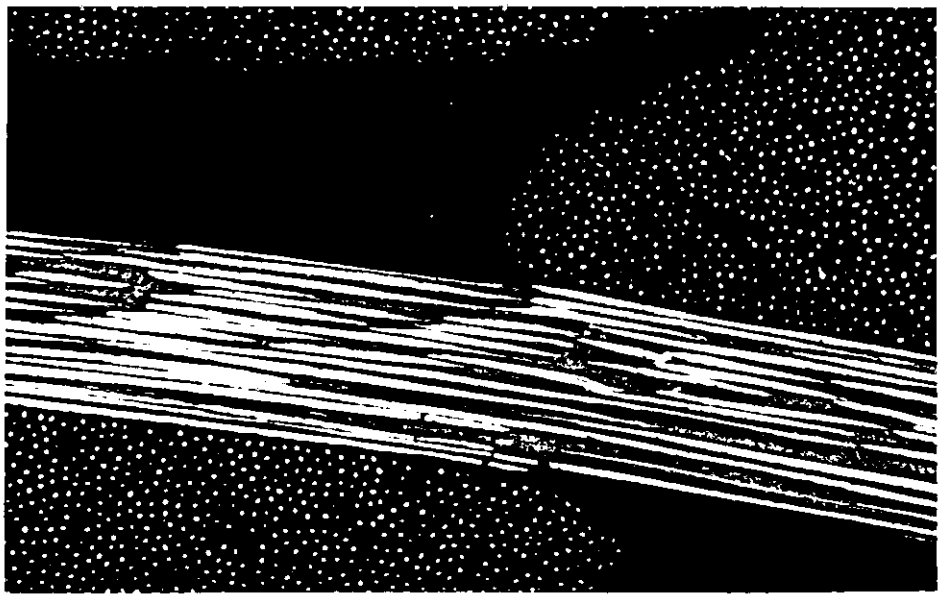

Plate 28 Fibre Microbuckling- Next to a Void (Magnification x197)

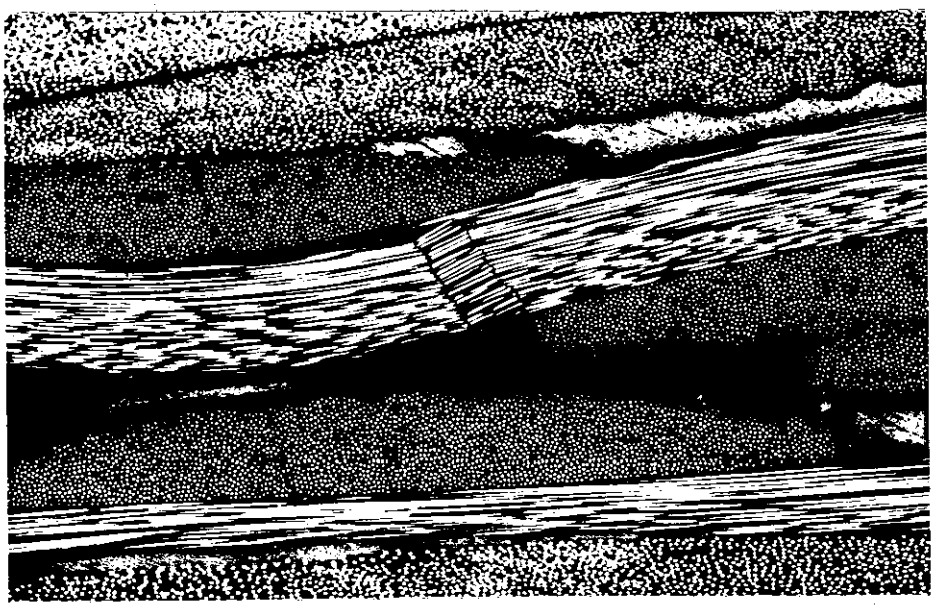

Plate 29 Kink-Band Formation (Magnification x80)

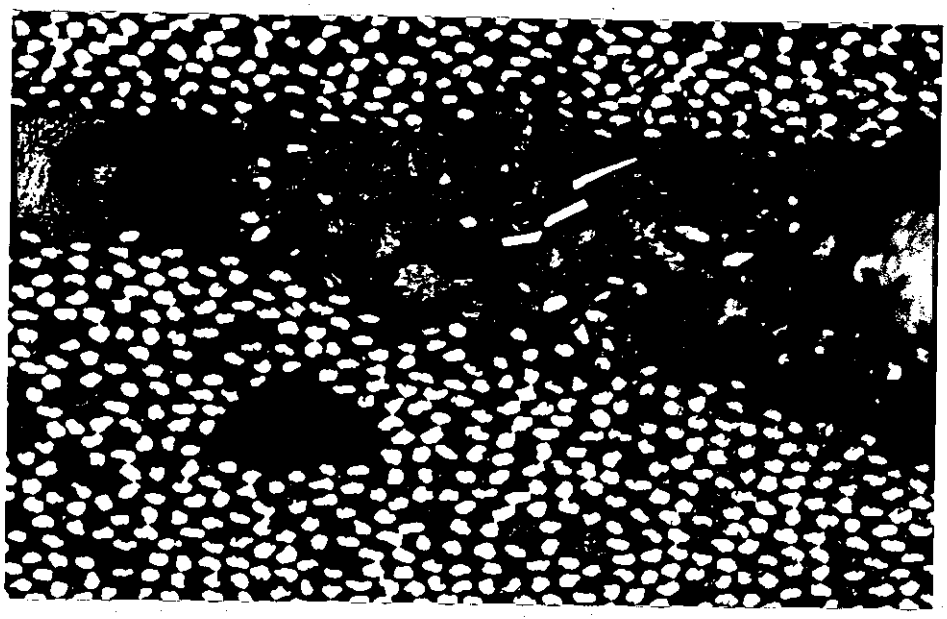

Plate 30 Broken Segments of Fibres (Magnification x296)

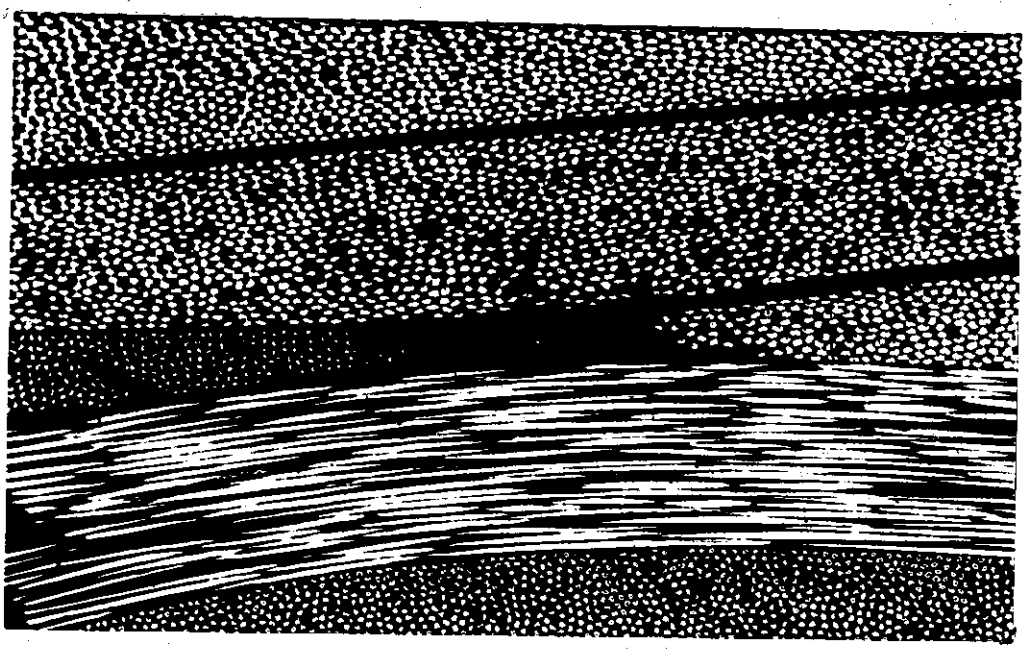

Plate 31 Laminate With 0-1% Void Content Cycling to Before Failure

(Magnification x158)

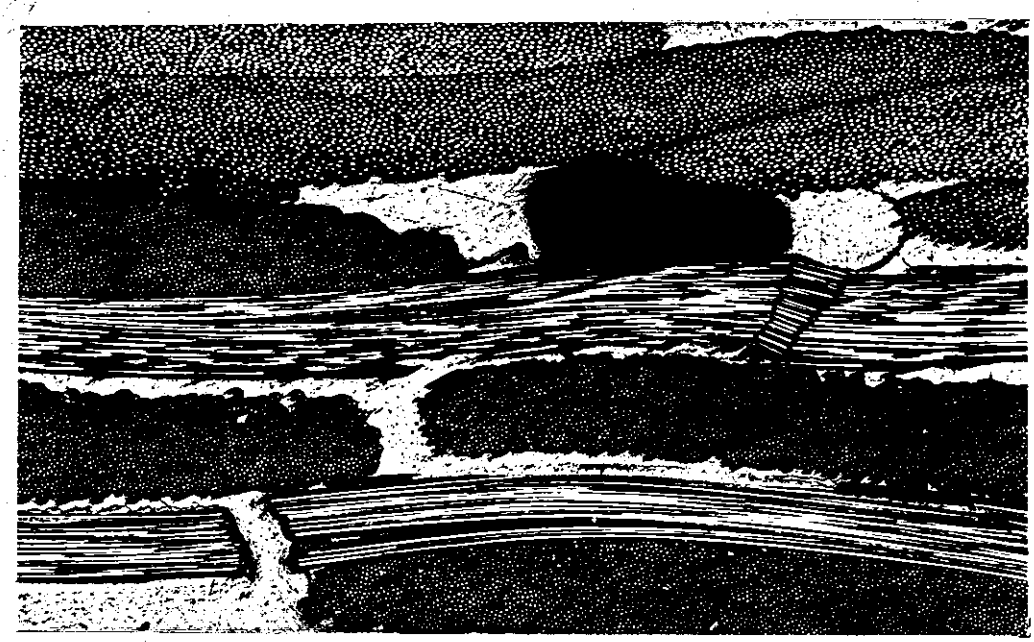

Plate 32 Laminate With 1-2% Void Content Cycling to Before Failure

(Magnification x80)

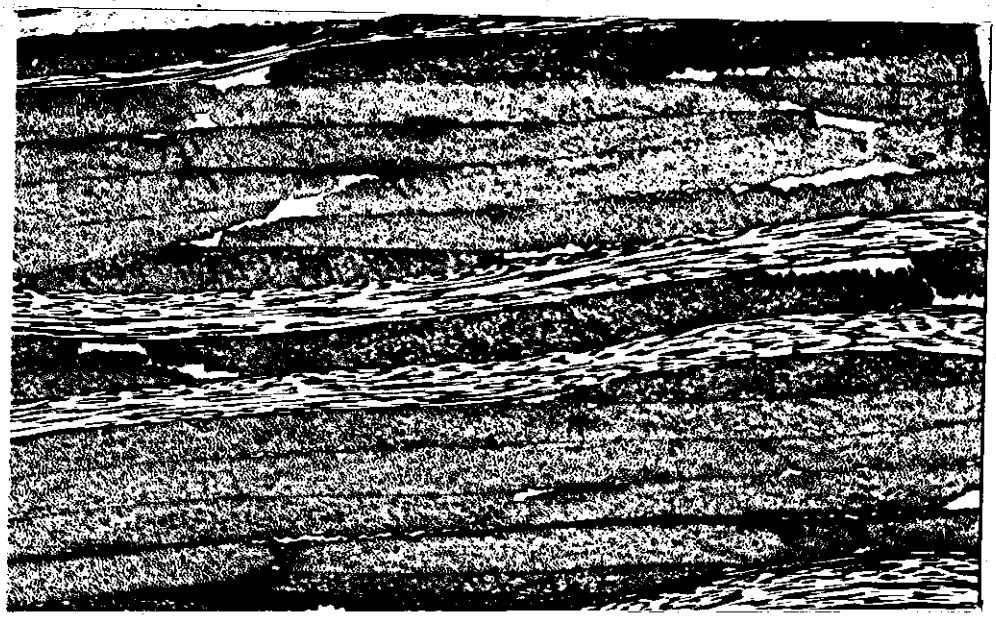

Plate 33 Specimen (0-1% Void Content) Fatigue Cycling to One Million Cycles (Magnification x40)

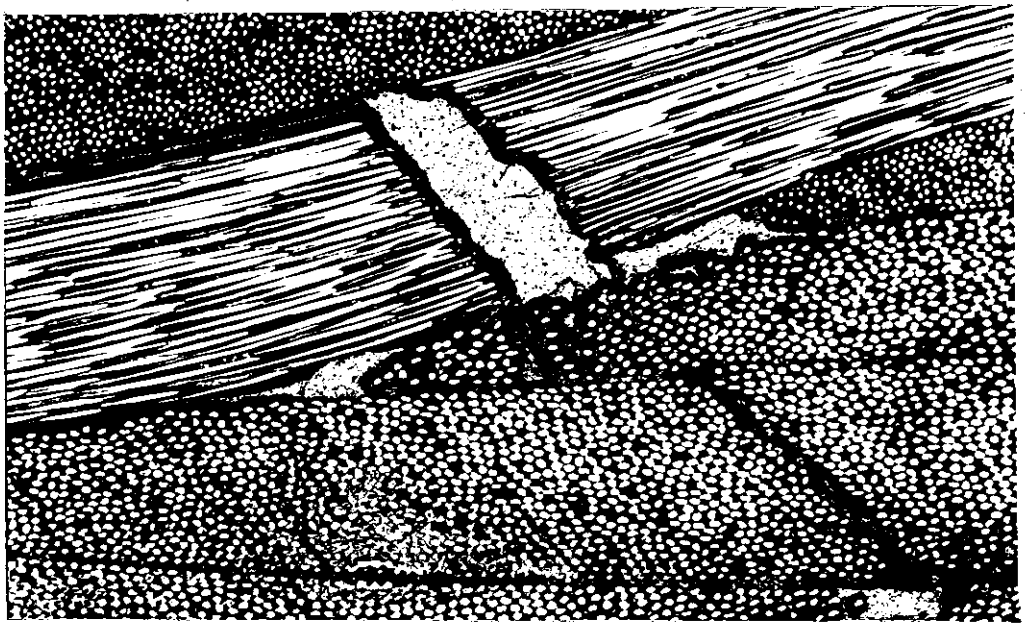

Plate 34 Specimen (1-2% Void Content) Fatigue Cycling to One Million Cycles (Magnification x158)

APPENDIX A

PHYSICAL TEST DATA

Table A1 Data Obtained From Solvent Addition
(Experiment 1)

SOLVENT	DENSITY (g/cm^3)	FIBRE VOLUME FRACTION	VOID CONTENT (%)
	2.1401	0.6596	- 0.20
PENTANE	2.1255	0.6578	0.01
	2.1319	0.6664	0.00
AVERAGE	**2.1325**	**0.6613**	**- 0.06**
	2.0738	0.6587	0.90
FREON	2.0155	0.6038	0.64
	2.1582	0.6691	- 0.32
AVERAGE	**2.0825**	**0.6439**	**0.41**
	2.1378	0.6751	0.22
WATER	2.0388	0.6391	1.91
	1.9640	0.6145	1.10
AVERAGE	**2.0469**	**0.6429**	**1.08**

Table A2 Data Obtained From The Effect of Curing Temperatures *(Experiment 2)*

TEMPERATURE (°C)	DENSITY (g/cm^3)	FIBRE VOLUME FRACTION	VOID CONTENT (%)	ILSS (MPa)
	1.5648	0.6633	2.59	47.85
150	1.5115	0.6068	4.71	47.38
	1.5751	0.6675	1.92	45.49
AVERAGE	**1.5505**	**0.6459**	**3.07**	**46.91**
	1.5952	0.6715	0.53	68.67
160	1.5242	0.6240	4.26	67.14
	1.5739	0.6689	1.78	69.19
AVERAGE	**1.5648**	**0.6548**	**2.19**	**68.33**
	1.5800	0.6547	1.13	77.67
165	1.5209	0.6240	4.61	73.98
	1.5798	0.6659	1.53	73.07
AVERAGE	**1.5602**	**0.6459**	**2.42**	**74.91**
	1.5566	0.6176	2.23	67.45
170	1.5693	0.6777	2.98	65.54
	1.5664	0.6639	2.47	67.83
AVERAGE	**1.5641**	**0.6531**	**2.56**	**66.94**
	1.6006	0.6658	- 0.07	67.67
175	1.4715	0.5961	7.23	63.68
	1.5631	0.6570	2.51	66.80
AVERAGE	**1.5451**	**0.6376**	**3.22**	**66.05**
	1.6007	0.6625	- 0.20	82.09
180	1.4533	0.5814	8.33	71.15
	1.5858	0.6728	1.31	73.59
AVERAGE	**1.5466**	**0.6389**	**3.15**	**75.61**

Table A3 Data Obtained From The Effect of Curing Pressures *(Experiment 3)*

PRESSURE (kN/m^2)	DENSITY (g/cm^3)	FIBRE VOLUME FRACTION	VOID CONTENT (%)	ILSS (MPa)
	1.5364	0.6143	3.08	81.72
327	1.5544	0.6183	1.83	83.91
	-	-	-	73.16
AVERAGE	**1.5454**	**0.6163**	**2.46**	**79.60**
	1.5553	0.6592	3.18	64.85
653	1.5342	0.6443	4.29	65.72
	-	-	-	65.85
AVERAGE	**1.5448**	**0.6518**	**3.74**	**65.47**
	1.5735	0.6677	2.07	66.68
980	1.5890	0.6797	1.30	63.92
	-	-	-	73.44
AVERAGE	**1.5813**	**0.6737**	**0.20**	**68.01**
	1.5951	0.6857	1.04	87.82
1307	1.6279	0.6941	0.20	77.24
	-	-	-	75.59
AVERAGE	**1.6115**	**0.6899**	**0.62**	**80.22**
	1.6376	0.7042	- 0.59	95.58
1633	1.6414	0.7097	- 0.70	95.09
	-	-	-	99.55
AVERAGE	**1.6395**	**0.7070**	**- 0.65**	**96.74**
	1.6389	0.7077	- 0.57	93.80
1960	1.6306	0.6926	- 0.45	90.67
	-	-	-	90.79
AVERAGE	**1.6348**	**0.7002**	**- 0.51**	**91.75**

Table A4 Data For Mouldings at 653 kN/m² Curing Pressure
(Experiment 4)

SPECIMEN NUMBER	DENSITY (g/cm³)	FIBRE VOLUME FRACTION	VOID CONTENT (%)	THICKNESS (mm)
1	1.5763	0.6165	0.09	2.251
2	1.5489	0.6107	2.00	2.277
3	1.5654	0.6093	0.68	2.271
4	1.5726	0.6170	0.39	2.257
5	1.5785	0.6285	0.34	2.214
6	1.5720	0.6165	0.42	2.245
7	1.5809	0.6262	0.07	2.216
MEAN	1.5707	0.6178	0.57	2.247
STD DEV	0.0108	0.0072	0.6629	0.0246

Table A5 Data For Mouldings at 1307 kN/m² Curing Pressure
(Experiment 4)

SPECIMEN NUMBER	DENSITY (g/cm³)	FIBRE VOLUME FRACTION	VOID CONTENT (%)	THICKNESS (mm)
1	1.5784	0.6300	0.39	2.202
2	1.5768	0.6208	0.20	2.216
3	1.5809	0.6317	0.18	2.194
4	1.5793	0.6318	0.39	2.207
5	1.5847	0.6323	-0.01	2.195
6	1.5834	0.6377	0.27	2.187
7	1.5809	0.6349	0.37	2.187
8	1.5764	0.6257	0.40	2.227
MEAN	1.5801	0.6306	0.27	2.202
STD DEV	0.0030	0.0053	0.1450	0.0140

Table A6 Data For Mouldings at 1960 kN/m^2 Curing Pressure *(Experiment 4)*

SPECIMEN NUMBER	DENSITY (g/cm^3)	FIBRE VOLUME FRACTION	VOID CONTENT (%)	THICKNESS (mm)
1	1.5651	0.5945	0.19	2.278
2	1.5661	0.5981	0.23	2.255
3	1.5711	0.6003	- 0.08	2.254
4	1.5716	0.5972	- 0.22	2.251
5	1.5681	0.5935	- 0.08	2.260
6	1.5832	0.6506	0.74	2.079
7	1.5858	0.6426	0.22	2.068
8	1.5778	0.6335	0.56	2.169
MEAN	1.5736	0.6138	0.20	2.202
STD DEV	0.0078	0.0241	0.3285	0.0855

Table A7 Data For Moulding at 653 kN/m^2 Curing Pressure
(Experiment 5)

SPECIMEN NUMBER	DENSITY (g/cm^3)	FIBRE VOLUME FRACTION	VOID CONTENT (%)	THICKNESS (mm)
1	1.5454	0.6078	2.16	2.279
2	1.5412	0.6089	2.52	2.294
3	1.5506	0.6106	1.86	2.282
4	1.5385	0.6021	2.50	2.292
5	1.5498	0.6139	2.03	2.273
6	1.5494	0.6089	1.89	2.265
7	1.5459	0.6103	2.21	2.257
8	1.5466	0.6128	2.31	2.280
9	1.5489	0.6050	1.80	2.272
10	1.5486	0.6100	1.99	2.249
11	1.5409	0.6045	2.39	2.269
12	1.5377	0.6026	2.57	2.310
13	1.5503	0.6086	1.81	2.287
14	1.5353	0.6041	2.81	2.278
15	1.5398	0.6077	2.59	2.291
16	1.5403	0.6095	2.61	2.289
17	1.5334	0.6019	2.88	2.265
MEAN	**1.5437**	**0.6076**	**2.29**	**2.278**
STD DEV	**0.0056**	**0.0037**	**0.3529**	**0.0150**

Table A8 Data For Moulding at 1633 kN/m^2 Curing Pressure
(Experiment 5)

SPECIMEN NUMBER	DENSITY (g/cm^3)	FIBRE VOLUME FRACTION	VOID CONTENT (%)	THICKNESS (mm)
1	1.5615	0.5976	0.57	2.195
2	1.5729	0.6227	0.56	2.200
3	1.5780	0.6266	0.30	2.199
4	1.5765	0.6275	0.45	2.197
5	1.5760	0.6339	0.36	2.204
6	1.5804	0.6333	0.35	2.186
7	1.5773	0.6331	0.58	2.188
8	1.5788	0.6303	0.37	2.179
9	1.5636	0.6028	0.59	2.146
10	1.5835	0.6329	0.10	2.185
11	1.5787	0.6310	0.40	2.187
12	1.5800	0.6286	0.22	2.189
13	1.5676	0.6097	0.52	2.184
14	1.5824	0.6270	- 0.01	2.211
15	1.5824	0.6285	0.03	2.200
16	1.5720	0.6210	0.57	2.212
17	1.5585	0.5843	0.34	2.175
MEAN	**1.5735**	**0.6212**	**0.37**	**2.190**
STD DEV	**0.0077**	**0.0142**	**0.1930**	**0.0155**

Table A9 Data For Moulding at 2940 kN/m^2 Curing Pressure
(Experiment 5)

SPECIMEN NUMBER	DENSITY (g/cm^3)	FIBRE VOLUME FRACTION	VOID CONTENT (%)	THICKNESS (mm)
1	1.5680	0.6000	0.15	2.123
2	1.5819	0.6322	0.20	2.170
3	1.5876	0.6356	-0.12	2.169
4	1.5876	0.6325	-0.23	2.192
5	1.5774	0.6344	0.62	2.157
6	1.5823	0.6335	0.22	2.177
7	1.5815	0.6327	0.25	2.191
8	1.5807	0.6321	0.29	2.177
9	1.5789	0.6170	-0.10	2.159
10	1.5842	0.6312	-0.01	2.181
11	1.5775	0.6276	0.38	2.187
12	1.5786	0.6246	0.19	2.195
13	1.5636	0.5943	0.30	2.154
14	1.5819	0.6350	0.30	2.171
15	1.5824	0.6325	0.21	2.174
16	1.5769	0.6271	0.40	2.160
17	1.5661	0.5842	-0.24	2.102
MEAN	1.5787	0.6240	0.17	2.167
STD DEV	0.0069	0.0158	0.2340	0.0240

Table A10 **Data For Moulding With Two Layers of Bleed Cloth and a Frame (1000 kN/m²)**
(Experiment 6)

SPECIMEN NUMBER	DENSITY (g/cm³)	FIBRE VOLUME FRACTION	VOID CONTENT (%)	THICKNESS (mm)
1	1.5530	0.6146	1.81	2.207
2	1.5668	0.6231	1.05	2.234
3	1.5577	0.6122	1.37	2.256
4	1.5611	0.6167	1.27	2.254
5	1.5523	0.6193	2.03	2.225
6	1.5528	0.6182	1.96	2.209
7	1.5644	0.6231	1.23	2.228
8	1.5603	0.6160	1.30	2.250
9	1.5501	0.6178	2.15	2.201
MEAN	1.5576	0.6179	1.57	2.230
STD DEV	0.0059	0.0036	0.4097	0.0210

Table A11 **Data For Moulding With Two Layers of Bleed Cloth Without a Frame (1000 kN/m²)**
(Expterimen 6)

SPECIMEN NUMBER	DENSITY (g/cm³)	FIBRE VOLUME FRACTION	VOID CONTENT (%)	THICKNESS (mm)
1	1.5678	0.6322	1.24	2.166
2	1.5777	0.6462	1.77	2.166
3	1.5725	0.6314	1.48	2.192
4	1.5748	0.6500	1.18	2.215
5	1.5670	0.6243	0.99	2.567
6	1.5615	0.6163	2.66	2.562
7	1.5757	0.6400	3.02	2.576
8	1.5786	0.6394	1.01	2.579
9	1.5729	0.6350	0.98	2.573
MEAN	1.5721	0.6317	1.59	2.188
STD DEV	0.0056	0.0085	0.7600	0.0240

Table A12 Data For Moulding With Four Layers of Bleed Cloth and a Frame (1000 kN/m^2)
(Experiment 6)

SPECIMEN NUMBER	DENSITY (g/cm^3)	FIBRE VOLUME FRACTION	VOID CONTENT (%)	THICKNESS (mm)
1	1.5605	0.6224	1.50	2.216
2	1.5656	0.6308	1.40	2.222
3	1.5664	0.6326	1.40	2.206
4	1.5676	0.6315	1.27	2.204
5	1.5649	0.6258	1.29	2.176
6	1.5651	0.6301	1.42	2.177
7	1.5649	0.6320	1.50	2.218
8	1.5667	0.6362	1.51	2.184
9	1.5564	0.6192	1.71	2.196
MEAN	1.5642	0.6290	1.44	2.200
STD DEV	0.0036	0.0054	0.1322	0.0175

Table A13 Data For Moulding With Four Layers of Bleed Cloth Without a Frame (1000 kN/m^2)
(Experiment 6)

SPECIMEN NUMBER	DENSITY (g/cm^3)	FIBRE VOLUME FRACTION	VOID CONTENT (%)	THICKNESS (mm)
1	1.5697	0.6472	1.66	2.128
2	1.5738	0.6502	1.44	2.153
3	1.5738	0.6489	1.40	2.159
4	1.5750	0.6504	1.36	2.148
5	1.5694	0.6454	1.62	2.142
6	1.5720	0.6463	1.45	2.138
7	1.5787	0.6547	1.23	2.140
8	1.5698	0.6472	1.65	2.157
9	1.5665	0.6422	1.73	2.143
MEAN	1.5721	0.6481	1.50	2.146
STD DEV	0.0037	0.0036	0.1670	0.0090

Table A14 Data For Moulding With Two Layers of Bleed Cloth and a Frame (3000 kN/m^2)
(Experiment 6)

SPECIMEN NUMBER	DENSITY (g/cm^3)	FIBRE VOLUME FRACTION	VOID CONTENT (%)	THICKNESS (mm)
1	1.5671	0.6030	0.33	2.053
2	1.5859	0.6544	0.66	2.110
3	1.5815	0.6512	0.89	2.129
4	1.5835	0.6543	0.84	2.125
5	1.5698	0.6141	0.51	2.096
6	1.5732	0.6264	0.67	2.030
7	1.5837	0.6570	0.92	2.108
8	1.5828	0.6516	0.80	2.124
9	1.5722	0.6215	0.57	2.105
MEAN	1.5777	0.6371	0.69	2.098
STD DEV	0.0071	0.0021	0.1950	0.0340

Table A15 Data For Moulding With Two Layers of Bleed Cloth Without a Frame (3000 kN/m^2)
(Experiment 6)

SPECIMEN NUMBER	DENSITY (g/cm^3)	FIBRE VOLUME FRACTION	VOID CONTENT (%)	THICKNESS (mm)
1	1.5849	0.6659	1.28	1.985
2	1.5873	0.6895	1.00	2.009
3	1.5894	0.6860	0.89	2.020
4	1.5974	0.6949	0.65	2.000
5	1.5937	0.6812	1.07	1.946
6	1.5258	0.6791	1.22	1.926
7	1.5732	0.6945	0.64	1.993
8	1.5950	0.6848	0.71	2.025
9	1.5863	0.6646	0.99	2.032
MEAN	1.5863	0.6827	0.94	1.993
STD DEV	0.0093	0.0011	0.2360	0.0360

Table A16 Data For Moulding With Four Layers of Bleed Cloth and a Frame (3000 kN/m^2)
(Exptérimen 6)

SPECIMEN NUMBER	DENSITY (g/cm^3)	FIBRE VOLUME FRACTION	VOID CONTENT (%)	THICKNESS (mm)
1	1.5739	0.6438	1.21	2.069
2	1.5898	0.6625	0.64	2.096
3	1.5907	0.6597	0.48	2.110
4	1.5892	0.6676	0.86	2.090
5	1.5825	0.6589	1.07	2.054
6	1.5790	0.6504	1.05	2.047
7	1.5907	0.6654	0.67	2.092
8	1.5887	0.6625	0.72	2.088
9	1.5730	0.6467	1.38	2.083
MEAN	1.5842	0.6575	0.90	2.081
STD DEV	0.0073	0.0085	0.2980	0.0203

Table A17 Data For Moulding With Four Layers of Bleed Cloth Without a Frame (3000 kN/m^2)
(Experiment 6)

SPECIMEN NUMBER	DENSITY (g/cm^3)	FIBRE VOLUME FRACTION	VOID CONTENT (%)	THICKNESS (mm)
1	1.5904	0.6754	1.04	1.975
2	1.5909	0.6843	1.31	2.040
3	1.5947	0.6762	0.74	2.067
4	1.5938	0.6723	0.68	2.080
5	1.5847	0.6606	0.97	2.050
6	1.5873	0.6642	0.89	2.043
7	1.5912	0.6786	1.09	2.055
8	1.5949	0.6859	1.06	2.040
9	1.5895	0.6748	1.09	1.949
MEAN	1.5908	0.6747	0.98	2.033
STD DEV	0.0034	0.0083	0.1946	0.0430

Table A18 Data For Moulding at Zero Minutes Partial Cure Time *(Experiment 7)*

SPECIMEN NUMBER	DENSITY (g/cm^3)	FIBRE VOLUME FRACTION	VOID CONTENT (%)	THICKNESS (mm)
1	1.5679	0.6121	0.58	2.058
2	1.5824	0.6441	0.57	2.136
3	1.5784	0.6360	0.60	2.165
4	1.5800	0.6337	0.40	2.172
5	1.5658	0.6153	0.85	2.166
6	1.5601	0.6080	1.04	2.173
7	1.5780	0.6348	0.59	2.171
8	1.5800	0.6403	0.63	2.148
9	1.5749	0.6304	0.67	2.106
MEAN	**1.5742**	**0.6288**	**0.66**	**2.144**
STD DEV	**0.0072**	**0.0131**	**0.1850**	**0.039**

Table A19 Data For Moulding at 5 Minutes Partial Cure Time *(Experiment 7)*

SPECIMEN NUMBER	DENSITY (g/cm^3)	FIBRE VOLUME FRACTION	VOID CONTENT (%)	THICKNESS (mm)
1	1.5757	0.6113	- 0.04	1.975
2	1.5737	0.6073	- 0.03	2.040
3	1.5658	0.5938	0.11	2.067
4	1.5656	0.5934	0.11	2.080
5	1.5750	0.6164	0.19	2.050
6	1.5636	0.5894	0.13	2.043
7	1.5522	0.5729	0.42	2.055
8	1.5752	0.6210	0.32	2.040
9	1.5708	0.6107	0.31	1.949
MEAN	**1.5686**	**0.6018**	**0.17**	**2.310**
STD DEV	**0.0077**	**0.0154**	**0.1593**	**0.0790**

Table A20 Data For Moulding at 10 Minutes Partial Cure Time *(Experiment 7)*

SPECIMEN NUMBER	DENSITY (g/cm^3)	FIBRE VOLUME FRACTION	VOID CONTENT (%)	THICKNESS (mm)
1	1.5333	0.5365	0.63	2.603
2	1.5240	0.5318	1.18	2.649
3	1.5121	0.5223	1.76	2.707
4	1.5189	0.5249	1.33	2.696
5	1.5283	0.5299	0.78	2.638
6	1.5073	0.5197	2.04	2.676
7	1.5163	0.5256	1.56	2.691
8	1.5214	0.5290	1.28	2.655
9	1.5406	0.5449	0.36	2.557
MEAN	**1.5225**	**0.5294**	**1.21**	**2.652**
STD DEV	**0.0104**	**0.0077**	**0.5450**	**0.0484**

Table A21 Data For Moulding at 15 Minutes Partial Cure Time *(Experiment 7)*

SPECIMEN NUMBER	DENSITY (g/cm^3)	FIBRE VOLUME FRACTION	VOID CONTENT (%)	THICKNESS (mm)
1	1.4648	0.5009	4.66	2.813
2	1.4707	0.5017	4.23	2.813
3	1.4766	0.5083	4.01	2.771
4	1.4808	0.5107	3.77	2.748
5	1.4908	0.5160	3.18	2.712
6	1.5021	0.5145	2.26	2.705
7	1.4872	0.5114	3.30	2.724
8	1.4608	0.5037	5.07	2.793
9	1.4636	0.5052	4.90	2.794
MEAN	**1.4775**	**0.5080**	**3.93**	**2.764**
STD DEV	**0.0140**	**0.0055**	**0.9113**	**0.0430**

Table A22 Data For Moulding at 30 Minutes Partial Cure Time *(Expterimen 7)*

SPECIMEN NUMBER	DENSITY (g/cm^3)	FIBRE VOLUME FRACTION	VOID CONTENT (%)	THICKNESS (mm)
1	1.4530	0.4954	5.38	3.064
2	1.4550	0.4978	5.31	3.121
3	1.4783	0.5072	3.84	3.151
4	1.4676	0.5056	4.61	3.113
5	1.4652	0.5083	4.89	3.030
6	1.4546	0.4987	5.37	2.993
7	1.4528	0.4968	5.44	3.083
8	1.4632	0.5034	4.87	3.161
9	1.4699	0.5075	4.50	3.102
MEAN	**1.4622**	**0.5024**	**4.91**	**3.091**
STD DEV	**0.0090**	**0.0052**	**0.5340**	**0.0550**

Table A23 Data For Moulding at 45 Minutes Partial Cure Time *(Experiment 7)*

SPECIMEN NUMBER	DENSITY (g/cm^3)	FIBRE VOLUME FRACTION	VOID CONTENT (%)	THICKNESS (mm)
1	1.4510	0.4982	5.63	2.942
2	1.4635	0.5044	4.89	2.992
3	1.4559	0.4987	5.27	3.015
4	1.4389	0.4943	6.42	2.977
5	1.4528	0.4990	5.52	2.901
6	1.4572	0.4992	5.19	2.911
7	1.4569	0.4999	5.23	2.978
8	1.4503	0.4982	5.68	3.007
9	1.4443	0.4803	5.52	2.958
MEAN	**1.4523**	**0.4969**	**5.48**	**2.964**
STD DEV	**0.0074**	**0.0067**	**0.4320**	**0.0400**

Table A24 Data For Mouldings at Zero Minutes Partial Cure Time *(Experiment 8)*

SPECIMEN NUMBER	DENSITY (g/cm^3)	FIBRE VOLUME FRACTION	VOID CONTENT (%)	THICKNESS (mm)
1	1.6004	0.6429	- 0.86	2.166
2	1.5771	0.6232	0.26	2.096
3	1.5882	0.6362	- 0.15	2.190
4	1.5907	0.6389	- 0.25	2.148
5	1.5766	0.6266	0.42	2.106
6	1.5827	0.6339	0.20	2.170
7	1.5595	0.6320	1.91	2.150
8	1.5863	0.6311	- 0.18	2.119
9	1.5818	0.6326	0.22	2.182
10	1.5863	0.6388	0.09	2.177
11	1.5849	0.6284	- 0.16	2.151
12	1.5907	0.6394	- 0.23	2.168
13	1.5887	0.6495	0.27	2.124
14	1.5801	0.6282	0.20	2.127
15	1.5779	0.6370	0.67	2.152
MEAN	1.5835	0.6346	0.13	2.149
STD DEV	0.0065	0.0068	0.6322	0.0289

Table A25 Data For Mouldings at 5 Minutes Partial Cure Time
(Experiment 8)

SPECIMEN NUMBER	DENSITY (g/cm^3)	FIBRE VOLUME FRACTION	VOID CONTENT (%)	THICKNESS (mm)
1	1.5770	0.6176	0.07	2.232
2	1.5901	0.6344	- 0.35	2.197
3	1.5764	0.6068	- 0.26	2.299
4	1.5851	0.6264	- 0.25	2.190
5	1.5689	0.6067	- 0.31	2.241
6	1.5817	0.6430	0.59	2.146
7	1.5866	0.6309	- 0.21	2.188
8	1.5782	0.6265	0.29	2.189
9	1.5689	0.6007	0.11	2.329
10	1.5800	0.6381	0.55	2.151
11	1.5696	0.6157	0.57	2.178
12	1.5676	0.6047	0.35	2.290
13	1.5823	0.6430	0.54	2.128
14	1.5767	0.6344	0.68	2.122
15	1.5790	0.6283	0.29	2.183
MEAN	**1.5779**	**0.6238**	**0.22**	**2.204**
STD DEV	**0.0069**	**0.0142**	**0.3488**	**0.0626**

Table A26 Data For Mouldings at 8 Minutes Partial Cure Time
(Experiment 8)

SPECIMEN NUMBER	DENSITY (g/cm^3)	FIBRE VOLUME FRACTION	VOID CONTENT (%)	THICKNESS (mm)
1	1.5085	0.4974	1.18	2.802
2	1.5296	0.5121	0.07	2.741
3	1.4963	0.4950	2.03	2.793
4	1.5703	0.6066	0.21	2.769
5	1.5692	0.6014	0.11	2.758
6	1.5217	0.5059	0.45	2.737
7	1.5434	0.5513	0.36	2.531
8	1.5390	0.5338	0.09	2.612
9	1.4919	0.4938	2.33	2.842
10	1.5498	0.5553	0.01	2.503
11	1.5437	0.5432	0.06	2.539
12	1.5126	0.5079	1.23	2.780
13	1.5337	0.5312	0.41	2.626
14	1.5294	0.5181	0.29	2.704
15	1.4775	0.4861	3.17	2.864
MEAN	**1.5278**	**0.5293**	**0.80**	**2.707**
STD DEV	**0.0270**	**0.0371**	**0.9800**	**0.1164**

Table A27 Data For Mouldings at 12 Minutes Partial Cure Time
(Experiment 8)

SPECIMEN NUMBER	DENSITY (g/cm^3)	FIBRE VOLUME FRACTION	VOID CONTENT (%)	THICKNESS (mm)
1	1.4852	0.4948	2.88	2.843
2	1.4990	0.5005	2.02	2.824
3	1.4926	0.4996	2.48	2.794
4	1.5246	0.5185	0.68	2.696
5	1.5246	0.5163	0.60	2.709
6	1.5012	0.5075	2.09	2.734
7	1.5168	0.5140	1.12	2.763
8	1.5119	0.5064	1.23	2.777
9	1.4587	0.4782	4.35	2.985
10	1.4619	0.5023	4.93	2.894
11	1.4473	0.4503	4.26	2.895
12	1.4782	0.4893	3.23	3.007
13	1.5285	0.5176	0.34	2.690
14	1.5223	0.5070	0.45	2.773
15	1.4755	0.4870	3.36	3.029
MEAN	1.4952	0.4993	2.27	2.828
STD DEV	0.0266	0.0180	1.5290	0.1123

Table A28 Data For Mouldings at 15 Minutes Partial Cure Time
(Experiment 8)

SPECIMEN NUMBER	DENSITY (g/cm^3)	FIBRE VOLUME FRACTION	VOID CONTENT (%)	THICKNESS (mm)
1	1.5015	0.5228	2.60	2.658
2	1.4914	0.5028	2.68	2.753
3	1.4881	0.5072	3.09	2.736
4	1.5615	0.5840	0.10	2.433
5	1.5604	0.5830	0.15	2.420
6	1.5546	0.5896	0.82	2.412
7	1.5036	0.5004	1.66	2.786
8	1.4857	0.4884	2.62	2.846
9	1.4582	0.4864	4.67	2.853
10	1.5324	0.5355	0.66	2.640
11	1.5240	0.5568	2.04	2.681
12	1.5076	0.5290	2.34	2.673
13	1.5217	0.5339	1.43	2.634
14	1.5299	0.5373	0.91	2.629
15	1.5163	0.5418	2.11	2.597
MEAN	1.5158	0.5333	1.86	2.650
STD DEV	0.0295	0.0337	1.2306	0.1410

Table A29 Data For Mouldings at 20 Minutes Partial Cure Time
(Experiment 8)

SPECIMEN NUMBER	DENSITY (g/cm^3)	FIBRE VOLUME FRACTION	VOID CONTENT (%)	THICKNESS (mm)
1	1.4545	0.5014	5.47	2.921
2	1.4566	0.5016	5.32	2.909
3	1.4644	0.5122	5.09	2.963
4	1.4789	0.5081	3.83	3.007
5	1.4757	0.5080	4.07	2.950
6	1.4656	0.5124	5.00	3.055
7	1.4877	0.5150	3.39	2.890
8	1.4934	0.5170	3.02	2.879
9	1.4957	0.5215	3.00	3.089
10	1.4775	0.5055	3.84	2.997
11	1.4823	0.5116	3.69	2.944
12	1.4787	0.5114	3.95	3.050
13	1.4711	0.5044	4.30	2.901
14	1.4642	0.5029	4.78	2.898
15	1.4963	0.5185	2.85	2.997
MEAN	**1.4762**	**0.5101**	**4.11**	**2.963**
STD DEV	**0.0135**	**0.0063**	**0.8633**	**0.0665**

Table A30 Data For Mouldings at 30 Minutes Partial Cure Time
(Experiment 8)

SPECIMEN NUMBER	DENSITY (g/cm^3)	FIBRE VOLUME FRACTION	VOID CONTENT (%)	THICKNESS (mm)
1	1.4242	0.4711	6.75	3.015
2	1.4332	0.4699	6.02	3.018
3	1.4333	0.4773	6.27	2.966
4	1.4587	0.4873	4.66	2.834
5	1.4899	0.5050	2.87	2.752
6	1.4535	0.4860	5.01	2.884
7	1.4452	0.4782	5.39	2.994
8	1.4480	0.4803	5.24	2.986
9	1.4202	0.4650	6.87	3.051
10	1.4585	0.4820	4.49	2.854
11	1.4695	0.4839	3.71	2.898
12	1.4342	0.4723	6.03	2.986
13	1.4585	0.4858	4.62	2.916
14	1.4580	0.4796	4.45	2.932
15	1.4280	0.4690	6.39	2.989
MEAN	**1.4475**	**0.4796**	**5.25**	**2.938**
STD DEV	**0.0190**	**0.0098**	**1.1480**	**0.0820**

APPENDIX B

STATIC TEST DATA

Table B1 Compressive Strength Data Using The Celanese Jig *(Experiment 4)*

SPECIMEN NUMBER	STATIC COMPRESSIVE STRENGTH (MPa)		
	653 kN/m^2	1307 kN/m^2	1960 kN/m^2
1	393	458	544
2	425	482	518
3	503	412	544
4	433	449	450
5	409	434	412
6	462	477	540
7	391	432	504
8	467	481	480
9	424	426	471
10	445	426	553
11	432	430	444
12	473	416	434
13	477	472	493
14	493	440	494
15	410	469	466
MEAN	442	447	490
STD DEV	35.30	24.37	44.14
COV*	7.98%	5.45%	9.00%

* COV : Coefficient of variation

Table B2 Compressive Strength Data Using The ABG-1 *(Experiment 4)*

SPECIMEN NUMBER	STATIC COMPRESSIVE STRENGTH (MPa)		
	653 kN/m^2	1307 kN/m^2	1960 kN/m^2
1	385	424	459
2	403	426	439
3	395	421	427
4	412	420	451
5	423	402	439
6	405	414	419
7	389	401	427
8	410	419	414
MEAN	403	416	434
STD DEV	12.63	9.55	15.52
COV	3.14%	2.30%	3.57%

Table B3 Compressive Strength Data Using The ABG-2 *(Expt 4)*

SPECIMEN NUMBER	STATIC COMPRESSIVE STRENGTH (MPa)		
	653 kN/m^2	1307 kN/m^2	1960 kN/m^2
1	399	413	394
2	343	412	426
3	380	374	375
4	376	386	404
5	348	395	380
MEAN	369	396	396
STD DEV	23.38	16.81	20.40
COV	6.33%	4.30%	5.15%

Table B4 Compressive Strength Data Using The CRAG Jig *(Experiment 4)*

SPECIMEN NUMBER	STATIC COMPRESSIVE STRENGTH (MPa)		
	653 kN/m^2	1307 kN/m^2	1960 kN/m^2
1	354	385	391
2	389	378	396
3	351	392	381
4	394	372	373
5	392	391	395
MEAN	376	384	387
STD DEV	21.55	8.56	9.91
COV	5.73%	2.23%	2.24%

Table B5 Secant Modulus Data Obtained Using The Celanese Jig *(Experiment 4)*

SPECIMEN NUMBER	SECANT MODULUS AT 0.25% STRAIN (GPa)		
	653 kN/m^2	1307 kN/m^2	1960 kN/m^2
1	41.7	48.2	49.2
2	45.2	44.2	48.7
3	48.8	50.4	47.7
4	-	-	48.9
5	-	-	43.3
6	-	-	45.1
7	-	-	44.2
8	-	-	43.9
MEAN	45.2	47.6	46.4
STD DEV	3.550	3.143	2.492
COV	7.85%	6.60%	5.37%

Table B6 Secant Modulus Data Obtained Using The ABG-1 *(Expt 4)*

SPECIMEN NUMBER	SECANT MODULUS AT 0.25% STRAIN (GPa)		
	653 kN/m^2	1307 kN/m^2	1960 kN/m^2
1	49.3	49.6	49.4
2	46.1	49.0	48.4
3	47.7	48.7	50.2
4	-	-	50.2
5	-	-	49.5
6	-	-	50.8
MEAN	47.7	49.1	49.8
STD DEV	1.600	0.458	0.838
COV	3.35%	0.93%	1.69%

Table B7 Failure Strain Data Obtained Using The Celanese Jig *(Experiment 4)*

SPECIMEN NUMBER	FAILURE STRAIN (%)		
	653 kN/m^2	1307 kN/m^2	1960 kN/m^2
1	0.94	0.86	0.82
2	0.89	0.82	0.68
3	0.90	1.04	0.95
4	-	0.99	1.09
5	-	-	1.30
6	-	-	0.70
7	-	-	0.89
8	-	-	0.80
MEAN	0.91	0.93	0.90
STD DEV	0.0265	0.1044	0.2082
COV	2.91%	11.25%	23.04%

Table B8 Failure Strain Data Obtained Using The ABG-1 *(Expt 4)*

SPECIMEN NUMBER	FAILURE STRAIN (%)		
	653 kN/m^2	1307 kN/m^2	1960 kN/m^2
1	0.88	0.98	0.94
2	0.92	0.81	0.93
3	0.87	0.81	0.97
4	-	-	0.92
5	-	-	0.93
6	-	-	0.88
MEAN	0.89	0.87	0.93
STD DEV	0.0265	0.0981	0.0293
COV	2.94%	11.32%	3.15%

Table B9 **Compressive Strength for Different Partial Cure Times** *(Experiment 8)*

SPECIMEN NUMBER	STATIC COMPRESSIVE STRENGTH (MPa) PARTIAL CURE TIME (MINS)						
	0	5	8	12	15	20	30
1	367	382	338	308	342	214	204
2	362	372	314	327	319	203	265
3	382	379	319	168	290	219	156
4	345	378	284	269	259	239	177
5	304	370	258	241	322	235	195
6	356	345	282	311	317	279	213
7	345	367	348	326	280	235	175
8	373	382	340	205	290	230	186
9	364	398	306	205	301	215	180
10	347	-	387	379	318	225	214
MEAN	355	375	318	274	304	229	197
STD DEV	21.58	14.36	37.65	67.44	24.40	20.77	30.17
COV	6.09%	3.81%	11.82%	24.54%	8.03%	9.07%	15.36%

Table B10 Secant Modulus for Different Partial Cure Times *(Experiment 8)*

SPECIMEN NUMBER	SECANT MODULUS AT 0.25% STRAIN (GPa)						
	PARTIAL CURE TIME (MINS)						
	0	5	8	12	15	20	30
1	48.5	47.6	39.0	40.1	39.0	34.6	31.3
2	51.2	45.8	38.5	32.8	36.9	37.7	34.3
3	48.4	44.7	38.5	38.3	37.0	35.5	30.4
4	49.3	45.2	40.8	31.4	38.1	36.9	32.4
5	49.2	48.3	37.3	40.4	39.5	32.9	30.0
MEAN	49.3	46.3	38.8	36.6	38.1	35.5	31.7
STD DEV	1.126	1.558	1.272	4.215	1.164	1.895	1.731
COV*	2.28%	3.36%	3.28%	11.52%	3.06%	5.34%	5.46%

Table B11 Failure Strain for Different Partial Cure Times *(Experiment 8)*

SPECIMEN NUMBER	FAILURE STRAIN (%)						
	PARTIAL CURE TIME (MINS)						
	0	5	8	12	15	20	30
1	0.75	0.61	0.85	0.81	0.70	0.62	0.62
2	0.71	0.93	0.97	0.94	0.76	0.75	0.66
3	0.80	0.93	0.93	0.75	0.86	0.64	0.66
4	0.79	0.83	0.66	0.64	0.90	0.69	0.72
5	0.61	0.66	0.82	0.64	0.88	0.75	0.67
MEAN	0.73	0.79	0.85	0.76	0.82	0.69	0.67
STD DEV	0.0769	0.1501	0.1201	0.1262	0.0860	0.0604	0.0358
COV	10.51%	18.95%	14.20%	16.69%	10.49%	8.76%	5.37%

Table B12 Effect of Partial Cure TIme on Residual Properties After Fatigue at 55% Stress Level *(Experiment 8)*

PARTIAL CURE TIME (MINS)	RESIDUAL COMP STR (MPa)	RESIDUAL SECANT MOD (GPa)	RESIDUAL FAIL STRAIN (%)
0*	344	38.4	0.80
5	280	45.0	0.74
8	303	36.3	0.84
12	293	33.8	0.92
15	277	35.5	0.81
20	270	34.6	0.65
30	174	31.9	0.56

* fatigued at 57% stress level

Table B13 **Effect of Partial Cure Time on Residual Properties After Fatigue at Various Stress Levels**
(Experiment 8)

PARTIAL CURE TIME (MINS)	STRESS LEVEL (%)	RESIDUAL COMP STR (MPa)	RESIDUAL SECANT MOD (GPa)	RESIDUAL FAIL STRAIN (%)
0	55	341	46.2	0.78
	55	346	30.6	0.82
5	50	245	46.9	0.52
	57	254	47.6	0.74
	57	305	42.4	0.74
8	55	326	36.3	0.84
	55	281	-	-
	60	319	33.4	1.36
12	50	267	35.5	0.82
	55	295	33.9	0.92
	55	292	33.6	0.86
15	55	278	36.1	0.81
	55	277	34.8	0.91
	60	263	-	-
20	50	216	35.1	0.65
	55	270	34.6	0.65
	65	254	34.5	0.76
30	50	170	-	-
	55	174	31.9	0.56

APPENDIX C

FATIGUE TEST DATA

Table C1 **Fatigue Life of Specimens Moulded at Different Curing Pressures *(Experiment 4)***

STRESS LEVEL (%)	NUMBER OF FATIGUE CYCLES		
	653 kN/m²	1307 kN/m²	1960 kN/m²
75	-	-	2900
70	14860	19840	18300
	-	-	35280
	-	-	95880
65	90730	51580	44380
	-	119540	80460
	-	126220	112300
60	68060	155100	71350
	75000	178300	160280
	253410	-	416000
	427760	-	737680
57	165300	-	-
	174290	-	-
	222560	-	-
55	280030	243110	152950
	300000	277650	293200
	-	-	423950
	-	-	470210
53	700180	1000000	-
	-	1000000	-
50	136420	600000	535000
	301490	1000000	704800
	1000000	-	778850
	-	-	1000000
45	-	-	1000000
	-	-	1000000

Table C2 **Fatigue Life of Specimens Moulded at Different Partial Cure Times *(Experiment 8)***

STRESS LEVEL	NUMBER OF FATIGUE CYCLES						
(%)	0 mins	5 mins	8 mins	12 mins	15 mins	20 mins	30 mins
75	8230	1410	590	90	1820	750	-
	29180	6260	880	150	2220	1900	-
	57050	6640	6920	93380	6710	41860	-
70	12230	46900	22200	1200	21510	11920	100
	46650	47920	50030	5120	48482	24710	220
	157450	70940	281050	9730	89930	113200	29170
67	- -	-	-	-	-	1970	
65	25770	43880	61410	6800	25000	14230	5750
	90900	155700	34730	35220	139400	29570	12270
	217970	370160	147600	297550	608440	187750	21160
	- -	-	-	-	1000000	-	
60	59070	166750	94100	100180	200740	325650	37340
	90990	363400	287150	355230	620460	381680	74410
	197050	726510	795060	481520	1000000	792250	624790
	- -	-	859140	-	-	-	
57	- 1000000		398670	-	-	-	676000
55	613250	671180	619770	315840	513850	476650	89660
	1000000	687920	1000000	1000000	1000000	760950	1000000
	1000000	1000000	-	-	-	1000000	-
50	- 1000000		-	27540	-	1000000	450080
	- -	-	910600	-	-	1000000	
	- -	-	1000000	-	-	-	

Table C3 **Residual Modulus For Mouldings at 1307 kN/m² Curing Pressure *(Experiment 4)***

NUMBER OF CYCLES	RESIDUAL MODULUS AT EACH STRESS LEVEL (GPa)				
	70 %	65 % (a)	65 % (b)	55 %	50 %
0	46.51	47.55	46.97	43.92	42.57
10000	44.00	45.92	-	-	-
14180	43.81	-	-	-	-
19840	41.69	-	-	-	-
15320	-	-	45.99	-	-
20000	-	45.56	-	-	-
35320	-	-	45.00	-	-
40000	-	-	-	-	42.57
46100	-	44.11	-	-	-
55320	-	-	44.71	-	-
77780	-	-	46.28	-	-
80000	-	-	-	-	42.84
97780	-	-	43.33	-	-
100000	-	-	-	42.47	-
119240	-	-	41.06	-	-
120000	-	-	-	-	42.93
160000	-	-	-	-	42.57
200000	-	-	-	42.18	-
217170	-	-	-	41.99	-
257970	-	-	-	41.70	-
300000	-	-	-	-	43.02
1000000	-	-	-	-	40.76
Failure Cycles	19840	51580	119540	277650	DNF*

* DNF : Did Not Fail (specimen completed one million cycles)

Table C4 Residual Modulus For Mouldings at 1960 kN/m^2 Curing Pressure *(Experiment 4)*

NUMBER OF CYCLES	RESIDUAL MODULUS AT EACH STRESS LEVEL (GPa)				
	70 %	65 %	60 %	55 %	50 %
0	74.30	44.84	45.72	45.86	45.55
10000	45.28	-	44.85	-	-
20000	44.36	42.89	-	44.10	-
30000	-	-	44.42	-	-
35270	41.97	-	-	-	-
40000	-	42.45	-	-	44.22
54000	-	-	44.42	-	-
60000	-	-	-	44.10	-
80000	-	41.57	-	-	43.78
100000	-	41.30	-	-	-
111030	-	-	-	43.22	-
112300	-	39.53	-	-	-
114000	-	-	43.98	-	-
125540	-	-	-	-	44.22
125600	-	-	-	40.84	-
145600	-	-	-	41.89	-
152950	-	-	-	38.81	-
154000	-	-	43.54	-	-
159680	-	-	42.93	-	-
160280	-	-	33.96	-	-
208430	-	-	-	-	43.78
285250	-	-	-	-	43.78
325250	-	-	-	-	43.61
393630	-	-	-	-	42.46
433630	-	-	-	-	42.19
484870	-	-	-	-	41.31
524870	-	-	-	-	40.42
Failure Cycles	35280	112300	160280	152950	535000

Table C5 **Residual Modulus For Mouldings at Zero Minutes Partial Cure Time *(Experiment 8)***

NUMBER OF CYCLES	RESIDUAL MODULUS AT EACH STRESS LEVEL (GPa)				
	75 %	70 %	65 %	60 %	55 %
0	46.71	46.09	46.20	45.28	45.03
20000	46.23	45.65	-	-	-
23570	-	45.47	-	-	-
29140	43.85	-	-	-	-
29930	-	-	-	-	44.74
55080	-	45.47	-	-	-
69450	-	-	45.05	-	-
89550	-	-	-	-	-
89800	-	-	43.28	-	-
90800	-	-	41.96	-	-
105200	-	45.47	-	-	-
109440	-	-	-	-	44.74
141070	-	45.20	-	-	-
141980	-	-	-	-	44.74
155600	-	43.68	-	-	-
276360	-	-	-	-	44.06
776830	-	-	-	-	43.28
1000000	-	-	-	-	42.31
Failure Cycles	29180	157450	90900	90990	DNF

Table C6 **Residual Modulus For Mouldings at 5 Minutes Partial Cure Time *(Experiment 8)***

NUMBER OF CYCLES	RESIDUAL MODULUS AT EACH STRESS LEVEL(GPa)				
	70 %	65 %	60 %	57 %	55 %
0	43.87	44.44	41.98	46.69	43.54
100	-	-	-	-	43.54
2000	43.80	-	-	-	-
4000	43.80	43.01	-	-	-
6000	43.80	-	-	-	-
8000	43.80	-	-	-	-
12000	-	42.77	-	-	-
18000	41.47	-	42.60	-	-
21520	41.01	-	-	-	-
28000	-	43.01	-	-	-
30000	41.94	-	-	-	-
36000	-	-	42.60	-	-
36570	41.01	-	-	-	-
39310	-	42.77	-	-	-
46130	39.61	-	-	-	-
50000	-	-	-	47.14	-
55310	-	41.44	-	-	-
79310	-	41.92	-	-	-
111330	-	40.49	-	-	-
114750	-	-	-	46.47	-
143330	-	40.25	-	-	-
155760	-	-	-	-	43.98
255760	-	-	-	-	43.54
286220	-	-	-	46.24	-
369900	-	-	-	-	43.54
377890	-	-	-	46.24	-
402700	-	-	42.60	-	-
432700	-	-	42.39	-	-
488290	-	-	-	46.02	-
489360	-	-	-	-	43.10
490610	-	-	41.78	-	-
550610	-	-	41.57	-	-
588360	-	-	-	-	43.54
589360	-	-	-	-	42.21
610610	-	-	40.46	-	-
632540	-	-	-	45.34	-
670610	-	-	40.55	-	-
676930	-	-	39.73	-	-
712670	-	-	38.09	-	-
732560	-	-	-	45.79	-
788840	-	-	-	-	42.65
809560	-	-	-	45.34	-
960260	-	-	-	-	42.87
997640	-	-	-	-	42.87
1000000	-	-	-	44.45	42.43
Failure Cycles	46900	155700	726510	DNF	DNF

Table C7 **Residual Modulus For Mouldings at 8 Minutes Partial Cure Time *(Experiment 8)***

NUMBER OF CYCLES	RESIDUAL MODULUS AT EACH STRESS LEVEL (GPa)			
	70 %	65 %	60 %	55 %
0	37.28	34.05	37.31	35.51
4970	-	33.72	-	-
6240	-	-	36.94	-
13870	-	-	-	34.79
20000	36.76	-	-	-
28400	-	33.06	-	-
35940	-	-	36.94	-
41640	36.54	-	-	-
65160	36.54	-	-	-
115160	36.17	-	-	-
116070	-	-	-	34.15
129660	36.17	-	-	-
135940	-	-	36.09	-
150600	35.43	-	-	-
223700	35.06	-	-	-
273090	33.58	-	-	-
280960	31.74	-	-	-
292310	-	-	-	33.35
348620	-	-	35.11	-
392310	-	-	-	34.07
426250	-	-	34.97	-
479410	-	-	34.01	-
497020	-	-	-	33.77
580160	-	-	34.01	-
633480	-	-	34.01	-
650540	-	-	33.28	-
759830	-	-	32.55	-
794280	-	-	31.45	-
Failure Cycles	281050	34730	795060	619770

Table C8 **Residual Modulus For Mouldings at 12 Minutes Partial Cure Time *(Experiment 8)***

NUMBER OF CYCLES	RESIDUAL MODULUS AT EACH STRESS LEVEL (GPa)			
	70 %	65 %	60 %	55 %
0	30.84	35.69	35.46	38.10
810	30.14	-	-	-
5000	-	35.69	-	-
10000	-	35.69	-	-
20000	-	35.34	-	-
21550	-	35.34	-	-
31550	-	35.34	-	-
50000	-	-	35.18	-
50130	-	-	-	37.33
51550	-	34.66	-	-
61550	-	35.34	-	-
74920	-	-	-	37.33
75450	-	-	34.46	-
86810	-	34.66	-	-
92120	-	34.66	-	-
132120	-	34.66	-	-
133840	-	-	34.82	-
183840	-	-	34.10	-
204310	-	-	-	-
206230	-	-	-	37.71
212120	-	33.63	-	-
226660	-	-	34.46	-
232120	-	33.63	-	-
237410	-	33.63	-	-
275710	-	32.94	-	-
276400	-	32.94	-	-
296120	-	31.23	-	-
326660	-	-	34.46	-
364280	-	-	-	37.33
406370	-	-	34.10	-
459400	-	-	34.10	-
515880	-	-	-	36.94
553000	-	-	34.10	-
638290	-	-	33.74	-
662700	-	-	33.74	-
684000	-	-	-	37.33
733620	-	-	33.38	-
859140	-	-	33.02	-
1000000	-	-	-	37.33
Failure Cycles	1200	297550	859140	DNF

Table C9 **Residual Modulus For Mouldings at 15 Minutes Partial Cure Time *(Experiment 8)***

NUMBER OF CYCLES	RESIDUAL MODULUS AT EACH STRESS LEVEL (GPa)				
	75 %	70 %	65 %	60 %	55 %
0	34.00	35.89	41.84	36.85	35.42
1000	33.02	-	-	-	-
10000	-	-	41.84	-	-
20600	-	34.45	-	-	-
35760	-	34.31	-	-	-
40000	-	-	41.27	-	-
50000	-	-	-	36.25	-
90000	-	-	40.63	-	-
97250	-	-	-	35.88	-
105830	-	-	-	-	34.07
129050	-	-	-	-	34.44
150770	-	-	40.63	-	-
197250	-	-	-	35.51	-
250770	-	-	39.66	-	-
255600	-	-	-	35.51	-
354140	-	-	-	-	34.29
355600	-	-	-	35.51	-
370770	-	-	39.42	-	-
455600	-	-	-	34.26	-
457340	-	-	-	-	34.07
490770	-	-	38.46	-	-
570920	-	-	36.61	-	-
650320	-	-	-	-	33.92
913550	-	-	-	-	33.32
1000000	-	-	-	-	32.57
Failure Cycles	2220	48482	608440	620460	DNF

Table C10 Residual Modulus For Mouldings at 20 Minutes Partial Cure Time *(Experiment 8)*

NUMBER OF CYCLES	RESIDUAL MODULUS AT EACH STRESS LEVEL (GPa)		
	67 %	65 %	60 %
0	32.17	34.41	35.25
5000	31.86	-	-
20000	-	32.22	-
25000	32.17	-	-
28010	-	-	34.97
70000	-	32.09	-
78910	-	-	34.61
95000	30.59	-	-
112230	-	-	34.61
113900	-	32.09	-
213900	-	31.90	-
227970	-	31.90	-
262230	-	-	34.61
320870	-	31.77	-
362230	-	-	34.61
420870	-	31.77	-
520870	-	31.14	-
532830	-	-	34.61
570870	-	31.14	-
632830	-	-	34.25
670870	-	30.64	-
732830	-	-	34.97
770870	-	30.32	-
792240	-	24.95	-
832830	-	-	34.25
1000000	-	-	33.89
Failure Cycles	113200	792250	DNF

Table C11 Residual Modulus For Mouldings at 30 Minutes Partial Cure Time *(Experiment 8)*

NUMBER OF CYCLES	RESIDUAL MODULUS AT EACH STRESS LEVEL (GPa)			
	67 %	65 %	60 %	55 %
0	27.45	28.20	30.76	31.83
1450	26.12	-	-	-
1870	25.79	-	-	-
1910	25.46	-	-	-
4000	-	28.53	-	-
5000	-	-	30.76	-
8000	-	28.37	-	-
12000	-	28.37	-	-
14000	-	28.37	-	-
15000	-	-	31.41	-
16040	-	27.87	-	-
18040	-	25.74	-	-
25000	-	-	31.09	-
35000	-	-	30.60	-
50000	-	-	30.60	-
53260	-	-	31.09	-
73260	-	-	31.09	-
83260	-	-	30.93	-
89620	-	-	-	24.37
126550	-	-	30.93	-
157030	-	-	30.76	-
215920	-	-	30.76	-
235920	-	-	30.60	-
296000	-	-	30.44	-
331610	-	-	30.44	-
385640	-	-	29.63	-
427410	-	-	29.47	-
575020	-	-	28.82	-
604980	-	-	28.01	-
624600	-	-	25.91	-
Failure Cycles	1970	21160	624790	476650

Table C12 Residual Modulus of Specimens Fatigue Loaded at 60% Stress Level Until Just Before Failure
(Experiment 8)

NUMBER OF CYCLES	RESIDUAL MODULUS (GPa)						
	0 mins	5 mins	8 mins	12 mins	15 mins	20 mins	30 mins
0	45.20	45.06	35.79	35.05	37.19	33.36	28.94
1640	-	44.15	-	-	-	-	-
1880	-	-	-	-	-	-	29.58
4790	-	-	-	-	-	-	29.58
5650	-	41.42	-	-	-	-	-
10000	-	-	-	34.70	-	-	-
16170	-	-	-	-	-	-	29.26
20000	45.20	-	-	-	-	-	-
21090	-	-	-	-	36.65	-	-
26170	-	-	-	-	-	-	28.62
31830	-	-	-	34.35	-	-	-
36380	45.20	-	-	-	-	-	-
36530	-	-	-	-	-	32.47	-
39190	-	-	-	34.25	-	-	-
46170	-	-	-	-	-	-	27.98
60780	45.97	-	-	-	-	-	-
61910	-	-	-	-	-	-	27.66
65650	-	43.70	-	-	-	-	-
71710	-	-	-	-	-	-	25.73
81740	-	-	-	-	-	32.03	-
96390	-	-	-	33.65	-	-	-
100000	-	-	34.71	-	-	32.09	-
116990	-	-	-	33.30	-	-	-
126360	-	-	-	-	35.64	-	-
131000	-	-	34.56	-	-	-	-
132640	-	-	34.20	-	-	-	-

*continue on next page

NUMBER OF CYCLES	RESIDUAL MODULUS (GPa)						
	0 mins	5 mins	8 mins	12 mins	15 mins	20 mins	30 mins
140780	45.68	-	-	-	-	-	-
150720	-	43.24	-	-	-	-	-
156990	-	-	-	33.30	-	-	-
200000	-	-	-	-	31.97	-	-
204310	-	-	-	32.60	-	-	-
205640	-	-	33.98	-	-	-	-
214190	-	-	33.62	-	-	-	-
231090	-	42.79	-	-	-	-	-
240780	45.20	-	-	-	-	-	-
242440	-	42.79	-	-	-	-	-
244310	-	-	-	31.90	-	-	-
246750	-	-	-	31.55	-	-	-
276360	-	-	-	-	33.70	-	-
290780	45.20	-	-	-	-	-	-
300000	-	-	-	-	31.73	-	-
331100	-	-	-	-	31.54	-	-
340620	-	43.24	-	-	-	-	-
340780	45.01	-	-	-	-	-	-
370130	-	-	-	-	31.33	-	-
447900	-	42.33	-	-	-	-	-
454480	-	41.88	-	-	-	-	-
475880	-	41.42	-	-	-	-	-
490780	44.72	-	-	-	-	-	-
535630	44.72	-	-	-	-	-	-
635630	44.72	-	-	-	-	-	-
680880	44.53	-	-	-	-	-	-
694860	44.24	-	-	-	-	-	-
744860	43.76	-	-	-	-	-	-